2010

Mechanistic photochemistry: From reactive intermediates to environmental remediation

Erin M. Rockafellow
Iowa State University

Mechanistic photochemistry: From reactive intermediates to environmental remediation

by

Erin M. Rockafellow

A dissertation submitted to the graduate faculty

in partial fulfillment of the requirements for the degree of

DOCTOR OF PHILOSOPHY

Major: Organic Chemistry

Program of Study Committee:
William S. Jenks, Major Professor
Mark S. Gordon
Nicola Pohl
Klaus Schmidt-Rohr
Yan Zhao

Iowa State University

Ames, Iowa

2010

TABLE OF CONTENTS

CHAPTER 1

General introduction

1.1 DISSERTATION ORGANIZATION

The eight chapters of this dissertation exemplify the utility of light in chemical research and technology. Certain photochemical processes, namely oxene generation and environmental remediation, will be the focus. Chapter 1 is a general introduction, which includes background on the basic unimolecular photochemical pathways of sulfoxides and selenoxides and photochemical methods for water and air purification, specifically TiO_2 photocatalysis for water remediation and ammonia mitigation from swine barn exhaust air through UV irradiation.

Chapter 2 is a paper that was published in *Journal of Photochemistry and Photobiology A: Chemistry* in 2008 which compares direct photolysis of dibenzothiophene-*S*-oxide and dibenzoselenophene-*Se*-oxide to sensitized photolysis using $n\pi^*$ sensitizers with various triplet energies. The author of this dissertation performed the steady state reactions and some flash photolysis studies and wrote a portion of the paper. Ryan McCulla also carried out some steady state experiments and flash photolysis studies, as well as drafting parts of the paper.

Chapter 3 is a paper that was published in 2009 in *Journal of Photochemistry and Photobiology A: Chemistry* exploring WO_x-modified TiO_2 as a potential visible light-active photocatalyst. The author of this dissertation performed all of the experiments using quinoline (**Q**) as a probe molecule, helped characterize the photocatalysts, and assisted in writing the paper. Youn-Chul Oh synthesized and characterized the modified titania used in this study. Timothy Hathway performed all of the experiments using 1-anisylneopentanol (**AN**) as a probe molecule and wrote the majority of the paper.

Chapter 4 is a collaborative work with Prof. Klaus Schmidt Rohr at Iowa State University published in *Chemistry of Materials* that tackles an analytical shortcoming of the popular characterization methods of carbon-modified TiO_2 by employing solid-state

NMR to identify the carbon species and location within the catalyst. The author of this dissertation prepared and characterized the C-TiO_2, excluding the SSNMR characterization, carried out photocatalytic studies, and wrote the initial draft of the paper. Xiaowen Fang ran all of the solid-state NMR experiments and wrote portions of the paper containing the SSNMR results. Brian Trewyn performed the TEM and nitrogen sorption studies.

Chapter 5 is a paper that was published in 2009 in *Applied Catalysis B: Environmental* concerning a popular main-group doped TiO_2 photocatalyst, S-TiO_2. This chapter investigates the functionality of S-TiO_2 as a visible light-active catalyst for the photochemical degradation of model pollutants. The author of this dissertation carried out all of the work using S-TiO_2 and wrote the paper. Laine Stewart completed the work involving S_8-TiO_2.

Chapter 6 explores the use of selenium as a dopant atom in TiO_2, and whether there are significant differences in reactivity when moving from sulfur to a heavier atom. The selenium center can act as an internal electron trap of photogenerated electrons, ultimately reducing the selenium from Se^{4+} to Se^0. This system absorbs visible light and likely creates a redox cycle at Se centers. The author of this dissertation performed most of the work and mentored undergraduate Jessica Haywood who assisted with point of zero charge measurements and leaching studies. Travis Witte, a graduate student in Dr. Robert Houk's laboratory, carried out the ICP-MS analyses.

The work discussed in Chapter 7 is an interdisciplinary collaboration at Iowa State University with Dr. Jacek Koziel and Dr. Steven Hoff (Agricultural and Biosystems Engineering), and Dr. Jeffery Zimmerman (Veterinary Diagnostic and Production Animal Medicine). This study explores the possibility of using UV light to abate ammonia from swine barn exhaust, and complements similar research done in the Koziel group.

Lastly, Chapter 8 draws some general conclusions and discusses future directions of sulfoxide photochemistry and photochemical remediation technologies.

1.2 A BRIEF REVIEW OF SELECTED SULFOXIDE AND SELENOXIDE PHOTOCHEMISTRY

The sulfoxide functional group has been of interest to the organic chemistry community for decades, particularly for its utility in thermal chemistry. Sulfoxides have proven very useful as chiral ligands in catalyzed asymmetric synthesis and in directing the stereochemistry in the synthesis of optically pure natural products.[1-4] Sulfoxides have also shown notable biological activity in some cases.[5,6]

The photochemistry of sulfoxides received limited attention with a brief exception the 1970s. Sulfoxides and selenoxides have exhibited unique photochemistry compared to other functional groups.[7,8] This section will briefly review nomenclature and specific photochemical properties relevant to the work contained in Chapter 2. Several excellent reviews on sulfoxide thermal chemistry and photochemistry are available for the reader to refer to for a more comprehensive discussion.[9-13]

1.2.1 Nomenclature of sulfur- and selenium-containing organic molecules

The International Union of Pure and Applied Chemistry has issued a full set of guidelines for naming compounds containing sulfur and selenium atoms.[14-16] The paragraphs below will survey the applicable trends in the nomenclature to prepare the reader for topics herein.

Sulfur-containing organic compounds. Sulfides contain the most reduced form of sulfur, where a sulfur atom is in the same bonding environment as an oxygen atom in an alcohol or ether, which gives a thiol or thioether, respectively. Thiols typically use the prefix "thio-" in the name to indicate the functional group. For example, the sulfur-containing analog of phenol is thiophenol. If the oxygen in ethanol is changed to a sulfur, the name becomes ethanethiol. It is also appropriate to name ethanethiol as ethyl mercaptan. In the same way, the thioether congener of diethyl ether can be called diethyl thioether. It is also common to simply use the sulfide functionality as a suffix to give the name diethyl sulfide.

Oxidation of a sulfide forms a sulfoxide or a sulfone depending on the extent of oxidation. The first oxidation leads to the sulfoxide, which is often viewed as the sulfur

analog of a carbonyl. However, calculations have shown that the S–O bond is consistent with a highly polarized σ–bond, and not a double bond that is present in the carbonyl system.[17] A second oxidation of the sulfur produces a sulfone, which contains two S-O ylide bonds.

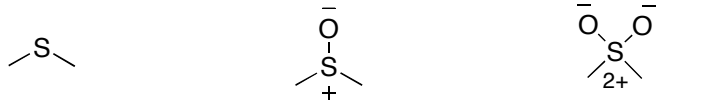

dimethyl sulfide dimethyl sulfoxide dimethyl sulfone

Several other organosulfur compounds exist, such as sulfur-containing esters, acids, and amides. In general, nomenclature for these sulfur compounds is based on the oxidation state of the sulfur and only differs by one vowel. Using sulfur-containing esters as an example, a sulf**e**nic ester (RS-OR) possesses a sulfur atom with a neutral oxidation state, a sulf**i**nic ester (RSO_2R) has a 1+ oxidation state on the sulfur, and a sulf**o**nic ester (RSO_3R) contains a sulfur with a 2+ oxidation state.

Selenium-containing organic compounds. Nomenclature of organoselenium compounds often parallels the naming of organosulfur compounds. Typically, only the "sulf" or "thio" in the name is replaced with "selen" or "seleno". For example, if the sulfur atom in the dimethylated sulfur compounds above was replaced with a selenium atom, the names would become dimethyl selenide, dimethyl selenoxide, and dimethyl selenone.

1.2.2 Unimolecular photochemical reactions of sulfoxides and selenoxides

Unimolecular sulfoxide photochemistry can be grouped into three major categories: α-cleavage, inversion, and deoxygenation. Homolytic α-cleavage is very common in carbonyl photochemistry and was recognized early in the history of sulfoxide chemistry, perhaps due to this analog. Inversion and unimolecular deoxygenation are unique to the sulfoxide functionality. Although intramolecular hydrogen abstraction is typical in carbonyl photochemistry, there is little evidence that supports this as a main

photochemical process for sulfoxides.[10,18] In fact, most photochemical reactions that appear to go by H-abstraction can be easily and more favorably explained by α-cleavage. This section briefly reviews each of the three common photochemical pathways of sulfoxides. Selenoxide photochemistry is generally analogous to that of sulfoxides, so it will not be explicitly reviewed here.[7,8]

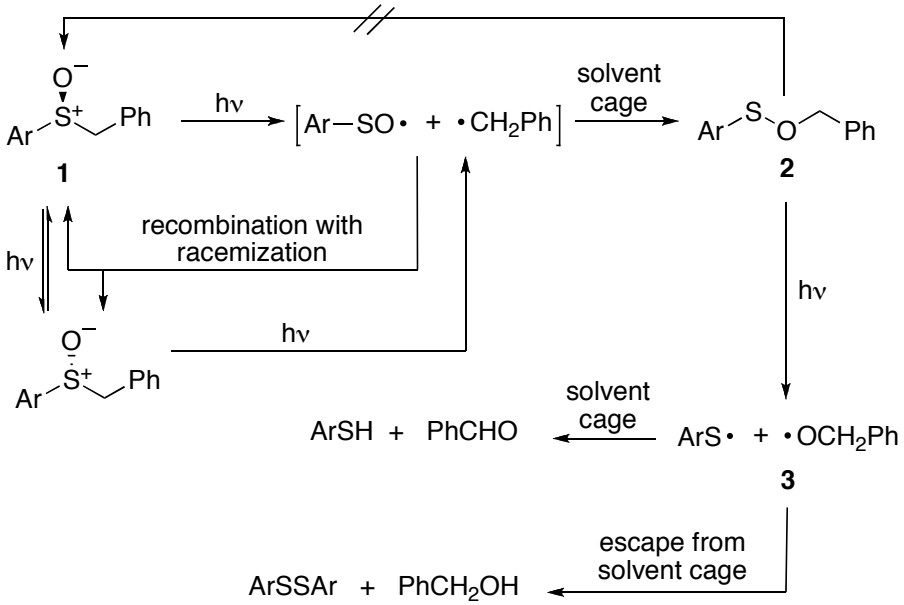

Scheme 1.1 Observed α-cleavage pathways using an aryl benzyl sulfoxide as the example.[18-20]

α-Cleavage. Homolytic cleavage of a C-S bond is very common in many sulfoxides as the S-O bond is typically stronger than a C-S bond. If anything, α-cleavage is more typical in sulfoxide photochemistry than in corresponding carbonyl systems. For example, under one-photon conditions, benzophenone does not undergo α-cleavage; however, C-S cleavage is observed for diphenylsulfoxide with a low quantum yield.[10] Appreciable quantum efficiencies can be obtained when the sulfoxide substituents lead to well-stabilized radicals. The Jenks group has demonstrated that aryl benzyl sulfoxides show high selectivity for alkyl-S cleavage with quantum yields for loss of the starting sulfoxide above 0.2, whereas 1˚ alkyl aryl sulfoxides exhibit cleavage of both C-S bonds with low quantum yields around 0.04.[21] In addition, when **1** is photolyzed with

wavelengths < 280 nm in an appropriate viscous solvent, **1** (with racemization) and sulfenic ester **2** are nearly the only products observed (Scheme 1.1).[18] If longer wavelengths were used, **2** is selectively photolyzed which leads to disproportionation products of the arenethiyl and alkoxyl radical pair **3**.

Inversion. As a result of the ylide nature of the S-O bond, the sulfur atom is a distorted pyramidal center.[19] Because inversion at room temperature is very slow, sulfoxides are often chiral compounds when they contain two different substituents. This feature makes them useful in synthesis as chiral auxiliaries.[10]

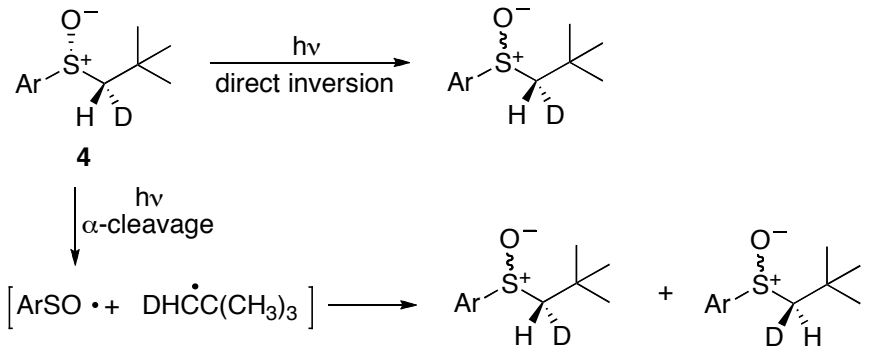

Scheme 1.2 Products expected from the direct inversion and α-cleavage mechanisms for sulfoxide stereomutation.[20]

Different mechanisms have been proposed for the photochemical racemization of enantiopure sulfoxides. One mechanism proposes homolytic α-cleavage followed by recombination, while another suggests direct inversion of the S-O center through geometric relaxation of an electronically excited state. In 2002, Vos *et al.* established strong evidence for direct inversion by showing that upon photolysis of **4**, stereomutation of only the sulfur center is predominant when there is an adjacent stereogenic center.[20] Scheme 1.2 shows the expected products for the direct inversion and α-cleavage products.

Deoxygenation. Direct photolysis of sulfoxides occasionally yields the

corresponding sulfide as a product. In specific cases where α-cleavage less favorable and easily reversible such as cyclic aryl systems, deoxygenation can be the major pathway.[22] Since this reaction was first discovered in the 1970s, several mechanisms have been proposed.[22-27] These are reviewed in section 2.2 of this dissertation.

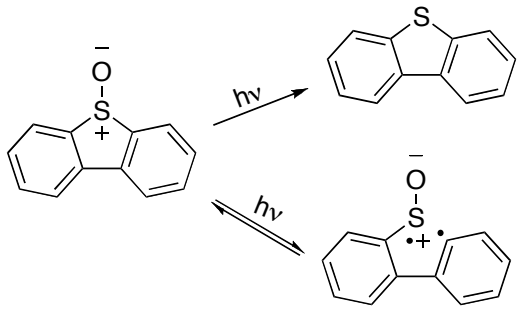

1.3 PHOTOCHEMICAL METHODS OF WATER AND AIR PURIFICATION

Pollution of air and water has been a pressing issue in our society for many years. Urban, military, and agricultural pollution significantly contribute to poor air and water quality.[28] Section 1.3.1 provides a very brief overview of common pollutants. Section 1.3.2 discusses available technology to either reduce or remove pollutants from water and air, particularly focusing on advanced oxidation processes (AOPs). This will lead into Sections 1.3.3 and 1.3.4, which introduce specific AOPs related to the research compiled in this dissertation.

1.3.1 Water and Air Pollution

Greenhouse gases, volatile organic compounds (VOCs), inorganic compounds and metals, particulate matter, commercial chemicals, pesticides and fertilizers, disinfectants, microbes, and radionuclides are several types of pollutants originating from urban and military sources.[28-31] Industrial emissions of greenhouse gases, such as N_2O, CH_4, CO_2, and fluorinated gases, are argued to contribute to global climate changes.[30] In addition, very poor air quality has plagued certain urban areas due to elevated levels of SO_2, NO_x, and VOCs.[31] Our rapidly developing industrial lifestyle also poses a considerable threat to the quality of our nation's drinking water. Of the contaminants found in drinking

water, organic compounds are more difficult to quantify and remove than inorganic pollutants due to the breadth of variety.[32] The abundance of various organic pollutants is reflected in the list of contaminants currently regulated by the EPA and recently recognized in the finalized third Contaminant Candidate List (CCL3) indicating the national dilemma at hand.[33,34]

Agricultural sources of water and air pollution include farm runoff, odor, fugitive dust, and animal waste. Fertilizers and pesticides drain from fields into rivers and lakes, and leach into groundwater, contaminating fresh water sources.[35] Certain pesticides can pose an obvious threat to water quality, and crop nutrients in fertilizers lead to elevated concentrations of nitrogen and phosphorus in water and soil. Ammonia emissions from animal waste are released to the air, where NH_3 can then suffer chemical transformations and contribute to the formation of particulate matter, increased nitrogen in soil and surface water, and changes in pH.[31]

Some species cannot tolerate the raised nitrogen and phosphorus content and are unable to survive, while other living things thrive in these conditions. For example, algal blooms only require a very small amount of essential nutrients, mainly nitrates and phosphates.[36] This amount is currently exceeded in many bodies of water due to farm runoff and emissions. As a result, an overgrowth of algae has led to a decrease of dissolved oxygen and sunlight that can reach the seafloor. These changes in habitat strain or kill many plants, fish, and invertebrates living in the water bodies affected by pollution.

1.3.2 Pollution Control Technology

Several methods have been employed to reduce or remove pollutants from air and water.[28,37,38] Methods of physical treatment include centrifugation, reverse osmosis, filtration and adsorption techniques using carbon or a resin. The downfall is that physical processes generally remove only solids or inorganic pollutants. In some cases, biological treatments are used, for instance activated sludge or waste lagoons, composting, and enzyme treatment. While biological methods are relatively inexpensive, they can be very slow relative to waste production. Chemical methods are also commonly used for treatment or recycling of waste, such as calcination, neutralization, oxidation, reduction,

sonochemical and photochemical techniques. The latter two are examples of advanced oxidation processes (AOPs) that often do not suffer from the same problems that conventional chemical processes face. For instance, conventional neutralization, oxidation, or reduction treatments are temperature dependent, often leave residues, and sometimes harmful or hazardous chemicals must be added (such as $KMnO_4$ for some oxidations). Many primary and secondary resources are available on general purification techniques, and it will not be further reviewed here.[28,31,35,38,39] Instead, the remainder of this section will introduce photo-initiated AOPs, as this background will facilitate the reader's comprehension of material discussed in subsequent chapters.

Advanced Photochemical Oxidation Processes (APOPs). APOPs have become popular techniques for remediation and disinfection as these methods promise several advantages over conventional water and air purification technologies.[38,39] For instance, most photochemical reactors or systems are very simple and can be easily designed for small or large scale applications. APOPs are also generally carried out under mild conditions, such as ambient temperature and pressure. In addition, the photochemical oxidation reactions generally occur very rapidly, particularly for gas phase applications, allowing for fast flow rates. Perhaps the greatest benefit of AOPs is the flexibility that they offer. Processes can be designed for specific applications by incorporating different reaction pathways through combinations of direct irradiation, oxidative auxiliaries, and photocatalysts.

The commonality between different APOPs is that oxidation occurs through reactions with reactive oxygen-containing species generated *in-situ* with short lifetimes, often the hydroxyl radical.[40] An array of effective APOPs are known and have been thoroughly reviewed, such as UV/H_2O_2, UV/O_3, UV direct photolysis, photo-Fenton reactions, and semiconductor photocatalysis.[38,41] Of these, several are routinely employed in laboratory and industrial technologies.[38,39,42] The following sections will focus on two popular APOPs used for purification, specifically TiO_2 photocatalysis for degradation of organic pollutants in water and UV-C irradiation in air for mitigation of odorous components.

1.3.3 TiO_2 photocatalysis

Several semiconductors have been studied as candidates for the photocatalytic degradation of organic pollutants, for instance TiO_2, FeO_3, ZnO, ZnS, and WO_3.[43,44] Of these, titanium dioxide has been considered the superior photocatalyst due to its superior thermal stability, low toxicity, low cost, and broad functionality.[43]

$$TiO_2 + h\nu \longrightarrow e^-_{cb} + h^+_{vb} \quad (1.1)$$

$$h^+_{vb} + H_2O_{ads} \longrightarrow HO^{\bullet}_{ads} + H^+ \quad (1.2)$$

$$e^-_{cb} + O_2 \longrightarrow O_2^{\bullet -} \quad (1.3)$$

$$O_2^{\bullet -} + H^+ \rightleftharpoons HO_2^{\bullet} \quad (1.4)$$

$$2\ HO_2^{\bullet} \longrightarrow H_2O_2 + O_2 \quad (1.5)$$

$$H_2O_2 + e^-_{cb} \longrightarrow HO^{\bullet} + HO^- \quad (1.6)$$

$$HO^{\bullet}_{ads} + M \longrightarrow [M\text{-}OH]^{\bullet +} \quad (1.7)$$

$$h^+_{vb} + M_{ads} \longrightarrow M^{\bullet +} \quad (1.8)$$

$$e^-_{cb} + M_{ads} \longrightarrow M^{\bullet -} \quad (1.9)$$

$$e^-_{cb} + h^+_{vb} \longrightarrow TiO_2 + \text{heat} \quad (1.10)$$

Upon absorption of a photon with sufficient energy, an electron is promoted from the semiconductor valence band to the conduction band (equation 1.1).[44] This creates a valence band hole (h^+_{vb}) and an available electron in the conduction band (e^-_{cb}). These photogenerated charges may then migrate to the surface where they can initiate a cascading series of reactions, provided they have the appropriate energy for oxidation or reduction (equations 1.2-1.10).[44] The h^+_{vb} can react with adsorbed water to form hydroxyl-like species and a proton (equation 1.2) and the e^-_{cb} can reduce molecular oxygen to yield superoxide (equation 1.3). Protonation of superoxide ultimately gives hydrogen peroxide, which can then react with an e^-_{cb} generating another source of hydroxyl radicals (equation 1.4-1.6). Hydroxyl radicals and related surface adsorbed

species can react with nearby organic molecules, known as hydroxyl-like oxidation ($HO\bullet_{ads}$) (equation 1.7). Surface adsorbed molecules can also be oxidized by directly transferring an electron to the h^{+}_{vb} of TiO_2, a process referred to as single electron transfer (SET) (equation 1.8). Using only O_2 and H_2O as reagents, organic molecules are completely degraded to CO_2 and appropriate inorganic ions (e.g., SO_4^{2-} or NO_3^{-}). An organic molecule could accept an electron from the e^{-}_{cb} (equation 1.9), but this process is minor compared to the reaction with the h^{+}_{vb} because the reducing power of the e^{-}_{cb} is often low and degradation pathways are generally oxidative.[43,44]

Equation 1.10 shows the final surface process, charge carrier recombination, which is simply a waste of light energy lost as heat. As a result, the quantum yield for oxidative pathways is only 5%.[41] Figure 1.1 provides a pictorial representation of TiO_2 mechanisms.

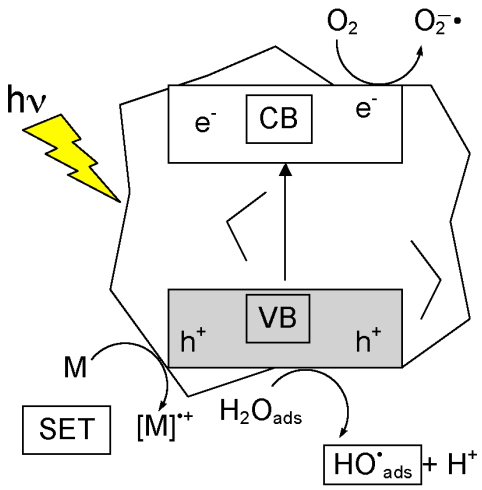

Figure 1.1 Illustration of the reaction pathways of the photogenerated charge-carriers formed upon irradiation of TiO_2.

The two oxidative pathways (SET and $HO\bullet_{ads}$) can often lead to different intermediate degradation products.[45] Several groups have studied select molecules and identified degradation products resulting from each pathway at low conversion, which has recently been reviewed by Jenks.[45] These well-studied molecules can then be used as organic probes to monitor and study the photocatalytic reactivity of TiO_2 photocatalysts.

This is a very critical aspect of TiO_2 photocatalysis because titania can be prepared with different crystal phases, particle sizes, shapes, and other modifications.

First generation TiO_2 photocatalysts. ***Pure TiO_2.*** TiO_2 has been prepared in different crystal phases for various photocatalysis applications.[46] TiO_2 nanoparticles have been applied in a spray for use as a thin film, typically in air purification, or simply left as loose powder suspended in a solution, which increases surface contact.[44,46] Initial studies on titanium dioxide determined conditions to optimize degradation rates, such as crystal phase and particle size.[44,47,48] TiO_2 has three phases: rutile, brookite, and anatase. Brookite has been considered to be photochemically inactive, and has not been well studied to date.[49-51] However, a recent study suggests that brookite may be very photochemically active, and is just difficult to obtain in a pure form.[52]

Early experimental and theoretical work was mostly done using rutile, which has a band gap of 3.0 eV (410 nm).[48] Rutile is the most thermally stable phase of TiO_2, photochemically active, and capable of utilizing an appreciable amount of sunlight. Yet, the rutile phase was found to be less effective in mediating the degradation of organic molecules than anatase (BG = 3.2 eV, 385 nm).[48,50] This has been attributed to fewer defects and tighter packing in the rutile crystal, which enhances recombination. Therefore, most recent work has focused on photocatalysis using anatase. The large bandgap allows for potentially broad functionality since the oxidizing power of the h^+_{vb} is necessarily higher, but unfortunately only allows for absorption of less than 10% of terrestrial solar radiation.[48]

Particle size has a direct effect on surface area and recombination.[53-55] A smaller particle size leads to a greater surface area per gram. While more surface area allows for more molecules to interact with the surface, it also increases recombination.[55] Particles in the nanometer range (5-100 nm) have been found to be the most effective for remediation.

Other approaches for improving the efficiency involved mixed catalysts. Multi-phase titania, such DeGussa's P25, which consists of about 75% anatase and 25% rutile, allows for a very slight red shift from the anatase band edge due the presence of rutile.

Gray has shown that the rutile phase absorbs near-visible light, and after charge separation, an electron is transferred to the anatase phase, supressing energy waste that occurs through recombination.[56,57] While P25 has a significantly increased quantum efficiency, it still does not take advantage of the visible portion of the solar spectrum, the cheapest light source available.

Noble metal deposition. Noble metals, particularly platinum and silver, have successfully improved the photocatalytic activity of TiO_2. These metals are present as pools on the surface and provide an electron trap, hindering the recombination process. Pt/TiO_2 has been particularly effective in the generation of H_2 as the metal provides a site of high electron availability.[48] Over time, the Pt is also oxidized by oxygen in the air to form PtO_2, which then reacts with the TiO_2 itself, leading to deactivation of the photocatalyst. Consequently, Pt/TiO_2 and other noble metal derivatives have not been cost-effective for use at a commercial level despite the enhanced reactivity.[58]

Second generation TiO_2 photocatalysts. Doping TiO_2 with metals and non-metals has been a popular method to improve solar absorption of TiO_2.[46] Addition of a dopant atom, either interstitially or through substitution, creates structural distortions and changes in chemical composition. These changes affect the electronic structure and as a result alter the optical response of the photocatalyst.[46]

Transistion metal doping. Incorporating transistion metal impuritites into the TiO_2 lattice extends the absorbance into the visible region in addition to providing an electron trap. The red shift is attributed to the formation new states in the band gap that act as donor/acceptor levels.[58] Choi reported on the photocatalytic activity of several metals used to modify titania nanoparticles.[59] The authors found that (1) increased photocatalytic activity is only observed in transition metals with open shells; and (2) the degree of enhancement was very sensitive to dopant concentration and distribution. In fact, contradictory results have been reported on the effect of vanadium doping.[54,59] Substitutional V^{4+} was shown to positively effect photocatalytic reactivity for both

oxidation and reduction, but further mechanistic investigations demonstrated that V^{4+} primarily acts as a recombination center. Enhancement of charge-carrier recombination was also observed for other transistion metals (Co^{3+}, Al^{3+}, and Cr^{3+}).[46,48]

Non-metal doping. In more recent years, attention has turned to doping with main group elements, particularly N, S, and C. In 2001, Asahi reported that nitrogen doping induced a shift of the valence band, therefore increasing visible light absorption.[60] Experimental and theoretical work has established that nitrogen doping actually introduces localized states within the bandgap just above the valence band.[61-66] The origin of visible absorbance has been attributed to stabilization interactions with oxygen vacancies induced by nitrogen doping.[67,68]

Nitrogen-doped TiO_2. Nitrogen modification to TiO_2 has received the most attention of any of the main group elements. Various methods have been developed to prepare N-doped anatase: (1) N_2/Ar sputtering (ion implantation);[60,69] (2) oxidative annealing of TiN;[70,71] (3) annealing under NH_3 or urea;[62,66,70,72-74] and (4) sol-gel methods for direct nitridation through controlled hydrolysis of $Ti(OiPr)_4$ or $TiCl_4$ in the presence of a nitrogenous source (ammonium salts, amines, hydrazine, urea).[65,67,74-78] Other preparations attempted to increase uniformity in the material through high pressure solvothermal reactions.[79,80] Burda reported a reflux synthetic route that allows control over the concentration of nitrogen.[81]

Information about the amount of dopant and bonding environment is obtained through surface techniques, frequently photoelectron spectroscopy (XPS). The N(1s) chemical shift assignments in XPS for N-doped TiO_2 has been debated. In general, a peak at 396-397 eV indicates the presence of a Ti-N bond (substitution for O) and a peak at *ca.* 399 eV can be assigned to a generic interstitial N-H species.[50,82] Burda and Gole have reported that material synthesized in their laboratories displayed XPS N(1s) features at 396.5 and 401 eV, which they attribute to a Ti-N and Ti-O-N species, respectively.[75,76] Reyes-Garcia *et al.* used solid-state NMR to characterize ^{15}N-doped TiO_2 prepared from direct nitridation of Degussa P25 or from $TiCl_4$ and $^{15}NH_4Cl$ or ^{15}N-urea.[74] The authors

obtained chemical shift data characteristic of several NH_x species (Figure 1.2) that became more highly oxidized with increasing calcination temperature, however XPS was not done, leaving the issue of concrete XPS assignment unresolved.

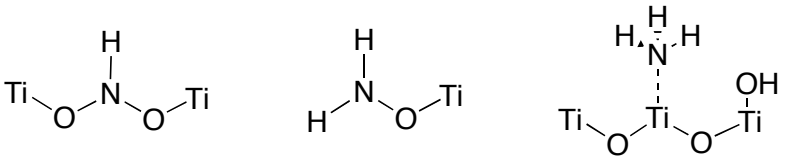

Figure 1.2 Proposed structures of N-doped TiO_2 characterized by NMR reproduced from reference [74].

A few studies have set out to establish which nitrogen species was responsible for inducing the changes resulting in visible absorption.[50,67,70,83,84] One report attributes the improved visible light activity to substitutional doping (Ti-N),[60] while another study claims the activating dopant is the interstitial N-species exhibiting an XPS chemical shift of 399.6 eV.[72] Diwald and coworkers found that nitrogen doping of rutile by ion implantaion actually resulted in an *decrease* of the adsorption edge.[69] This preparation method produces a doped material (Ti-N) displaying an XPS N(1s) binding energy of 396.5, which suggests substitutional doping (Ti-N) is not solely responsible for inducing the red shift. Computational work by DiValentin *et al.* agrees with the experimentally observed difference in photothreshold energy of N-doped anatase and rutile.[85]

Experiments to probe the degradative activity were typically carried out using small organic molecules and dyes.[60,62,75,76] While researchers were able to demonstrate cases where N-TiO_2 could degrade specific molecules, detailed information of the actual organic oxidation mechanism(s) was not always available. In particular, methylene blue has been a popular choice for an organic probe molecule.[60,75,76] However, dyes are not the best choice for gaining insight on the oxidation chemistry since they are also very susceptible to reductive degradation pathways.[86]

Carbon-doped TiO_2. Several methods have been used to prepare carbon-doped catalysts.[87-95] Among them is treatment of titanium carbide by sputtering or heating in an

oxidative atmosphere. Khan *et al.* reported that flame pyrolysis of Ti metal with natural gas produced a dark gray material.[95] The color was attributed to carbon impurities remaining in the material, which was capable of splitting water with visible light. Simple sol-gel techniques have also been used to produce C-doped titania. Lettman *et al.* reported a coke-containing catalyst prepared through acid-catalyzed condensation of various titanium alkoxide precursors at low temperature.[88] Ohno generated carbonate species within the TiO_2 using urea as a carbon source.[96] It was demonstrated by Sakthivel and Kisch that even tetrabutyl ammonium hydroxide could end up leaving carbon in the titania prepared by sol-gel methods.[89,97] Xu *et al*. prepared carbon-doped titania powder and films using glucose as a source of carbon.[98,99]

Very promising structural information has been reported based on XPS results. It was found that oxidation of TiC to carbon-doped TiO_2 yields materials in which reduced carbon species remain from some of the Ti-C bonds being preserved through incomplete oxidation.[61,91,100] In contrast, Xu *et al.* used IR and powder diffraction to demonstrate the absence of Ti-C bonds in their materials.[98,99] Others report carbonate; however, many reports are ambiguous on the presence of coke.[93,96]

The C(1s) peak observed in XP spectra around 284.8 eV arises from adventitious C-H and C-C species present on material surfaces and from the spectrometer itself.[82] In fact, the C(1s) peak is used for spectral calibration. Any true condensed carbon on the surface of the TiO_2 powder would overlap in this region. This presents an analytical short-coming as the actual source and quantity of carbon species of this nature cannot be accurately identified. Chapter 4 includes more information on carbon doping of TiO_2 and the use of solid-state NMR to fully characterize the carbon species.

Sulfur-doped TiO_2. There are two common synthetic routes in the literature to prepare S-TiO_2: (1) oxidation of TiS_2 (under air[101] or hydrothermally in a high pressure autoclave[102]) and (2) sol-gel methods which involve addition of an alcoholic solution of a titanium (IV) alkoxide precursor to thiourea dissolved in alcohol.[63,103,104] Oxidation of TiS_2 causes S atoms to be slowly replaced by O atoms resulting in TiO_2 with residual S impurities. This method produces titania doped with S^{2-} (substitution for O).[101] Sol-gel

methods typically lead to substitution of a Ti atom with an S^{4+} atom upon annealing as indicated by XPS results.[103]

The effects of the two types of preparation have been directly compared.[102,105] The first study showed that oxidation of TiS_2 resulted in micrometer-size particles with S^{2-} impurities localized within the bulk of the material, whereas sol-gel preparations with thiourea gave nanometer particles with S^{4+} evenly distributed throughout the titania.[105] The S^{4+}-TiO_2 showed increased visible absorbance and good charge-carrier mobility based on its reactivity with adsorbed gases under visible light, but it was unable to oxidize water, even under UV light, which was suggested to be a result of trap states near the surface. S^{2-}-TiO_2 displayed similar reactivity to that of undoped TiO_2 under UV light, but showed limited charge-carrier mobility to adsorbed gases and failed as a photocatalyst when 532 nm was used as the excitation source due to the large particle size and the central location of impurities. The second study, which prepared nanometer S^{2-}-TiO_2, observed enhanced photocatalytic degradation of 4-chlorophenol under >400 nm irradiation when compared to S^{4+}-TiO_2.[102] This was thought to be a result of increased charge-carrier mobility attributable to the particle size reduction of the S^{2-}-TiO_2.[102] Reports have shown that S^{4+}-TiO_2 is capable of degrading methylene blue, hydroxylating adamantane, and oxidizing isopropanol,[103] but is unable to oxidize 4-(methylthio)phenyl methanol.[63] The discrepancies over the functionality of S^{4+}-TiO_2 are discussed further in section 5.5.

Nonmetallic heavy atom dopants. Larger main group elements, such as iodine, have been reported to enhance photocatalytic activity.[106-110] Although there are relatively few publications currently available on iodine doping, different types of iodine have been identified in modified titana. Functioning redox cycles have been successful for TiO_2 modified by I_2 encapsulation as well as substitutional I doping.[110] Recent theoretical work also suggests that I doping (I^{5+}) could create promising changes to the band structure.[111] This was in agreement with experimental reports that observed a significant increase in the phocatalytic activity of I-TiO_2.[106-108,110] However, Majima and coworkers found that while charge-carriers were sufficiently produced under both UV and visible

light, hole attack was not seen in the presence of a quencher.[106] This indicates the h^+ was being trapped at the iodine centers. In addition, XPS assignments for iodine oxidation states differ from one report to another, particularly between I^{5+} and I^{7+}.[107,108]

Zhang *et al.* prepared an SeO_2/TiO_2 composite that exhibits a blue shift for the annealed material, but after chemical reduction of the Se, the desired red shift was observed.[109] The authors attribute the visible absorbance to the presence of Se^0, which can absorb visible light and participate in an oxidation/reduction cycle. Se-modification is discussed further in Chapter 6.

1.3.4 UV-initiated remediation of air pollutants

Many compounds that contribute to what is simply categorized as "odor" absorb wavelengths of <300 nm light.[39] Thus, the molecular components can be converted to odorless compounds through photochemical oxidation initiated by inexpensive, quartz-walled low-pressure mercury lamps, which have a major emission at 254 nm. Recycling and food processing industries currently use UV irradiation for air purification. Exhaust is blown through a filter to remove small particulates and aerosols, followed by passing through an irradiation chamber, and then released to the air. In these cases, emissions have been reduced by as much as 96%.[39]

Commercial swine farms, another odor-producing industry, emit NH_3, H_2S, VOCs, and other compounds at levels that have become a national environmental concern.[31,35,112] Ammonia has a strong, pungent odor that is easily detectable at 50 ppm by the human nose, which creates an imposition on neighbors, both residential and commercial. UV-technology would be ideal for the mitigation of ammonia. Lamps must be prepared with quartz tubing that will allow the minor 185 nm Hg emission to pass, which is a very small amount relative to the 254 nm line. Upon exposure to 185 nm light, molecular oxygen in the air will absorb a photon and produce reactive species that may then react with ammonia and potentially convert NH_3 to something less noxious. In Chapter 7, the possibility to use UV irradiation for abatement of NH_3 from farm exhaust is examined.

1.4 REFERENCES

(1) Hiroi, K.; Sone, T. *Current Organic Synthesis* **2008**, *5*, 305-320.

(2) Ruano, J. L. G.; De la Plata, B. C. *Topics in Current Chemistry* **1999**, *204*, 1-126.

(3) Carreno, M. C. *Chemical Reviews (Washington, D. C.)* **1995**, *95*, 1717-60.

(4) Labat, Y. *Phosphorus, Sulfur and Silicon and the Related Elements* **1993**, *74*, 173-94.

(5) Kalir, A.; Kalir, H. H. *Chemistry of Sulphur-Containing Functional Groups* **1993**, 957-73.

(6) Legros, J.; Dehli, J. R.; Bolm, C. *Advanced Synthesis & Catalysis* **2005**, *347*, 19-31.

(7) McCulla, R. D.; Jenks, W. S. *Journal of the American Chemical Society* **2004**, *126*, 16058-16065.

(8) Yamazaki, Y.; Tsuchiya, T.; Hasegawa, T. *Bulletin of the Chemical Society of Japan* **2003**, *76*, 201-202.

(9) Jenks, W. S. *Spectrum (Bowling Green, OH, United States)* **2001**, *14*, 1, 3-7.

(10) Jenks, W. S.; Gregory, D. D.; Guo, Y.; Lee, W.; Tetzlaff, T. *Molecular and Supramolecular Photochemistry* **1997**, *1*, 1-56.

(11) Chanon, M.; Samat, A. **1988**, 1047-80.

(12) Still, I. W. J. **1988**, 873-87.

(13) Mislow, K. *Record of Chemical Progress* **1967**, *28*, 217-40.

(14) Loening, K. L. In *Sulfur in Organic and Inorganic Chemistry*; Senning, A., Ed.; Dekker: New York, 1972; Vol. 3, p 339-354.

(15) *Information Bulletin - International Union of Pure and Applied Chemistry, Appendices on Tentative Nomenclature, Symbols, Units, and Standards* **1973**, *31*, 149 pp.

(16) Panico, R.; Powell, W. H.; Richer, J. C.; Editors *A Guide to IUPAC Nomenclature of Organic Compounds: Recomendations 1993. International Union of Pure and Applied Chemistry (IUPAC); Organic Chemistry Division, Commision on Nomenclature of Organic Chemistry (III.1)*, 1993.

(17) Dobado, J. A.; Martinez-Garcia, H.; Molina; Sundberg, M. R. *Journal of the American Chemical Society* **1999**, *121*, 3156-3164.

(18) Guo, Y.; Jenks, W. S. *Journal of Organic Chemistry* **1995**, *60*, 5480-5486.

(19) Cubbage, J. W.; Jenks, W. S. *The Journal of Physical Chemistry A* **2001**, *105*, 10588-10595.

(20) Vos, B. W.; Jenks, W. S. *Journal of the American Chemical Society* **2002**, *124*, 2544-2547.

(21) Guo, Y.; Jenks, W. S. *Journal of Organic Chemistry* **1997**, *62*, 857-864.

(22) Gregory, D. D.; Wan, Z.; Jenks, W. S. *Journal of the American Chemical Society* **1997**, *119*, 94-102.

(23) Gurria, G. M.; Posner, G. H. *J. Org. Chem.* **1973**, *38*, 2419-2420.

(24) Shelton, J. R.; Davis, K. E. *Int. J. Sulfur Chem.* **1973**, *8*, 217-228.

(25) Khait, I.; Luedersdorf, R.; Muszkat, K. A.; Praefcke, K. *Journal of the Chemical Society, Perkin Transactions 2: Physical Organic Chemistry (1972-1999)* **1981**, 1417-29.

(26) Lüdersdorf, R.; Khait, I.; Muszkat, K. A.; Praefcke, K.; Margaretha, P. *Phosphorus and Sulfur and the Related Elements* **1981**, *12*, 37-54.

(27) Wan, Z.; Jenks, W. S. *J. Am. Chem. Soc.* **1995**, *117*, 2667-2668.

(28) *The Handbook of Water Purification*; Lorch, W., Ed.; McGraw-Hill: London, 1981.

(29) Patterson, G. G.; Focazio, M. J. *Contaminants and Drinking-Water Sources in 2001: Recent Findings of the U.S. Geological Survey*, 2001.

(30) USEPA. http://www.epa.gov/climatechange/emissions/index.html.

(31) *Emissions of Air Pollutants*; Friedrich, R.; Reis, S., Eds.; Springer-Verlag: Berlin, 2004.

(32) Benfenati, E.; Porazzi, E.; Martinez, M. P. In *The Handbook of Environmental Chemistry*; Springer-Verlag: Berlin, 2004; Vol. 5, Part I, p 71-97.

(33) USEPA. http://www.epa.gov/safewater/contaminants/index.html.

(34) USEPA. *Federal Register* **2009**, *74*, 51850-51862.

(35) *Animal Agriculture and the Environment*; Rice, J. M.; Caldwell, D. F.; Humenik, F. J., Eds.; American Society of Agricultural and Biological Engineers: St. Joseph, MI, 2006.

(36) Bricker, S. B.; Longstaff, B.; Dennison, W.; Jones, A.; Boicourt, K.; Wicks, C.; Woerner, J. *Harmful Algae* **2008**, *8*, 21-32.

(37) Dupont, R. R.; Theodore, L.; Ganesan, K. *Pollution Prevention: The Waste Management Approach for the 21st Century*; CRC Press LLC: Boca Raton, FL, 2000.

(38) *Chemical Degradation Methods for Wastes and Pollutants*; Tarr, M. A., Ed.; Marcel Dekker, Inc.: New York, NY, 2003.

(39) Oppenlander, T. *Photochemical Purification of Water and Air*; WILEY-VCH Verlag: Weinheim, Germany, 2003.

(40) Glaze, W. H.; Kang, J. W.; Chapin, D. H. *Ozone Science and Engineering* **1987**, *9*, 335-342.

(41) Legrini, O.; Oliveros, E.; Braun, A. M. *Chem. Rev.* **1993**, *93*, 671-698.

(42) USEPA. *Handbook: Advanced Photochemical Oxidation Processes*, 1999.

(43) Fox, M. A.; Dulay, M. T. *Chem. Rev.* **1993**, *93*, 341-357.

(44) Hoffmann, M. R.; Martin, S. T.; Choi, W.; Bahnemann, D. W. *Chem. Rev.* **1995**, *95*, 69-96.

(45) Jenks, W. S. In *Environmental Catalysis*; Grassian, V. H., Ed.; Taylor & Francis Boca Raton, 2005, p 307-346.

(46) Chen, X.; Mao, S. S. *Chemical Reviews* **2007**, *107*, 2891-2959.

(47) Wang, C.-C.; Ying, J. Y. *Chemistry of Materials* **1999**, *11*, 3113-3120.

(48) Linsebigler, A. L.; Lu, G.; Yates, J. T., Jr. *Chem. Rev.* **1995**, *95*, 735-758.

(49) Mills, A.; Davies, R. H.; Worsley, D. *Chemical Society Reviews* **1993**, *22*, 417-25.

(50) Thompson, T. L.; Yates, J. T., Jr. *Chemical Reviews (Washington, DC, United States)* **2006**, *106*, 4428-4453.

(51) Li, G.; Gray, K. A. *Chemistry of Materials* **2007**, *19*, 1143-1146.

(52) Li, J.-G.; Ishigaki, T.; Sun, X. *The Journal of Physical Chemistry C* **2007**, *111*, 4969-4976.

(53) Bahnemann, D. W.; Hilgendorff, M.; Memming, R. *Journal of Physical Chemistry B* **1997**, *101*, 4265-4275.

(54) Martin, S. T.; Morrison, C. L.; Hoffmann, M. R. *Journal of Physical Chemistry* **1994**, *98*, 13695-704.

(55) Rothenberger, G.; Moser, J.; Graetzel, M.; Serpone, N.; Sharma, D. K. *Journal of the American Chemical Society* **1985**, *107*, 8054-9.

(56) Hurum, D. C.; Gray, K. A.; Rajh, T.; Thurnauer, M. C. *Journal of Physical Chemistry B* **2005**, *109*, 5388.

(57) Hurum, D. C.; Gray, K. A.; Rajh, T.; Thurnauer, M. C. *Journal of Physical Chemistry B* **2005**, *109*, 977-980.

(58) Nowotny, M. K.; Sheppard, L. R.; Bak, T.; Nowotny, J. *Journal of Physical Chemistry C* **2008**, *112*, 5275-5300.

(59) Choi, W.; Termin, A.; Hoffmann, M. R. *The Journal of Physical Chemistry* **1994**, *98*, 13669-13679.

(60) Asahi, R.; Morikawa, T.; Ohwaki, T.; Aoki, K.; Taga, Y. *Science (Washington, DC, United States)* **2001**, *293*, 269-271.

(61) Liu, H.; Imanishi, A.; Nakato, Y. *Journal of Physical Chemistry C* **2007**, *111*, 8603-8610.

(62) Tachikawa, T.; Takai, Y.; Tojo, S.; Fujitsuka, M.; Irie, H.; Hashimoto, K.; Majima, T. *Journal of Physical Chemistry B* **2006**, *110*, 13158-13165.

(63) Tachikawa, T.; Tojo, S.; Kawai, K.; Endo, M.; Fujitsuka, M.; Ohno, T.; Nishijima, K.; Miyamoto, Z.; Majima, T. *Journal of Physical Chemistry B* **2004**, *108*, 19299-19306.

(64) Sakthivel, S.; Janczarek, M.; Kisch, H. *Journal of Physical Chemistry B* **2004**, *108*, 19384-19387.

(65) Sato, S.; Nakamura, R.; Abe, S. *Applied Catalysis, A: General* **2005**, *284*, 131-137.

(66) Irie, H.; Watanabe, Y.; Hashimoto, K. *Journal of Physical Chemistry B* **2003**, *107*, 5483-5486.

(67) Di Valentin, C.; Finazzi, E.; Pacchioni, G.; Selloni, A.; Livraghi, S.; Paganini, M. C.; Giamello, E. *Chemical Physics* **2007**, *339*, 44-56.

(68) Emeline, A. V.; Sheremetyeva, N. V.; Khomchenko, N. V.; Ryabchuk, V. K.; Serpone, N. *Journal of Physical Chemistry C* **2007**, *111*, 11456-11462.

(69) Diwald, O.; Thompson, T. L.; Goralski, E. G.; Walck, S. D.; Yates, J. T., Jr. *Journal of Physical Chemistry B* **2004**, *108*, 52-57.

(70) Balcerski, W.; Ryu, S. Y.; Hoffmann, M. R. *Journal of Physical Chemistry C* **2007**, *111*, 15357-15362.

(71) Morikawa, T.; Asahi, R.; Ohwaki, T.; Aoki, K.; Taga, Y. *Japanese Journal of Applied Physics, Part 2: Letters* **2001**, *40*, L561-L563.

(72) Diwald, O.; Thompson, T. L.; Zubkov, T.; Goralski, E. G.; Walck, S. D.; Yates, J. T., Jr. *Journal of Physical Chemistry B* **2004**, *108*, 6004-6008.

(73) Mrowetz, M.; Balcerski, W.; Colussi, A. J.; Hoffmann, M. R. *Journal of Physical Chemistry B* **2004**, *108*, 17269-17273.

(74) Reyes-Garcia, E. A.; Sun, Y.; Reyes-Gil, K.; Raftery, D. *Journal of Physical Chemistry C* **2007**, *111*, 2738-2748.

(75) Chen, X.; Lou, Y.; Samia, A. C. S.; Burda, C.; Gole, J. L. *Advanced Functional Materials* **2005**, *15*, 41-49.

(76) Gole, J. L.; Stout, J. D.; Burda, C.; Lou, Y.; Chen, X. *Journal of Physical Chemistry B* **2004**, *108*, 1230-1240.

(77) Sakthivel, S.; Kisch, H. *ChemPhysChem* **2003**, *4*, 487-490.

(78) Sato, S. *Chemical Physics Letters* **1986**, *123*, 126-8.

(79) Huang, D.-G.; Liao, S.-J.; Liu, J.-M.; Dang, Z.; Petrik, L. *Journal of Photochemistry and Photobiology, A: Chemistry* **2006**, *184*, 282-288.

(80) Yin, S.; Ihara, K.; Aita, Y.; Komatsu, M.; Sato, T. *Journal of Photochemistry and Photobiology, A: Chemistry* **2006**, *179*, 105-114.

(81) Qiu, X.; Burda, C. *Chemical Physics* **2007**, *339*, 1-10.

(82) Moulder, J. F.; Stickle, W. F.; Sobol, P. E.; Bomben, K. D. *Handbook of X-Ray Photoelectron Spectroscopy*; Perkin-Elmer Corporation (Physical Electronics): Eden Prairie, MN, 1992.

(83) Yates, H. M.; Nolan, M. G.; Sheel, D. W.; Pemble, M. E. *Journal of Photochemistry and Photobiology, A: Chemistry* **2006**, *179*, 213-223.

(84) Di Valentin, C.; Pacchioni, G.; Selloni, A.; Livraghi, S.; Giamello, E. *Journal of Physical Chemistry B* **2005**, *109*, 11414-11419.

(85) Di Valentin, C.; Pacchioni, G.; Selloni, A. *Physical Review B: Condensed Matter and Materials Physics* **2004**, *70*, 085116/1-085116/4.

(86) Ohno, T.; Tsubota, T.; Nishijima, K.; Miyamoto, Z. *Chemistry Letters* **2004**, *33*, 750-751.

(87) Ohno, T.; Tsubota, T.; Toyofuku, M.; Inaba, R. *Catal. Lett.* **2004**, *98*, 255-258.

(88) Lettmann, C.; Hildenbrand, K.; Kisch, H.; Macyk, W.; Maier, W. F. *Applied Catalysis, B: Environmental* **2001**, *32*, 215-227.

(89) Sakthivel, S.; Kisch, H. *Angewandte Chemie International Edition* **2003**, *42*, 4908-4911.

(90) Irie, H.; Watanabe, Y.; Hashimoto, K. *Chemistry Letters* **2003**, *32*, 772-773.

(91) Choi, Y.; Umebayashi, T.; Yoshikawa, M. *J. Mater. Sci.* **2004**, *39*, 1837-1839.

(92) Ren, W.; Ai, Z.; Jia, F.; Zhang, L.; Fan, X.; Zou, Z. *Applied Catalysis, B: Environmental* **2007**, *69*, 138-144.

(93) Wang, X.; Meng, S.; Zhang, X.; Wang, H.; Zhong, W.; Du, Q. *Chemical Physics Letters* **2007**, *444*, 292-296.

(94) Li, Y.; Hwang, D.-S.; Lee, N. H.; Kim, S.-J. *Chemical Physics Letters* **2005**, *404*, 25-29.

(95) Khan, S. U. M.; Al-Shahry, M.; Ingler, W. B., Jr. *Science (Washington, DC)* **2002**, *297*, 2243-2245.

(96) Ohno, T.; Tsubota, T.; Nishijima, K.; Miyamoto, Z. *Chemistry Letters* **2004**, *33*, 750-751.

(97) Sakthivel, S.; Neppolian, B.; Shankar, M. V.; Arabindoo, B.; Palanichamy, M.; Murugesan, V. *Solar Energy Materials and Solar Cells* **2003**, *77*, 65-82.

(98) Xu, C.; Killmeyer, R.; Gray, M. L.; Khan, S. U. M. *Applied Catalysis, B: Environmental* **2006**, *64*, 312-317.

(99) Xu, C.; Khan, S. U. M. *Electrochemical and Solid-State Letters* **2007**, *10*, B56-B59.

(100) Irie, H.; Watanabe, Y.; Hashimoto, K. *Chemistry Letters* **2003**, *32*, 772-773.

(101) Umebayashi, T.; Yamaki, T.; Itoh, H.; Asai, K. *Applied Physics Letters* **2002**,

81, 454-456.

(102) Ho, W.; Yu, J. C.; Lee, S. *Journal of Solid State Chemistry* **2006**, *179*, 1171-1176.

(103) Ohno, T.; Akiyoshi, M.; Umebayashi, T.; Asai, K.; Mitsui, T.; Matsumura, M. *Applied Catalysis, A: General* **2004**, *265*, 115-121.

(104) Ohno, T.; Mitsui, T.; Matsumura, M. *Chemistry Letters* **2003**, *32*, 364-365.

(105) Takeshita, K.; Yamakata, A.; Ishibashi, T.-A.; Onishi, H.; Nishijima, K.; Ohno, T. *Journal of Photochemistry and Photobiology, A: Chemistry* **2006**, *177*, 269-275.

(106) Tojo, S.; Tachikawa, T.; Fujitsuka, M.; Majima, T. *Journal of Physical Chemistry C* **2008**, *112*, 14948-14954.

(107) Su, W.; Zhang, Y.; Li, Z.; Wu, L.; Wang, X.; Li, J.; Fu, X. *Langmuir* **2008**, *24*, 3422-3428.

(108) Hong, X.; Wang, Z.; Cai, W.; Lu, F.; Zhang, J.; Yang, Y.; Ma, N.; Liu, Y. *Chemistry of Materials* **2005**, *17*, 1548-1552.

(109) Zhang, S.-Y.; Chen, X.-J.; Tian, Y.-P.; Jin, B.-K.; Yang, J.-X. *Journal of Crystal Growth* **2007**, *304*, 42-46.

(110) Usseglio, S.; Damin, A.; Scarano, D.; Bordiga, S.; Zecchina, A.; Lamberti, C. *Journal of the American Chemical Society* **2007**, *129*, 2822-2828.

(111) Yang, K.; Dai, Y.; Huang, B.; Whangbo, M.-H. *Chemistry of Materials* **2008**, *20*, 6528-6534.

(112) USEPA. http://www.epa.gov/ttn/chief/net/2002inventory.html, 2005.

CHAPTER 2

Deoxygenation of dibenzothiophene-*S*-oxide and dibenzoselenophene-*Se*-oxide: A comparison of direct and sensitized photolysis

Reproduced from *Journal of Photochemistry and Photobiology A: Chemistry* **2008**, 198(1), 45, with permission from Elsevier.

Erin M. Rockafellow, Ryan D. McCulla, and William S. Jenks*
Department of Chemistry, Iowa State University, Ames, IA 50011-3111

2.1 ABSTRACT

Photolysis of dibenzothiophene-*S*-oxide (DBTO) and dibenzoselenophene-*Se*-oxide (DBSeO) was examined under direct and sensitized conditions. Quantum yield and solvent oxidation data are used to separate the direct irradiation conditions, plus benzophenone-sensitized and anthraquinone-sensitized irradiation of DBSeO, into one mechanistic class. Acridine-sensitized photolysis of DBSeO and triplet sensizitization of DBTO result in deoxygenation, but go by different mechanisms than the direct irradations. The two sensitized cases that appear mechanistically linked to direct DBTO photolysis are ones in which the spectroscopic triplet of DBSeO, which is very likely of comparable energy to the Se—O BDE, is populated by triplet energy transfer.

2.2 INTRODUCTION

Three primary processes are observed in unimolecular sulfoxide photochemistry: photochemical stereomutation of the S-O bond,[1-8] α-cleavage,[9-14] and deoxygenation.[14-22] Although the last of these is typically a minor process, it gives high chemical yields some cases, notably derivatives of dibenzothiophene-*S*-oxide (DBTO). An analogous process, with higher quantum yield, is observed for the selenium analog, dibenzoselenophene-*Se*-oxide (DBSeO).[23] Deoxygenation is perhaps the most interesting photochemical reaction of sulfoxides, in that the S-O bond is much stronger than either of the C-S bonds, and the pathway by which loss of the oxygen atom occurs has been a matter of study since the

reaction was first discovered in the 1970s.[1]

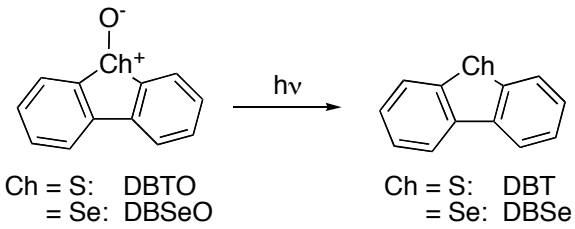

Several mechanisms for photodeoxygenation of sulfoxides have been proposed, but most can now be rejected.[17,20] An early postulated mechanism proceded by the formation of a dimer: a triplet sulfoxide was trapped by ground state sulfoxide, leading ultimately to the generation of two sulfide molecules and molecular oxygen. Cross-labeling experiments, low temperature results, and ^{18}O labeling now contradict this. Another proposed mechanism based on O-atom transfer by a sulfinyl radical (RSO•) subsequent to α-cleavage is energetically infeasible.[24] A mechanism based on hydrogen abstraction by the oxygen atom to form the unstable 9-electron sulfuranyl radical can be eliminated because the reaction proceeds in solvents entirely lacking hydrogen atoms.[17]

We proposed that the deoxygenation of certain aromatic sulfoxides on direct photolysis proceeds by unimolecular cleavage of the S-O bond to form $O(^3P)$.[17] (We acknowledge that there are additional bimolecular pathways in certain circumstances, such as carbazole or aniline sensitization.)[25-27] Perhaps the strongest positive evidence for this mechanism is the pattern of solvent oxidation observed on photolysis of dibenzothiophene-*S*-oxide (DBTO), as illustrated in Scheme 2.1.[16,17,20] Several subsequent investigations have been carried out to test this assertion, and though none has produced direct detection of atomic oxygen, all are consistent with its formation.[19,28,29] Recently, we have also shown that a common intermediate is formed on direct photolysis of DBTO and DBSeO.[23] Additionally, we have directly detected the nitrene formed on photolysis of the *N*-benzoyl analog of DBTO, *N*-benzoyldibenzothiophene sulfilimine,[30] and have provided indirect evidence of carbene formation from the *S,C*-sulfonium ylides derived from dimethylmalonate and DBT.[31]

Scheme 2.1

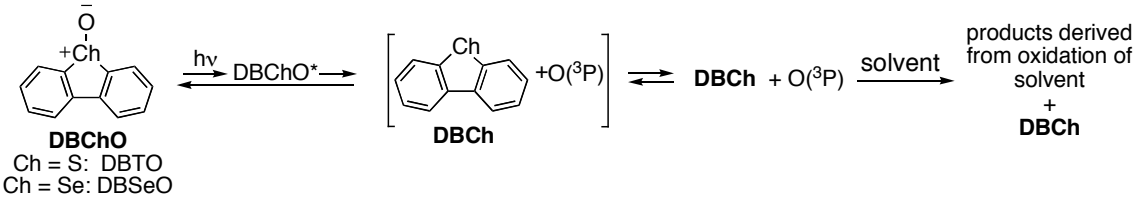

Nonetheless, there is an important aspect of this proposed mechanism of sulfoxide deoxygenation that remains unresolved. As noted previously for DBTO,[32,33] there is not sufficient energy in the spectroscopic triplet state of DBTO (ca. 61 kcal/mol) for cleavage (ca. 76 kcal/mol). In our previous work, we simply avoided this issue entirely by carrying out direct irradiation only, and stated that the reaction that produced O(^{3}P) could not proceed through the spectroscopic triplet of DBTO. Here, we address the issue of sensitized deoxygenation directly, in large part because it can be an important test of the unimolecular cleavage mechanism. Data showing that triplet sensitization provides the same oxidizing intermediate as direct photolysis would cast very strong doubt on the proposed direct photolysis mechanism. Here we report a study, using literature-established sensitizers, to test just that. To the best of our knowledge, there are no previous reports examining the sensitized photochemistry of selenoxides, and only a few studies have been reported on their direct photolysis.[23,34-36]

The earliest studies on deoxygenation were done before the relevant triplet energies were all known.[14,15] Due to the now-known energies of the relevant triplet states, it seems likely that at least many of these sensitized reactions occurred through electron transfer or solvent-mediated chain mechanisms, because triplet energy transfer is not plausible. Again, evidence differentiating such a mechanism from that of direct photolysis is required for the O(^{3}P) mechanism to be correct.

Recently, de Lucas and coworkers published a transient absorption study on the benzophenone sensitized photolysis of DBTO.[37] They were able to detect a 370 nm-absorbing transient and ascribed it to a short-lived (143 ns) triplet state of DBTO. Similarly, they observed a somewhat longer-lived transient they associated with the triplet state of the benzannulated analog benzo[*b*]naptho[2,1,d]thiophene-11-oxide (BNTO) originally investigated by Greer.[20] In each case, they concurred with previous

work that the spectroscopic triplet was not sufficiently energetic for S-O bond scission, but any evidence regarding the similarity or contrast between the direct and sensitized deoxygenation mechanism was indirect.

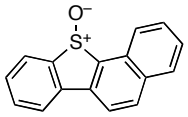

BNTO

Even the direct photolysis of DBTO requires an unusual explanation for the apparently spin forbidden reaction of producing $O(^3P)$ without going through T_1. We have previously proposed that intersystem crossing from ^{1}DBTO* could accompany the bond stretching motion. However, the wavelength dependence reported previously would also be consistent with a mechanism involving a non-spectroscopic T_2 state that lies near the S_1 state in energy.[17]

For this study comparing direct and sensitized deoxygenation, we take a two-fold approach. The first is the straightforward measurement of rate constants and quantum yields. The second is a product-based approach in which we characterize the oxidation products formed *as a result of* the deoxygenation, i.e., what happens to the oxygen atom that is lost from DBTO or DBSeO, regardless of the mechanism. With many solvents (or added reactive traps), oxygenated or otherwise oxidized compounds can be identified. This provides an opportunity for a test against related, but sensitized, conditions for a common intermediate, since a given intermediate should react with a mixture of traps or a multifunctional trap in a characteristic product ratio (its "oxidation fingerprint"). Grossly different fingerprints for two reaction conditions can be taken to show that different oxidizing species are involved in the reaction conditions being compared.

Details of the sensitization mechanism(s) remain ambiguous, but we now show that direct photolysis of DBTO is distinct from the sensitized path. Sensitized deoxygenation of DBSeO also proceeds by a mechanism other than that observed on direct photolysis when sensitizers with a low triplet energy are employed. In certain conditions, the energetics are such that a unimolecular cleavage becomes possible when a sensitizer with

a triplet energy greater than the Se-O bond strength is used.

2.3 EXPERIMENTAL

2.3.1 Materials

Commercial materials were obtained from Aldrich and Fisher unless specified otherwise. HPLC grade toluene was further purified[38] by washing with cold H_2SO_4, then once with water, once 5% NaOH, followed with one more wash with water, dried with magnesium sulfate, and distilled from potassium under argon. Benzene and dichloromethane were distilled over CaH_2 under argon. Cyclohexane was purified as described in Perrin and Armarego[38] then dried and distilled from sodium under argon. Peroxides were removed from cyclohexene.[38] Benzophenone was recrystallized from methanol until ≥ 99% pure by GC. All other sensitizers were found to be at least 99% pure by GC as received. Dibenzothiophene-*S*-oxide and dibenzoselenophene-*Se*-oxide were prepared by literature methods.[23] and further purified by recrystallizations in acetone and dichloromethane, respectively.

Photochemical reactions were monitored by GC, HPLC, or both. HPLC separations were done using a Discovery HS C18 reverse phase column and a diode array UV/VIS detector. GC analysis was done with a flame ionization detector and 30 m ZB-5 capillary column or a 15 m RTX-1 capillary column. Reported error limits are the standard deviations of multiple runs, and thus reflect the reproducibility of the result, rather than an error limit including any systematic errors.

2.3.2 Irradiations

Photochemical reactions were irradiated with a 75 W Xe arc lamp focused on a monochrometer. Slit widths allowed ± 12 nm linear dispersion from the set wavelength. Samples in a 1 cm square quartz cell were put in a permanently mounted cell holder positioned such that all the exiting light hits the sample cell without further focusing. Photolysis of azoxybenzene was used as an actinometer.[39] Degassing was done by purging with Ar for at least 10 minutes except as noted. With nπ*-triplet sensitizers, this led to modest quantities of oxygenated products in control photolyses that did not have

the sulfoxide or selenoxide due to reaction with residual oxygen. The formation of these products is not linear with time, but is rapid intially and tails off as the oxygen is consumed. Other experiments were carried out under freeze-pump-thaw degassing conditions, and the background oxygenation products could be eliminated.

All photolyses were done at ambient temperature. Reactions were typically carried out to about 30% conversion in order to measure the small amounts of minor products. In some cases, it was necessary to carry the reaction to nearly 50% to quantify some products that could only be reliably quantified beginning at about 25% conversion. Both loss of substrate and growth of products were consistently linear with time under these conditions. Control experiments showed that no reaction (either deoxygenation or solvent oxidation) occurred in the dark at temperatures of 40 ˚C over several hours.

2.3.3 Spectroscopy

Transient absorption studies were done with a home-built nanosecond transient absorption spectrometer, which has been described previously.[13] Samples were irradiated with the third harmonic of a Nd:YAG (355 nm, 5 ns, 2-25 mJ/pulse, 3 mm beam radius). The spectroscopic detection system included a 75 W Xe arc lamp, a monochrometer, an 1P-28 photomultiplier (R_1 = 50 Ω), and a 100 MHz digitizer. Irradiations were carried out in 1 cm square quartz cell. The decay kinetics were typically averaged over 100 laser pulses. Steady state absorption spectra were recorded on a double-beam instrument at room temperature.

2.4 RESULTS AND DISCUSSION

Two technical problems made the experiments more difficult than might have been anticipated. They were related to setting up the sensitization reactions ideally (100% light absorption by sensitizer and 100% quenching of sensitizer by substrate) and the reactivity of even small amounts of residual molecular oxygen. Because the sensitizers (benzophenone, anthraquinone and acridine) are known hydrogen abstractors, the inevitable radical chemistry in less than ideal conditions leads to oxygenated products. The problem regarding sensitization could not sensibly be relieved by choice of alternate sensitizers, because the primary goal was to investigate the mechanism of representative

known reactions from the literature.[14,15] These limitations make the data also less than ideal; however, important qualitative conclusions can still be drawn.

2.4.1 Rate Constants and Quantum Yields

DBTO and DBSeO begin to absorb at wavelengths shorter than about 360 nm, with significant extinction coefficients ranging from ~6000 to 2000 $M^{-1}cm^{-1}$ from 270 nm to 320 nm. The selected sensitizers have nπ* states and appreciable extinction coefficients over 350 nm. In instances where sensitizer absorption was not intense at wavelengths of at least 350 nm, the sensitizers were used in excess. In all cases, conditions were such that >99% of the light was being absorbed by the sensitizer.

Table 2.1 Rate constants for quenching of sensitizers by DBTO and DBSeO.

Sensitizer	Quencher	Solvent	k_q, (M^{-1} s^{-1})	$1/\tau_o$, (s^{-1})
Acridine	DBTO	Acetonitrile	$< 10^5$	4.3×10^5
	DBTO	CH_2Cl_2	$< 10^5$	2.7×10^4
	DBTO	Toluene	4.7×10^5	5.0×10^3
Anthraquinone	DBTO	CH_2Cl_2	5.7×10^8	4.2×10^6
Benzophenone	DBTO	Acetone	4.2×10^9	1.6×10^5
	DBTO	CH_2Cl_2	2.8×10^9	5.4×10^5
	DBTO	Toluene	4.4×10^9	3.8×10^5
Acridine	DBSeO	CH_2Cl_2	$<10^5$	4.30×10^5
Anthraquinone	DBSeO	CH_2Cl_2	1×10^9	4.20×10^6
Benzophenone	DBSeO	CH_2Cl_2	4.8×10^9	5.35×10^5

Quenching rate constants and sensitizer triplet lifetimes were measured to attempt to set up conditions where all or nearly all the sensitizer would be quenched by DBTO or DBSeO. These measurements were made by standard transient absorption techniques, using the well-known triplet absorption spectra of the sensitizers.[40] The results are given in Table 2.1 and typical data are shown in Figures 2.1 and 2.2. de Lucas reported a rate

constant of 9 x 10^9 M^{-1} s^{-1} for the quenching of benzophenone by DBTO in acetonitrile,[37] in keeping with the current data.

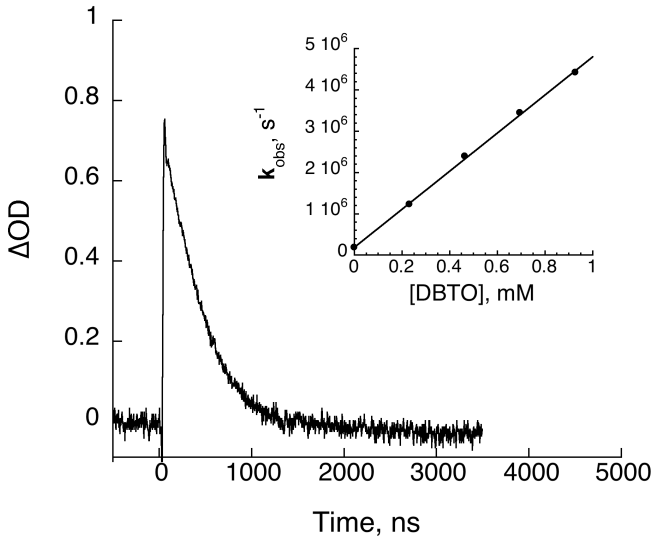

Figure 2.1 Kinetic trace at 515 nm acquired after 355 nm excitation of 9 x 10^{-3} M benzophenone and 0.5 x 10^{-3} M DBTO in acetone. *Insert*: The rate of decay or the 530 nm transient as a function of the concentration of DBTO.

The data in Table 2.1, in combination with equation 2.1, show that in the range of several mM initial concentration, DBTO and DBSeO both quench a very large fraction of benzophenone, but that a small amount of sensitizer remains unquenched (Table 2.2).

$$\Phi_{sens} = \frac{k_q[Q]}{k_q[Q] + \tau_0^{-1}} \qquad (2.1)$$

Increasing the concentration of DBTO or DBSeO too far means increasing the small fraction of direct irradiation and is undesirable for straightforward data interpretation [41]. For the sensitizers other than benzophenone, this is more severe: smaller fractions of the sensitizer are quenched at reasonable DBTO/DBSeO concentrations. This affects both quantum yield measurements and product distributions (vide infra).

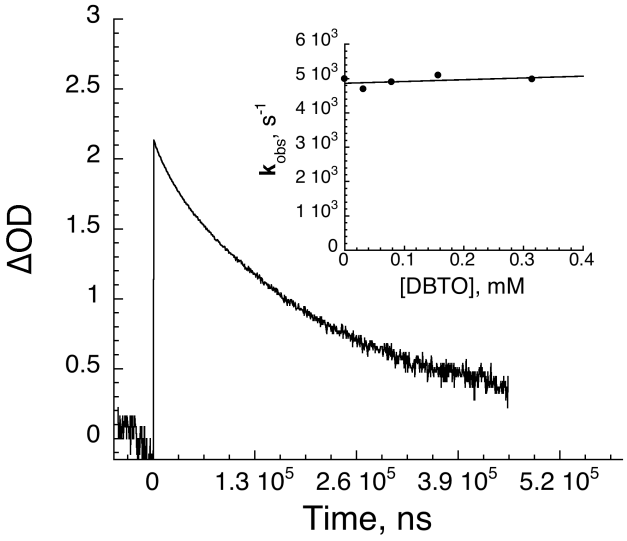

Figure 2.2 Kinetic trace at 440 nm acquired after 355 nm excitation of 0.2 x 10^{-4} M acridine and 3 x 10^{-4} M DBTO in toluene. *Insert*: The rate of decay or the 440 nm transient as a function of the concentration of DBTO.

In previous work, we have shown that the triplet energy of DBTO, as judged by the blue edge shoulder of phosphorescence, varies between 60 and 65 kcal/mol depending on the polarity of the solvent.[32] We were not successful in obtaining a phosphorescence spectrum for DBSeO at 77 K in organic glasses.[2342] However, based on the similarity of the triplet energy of DBT and DBSe, and the fact that the oxidation tends to remove the S or Se as a part of the active chromophore, we presume that the "spectroscopic" triplet energy of DBSeO is about the same as that of DBTO, i.e., between 60 and 65 kcal/mol.

Triplet energy transfer is plausible as a quenching mechanism for benzophenone (E_T ~ 69 kcal/mol) and anthraquinone (E_T ~ 63 kcal/mol), but not for acridine (E_T ~ 45 kcal/mol) [40]. The rapid quenching of benzophenone (Figure 2.1) and somewhat slower quenching of anthraquinone are consistent with exothermic and near-thermoneutral energy transfer. The low rate constant for acridine quenching by DBTO or DBSeO (e.g., Figure 2.2) is consistent with a slower mechanism, such as, for example, endothermic

electron transfer. We have previously concluded that DBTO undergoes electron transfer reactivity with *N*-methylcarbazole [26].

Table 2.2 Quantum yields for loss of oxide from sensitized DBTO or DBSeO photolyses.[a]

Entry		Sensitizer	[Sens], mM	λ_{ex} (nm)	Φ_{obs}	Φ_T	Φ_{sens}	Φ_{rxn}
1	DBTO[a]	None	--	313	0.0118 ± 0.0013	--	--	0.012
2	DBTO	Acridine	11	357	0.0048 ± 0.0004	0.5[b]	0.16	0.061
3	DBTO	Anthraquinone	10	355	0.0313 ± 0.0016	0.9	0.58	0.060
4	DBTO	Benzophenone	100	365	0.0074 ± 0.0005	1.0	0.92	0.0080
5	DBTO	*N*-Methylcarbazole	25	350	0.0152 ± 0.0016	0.4		
6	DBSeO[a]	None	--	320	0.301 ± 0.056	--	--	0.30
7	DBSeO	Acridine	11	357	0.048 ± 0.011	0.5	[c]	[c]
8	DBSeO	Anthraquinone	10	355	0.709 ± 0.052	0.9	0.704	1.2
9	DBSeO	Benzophenone	80 - 100	365	0.326 ± 0.021	1.0	0.900	0.36

[a] Solutions of DBTO and DBSeO were originally 0.4-5 mM and flushed with Ar to remove air. Solvent for DBTO was toluene. Due to solubility issues, the solvent for DBSeO was toluene with 4% chloroform as a co-solvent. Under these conditions all of the light is absorbed by the sensitizer. [b] Ref 40 or 43. [c] Unable to calculate due to low k_q.

Tables 2.2 and 2.3 give the observed quantum yields for loss of DBTO/DBSeO and formation of DBT/DBSe, respectively, along with the conditions used for the measurements.[43] Given the quenching rate constants, the inherent quantum yield for the sensitized reaction can be calculated according to equation 2.2, where equation 2.1 is used to estimate Φ_{sens}. We used $\Phi_{triplet}$ = 1, 0.9, 0.5, and 0.44 for benzophenone, anthraquinone, acridine, and *N*-methylcarbazole, respectively.[40,44]

$$\Phi_{obs} = \Phi_{triplet} \cdot \Phi_{sens} \cdot \Phi_{rxn} \qquad (2.2)$$

Table 2.3 Quantum yields for formation of sulfide or selenide from sensitized DBTO or DBSeO photolyses.[a]

Entry		Sensitizer	[Sens], mM	λ_{ex} (nm)	$\Phi_{\text{-oxide}}$[b]	Φ_{obs}[c]	Φ_T	Φ_{sens}	Φ_{rxn}
1	DBTO[a]	None	--	313	0.0118 ± 0.0013	0.0046 ± 0.0007	--	--	0.0046
2	DBTO	Acridine	11	357	0.0048 ± 0.0004	0.0035 ± 0.0003	0.5[d]	0.158	0.0443
3	DBTO	Anthraquinone	10	355	0.0313 ± 0.0016	0.0260 ± 0.0021	0.9	0.575	0.0502
4	DBTO	Benzophenone	100	365	0.0074 ± 0.0005	0.0070 ± 0.0010	1.0	0.920	0.0076
5	DBTO	*N*-Methylcarbazole	25	350	0.0152 ± 0.0016	0.0116 ± 0.0001	0.4		
6	DBSeO[a]	None	--	320	0.301 ± 0.056	0.236 ± 0.025	--	--	0.236
7	DBSeO	Acridine	11	357	0.048 ± 0.011	0.027 ± 0.002	0.5	[e]	[3]
8	DBSeO	Anthraquinone	10	355	0.709 ± 0.052	0.531 ± 0.037	0.9	0.704	0.838
9	DBSeO	Benzophenone	80 - 100	365	0.326 ± 0.021	0.207 ± 0.009	1.0	0.900	0.230

[a] Solutions of DBTO and DBSeO were originally 0.4-5 mM and flushed with Ar to remove air. Solvent for DBTO was toluene. The solvent for DBSeO was toluene with 4% chloroform as a co-solvent. All of the light is absorbed by the sensitizer. [b] Observed quantum yield for loss of DBTO or DBSeO, respectively. [c] Observed quantum yield for formation of DBT or DBSe, respectively. [d] Ref 40 or 43. [e]Unable to calculate due to low k_q.

Equations 2.1 and 2.2 are used under the assumption that the reaction is based on a simple sensitization/quenching scheme. They thus have an upper limit for Φ_{rxn} of 1. The observed value of 1.2 for anthraquinone and DBSeO (entry 8, Table 2.2) is probably within experimental error of that limit. We cannot calculate a value for acridine because the quenching rate constant is too low. This is *prima facie* evidence that at least acridine-sensitized DBSeO photolysis does not go by any simple sensitized mechanism. The most likely explanation is radical-mediated chemistry, probably initiated by hydrogen abstraction by the acridine. Notable also is that the Φ_{rxn} value is similar for direct direct irradiation (entry 6) and benzophenone-sensitized chemistry (entry 9), with the latter

higher by about 20%. Since the benzophenone-sensitized data presumably reflect the fate of all of the ^{3}DBSeO that is formed, the somewhat smaller, but comparable, value on direct irradiation is consistent with the two processes having the same general mechanism (i.e., through ^{3}DBSeO), as long as the quantum yield for ^{3}DBSeO formation on direct irradiation is in the range of 0.7-0.8.

The Φ_{rxn} quantum yields recorded for acridine and anthraquinone and DBTO (entries 2 and 3 in Table 2.2) are essentially identical, but almost an order of magnitude larger than that when using benzophenone (entry 4). As will become clear below, we conclude that the mechanism for deoxygenation of DBTO under direct irradiation is different than that under sensitized conditions, regardless of which sensitizer is used. (However, this does not necessarily imply that all of the sensitized reactions follow the same mechanism.) Assuming the mechanism for DBTO deoxygenation does not directly involve ^{3}DBTO — as concluded for entry 8 with DBSeO — there is no particular reason that these then-meaningless Φ_{rxn} values should coincide for various sensitizers. We thus do not derive any particular meaning from their difference.

2.4.2 Oxidation fingerprint experiments

In our original report on DBSeO photochemistry, we demonstrated that DBSeO and DBTO gave very similar "fingerprints" on oxidation of toluene, with a predominance of cresols being formed over products from benzyl oxidation (benzyl alcohol and benzaldehyde) [23].

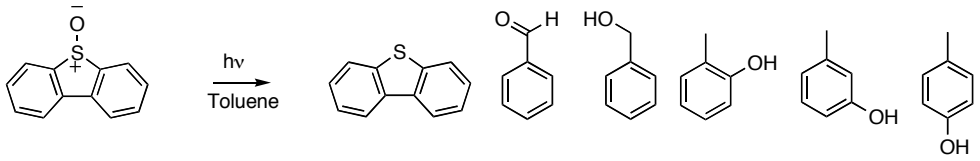

Toluene was chosen as an initial solvent and trap, due to the mix of easily identifiable products: the three possible cresols, benzyl alcohol, and its over-oxidation product, benzaldehyde. *m*-Cresol and *p*-cresol were quantified as a single peak by GC because of the difficulty of their separation. Table 4 lists the percent yields of sulfide

(DBT) relative to loss of sulfoxide (DBTO) in entries 1-5. The yields of oxidized products, relative to the formation of DBT, are given in the other columns.

Analogous data are given for the DBSeO reaction in entries 6-9. It was determined that addition of a small amount of chloroform (4% by volume) enhanced the solubility of DBSeO in toluene and was necessary for homogenous solutions. Control experiments with DBTO showed that addition of this amount of chloroform to the toluene did not affect the data.

Fairly large error bars are associated with the data for benzyl alcohol and benzaldehyde. Empirical experimentation with deoxygenation techniques indicated that the *sum* of these two products was much more reproducible than either individual number, and that the "overoxidation" of the benzyl alcohol to benzaldehyde was probably correlated with residual oxygen in solution. Further experiments using the more rigorous freeze-pump-thaw method for deoxygenation of DBSeO under direct, benzophenone-sensitized, and anthraquinone-sensitized conditions showed that benzaldehyde could be eliminated from the product mixture. FPT degassing was not used in most experiments, though, because only a single time point can be taken from the sample.

Because of the low concentrations of oxygenated species being detected in the measurements and the potential for their formation by reactions between the sensitizer, solvent, and residual O_2, appropriate control experiments were run. Solutions were prepared without DBTO or DBSeO, but otherwise identically to those of the ordinary runs, i.e., they contained the sensitizers at the appropriate concentrations and were deoxygenated the same way. The following key results were obtained: (1) In no case was any cresol detected; (2) Though small amounts of $PhCH_2OH$ and PhCHO were detected, in no case did those quantities exceed one-tenth that observed in the measurements that contained sensitizer and DBTO that were photolyzed for the same amount of time, particularly for higher conversions. An analogous conclusion holds for DBSeO [45].

Table 2.4 Product yields of photolysis of DBTO and DBSeO in toluene.[a]

Entry		Sensitizer	[Sens], mM	λ_{ex}, nm	$\%_{DBT}$[b]	Benzyl oxidations[c]		Cresols[c]		Benzyl: Cresol
						PhCHO	BnOH	*o*	*m* and *p*[d]	
1	DBTO[a]	None	--	313	55 ± 11	17 ± 4	13± 4	26 ± 5	22 ± 5	1:1.6
2	DBTO	Acridine	11	357	75 ± 8	45 ± 5	26 ± 5	6.5 ± 0.5	-	-
3	DBTO	Anthraquinone	10	355	83 ± 8	9.6 ± 2.2	8.9 ± 0.6	3.5 ± 0.4	1.8 ± 0.4	3.5:1
4	DBTO	Benzophenone	100	365	94 ± 9	30 ± 3	27 ± 3	3.4 ± 0.5	3.6 ± 0.7	8.1:1
5	DBTO	*N*-Methylcarbazole	25	350	77 ± 8	3.2 ± 0.8	3.4 ± 0.8	3.3 ± 0.1	1.1 ± 0.2	1.5:1
6	DBSeO[a]	None	--	320	80 ± 7.6	6.7 ± 1.6	-	12 ± 0.5	5.2 ± 0.4	1:2.6
7	DBSeO	Acridine	11	357	58 ± 10	23 ± 3	3.9 ± 1.5	7.0 ± 0.7	2.8 ± 0.5	2.7:1
8	DBSeO	Anthraquinone	10	355	75 ± 4	17 ± 1.5	7.7 ± 1.5	5.8 ± 1.5	3.3 ± 1.1	2.7:1
9	DBSeO	Benzophenone	80 - 100	365	64 ± 1.3	6.0 ± 1.9	1.2 ± 2.6	12 ± 2.3	7.6 ± 0.4	1:2.7

[a] Solutions of DBTO were originally 1-5 mM and flushed with Ar to remove O_2. Solutions of DBSeO were originally 0.4-2 mM and flushed with Ar to remove O_2. Chloroform (4%) was added as a co-solvent to increase DBSeO solubility. [b] Yield, relative to loss of DBTO or DBSeO. [c] Yield relative to formation of DBT or DBSe. [d] Measured as one peak.

However, Entry 8 in Tables 2.2, 2.3, and 2.4 merits special discussion. Photolysis of anthraquinone in the absence of DBSeO with Ar-flushing deoxygenation does lead to benzyl oxidation products that are significant to the concentrations reported in the table. (Again, cresols were not observed.) With the measurements reported in these tables, only about 10% of the anthraquinone is actually quenched, with anthraquinone absorbing >99% of the light. Because of solubility limitations, a significantly higher fraction of anthraquinone quenching could not be achieved. Thus, most of the anthraquinone "control chemistry" is still occurring under these experimental conditions, and most of the benzyl oxidation products in entry 8 comes from this direct interaction between anthraquinone and solvent. *In contrast, under FPT degassing, the oxidation fingerprint for anthraquinone-sensitized DBSeO photolysis is dominated by cresol formation, quite similar to direct or DBSeO or benzophenone-sensitized photolysis of DBSeO.*

Table 2.4 immediately draws attention to the difference between direct photolysis and the other conditions by presenting the ratio of benzyl oxidation products (benzyl alcohol and benzaldehyde) to cresols. Even allowing for relatively large uncertainties in the data due to the low concentrations being measured, the preponderance of cresol products over benzyl oxidation for direct irradiation is in direct contrast to all the other cases. Our current data give slightly different ratios for direct irradiation of both DBTO and DBSeO (entries 1 and 6) than our previous report in such a way as to make the data for the two compounds look less similar. (The ratios were 2.0 and 2.8, rather than 1.6 and 2.6, for DBTO and DBSeO, respectively [23].) We attribute this to the difficulties with residual O_2. Nonetheless, the salient result remains that direct irradiation of the two compounds leads to the cresols as the major product, with a substantial minor pathway giving benzyl alcohol and benzaldehyde. In contrast, all of the sensitized DBTO reactions (entries 2-5) lead to large majorities of benzyl oxidations. Among the DBSeO reactions, the benzophenone sensitization (entry 9) stands out as being much more like the direct irradiations than the other sensitized reactions (entries 7 and 8), in addition to anthraquinone-sensitized DBSeO photolysis when FPT is used.

An alternative second trap was pursued. Originally, we examined cyclohexene,

which produces the epoxide and cyclohexenol on treatment with DBTO,[16,17] but this trap was fraught with reproducibility-related difficulties when the sensitizers that could also accomplish hydrogen abstraction were used.

Ultimately a 3:1 (v/v) mixture of benzene and cyclohexane was used, based on selectivity results reported previously.[17] Cyclohexanol and phenol were used as the fingerprint products. To best accommodate solubility, this mixture was used as a 20% cosolvent with 80% dichloromethane. Results for direct and benzophenone-sensitized photolysis are given in Table 2.5.

Table 2.5 Product yields from photolysis of DBTO in dichloromethane and 20% 3:1 benzene:cyclohexane.[a]

Entry		Sensitizer	[Sens], mM	λ_{ex}, nm	% sulfide/selenide[b]	% cyclohexanol[c]	% phenol[c]
1	DBTO	None		320	49 ± 4	32 ± 5	10 ± 0.1
2	DBTO	Benzophenone	100	365	95 ± 1	20 ± 5	-
3	DBSeO	None		320	61 ± 10	3.8 ± 0.3	2.4 ± 0.5
4	DBSeO	Benzophenone	100	365	86 ± 9	14 ± 3	3.0 ± 0.6

[a] Initial concentrations of DBTO or DBSeO were 1-2 mM and flushed with Ar to remove oxygen.
[b] Percent yield, relative to loss of DBTO or DBSeO. [c] Percent yield, relative to formation of DBT or DBSe.

Despite the poor mass balances reflected in Table 2.5, particularly for DBSeO, we believe some analysis can still be made. An approximately 3:1 ratio of cyclohexenol:phenol is achieved by direct photolysis of DBTO. The observed ratio for DBSeO is somewhat lower (entry 3, direct) or higher (entry 4, benzophenone-sensitized). However, it should also be noted that the absolute yields of the oxygenated products are low in this solvent mixture, particularly for DBSeO. They are thus subject to a larger proportion of systematic error due to the presence of residual oxygen and radical chemistry. Nonetheless, we suggest these imperfect data still show that entries 1 and 2 are mechanistically distinct from one another. Conclusions regarding DBSeO must be

considerably more tentative, but that entries 3 and 4 produce similar results is consistent with the toluene data and the hypothesis that benzophenone-sensitized deoxygenation of DBSeO may go through the same mechanism as direct irradiation of DBSeO.

2.4.3 Differentiating mechanisms

As discussed previously, we have estimated that the T_1 energy of DBTO is between 60 and 65 kcal/mol, depending on the solvent; DBSeO should be very similar.[32] However, while the S-O BDE of DBTO is about 76 kcal/mol, we have estimated that the Se-O BDE for DBSeO is only about 64 kcal/mol.[46] Thus, it is at least plausible that DBSeO may undergo dissociation to DBSe and O(^{3}P) from the T_1 state of DBSeO. On the other hand, T_1 simply is not energetic enough for S-O dissociation in DBTO.

It is thus satisfying that, while the data presented in this paper are less than perfect, in each case, they can be broken into two qualitative groups. In the first group reside data from direct photolysis of both precursors, benzophenone-sensitized photolysis of DBSeO, and anthraquinone-sensitized photolysis of DBSeO (if done with FPT degassing). The other group, consisting of the rest of the condition sets, is more diverse in terms of its results, but all of them contrast to the first group. We conclude that the two groups do not share a common intermediate or mechanistic path.

2.5 CONCLUSIONS

The results reported here place the chemistry of direct irradiation of DBTO, direct irradiation of DBSeO, and either benzophenone- or anthraquinone-sensitized photolysis of DBSeO into a single group of reactions with regard to oxidative selectivity. Though it must be acknowledged that the data are not perfect, this is a sensible grouping. Direct irradiation of DBTO and DBSeO both produce O(^{3}P), we have argued. The two sensitized cases in this group are those where energy transfer to form triplet DBSeO is plausible, and we estimate that ^{3}DBSeO probably has enough energy for unimolecular Se-O scission.

In contrast, the other sensitizing combinations lead to cases that cannot directly form O(^{3}P). Formation of triplet DBTO (from benzophenone and probably anthraquinone) may result in deoxygenation, but not by the same mechanism as direct irradiation.

Sensitization of either substrate with acridine simply cannot result in triplet formation. Thus, it is no surprise that the oxidation patterns of this second group differ from that of the first. These experiments do not shed significant light on the mechanism(s) of the sensitized deoxygenations, but they are set apart from the conditions of the former group.

Thus, we again conclude that the data here add to the circumstantial evidence that photolysis of DBTO or DBSeO produces atomic oxygen.

2.6 ACKNOWLEDGEMENT

The authors thank the National Science Foundation (CHE 0211371) for support of this work.

2.7 REFERENCES

(1)Mislow, K.; Axelrod, M.; Rayner, D. R.; Gotthardt, H.; Coyne, L. M.; Hammond, G. S. *Journal of the American Chemical Society* **1965**, *87*, 4958-9.

(2)El Amoudi, M. S. E. F.; Geneste, P.; Olivé, J.-L. *J. Org. Chem.* **1981**, *46*, 4258-4262.

(3)Archer, R. A.; Kitchell, B. S. *J. Am. Chem. Soc.* **1966**, *88*, 3462-3463.

(4)Archer, R. A.; De Marck, P. V. *J. Am. Chem. Soc.* **1969**, *91*, 1530-1532.

(5)Spry, D. O. *J. Am. Chem. Soc.* **1970**, *92*, 5006-5008.

(6)Lee, W.; Jenks, W. S. *J. Org. Chem.* **2001**, *66*, 474-480.

(7)Tsurutani, Y.; Yamashita, T.; Horie, K. *Polymer Journal* **1998**, *30*, 11-16.

(8)Tsurutani, Y.; Machida, S.; Horie, K.; Kawashima, Y.; Nakano, H.; Hirao, K. *J. Photochem. Photobiol. A* **1999**, *122*, 161-168.

(9)Sato, T.; Goto, Y.; Tohyama, T.; Hayashi, S.; Hata, K. *Bulletin of the Chemical Society of Japan* **1967**, *40*, 2975-6.

(10) Sato, T.; Yamada, E.; Akiyama, T.; Inoue, H.; Hata, K. *Bull. Chem. Soc. Japan* **1965**, *38*, 1225.

(11) Still, I. W. J. In *The Chemistry of Sulfones and Sulfoxides*; Patai, S., Rappaport, Z., Stirling, C. J. M., Eds.; John Wiley & Sons Ltd.: New York, 1988, p 873-887.

(12) Guo, Y.; Jenks, W. S. *J. Org. Chem.* **1997**, *62*, 857-864.

(13) Darmanyan, A. P.; Gregory, D. D.; Guo, Y.; Jenks, W. S. *J. Phys. Chem. A* **1997**, *101*, 6855-6863.

(14) Shelton, J. R.; Davis, K. E. *Int. J. Sulfur Chem.* **1973**, *8*, 217-228.

(15) Gurria, G. M.; Posner, G. H. *J. Org. Chem.* **1973**, *38*, 2419-2420.

(16) Wan, Z.; Jenks, W. S. *J. Am. Chem. Soc.* **1995**, *117*, 2667-2668.

(17) Gregory, D. D.; Wan, Z.; Jenks, W. S. *J. Am. Chem. Soc.* **1997**, *119*, 94-102.

(18) Thiemann, T.; Ohira, D.; Arima, K.; Sawada, T.; Mataka, S.; Marken, F.; Compton, R. G.; Bull, S.; Davies, S. G. *J. Phys. Org. Chem.* **2000**, *13*, 648-653.

(19) Thomas, K. B.; Greer, A. *J. Org. Chem.* **2003**, *68*, 1886-1891.
(20) Lucien, E.; Greer, A. *J. Org. Chem.* **2001**, *66*, 4576-4579.
(21) Lüdersdorf, R.; Khait, I.; Muszkat, K. A.; Praefcke, K.; Margaretha, P. *Phosphorus and Sulfur and the Related Elements* **1981**, *12*, 37-54.
(22) Khait, I.; Lüdersdorf, R.; Muszkat, K. A.; Praefcke, K. *J. Chem. Soc., Perkins Trans 2* **1981**, 1417-1429.
(23) McCulla, R. D.; Jenks, W. S. *J. Am. Chem. Soc.* **2004**, *126*, 16058-16065.
(24) Gregory, D. D.; Jenks, W. S. *J. Org. Chem.* **1998**, *63*, 3859-3865.
(25) Kropp, P. J.; Fryxell, G. E.; Tubergen, M. W.; Hager, M. W.; Harris, G. D., Jr.; McDermott, T. P., Jr.; Tornero-Velez, R. *Journal of the American Chemical Society* **1991**, *113*, 7300-10.
(26) Cubbage, J. W.; Tetzlaff, T. A.; Groundwater, H.; McCulla, R. D.; Nag, M.; Jenks, W. S. *J. Org. Chem.* **2001**, *66*, 8621-8628.
(27) Arima, K.; Ohira, D.; Watanabe, M.; Miura, A.; Mataka, S.; Thiemann, T.; Valcarcel, J. I.; Walton, D. J. *Photochemical & Photobiological Sciences* **2005**, *4*, 808-816.
(28) Nag, M.; Jenks, W. S. *J. Org. Chem.* **2004**, *69*, 8177-8182.
(29) Nag, M.; Jenks, W. S. *J. Org. Chem.* **2005**, *70*, 3458-3463.
(30) Desikan, V.; Liu, Y.; Toscano, J. P.; Jenks, W. S. *Journal of Organic Chemistry* **2007**, *72*, 6848-6859.
(31) Stoffregen, S. A.; Heying, M.; Jenks, W. S. *Journal of the American Chemical Society* **2008**, *accepted*.
(32) Jenks, W. S.; Lee, W.; Shutters, D. *J. Phys. Chem.* **1994**, *98*, 2282-2289.
(33) Jenks, W. S.; Matsunaga, N.; Gordon, M. *J. Org. Chem.* **1996**, *61*, 1275-1283.
(34) Yamazaki, Y.; Tsuchiya, T.; Hasegawa, T. *Bull. Chem. Soc. Jpn.* **2003**, 201-202.
(35) Tezuka, T.; Suzuki, H.; Miyazaki, H. *Tetrahedron Lett.* **1978**, 4885-4886.
(36) Goldschmidt, Z. In *The Chemistry of Organic Selenium and Tellurium Compounds Volume 2*; Patai, S., Ed.; Wiley: New York, 1986, p 275-337.
(37) de Lucas, N. C.; Albuquerque, A. C. C.; Santos, A. C. A. S.; Garden, S. J.; Nicodem, D. E. *Journal of Photochemistry and Photobiology, A: Chemistry* **2007**, *188*, 293-297.
(38) Perrin, D. D.; Armarego, W. L. F. *Purification of Laboratory Chemicals. 3rd Ed*, 1988.
(39) Bunce, N. J.; LaMarre, J.; Vaish, S. P. *Photochem. Photobiol.* **1984**, *39*, 531-533.
(40) Murov, S. L.; Carmichael, I.; Hug, G. L. *Handbook of Photochemistry*; 2nd ed.; Marcel Dekker, Inc.: New York, 1993.
(41) In some cases, solubility also becomes a limitation.
(42) A careful reading of reference 32 will reveal that a majority of this type of sulfoxides does not produce useful phosphorescence data, i.e., DBTO was one of the few exceptions. We routinely examine new sulfoxides or selenoxides for phosphorescence at 77 K, but are not surprised when a useful spectrum is not obtained.
(43) The values here reported here were remeasured for this work, as we have

done for each paper in the series that addresses this reaction. We find that measured quantum yields are quite reproducible when measured repeatedly over a short time span for a project such as the current one. However, some variation from previously reported values for DBTO photolysis is common, and not unexpected due to the fairly severe dependence on wavelength, solvent-dependence, and inherently low value.

(44) Bonesi, S. M.; Erra-Balsells, R. *Journal of Luminescence* **2001**, *93*, 51-74.

(45) A disproportionate fraction of theoxygenated solvent is produced very quickly. Thus, care must be taken in comparing DBSeO product oxidations to these control experiments.

(46) Stoffregen, S. A.; McCulla Ryan, D.; Wilson, R.; Cercone, S.; Miller, J.; Jenks, W. S. *Journal of Organic Chemistry* **2007**, *72*, 8235-8242.

CHAPTER 3

Photocatalytic degradation using tungsten-modified TiO_2 and visible light: kinetic and mechanistic effects using multiple catalyst doping strategies

Reproduced from *The Journal of Photochemistry and Photobiology, A: Chemistry* **2009**, 207(2-3), 197, with permission from Elsevier.

Timothy Hathway, Erin M. Rockafellow, Youn-Chul Oh and William S. Jenks*
Department of Chemistry, Iowa State University, Ames, IA 50011-3111

3.1 ABSTRACT

Tungsten-modified titanium dioxide catalysts prepared from sol-gel methods and obtained commercially were compared for their photocatalytic activity using mechanistic probes designed to examine chemical pathways of oxidation. No special visible absorbance was noted for the sol-gel catalyts. However, an increase in the single-electron transfer chemistry with the presence of WO_x was noted, and a distinct wavelength dependence on the product ratios.

3.2 INTRODUCTION

Titanium dioxide is an excellent photocatalyst for the degradation of organic contaminants in water and air. Most organic compounds are degraded to CO_2, H_2O, and appropriate inorganic ions on exposure to TiO_2 in the presence of light and oxygen.[1-7] A distinct hindrance, however, for more widespread application of TiO_2 as a catalyst for removal of organic pollutants is its lack of absorption in the visible spectrum, as betrayed by its appearance as a white powder. Another is its relatively low efficiency. Modification of TiO_2 is thus an active and important field of research.

Of the three common phases of crystalline TiO_2, it is widely held that anatase (band gap = 3.2 eV, absorption $\leq$ 385 nm) is the most photocatalytically active, yet rutile (band gap = 3.0 eV, absorption $\leq$410 nm) absorbs light to the red of the anatase band edge.

This poses an obvious advantage, when considering the utility of solar light, but still does not extend far into the visible, where the majority terrestrial solar energy lies. The most commonly used and most effective TiO_2 photocatalyst is probably DeGussa's P25, which contains adjoining anatase and rutile microcrystalline regions. Gray has shown that this extended functionality is due in large part to the extended near-visible absorption of the rutile phase, followed by rapid electron transfer between the phases, leading to enhanced charge separation and reduced energy wastage by electron-hole recombination.[8,9]

In this sense, DeGussa P25 and other mixed-phase TiO_2 samples are inherently multicomponent catalysts, but other multi-component strategies for enhancing photocatalysts have emerged as well[10,11] One approach to building multi-component catalysts to increase physical charge separation and/or visible light absorption include nanodeposits of noble metal pools on the exterior of TiO_2 particles.[12-15] Another, more in the spirit of P25, is the overt use of additional semiconductors, such as CdS or WO_3, coupled to TiO_2.[16-20] Kamat has outlined both core-shell and coupled geometries.[16,17] but for practical purposes, we are concerned with the coupled case, which may be envisioned as small adjoining nanodomains. Here, both photogenerated holes and electrons are potentially accessible at the particle surface.

In this paper, we examine the photocatalytic chemistry of a series of WO_3-modified titanium dioxide samples.[21-24] The band gap of bulk WO_3 is 2.5 eV, which corresponds to absorption out to approximately 500 nm, well into the visible. Moreover, because of the absolute positions of the bands, conduction bond electrons from TiO_2 can migrate to WO_3, while the complementary migration can occur for valence band holes. With small percentages of tungsten, relative to titanium, it is also possible that simple substitutional doping may occur, with less predictable results.

A key issue, however, is whether the ordinary modes of reactivity for TiO_2 are maintained, enhanced, or destroyed.[25] We and others have generally drawn a distinction between hydroxyl-like ($HO\bullet_{ads}$) and SET-initiated chemistry. (See, for example, ref [26]) Bahnemann has referred to these phenomenologically different reactivities as deriving from "deeply" and "surface" trapped holes, respectively.[27] Others, as summarized by Fujishima,[7] argue that the hydroxyl-like chemistry can occur away from the particle

surface, indicative of a diffusible intermediate (presumably HO• itself). Regardless of the claims of true action-at-a-distance, we have argued that SET chemistry has a more stringent requirement for pre-adsorption to the catalyst and shown this to be the case for both oxidative and reductive SET reactions.[26,28]

In principle, if reactivity in WO_x-modified TiO_2 derives from the oxidative reactivity of holes residing in TiO_2 alone (surface or "deep"), then both the typical hydroxyl-like and single-electron transfer initiated chemistry ought still occur, assuming the reactivity is still dominated by adsorption on TiO_2 sites. The valence band for bulk WO_3 is at a higher potential than for TiO_2, which could result in hole trapping concentrated on these sites, which might, in turn, be observable in the oxidative behavior. There is also a possibility of true wavelength dependence of the chemistry because of the dopant, depending on the dynamics of hole trapping vs. substrate oxidation. However, if isolated WO_x sites are dilute within the TiO_2 matrix, the effects are harder to predict.

There are multiple methods of making WO_x-modified TiO_2, including an incipient wetness method, in which TiO_2 is at least partially coated with WO_x from solution deposition, and sol-gel methods, in which the tungsten is coprecipitated with the titanium and is presumably distributed throughout the catalyst. (We will use the term W-TiO_2 below to mean tungsten-modified TiO_2 in the most general sense, and will be more precise when referring to specific preparations.)

We examine the oxidative chemistry of two sets of catalysts. First, we compare two commercial catalysts: PC50 and DT52 from Millenium chemicals. The latter of these is derived by treatment of the former to coat it with WO_x by an incipient wetness method, such as that described by Do [21]. This process presumably results in segregated regions of WO_x on the TiO_2 particle. A second series is a set of sol-gel-prepared W-TiO_2 catalysts with 0-5% tungsten, prepared according to the method of Li.[23] By contrast, there is no evidence to suggest anything but a randomly formed mixed oxide for these materials. Rather than evaluate the chemistry by disappearance of a dye such as methylene blue,[29] we use chemical probes originally proposed by Ranchella[30] and Pichat[31,32] that provide more detailed information regarding the chemical mechanisms of oxidation of these catalysts, revealing pathways through product analysis.

3.3 EXPERIMENTAL

3.3.1 General materials

1-*p*-Anisylneopentanol (**AN**) and the oxidized products of its degradation were synthesized and characterized as published previously.[25] Quinoline and its major oxidized products were obtained from Aldrich. Distilled water was purified from a Millipore MilliQ UV system and had a resistivity of ≥ 18 MΩ cm^{-1}. Commercial titania samples were PC50 and DT52 obtained from Millennium Chemical.

3.3.2 Preparation of W-TiO_2 catalysts

W-TiO_2 was prepared by a sol-gel method based closely on that of Li.[23] A TiO_2 transparent sol was prepared by combining 17.5 g Ti(O-*n*Bu)$_4$, 120 mL ethanol, 15 mL acetic acid, and 5 mL de-ionized water. The mixture was aged for 1 day, stirring at room temperature. To this sol was added dropwise added 60 mL of aqueous solution of containing 4.56 g of ammonium paratungstate ($(NH_4)_{10}W_{12}O_{41}$, F.W.= 3042.55) under vigorous stirring over 2 hours until WO_x-TiO_2 (3 mol % WO_x to TiO_2) gel is formed. Similarly, 0%, 1%, and 5% WO_x-TiO_2 samples were prepared by using appropriate amounts of ammonium paratungstate. Ammonium tungstate was also used in the same way to prepare a 3% WO_x-TiO_2 gel with a different W source; no detectable difference was found between materials made from the two precursors.

The W-TiO_2 gels were aged two days with vigorous stirring, then one day undisturbed followed by one more day with vigorous stirring. The W-TiO_2 gels were then dried with a rotary evaporator at 358 K. As the gels dried, they shrunk and coated the surface of their flasks, eventually forming powders. After drying, the samples were ground for eight minutes in an agate ball mill.

Sintering was then carried out in porcelain crucibles. The furnace was heated at a moderate rate (10 K/min) to ensure that ejection of the volatiles did not discharge powder from the crucibles. The furnace was allowed to reach 923 K, which then stayed constant for two hours. A calibrated thermocouple was placed in the center of the cluster of crucibles to continuously monitor the temperature at the location of the samples. The furnace was then allowed to cool down over the course of two hours. The cooled

powders were immediately transferred to storage vials.

3.3.3 Catalyst characterization

Powder x-ray diffraction (XRD) measurements were carried out at room temperature using a diffractometer with Cu K_α radiation. An accelerating voltage of 40 kV and an emission current of 30 mA were used.

X-ray photoelectron spectroscopy (XPS) was performed with a multi-technique spectrometer employing monochromatized Al K_α radiation. The instrumental Gaussian full-width at half maximum (GFWHM), which characterizes the resolution, was 0.65 eV for the Al source. The take-off angle was fixed at 45˚ and the x-ray source was run at 14 kV and 250 W. The emitted photoelectrons were sampled from a 1 mm^2 area. The XPS energy scale was calibrated against Au $4f_{7/2}$ and Ag $3d_{5/2}$ peaks at 84.0 and 368.27 eV, respectively. The sample was mounted on an indium foil for XPS analysis and placed in the XPS chamber, whose base pressure was about 3 x 10^{-10} Torr. Temperature was measured with a Type K thermocouple.

Particles were examined by scanning electron microscopy (SEM) using a variable pressure scanning electron microscope with 20 kV accelerating voltage and ~0.5 nA of beam current for imaging in 25 mm working distance. SEM-EDX analyses were performed to check for segregation of the tungsten. A high-purity Ge light-element x-ray detector was employed and the take-off angle was fixed at 30˚.

3.3.4 Suspensions and Photolyses

Photocatalytic degradations were carried out as described previously.[25,33] Broadly emitting fluorescent lamps centered at 419 nm (roughly 390 – 500 nm total range) or 350 nm (roughly 320-380 nm) were used. The spectral distributions are available in the supporting information. Ferrioxalate actinometry was employed in order to compare the rates between UV and visible reactions.[34,35] Initial conditions were 300 μM **AN** or 150 μM **Q** in water containing 1 g/L catalyst and all solutions were purged with O_2. The pH was controlled throughout the kinetic run reactions by careful addition of aqueous NaOH as necessary. The reported initial degradation rates were normalized for total lamp flux by means of potassium ferrioxalate actinometry.

3.4 RESULTS

3.4.1 Catalyst characterization

Based on SEM analysis, the average particle size of the sintered, tungstated catalysts was in the range of 100 nm to 3 μm, which is much larger than P25 particles (Figure 3.1d). Ball-milling was used to successfully grind the particles into the 20 nm regime (Figure 2e), yielding both smaller particles and a tighter distribution of sizes.

As was noted by Li,[23] addition of WO_x to the sol-gel preparation of TiO_2 inhibited the conversion of anatase to rutile on annealing at 923 K. Studies of similar substitutionally W-doped titania catalysts show that W^{6+} exists in distorted octahedra. These cause long-range distortions that lead to anatase being favored over rutile up to temperatures higher than for undoped catalysts.[36]

Figure 3.1a shows the powder XRD of P25 (anatase and rutile), the undoped catalyst (0% WO_x-TiO_2, mainly rutile), and the doped materials (mainly anatase). Using the Scherrer equation, average crystallite sizes were found to be 15 nm, 18 nm, 23 nm, 28 nm, and 19 nm for 5% WO_x, 3% WO_x, 1% WO_x, 0% WO_x, and DeGussa P25, respectively.

XPS was used to determine the oxidation state of W near the surface of the catalysts. Figure 3.2b shows the underlying Ti 3p signal at 36.6 eV for the undoped sample. For the 3% WO_x-TiO_2 sample, the signal for the W^{6+} $4f_{7/2}$-$4f_{5/2}$ doublet at 36.0 eV is an inherently stronger peak and dominates the spectrum, with the apparent loss of resolution between the double peaks being due to the underlying Ti signal. Small contributions of other states are possible due to broad peaks.[37] Data from the XPS were also used to confirm the overall doping percentage (1.87% W, 32.80% Ti, remainder O, corresponding to 3 mol% W, relative to Ti, in TiO_2).

Diffuse reflectance UV-visible spectrophotometry (Figure 3.2c) shows that there was not a dramatic shift in the absorption spectra of the catalysts outside of what is predictable from the XRD data. P25 shows the typical band edge of TiO_2, with a slight tail into the red due to rutile. DT52 and the PC50 from which it is made had nearly identical spectra. The most red-shifted absorption came from the 0% WO_xTiO_2. However, this effect can be attributed entirely to the great fraction of rutile in this

material. We do not know why these materials exhibit a different result than the materials reported by Li, *et al.*[23]

SEM-EDX was used to check for segregation of WO_3. The data in Figure 3.2 show an even distribution of W in the 3% W catalyst, though the resolution of the images (ca. 0.2 μm) is not good enough to demonstrate whether there are nano-sized aggregations on the TiO_2 particles, or whether the W is homogeneously dispersed on the atomic scale. The same results were obtained for the 1% and 5% WO_x catalysts. More SEM and SEM-EDX data are available in the Supporting Information.

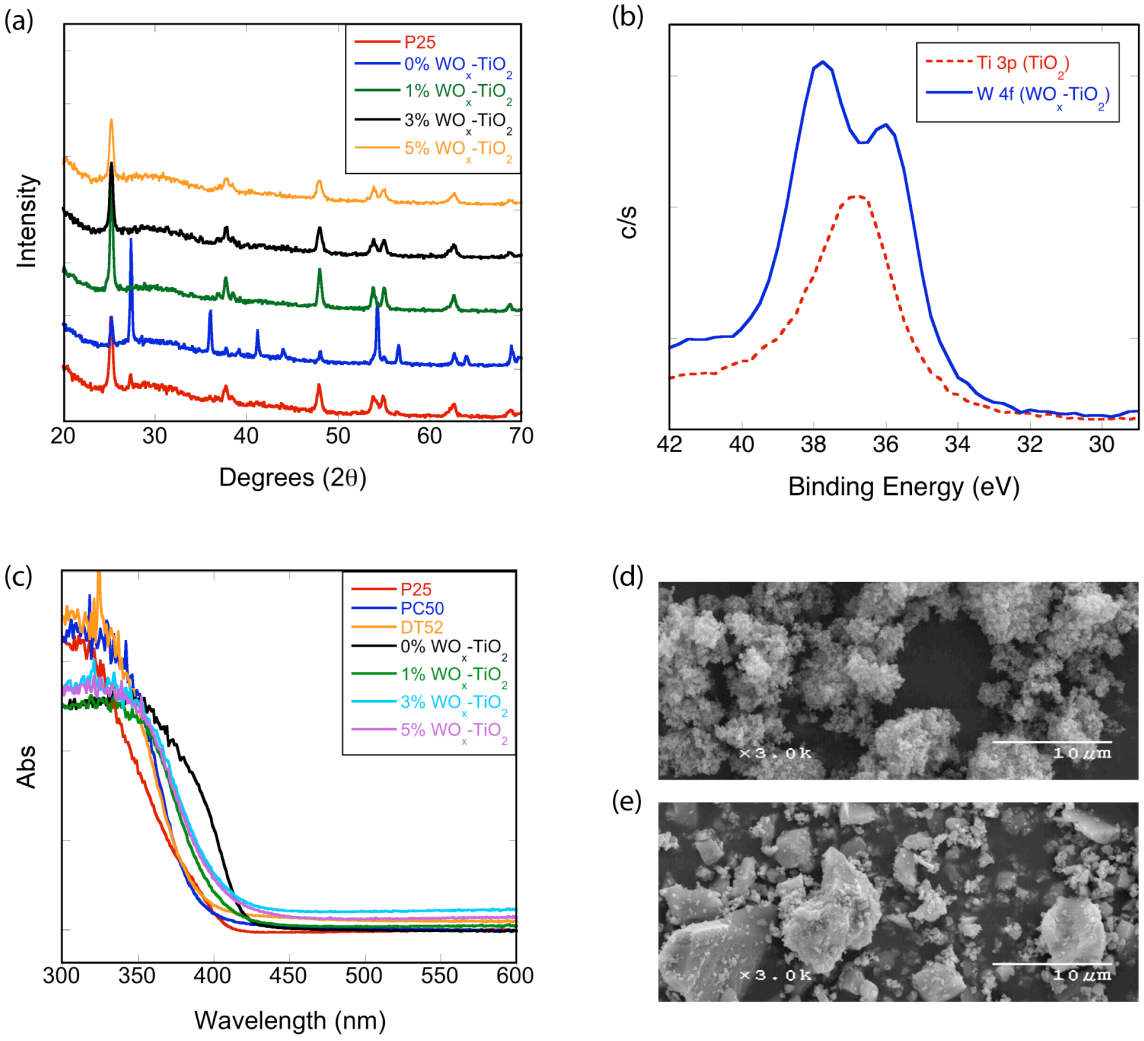

Figure 3.1 Characterization of sol-gel catalysts. (a) Powder XRD patterns; (b) Detail of XP spectrum of 3% WO_x-TiO_2; (c), Diffuse reflectance UV-vis spectra; (d and e) SEM images of P25 (d) and 5% WO_x-TiO_2 after milling (e) on the same scale.

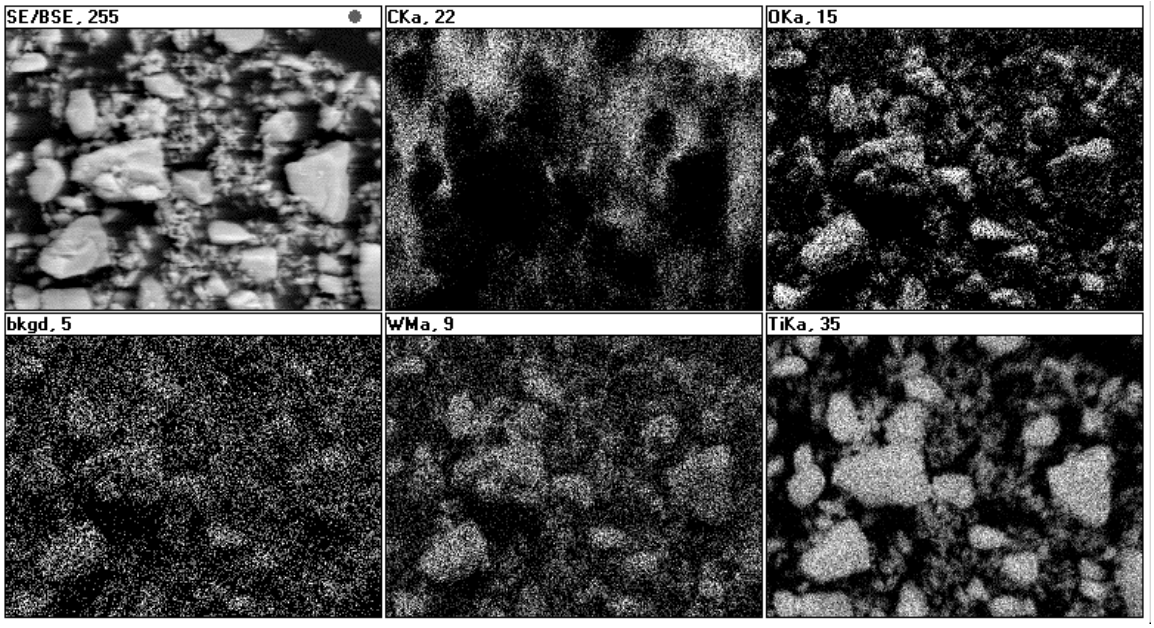

Figure 3.2 SEM-EDX images of the 3% WO_x catalyst on the same scale as Figure 1d and 1e. Clockwise from the top left: overall SEM, C signal, O signal, background, W signal, Ti signal.

3.4.2 Probe Degradations

Because one of the important questions of modified photocatalysts is whether they are more functional with visible light than undoped TiO_2, the experiments described below were carried out with lamps whose irradiation is centered at 419 nm, to the red of the onset of absorption of the bare catalysts as documented in Figure 1. This light source rests on the edge of the range separating near UV and visible light, but clearly enough, there is more light of this range available from ambient sunlight (the ideal light source) than the more commonly used true UV wavelengths. The irradiation frequencies of this lamp, however, are such that a small amount of light below 380 nm is available. As noted, other irradiations used lamps centered at 350 nm. No irradiations were done using light sources well into the visible (e.g., 500 nm and longer) because the catalysts do not directly absorb any light in these regions.

Initially, 4-methoxyresorcinol (2,4-dihydroxyanisole), was chosen as a probe because it exhibits a mixture of SET and hydroxyl chemistry with P25 and the PC series of catalysts [25,26]. However, initial experiments using 420 nm irradiation indicated a high

degradation efficiency. Subsequent preliminary experiments using a white light source and a 435 nm high pass cutoff filter suggested that any differences between the catalysts were being overwhelmed by visible-light mediated degradation that could be attributed to the formation of a charge transfer complex between this very electron rich arene and TiO_2, analogous to the reports of Agrios and Gray [38,39]. We therefore resorted to the less electron rich probes shown in Scheme 3.1.

3.4.3 Kinetic Traces

The initial degradative steps of probe molecules quinoline (**Q**) and 1-*p*-anisylneopentanol (**AN**) have been discussed at length previously [25,30,31]; the essentials are illustrated in Scheme 3.1 and can be summarized by noting the differing products predominant for single electron transfer (SET) chemistry and hydroxyl-type chemistry. These two probes were chosen for their lack of strong adsorption to the TiO_2 and for their well-defined partial degradation chemistry. Conditions were chosen on the basis of previous work [25] under which both SET and hydroxyl products would normally be observed.

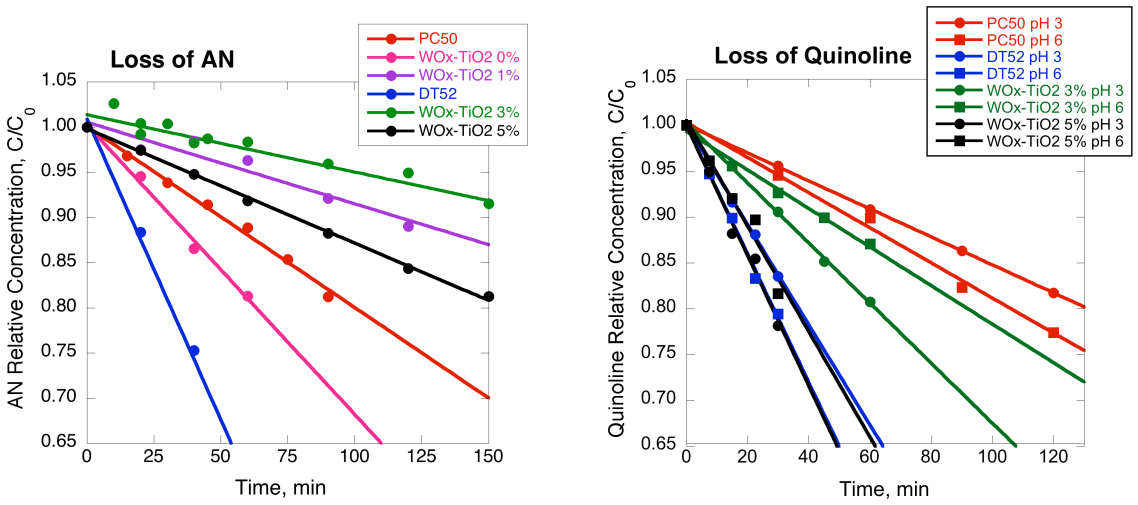

Figure 3.3 Kinetic traces for degradation of **AN** (pH 2) and **Q** (pH 3 or 6) by various photocatalysts using irradiation centered at 419 nm.

Kinetic traces were obtained. As seen in Figure 3.3, which illustrates the data

obtained at 419 nm, the traces could be acceptably fit to zero order decays for degradation of up to approximately 25%. The results are given numerically in Table 3.1, and the values were reproducible within a 5% standard deviation. Immediately striking is the two order of magnitude increase in rate at 350 nm, relative to 419 nm.

Scheme 3.1

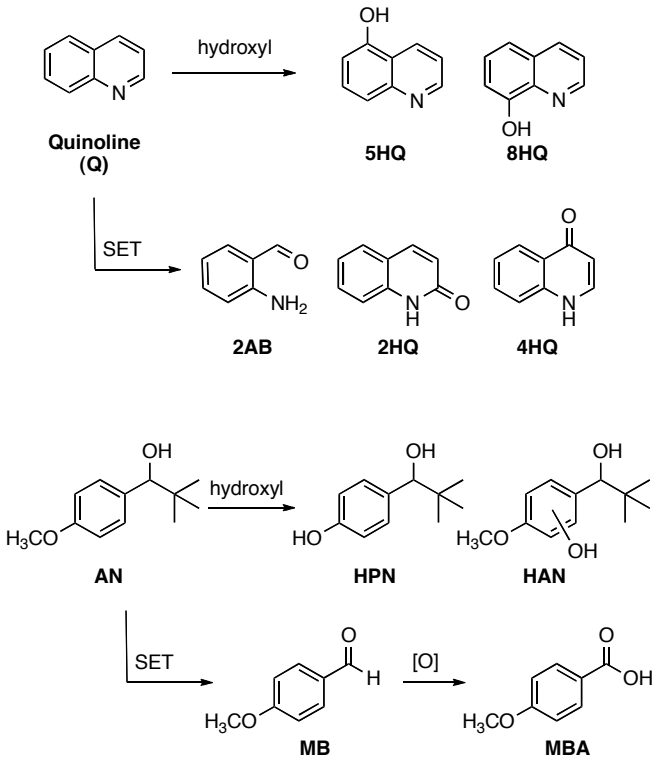

For **AN**, the clearly superior catalyst is DT52, with the others varying without a discernable pattern. The rate of degradation of quinoline is not especially pH sensitive, despite its pKa being between 4.5 and 5, such that the protonated and deprotonated forms are predominant at pH 3 and 6, respectively. Adsorption is difficult to measure quantitatively, but it is expected that quinolinium, due to its greater water solubility and positive charge, would be less adsorbed to the catalyst, which is also positively charged at pH 3. At pH 6, adsorption of quinoline through the nitrogen lone pair is expected. The rate of degradation does not vary much, however, suggesting that adsorption to the catalyst is not rate-determining for this compound.

Table 3.1 Degradation rates of **AN** and **Q** with various catalysts.

Catalyst	Rate (μM/min) [a]					
	AN pH 2 420 nm	**Q** pH 3 420 nm	**Q** pH 6 420 nm	**AN** pH 2 350 nm	**Q** pH 3 350 nm	**Q** pH 6 350 nm
PC50	2.00	1.52	1.91	354	154	287
3% DT52	6.70	5.45	6.99		597	616
0% WO_x–TiO_2	3.20					
1% WO_x–TiO_2	0.90					
3% WO_x–TiO_2	0.63	3.27	2.10		145	329
5% WO_x–TiO_2	1.27	7.09	5.75	179	605	228

[a] All rages were reproducible to standard deviations of ≤5%

3.4.4 Product Studies

The sole product obtained for low conversion of **AN** with the 419 nm bulbs was *p*-methoxybenzoic acid (**MBA**). This is clearly the result of a two-step oxidation whose initial product is *p*-methoxybenzaldehyde (**MB**). The second oxidation step may be photochemical or a result of the formation of hydrogen peroxide and either autoxidation or Bayer-Villager chemistry. In any case, it is clear that **MB** is oxidized more rapidly than it is formed and thus does not accumulate. For the 5% WO_x-TO_2 catalyst, both the usual **MBA** and hydroxylated products (Scheme 3.1) were observed, though the total accumulated intensity of the products was only about 10% of that of the other catalysts. The simplest explanation for the lower accumulation of intermediates is that they are degraded faster than they are formed, implying that the 5% WO_x-TiO_2 catalyst was superior from this perspective.

Table 3.2 Ratio of initial SET products to hydroxyl-type products[a] in quinoline degradations.

Catalyst	pH 3 420 nm	pH 6 420 nm	pH 3 350 nm	pH 6 350 nm
PC50	0.08	9.5	0.11	0.63
3% DT52	0.54	11	0.13	1.2
3% WO_x–TiO_2	0.15	15	0.43	4.3
5% WO_x–TiO_2	0.25	4.2	<0.01	0.89

[a] See Scheme 1.

The 350 nm bulbs were also used to determine product ratios under UV irradiation. In distinct contrast to the 419 nm irradiations, all four products (**MB**, **MBA**, **HPN**, and **HAN**) were found in very comparable amounts for low conversion.

For degradation of **Q**, both $HO•_{ads}$-type products (**5HQ** and **8HQ**) and SET products (**2AB, 2HQ**, and **4HQ**) are observed on 419 nm irradiation. At low pH, where quinoline is protonated, the hydroxyl type products predominate, whereas the SET products are found at higher concentration at pH 6. The ratios of initially formed (SET products)/($HO•_{ads}$-type products) are given in Table 3.2. With 350 nm irradiation at pH 3, the hydroxyl products still predominate; at pH 6, the dominance of SET products declines, relative to the 419 nm values.

3.5 DISCUSSION

In keeping with other publications examining the efficacy of tungstated titanium dioxide catalysts, we find DT52, the tungsten-treated PC50 derivative is more active than its parent material. The same cannot be directly concluded for the sol-gel samples examined here, because the crystal composition of the undoped sol-gel sample is a

qualitatively different mix of anatase and rutile nanodomains than the others, as demonstrated in Figure 1a. From this point of view, it appears that incipient wetness tungsten-coating of otherwise optimized TiO_2 photocatalysts may be an important empirical parameter for use in achieving the most active catalyst possible. Empirically, we are unaware of any evidence suggesting that the presumably homogeneous distribution of WO_x throughout the particle by the sol gel (or other related) methods presents any special advantage in photocatalytic degradations besides stabilizing the anatase crystal structure (the more active titania polymorph) at high temperatures during catalyst preparation.

Two causes for increased reactivity of WO_x-modified TiO_2 have been proposed: the ability of the WO_3 to trap electrons (and thus preserve holes), and an increase of surface acidity, which is thought to improve the binding of Lewis bases [40]. There is not a consistent pattern of rates among the sol-gel prepared samples, but there is a consistent increase in both rate and proportion of SET products, comparing DT52 to PC50. This latter result suggests that enhanced surface binding may be important.

The materials we prepared (and DT52) do not have extensive absorption into the visible. Nonetheless, the 419 nm lamps we used overemphasize irradiation at the very red edge; only a modest percentage of the lamps' output is below 400 nm, and very little below 380 nm. The two order of magnitude change in rates of photolysis comparing 350 to 419 nm bulbs is at least in very large part due to the much smaller absorption of light by our catalysts in the latter case, since the actinometer counts all of the photons, absorbed by catalyst or not.

In our previously published work [25], partial degradation of **AN** with PC50 (or related catalysts) and 350 nm irradiation at pH 2 yielded a product mixture containing similar amounts of SET and $HO\bullet_{ads}$ products. The present data, with the tungstated catalysts, give the same result. However, we find that only the electron transfer products are observed when irradiating at the red edge of the absorption band, with one exception (5% WO_x-TiO_2). A much smaller total sum of products and some hydroxyl chemistry was observed for the 5% WO_x-TiO_2. This result is probably due to more efficient degradation of **MBA** by 5% WO_x-TiO_2. The observation of a small amount of **HAB** and **HPN** is

consistent with the idea that the **MB** and **MBA**, out-compete the **AN** for the specific adsorption locations that lead to SET reactivity (and get degraded in the process). However, it is not obvious why the phenomenon of the more efficient degradation of **MB** and **MBA** is limited to the 5% WO_x sample.

The red edge irradiation used with quinoline as a probe at pH 6 also shows a relative increase for SET products for every catalyst. At pH 3, the effect is less dramatic. In that the relative increase of SET chemistry at 419 nm is observed for PC50 and the undoped sol-gel TiO_2, it is clearly not a special feature due to the tungsten; rather it is an inherent feature of the interaction between the probes and TiO_2. The two simplest explanations are (1) there is a wavelength dependence on TiO_2 photocatalysis at the red edge of absorption that is generally unnoticed because it represents such a small portion of the excitation spectrum; (2) there is a charge-transfer band or other specific interaction between the small population of adsorbed probes and TiO_2 whose light absorption may extend further into the visible than the classic red edge of the catalyst absorption. Charge transfer interactions between arenes and TiO_2 are well documented in more functionalized cases [39,41]. We cannot be definitive here, but prefer the second explanation, given that the effect is much smaller for quinolinium ion at pH 3 than for the other two cases. Qunolinium's positively charged nature presumably inhibits binding to the positively charged TiO_2, and acts as a control – in combination with **AN** at pH 2 – for the effect being mitigated solely by the protonation state of the catalyst under acidic conditions.

3.6 CONCLUSIONS

The results reported here add to the literature that suggests that tungstated TiO_2 can be a catalyst that is functionally superior to its unmodified parent in terms of the speed of degradation for photocatalytic applications. No special advantage was found for sol-gel preparations that presumably disperse WO_x throughout the catalyst over comparable surface-modified species.

As documented by the diffuse reflectance spectra, surface coating of WO_x (e.g., DT52) does not have a significant effect on the light absorbed by the bare photocatalyst.

Any effects on the absorption of the photocatalysts made by the sol gel method may easily derive more from subtly different ratios of anatase and rutile in the annealed catalysts, since WO_x inhibits the conversion to rutile.

Product distributions for partial degradation are affected by the modification of the TiO_2. With surface modification (DT52 vs. PC50), the tendency was for the added tungsten to increase the fraction of SET-derived products, which accompanied an acceleration of overall reaction. This might be explained either by greater adsorption of the organic to the modified catalyst or by a longer lifetime of the SET-active "hole" before finding an alternative trap site that results in hydroxyl chemistry. Of these, the former, simpler explanation is more appealing, but more evidence would be required to be certain.

Also, a wavelength dependence was found. Irradiation at the red edge of TiO_2 absorption (and beyond) favored the cleavage reactions that have been attributed to SET chemistry for **AN** and the regiochemistry of hydroxylation that indicates SET chemistry for **Q**. In the absence of evidence to the contrary, the simplest explanation is a previously unknown charge transfer band formed on adsorption to the catalyst by almost any arene.

3.7 ACKNOWLEDGEMENT

The authors thank the National Science Foundation (CHE 0518586) for financial support of this work. We are grateful to Clemens Burda for allowing us to obtain diffuse reflection spectra on his instrumentation. We also gratefully acknowledge the assistance of Jim Anderegg with the XPS data.

3.8 REFERNECES

(1) Robertson, P. K. J.; Bahnemann, D. W.; Robertson, J. M. C.; Wood, F. *Handbook of Environmental Chemistry* **2005**, *2*, 367-423.

(2) Bahnemann, D.; Cunningham, J.; Fox, M. A.; Pelizzetti, E.; Pichat, P.; Serpone, N. In *Aquat. Surf. Photochem.*; Helz, G. R., Zepp, R. G., Crosby, D. G., Eds. 1994, p 261-316.

(3) Pichat, P. *Environmental Science and Pollution Control Series* **2003**, *26*, 77-119.

(4) Jenks, W. S. In *Environmental Catalysis*; Grassian, V. H., Ed.; CRC Press: Boca Raton, 2005, p 307-346.

(5) Ollis, D. F.; Pelizzettti, E.; Serpone, N. In *Photocatalysis: Fundamentals and*

Applications; Serpone, N., Pelizzetti, E., Eds.; John Wiley & Sons: New York, 1989, p 603-637.

(6) *Photocatalysis: Fundamentals and Applications*; Serpone, N.; Pelizzetti, E., Eds.; John Wiley & Sons: New York, 1989.

(7) Fujishima, A.; Zhang, X.; Tryk, D. A. *Surface Science Reports* **2008**, *63*, 515-582.

(8) Hurum, D. C.; Agrios, A. G.; Gray, K. A.; Rajh, T.; Thurnauer, M. C. *J. Phys. Chem. B* **2003**, *107*, 4545-4549.

(9) Hurum, D. C.; Gray, K. A. *Journal of Physical Chemistry B* **2005**, *109*, 977-980.

(10) Agrios, A. G.; Pichat, P. *Journal of Applied Electrochemistry* **2005**, *35*, 655-663.

(11) Agrios, A. G.; Gray, K. A. In *Environmental Catalysis*; Grassian, V. H., Ed.; Taylor and Francis: Boca Raton, 2005, p 369-390.

(12) Izumi, I.; Dunn, W. W.; Wilbourn, K. O.; Fan, F.-R. F.; Bard, A. J. *J. Phys. Chem.* **1980**, *84*, 3207-10.

(13) Goren, Z.; Willner, I.; Nelson, A. J.; Frank, A. J. *Journal of Physical Chemistry* **1990**, *94*, 3784-90.

(14) Gao, Y. M.; Lee, W.; Trehan, R.; Kershaw, R.; Dwight, K.; Wold, A. *Materials Research Bulletin* **1991**, *26*, 1247-54.

(15) Herrmann, J. M.; Disdier, J.; Pichat, P.; Fernandez, A.; Gonzalez-Elipe, A.; Munuera, G.; Leclercq, C. *Journal of Catalysis* **1991**, *132*, 490-7.

(16) Liu, D.; Kamat, P. *J. Phys. Chem.* **1993**, *97*, 10769-10773.

(17) Nasr, C.; Kamat, P. V.; Hotchandani, S. *Journal of Electroanalytical Chemistry* **1997**, *420*, 201-207.

(18) Hotchandani, S.; Kamat, P. V. *Chemical Physics Letters* **1992**, *191*, 320-6.

(19) Vinodgopal, K.; Bedja, I.; Kamat, P. V. *Chem. Mater.* **1996**, *8*, 2180-2187.

(20) Nasr, C.; Hotchandani, S.; Kamat, P. V. *Proceedings - Electrochemical Society* **1997**, *97-20*, 130-140.

(21) Do, Y. R.; Lee, W.; Dwight, K.; Wold, A. *J. Solid State Chem.* **1994**, *108*, 198-201.

(22) Ramis, G.; Busca, G.; Cristiani, C.; Lietti, L.; Forzatti, P.; Bregani, F. *Langmuir* **1992**, *8*, 1744-9.

(23) Li, X. Z.; Li, F. B.; Yang, C. L.; Ge, W. K. *J. Photochem. Photobiol., A* **2001**, *141*, 209-217.

(24) Papp, J.; Soled, S.; Dwight, K.; Wold, A. *Chem. Mater.* **1994**, *6*, 496-500.

(25) Hathway, T.; Jenks, W. S. *J. Photochem. Photobiol. A* **2008**, *200*, 216-224.

(26) Li, X.; Cubbage, J. W.; Jenks, W. S. *J. Photochem. Photobiol. A* **2001**, *143*, 69-85.

(27) Bahnemann, D. In *Handbook of Environmental Chemistry*; Boule, P., Ed.; Springer: Berlin, Germany, 1999; Vol. 2 L, p 285-351.

(28) Oh, Y.-C.; Li, X.; Cubbage, J. W.; Jenks William, S. *Appl. Catal. B: Environmental* **2004**, *54*, 105-114.

(29) Yan, X.; Ohno, T.; Nishijima, K.; Abe, R.; Ohtani, B. *Chemical Physics Letters* **2006**, *429*, 606-610.

(30) Ranchella, M.; Rol, C.; Sebastiani, G. V. *J. Chem. Soc. Perkin Trans. 2* **2000**, 311-315.

(31) Cermenati, L.; Pichat, P.; Guillard, C.; Albini, A. *J. Phys. Chem. B* **1997**, *101*, 2650-2658.

(32) Cermenati, L.; Albini, A.; Pichat, P.; Guillard, C. *Res. Chem. Intermed.* **2000**, *26*, 221-234.

(33) Rockafellow, E. M.; Fang, X.; Trewyn, B. G.; Schmidt-Rohr, K.; Jenks, W. S. *Chemistry of Materials* **2009**, *Revision submitted*.

(34) Chakraborti, A. K.; Sharma, L.; Nayak, M. K. *Journal of Organic Chemistry* **2002**, *67*, 6406-6414.

(35) Hatchard, C. G.; Parker, C. A. *Proceeding of the Royal Society of London. Series A, Mathematical and Physical Sciences* **1956**, *235*, 518-536.

(36) Fernandez-Garcia, M.; Martinez-Arias, A.; Fuerte, A.; Conesa, J. C. *Journal of Physical Chemistry B* **2005**, *109*, 6075-6083.

(37) Moulder, J. F.; Stickle, W. F.; Sobol, P. E.; Bomben, K. D. *Handbook of X-Ray Photoelectron Spectroscopy*; Perkin-Elmer Corporation (Physical Electronics): Eden Prairie, MN, 1992.

(38) Agrios, A. G.; Gray, K. A.; Weitz, E. *Langmuir* **2003**, *19*, 5178.

(39) Agrios, A. G.; Gray, K. A.; Weitz, E. *Langmuir* **2004**, *20*, 5911-5917.

(40) Tennakone, K.; Ileperuma, O. A.; Bandara, J. M. S.; Kiridena, W. C. B. *Semicond. Sci. Technol.* **1992**, *7*, 423-424.

(41) Agrios, A. G.; Gray, K. A.; Weitz, E. *Langmuir* **2003**, *19*, 1402-1409.

3.9 SUPPORTING INFORMATION

3.9.1 SEM Images

SEM data (Figures 3.S1-3.S5) were collected as mentioned in the experimental section. The homemade W-TiO_2 samples were imaged after annealing and ball-milling. The pictures shown below were chosen as "average" representations of each catalyst, taken at 3,000 times magnification.

Figure 3.S1 SEM image of the 0% WO_x catalyst.

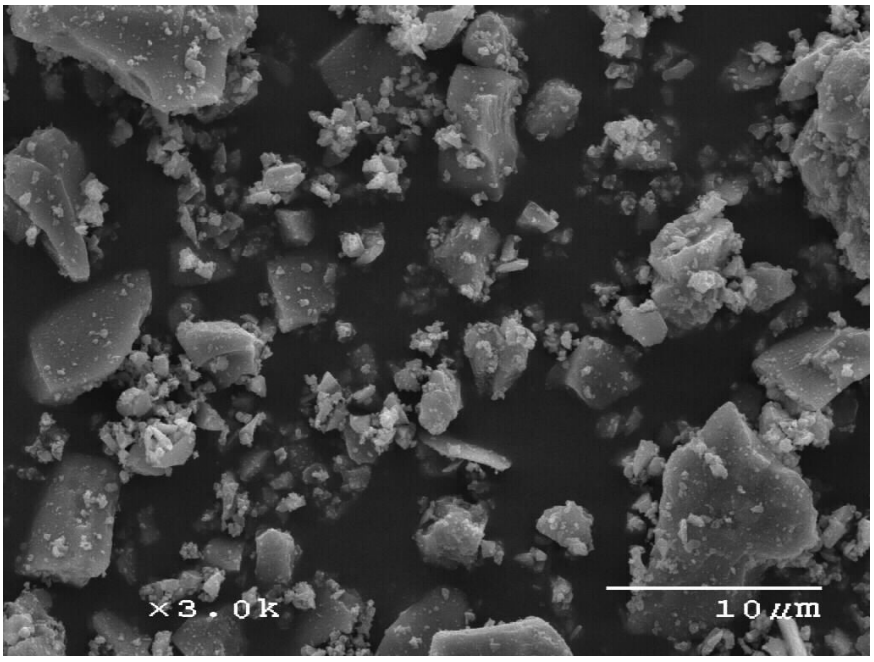

Figure 3.S2 SEM image of the 1% WO_x catalyst.

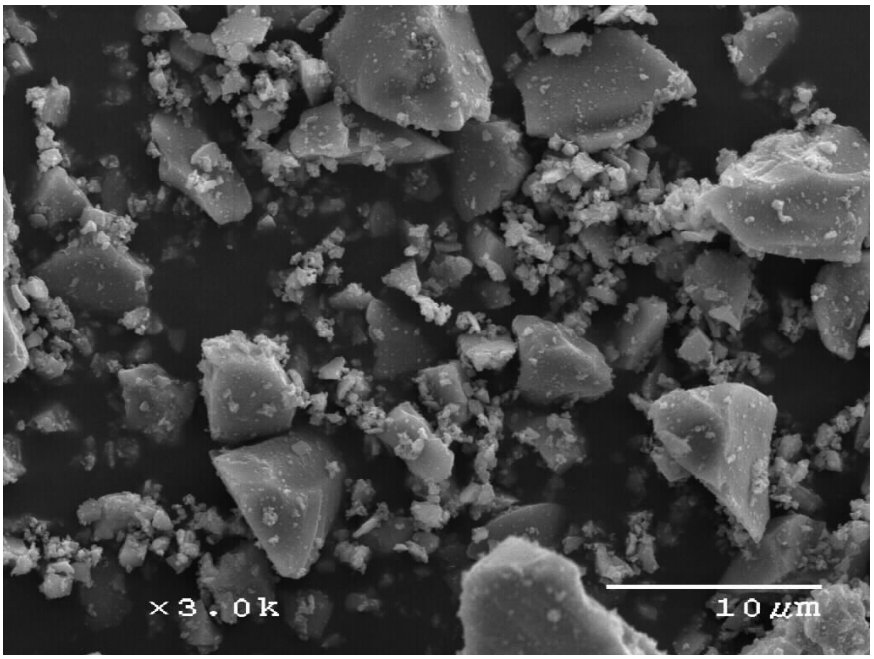

Figure 3.S3 SEM image of the 3% WO_x catalyst.

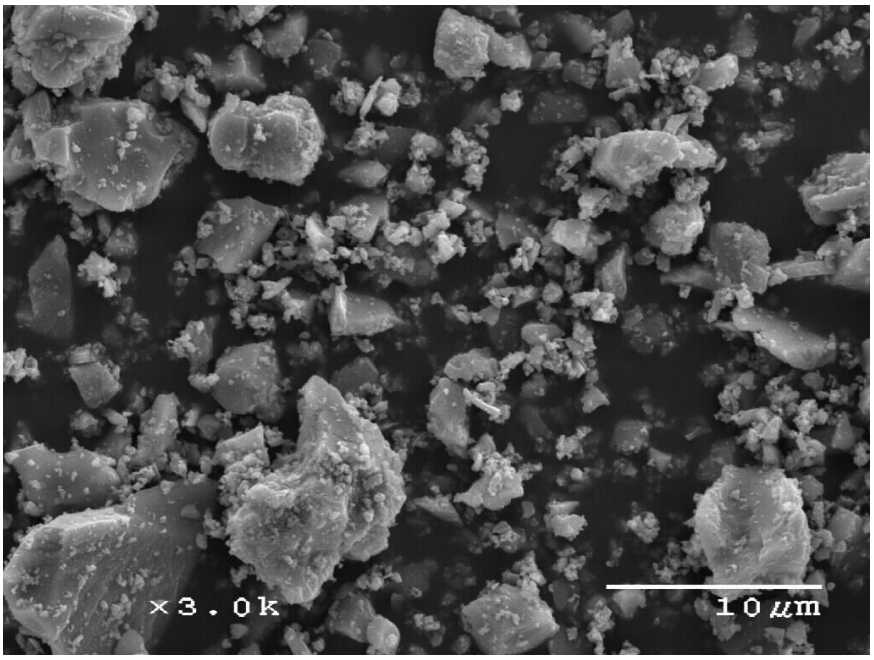

Figure 3.S4 SEM image of the 5% WO_x catalyst.

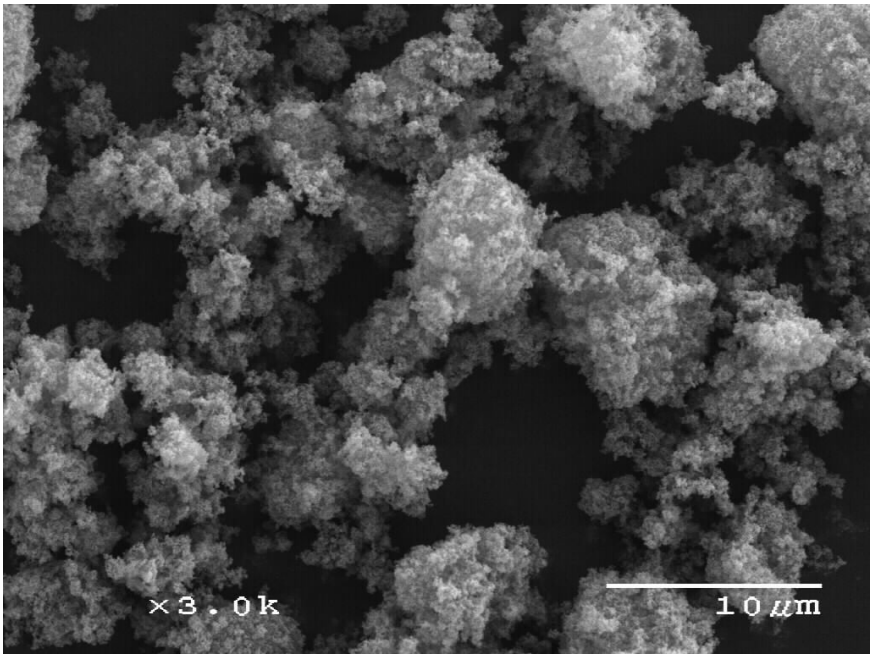

Figure S5. SEM image of the P25 catalyst.

3.9.2 SEM-EDX Maps

SEM-EDX data (Figures 3.S6-3.S10) were collected as mentioned in the experimental section. The homemade W-TiO_2 samples were imaged after annealing and ball-milling. The maps contain six panels: (clockwise from the top left) total SEM, carbon channel, oxygen channel, titanium channel, tungsten channel, and background channel. Each map is shown at 2,000 times magnification, except DT52, which is shown at 10,000 times magnification.

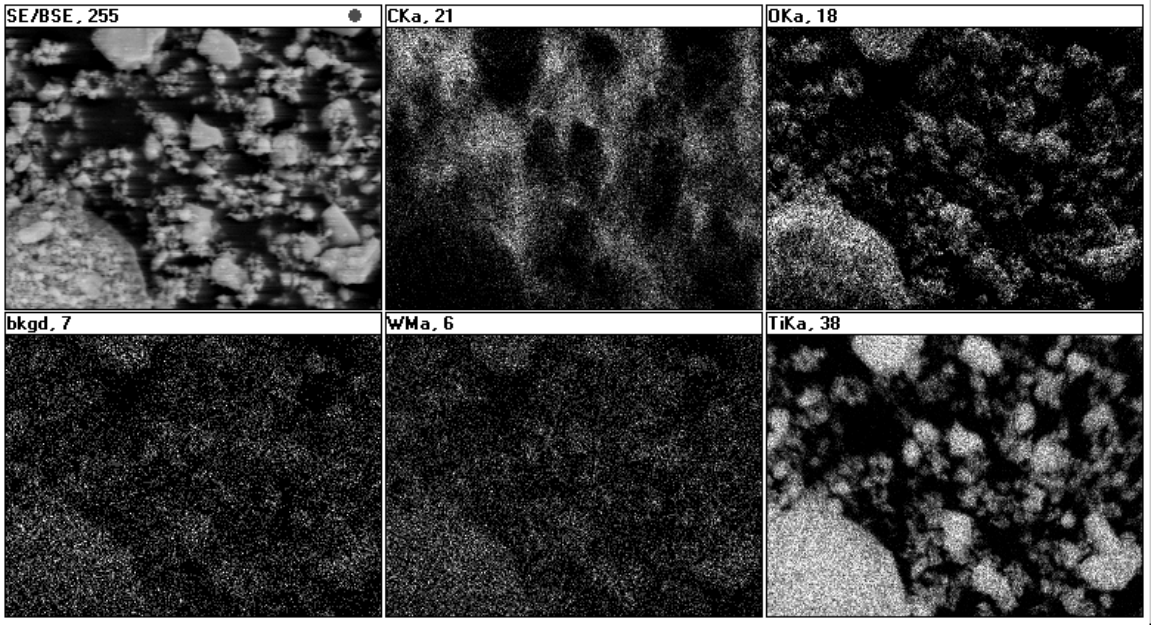

Figure 3.S6 SEM-EDX map of the 0% WO_x catalyst.

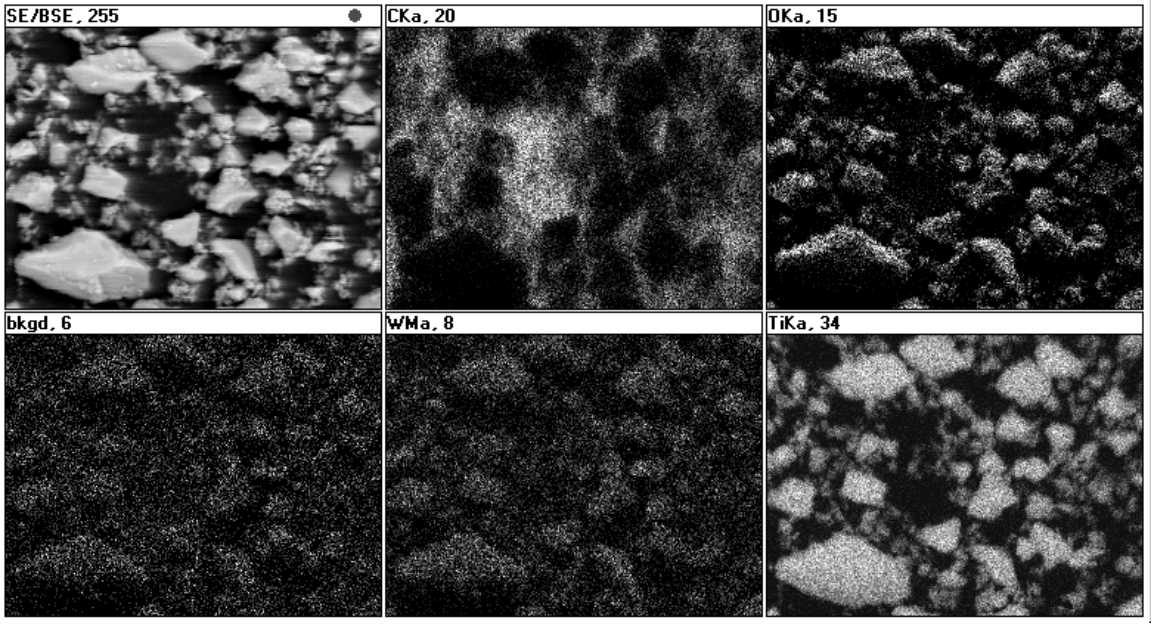

Figure 3.S7 SEM-EDX map of the 1% WO_x catalyst.

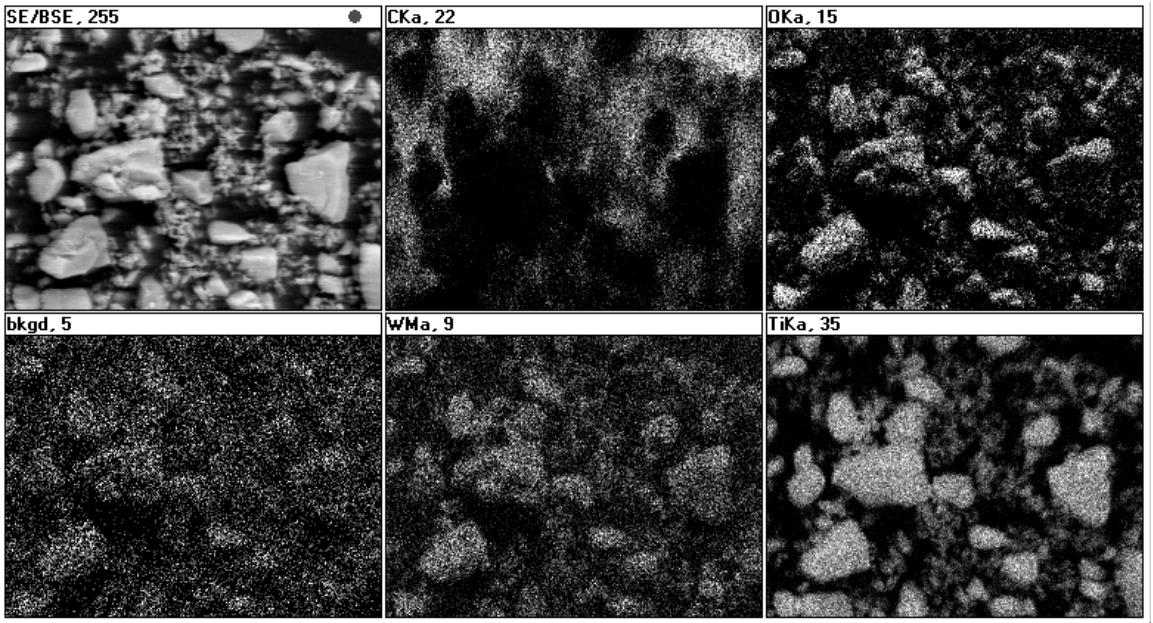

Figure 3.S8 SEM-EDX map of the 3% WO_x catalyst.

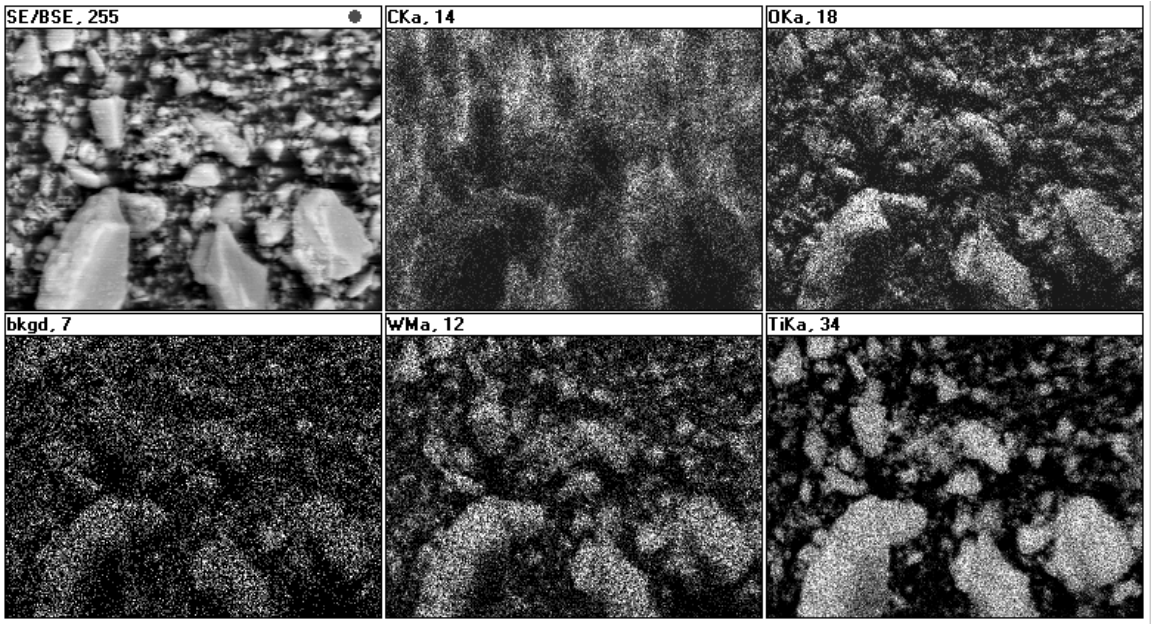

Figure 3.S9 SEM-EDX map of the 5% WO_x catalyst.

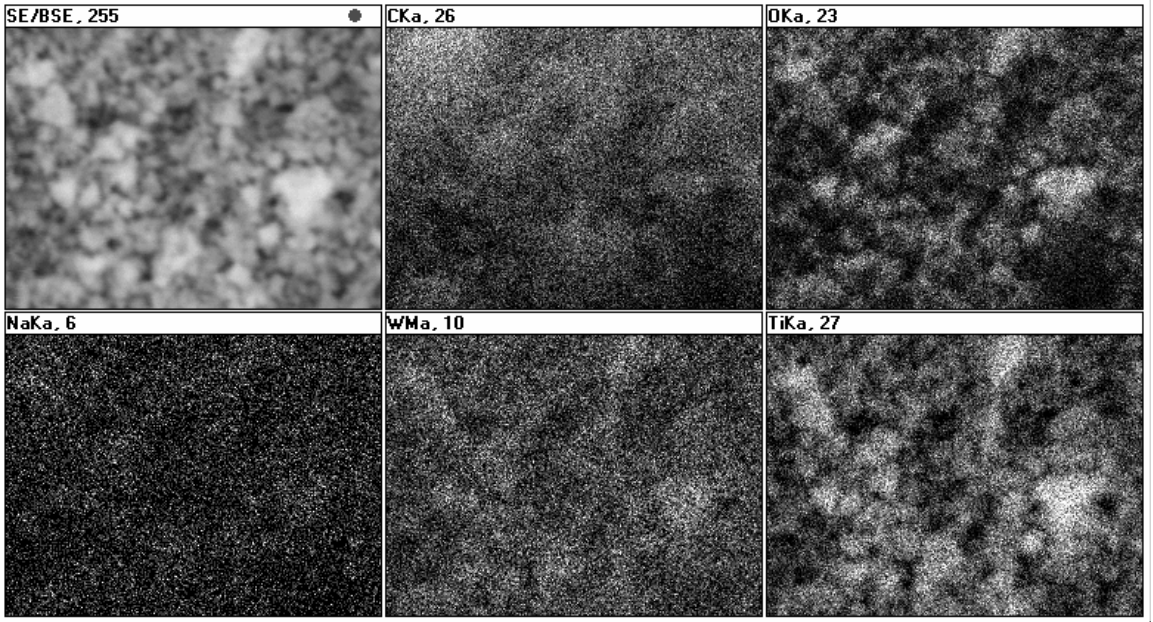

Figure 3.S10 SEM-EDX map of the DT52 catalyst.

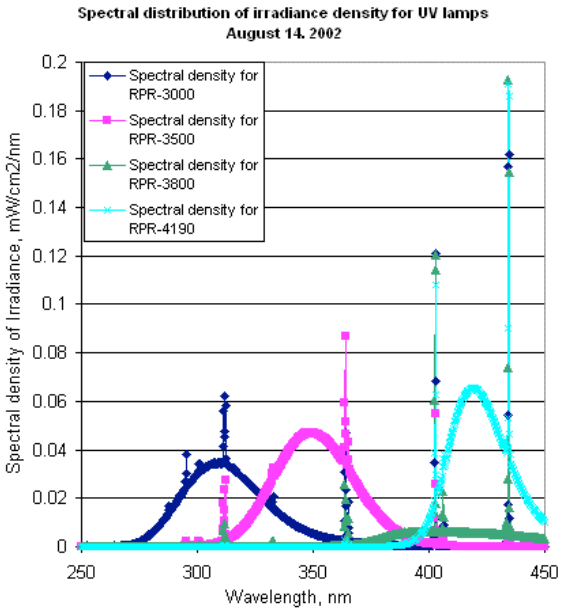

Figure 3.S11 Linear spectral distributions of Rayonet lamps (obtained from http://www.rayonet.org/spectral-graphs.htm, accessed 11/11/2008)

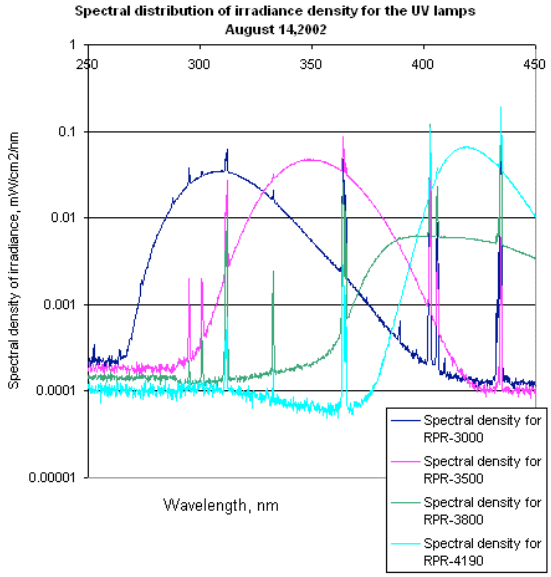

Figure 3.S12 Logarithmic spectral distributions of Rayonet lamps (obtained from http://www.rayonet.org/spectral-graphs.htm, accessed 11/11/2008)

CHAPTER 4

Solid-State ^{13}C NMR Characterization of Carbon-Modified TiO_2

Reproduced from *Chemistry of Materials* **2009**, 21(7), 1187, with permission from American Chemical Society.

Erin M. Rockafellow, Xiaowen Fang, Brian G. Trewyn, Klaus Schmidt-Rohr,* and William S. Jenks*
Department of Chemistry, Iowa State University, Ames, IA 50011-3111

4.1 ABSTRACT

^{13}C-modified TiO_2 was prepared in order to facilitate study of the dopant atoms and trace their chemical fate throughout the process. In the pre-annealed material, NMR showed strong evidence of many Ti-O-C bonds. After annealing, surface-bound coke is a major component. NMR also showed that a washing step before annealing led to the generation of orthocarbonate ($C[OR]_4$) centers, observed at 126 ppm, which are located deep inside the TiO_2 particles. Both NMR and XPS confirmed the presence of small amounts of regular sp^2-hybridized carbonate species in all briefly annealed samples, while annealing for longer times led to a reduction removal of the CO_n centers. Quantitative NMR also shows the degree of carbon loss that accompanies annealing. Some variation in the chemical degradation of quinoline is noted among the catalysts, but coke-containing TiO_2 catalysts are not qualitatively better catalysts for use with visible light with this substrate.

4.2 INTRODUCTION

It is well known that titanium dioxide is one of the most effective photocatalysts for the complete mineralization of pollutants in water and air.[1-8] However, although TiO_2 is cheap, robust, and thermally stable, it is not yet ideal.[9,10] The two most important shortcomings are a low efficiency of photon usage due to rapid recombination of

separated charges and that the onset of absorption, near 400 nm, does not allow sufficient use of terrestrial solar light.

Doping the TiO_2, either with main group elements or transition metals, has emerged as a promising approach for improving the catalyst.[8,10,11] Transition metal dopants have been shown to increase visible absorbance, but the experimental observations often include a decrease in the overall efficiency of the photocatalyst, and sometimes thermal instability.[12-16]

Nitrogen-,[17-21] sulfur-,[22-25] and carbon-doped[24,26-33] titanium dioxides have displayed efficient photocatalytic degradation of some small organic molecules and dyes under visible irradiation. In these materials, the recombination center problem is minimized, if not eliminated.[34-37] Main group doping increases visible absorption by creating narrow, localized bands of orbitals within the band gap, as well as by promoting other defects of the TiO_2 lattice.[38-45] For example, nitrogen doping of TiO_2 has been correlated to an increase in oxygen vacancies, which are believed to be involved with the observed increased visible light activity.[39,41,44,45]

Among the most promising materials is carbon-doped TiO_2,[24,26-33,46-52] hereafter called C-TiO_2. It has been prepared in several ways. Khan *et al.* reported that flame pyrolysis of Ti metal with natural gas produced a dark gray material.[50] The color was attributed to (presumably graphitic) carbon impurities remaining in the material. Simple sol-gel techniques have also been used to produce C-TiO_2 using a wide variety of carbon sources, including the titanium alkoxide precursor itself.[26,53-58]

Characterization of the resulting carbon dopant obviously becomes very important, particularly given the divergent synthetic methods. Both coke[26] and carbonate-type species[54,56-59] have been reported. It was also found that oxidation of TiC to C-TiO_2 yield materials in which reduced carbon species remain from some of the Ti-C bonds being preserved through incomplete oxidation.[29,32,60]

In coming to these conclusions, groups report the results of surface-sensitive techniques, such as X-ray photoelectron spectroscopy (XPS), energy-dispersive X-ray spectroscopy (EDX), or IR spectroscopy. XPS can be particularly useful, in that oxidation states can be immediately determined, but it is not without shortcomings.

While XPS gives a good indication of the higher oxidation states of the carbon dopant, signals from adsorbed ambient carbonaceous materials interfere with those of more reduced oxidation states, making identification and quantification of coke difficult. Argon etching can be used to remove adventitious carbon, but often results in destroying or completely removing the very surface species that may be crucial to the visible photoactivity of the material.[20] The concentration of carbon can instead be determined by EDX, but this technique also suffers from the exposure to ambient carbon.

We report here a study of C-TiO_2 prepared from ^{13}C-labeled glucose following the precedent of Xu *et al*.[56] Labeling with ^{13}C allows the structural tool of solid state NMR to be added to the array of characterization tools to determine the chemical nature of the dopant. We are also able to show that part of the glucose is covalently bound – with extensive rearrangement — to the TiO_2 during the low-temperature aging process and that the catalyst remains chemically effective.

An analogous study has been carried out with several ^{15}N-labeled nitrogen precursors in N-TiO_2.[21] Reyes-Garcia *et al*. were able to observe probable amino, ammonium, nitrate, and imido species. We expand on the techniques used by these authors, allowing us to remark upon the functionality, quantity, and location of carbon within the samples. The photocatalytic ability of the carbon-modified TiO_2 samples is also reported, using quinoline as an organic probe molecule.

4.3 EXPERIMENTAL

Detailed descriptions of the synthetic and analytic methods, along with the degradations, are given in the Supporting information.

4.3.1 Preparation of photocatalysts

The preparation is based on the procedure reported by Xu et al.[56] Briefly, a 20 mM solution of glucose in ethanol was chilled to near 0 ˚C and combined with $TiCl_4$ up to a final Ti concentration of 0.1 M. Aqueous NaOH was added to bring the pH to 5.5, and a yellow material was obtained after standing for ~150 hours. This was dried at 70 ˚C for 12 hours and re-ground.

In that one purpose of our investigation was to understand the chemical fate of the

glucose throughout the process, after grinding, samples were treated in different ways. In some cases (to remove both water soluble salts and any glucose-derived material not covalently bound to the TiO_2), the ground samples were thoroughly washed with water before annealing. This step was not part of the Xu protocol.[56] Either without washing or afterwards, samples were annealed under air at 500 ˚C for 5 minutes, 120 minutes, or not at all.

Table 4.1 Description of preparation and nomenclature for synthesized photocatalysts.

Photocatalyst	Synthesis Description
Undoped TiO_2	Prepared without carbon source; annealing time of 5 minutes
C-TiO_2-5	Prepared with glucose as carbon source; annealing time of 5 minutes
$^{13}C_6$-TiO_2-0	Prepared with uniformly ^{13}C labeled glucose; not annealed
$^{13}C_6$-TiO_2-5	Prepared with uniformly ^{13}C labeled glucose; annealing time of 5 minutes
$^{13}C1$-TiO_2-0	Prepared with glucose containing ^{13}C label at carbon 1; not annealed
$^{13}C_6$-TiO_2-W0	Prepared with glucose containing ^{13}C label at carbon 1; washed after oven drying; not annealed
$^{13}C1$-TiO_2-5	Prepared with glucose containing ^{13}C label at carbon 1; annealing time of 5 minutes
C-TiO_2-W5	Prepared with glucose as carbon source; washed between oven drying and annealing; annealing time of 5 minutes
$^{13}C_6$-TiO_2-W5	Prepared with uniformly ^{13}C labeled glucose; washed between oven drying and annealing; annealing time of 5 minutes
$^{13}C1$-TiO_2-W5	Prepared with glucose containing ^{13}C label at carbon 1; washed between oven drying and annealing; annealing time of 5 minutes
C-TiO_2-120	Prepared with glucose as carbon source; annealing time of 120 minutes

To keep track of these varying materials, a notation is required. The nomenclature used hereafter for the materials follows the format (C)-TiO_2-(prewashed or

not)(calcination time, in minutes), as shown in Table 4.1. "C" represents the presence of carbon and the type of glucose precursor: C is used when the glucose isotopes were at natural abundance, $^{13}C_6$ is for uniformly labeled glucose, and $^{13}C1$ is for the ^{13}C label only at carbon 1. The number after TiO_2 indicates the duration of the annealing time, in minutes. A "W" is added before the calcination number if the sample was washed before annealing.

4.3.2 Routine physical characterization

Physical characterization was carried out using powder X-ray diffraction (XRD), X-ray photoelectron spectroscopy (XPS), and transmission electron microscopy (TEM). Surface area analysis of the materials was performed by nitrogen sorption isotherms in a sorptometer. The surface areas were calculated by the Brunauer-Emmett-Teller (BET) method.

4.3.3 NMR parameters

The NMR experiments were performed on a Bruker DSX400 spectrometer at 400 MHz for ^{1}H, 100 MHz for ^{13}C. A Bruker 4-mm triple-resonance magic-angle spinning (MAS) probe head was used for measurements at various MAS speeds. ^{13}C and ^{1}H chemical shifts were referenced to TMS, using the COO resonance of α-glycine at 176.49 ppm as a secondary ^{13}C reference and the proton resonance of NIST hydroxyapatite at 0.18 ppm as a secondary ^{1}H reference. The 90° pulse lengths were 4 μs for both ^{13}C and ^{1}H.

High-speed quantitative ^{13}C DP/echo/MAS NMR. In order to quantitatively account for the glucose carbon in TiO_2 particles, quantitative direct polarization (DP) /MAS ^{13}C NMR spectra were acquired at 14 kHz MAS. A Hahn echo was used to avoid baseline distortions and two-pulse phase modulation (TPPM) decoupling was applied during detection. The recycle delays were estimated by measuring cross-polarization (CP)/T_1/TOSS[61] (total suppression of sidebands) spectra with two or three different $T_{1,C}$ filter times. The $T_{1,C}$ filter time where the remaining carbon signals were less than 5% of the full intensity was chosen as the recycle delay of the quantitative DP/MAS experiment to ensure that all carbons are essentially fully relaxed. More details are given in ref [62].

The recycle delays ranged between 6 and 25 s for the uniformly ^{13}C-labeled materials, and were 100 s for the samples made from singly (^{13}C1-)labeled glucose. The measuring time per spectrum was typically 1.5 h. Corresponding quantitative ^{13}C NMR spectra of nonprotonated carbons and of mobile segments were obtained after recoupled dipolar dephasing of 68 μs duration.

^{13}C chemical-shift-anisotropy filter. The ^{13}C chemical-shift-anisotropy (CSA) filter technique[63,64] with five pulses was used to select signals of sp^3-hybridized (alkyl) carbons, which have small CSAs due to their nearly tetrahedral bonding symmetry. A filter time of 38 μs and a spinning frequency of 5 kHz were used. For samples that had not been annealed, cross polarization was used to generate the signal, while direct polarization was used for annealed samples. During detection, TPPM decoupling was applied.

CH spectral editing. The signals of methine (CH) carbons can be selectively observed based on the CH-group multiple-quantum coherence not being dephased by the spin-pair CH dipolar coupling, while CH_2 group coherence is dephased by the dipolar coupling of the carbon to the second proton.[65] The residual quaternary carbon and partial CH_3 carbon signals were subtracted out by acquiring a second spectrum under the same conditions with an additional 40 μs gated decoupling before detection. The spinning frequency was 5.787 kHz and the recycle delay was 1.5 s.

CH_2 spectral editing. Spectral editing of CH_2 signals was achieved by selection of the three-spin coherence of CH_2 groups, using a ^{13}C 90^o pulse and ^{1}H 0^o/180^o pulses applied after the first quarter of one rotation period with MREV-8 decoupling.[66] The spinning frequency was 5.787 kHz.

Two-dimensional ^{13}C-^{13}C spin exchange. In order to see the C-C connectivities in the C_6-TiO_2-0 sample, a mixing time of 50 ms was used to produce the dipolar ^{13}C-^{13}C spin exchange. For sideband suppression, TOSS was applied before and time-reversed TOSS after the evolution time,[67,68] and normal TOSS was used before detection. Direct polarization with an 8-s recycle delay was used, at an MAS frequency of 7 kHz. The total measurement time was 10 h.

Selection of signals of isolated ^{13}C spins. In order to determine if the ^{13}C giving

rise to a specific resonance is bonded to another ^{13}C, dephasing by the homonuclear J-coupling was measured. The dephased signal S after 10 ms of evolution under the J-coupling shows only the signals from isolated ^{13}C spins. A reference signal S_0 of all spin pairs and isolated ^{13}C spins was generated by a Hahn-solid-Hahn echo[69] that refocuses the J-coupling.[70] Direct polarization (DP) at an MAS frequency of 14 kHz was used to obtain clear signals from all carbons.

$^{13}C\{^1H\}$ HARDSHIP NMR. HeteronucleAr Recoupling with Dephasing by Strong Homonuclear Interactions of Protons (HARDSHIP)[71] NMR experiments were performed in order to estimate the distance of the orthocarbonate carbons from the nearest ^1H spins, presumably at the surface of the TiO_2 particles. The spinning frequency was 6.5 kHz.

^{13}C T_1 relaxation measurements. The ^{13}C T_1 relaxation behavior was measured by DP/T_1/TOSS with a 20-s recycle delay.[72] The T_1-filter times varied from 0 to 20 s.

4.3.4 Degradations

Suspensions containing 150 μM quinoline and the catalyst (1.0 g/L) were prepared, thoroughly stirred and saturated with O_2 before photolysis. Reactions were irradiated using the output of broad range 4 W fluorescent tubes centered at 350 nm or light from a 75 W Xe arc lamp passed through a water filter and a 495 nm long pass filter. Small aliquots were removed at appropriate time for kinetics runs, and the concentrations of the partial degradation products were determined by HPLC after removal of the TiO_2.

4.4 RESULTS AND DISCUSSION

4.4.1 Catalyst preparation.

The preparation of C-TiO_2 by Xu *et al.*[56] presented a chemically sensible means by which carbon could be covalently attached to the developing TiO_2 framework and was adopted as a model. In most respects, the reported method was used in preparing the current carbon-doped catalysts from glucose and $TiCl_4$.[56] An aging time of 150 h was used, following Xu's report of greatest visible light activity. The material obtained after centrifuging the sol-gel was oven dried at 70 ˚C for about 12 hours.

Characterization of the carbon component by NMR at various stages of the synthesis

was a consideration, so after the drying stage, different treatment sequences were undertaken, as shown in Table 1. The variables were whether the dried sample was washed with water before annealing (to remove NaCl and water-soluble glucose-derived components present only as a physical mixture in the TiO_2) and the length of time of annealing at 500 ˚C under air. Annealing times were 0, 5, or 120 min, as noted.[73] All carbon-modified materials annealed for 5 minutes without the additional washing step were dark gray in color. The other annealed samples were an obviously lighter shade of gray.

4.4.2 Characterization of annealed samples by XRD, TEM, XPS, and UV/Vis.

Four classes of samples, including the undoped control material TiO_2-5, were thoroughly characterized by the classic methods used for these photocatalytic materials, as shown in Figures 4.1 and 4.2. The material prepared under conditions most similar to Xu was C-TiO_2-5. C-TiO_2-120 was used to determine whether C-TiO_2-5 would undergo further changes if held at the annealing temperature of 500 ˚C for a longer time, and C-TiO_2-W5 was used to help determine whether all of the dopant material was covalently bound to the TiO_2 matrix before the annealing step.

Analysis of all four samples by XRD (Figure 4.1a) showed them all to be anatase, with average particle diameters of 9-10 nm, as determined by Scherrer's formula ($d = 0.9\lambda/\beta_{1/2}\cos\theta$). TEM images (Figure 4.2) showed particles with sizes ranging from 5-15 nm, in good agreement. Surface areas, determined by the BET method of N_2-sorption, were also similar, e.g., 100 m^2/g for C-TiO_2-5, 110 m^2/g for C-TiO_2-5, and 114 m^2/g for C-TiO_2-120.

Diffuse reflectance UV/Vis spectra (Figure 4.1b) showed the typical onset of absorption near 380 nm for TiO_2-5, i.e., the undoped TiO_2. Only a subtle red-shift in this absorption is observed in the doped samples. A dramatic increase in non-specific absorption throughout the visible was observed for C-TiO_2-5, consistent with its gray color. DiValentin has suggested that carbon substituting for Ti (see below) does not significantly alter the band structure of the TiO_2, potentially resulting in materials with little visible-light activity.[42] Evidence for several other carbon-containing functional

group structures, including coke – which is probably responsible for the non-specific visible absorption – is presented below.

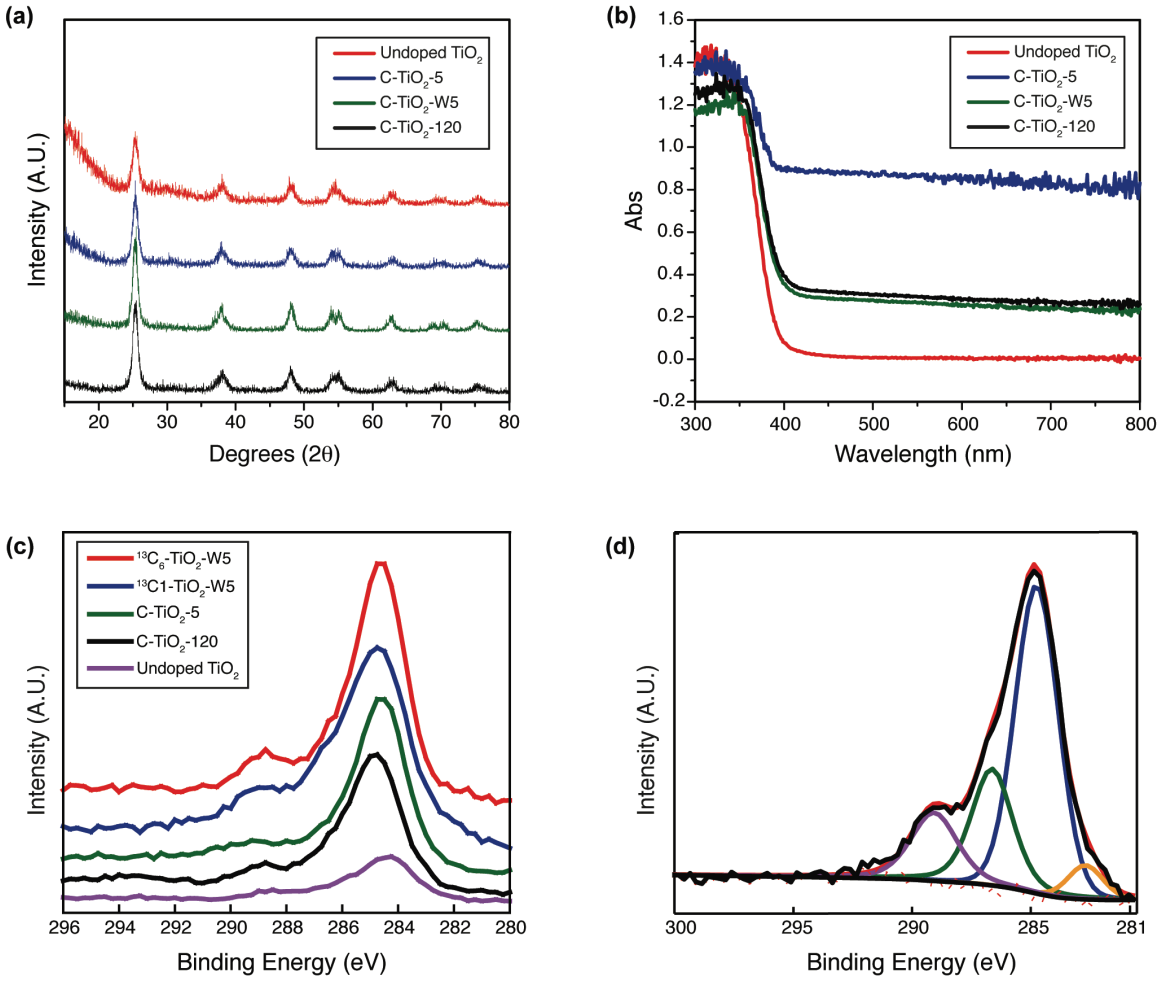

Figure 4.1 (a) X-Ray powder diffraction patterns, (b) diffuse reflectance spectra and (c) XP spectra of undoped and doped titania. (d) Fitted XP spectrum of ^{13}C1-TiO$_2$-W5. Maxima are at 282.4 eV, 284.7 eV, 286.5 eV, and 288.9 eV. See text for discussion.

XPS was used initially to address the character of the carbon dopant in C-TiO$_2$-5, the "baseline" doped catalyst and look for other impurities. Both sodium and chloride were detected in C-TiO$_2$-5, presumably due to the presence of these ions in the sol-gel reaction mixture. Multiple types of carbon centers were observed. There are three major components in the C1s region with binding energies of 288.9 eV, 286.5 eV, and 284.7 eV (Figure 4.1c). The first two are assigned to carbonate esters and carbonyls (C=O)

respectively, based on known chemical shifts.[74] The 284.7 eV peak is attributable to other reduced carbonaceous material (C-C/C-H), which can be coke and/or ambient atmospheric species deposited on the surface. Fitting the data to Gauss-Lorentz curves (70 – 95% Gauss) reveals a small shoulder at 282.4 eV, possibly arising from a Ti-C bond. This phenomenon is illustrated using the spectrum of C-TiO_2-W5 in Figure 4.1d. Argon etching and remeasurement generally resulted in significant reduction of the peaks attributed to oxidized carbon species, leaving mostly C-C/C-H species and the shoulder at 282.4 eV. The signal at 282.4 eV often became more prevalent after argon etching. Since the materials are annealed under oxidative conditions, it is more likely that this Ti-C species suggested by the 282.4 eV peak is present as an interstitial carbon also bound to oxygen, as opposed to a highly reduced carbon substituting for oxygen.[42,75]

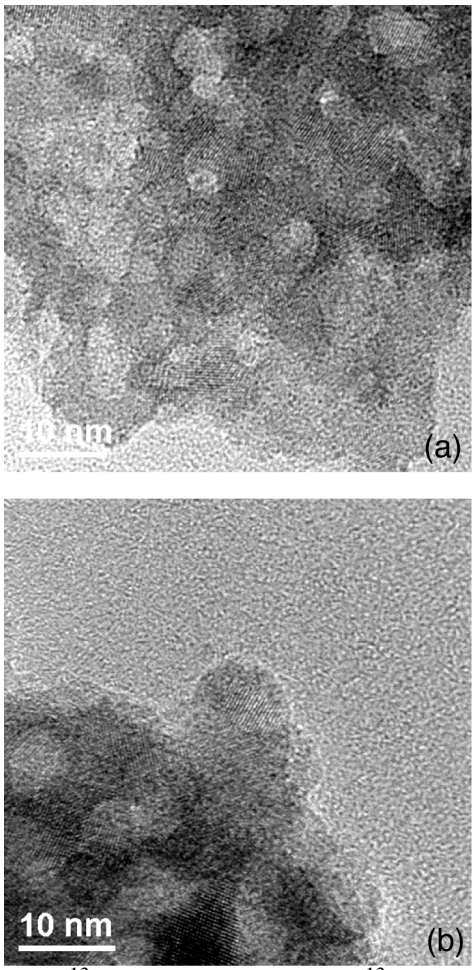

Figure 4.2 TEM images of (a) ^{13}C1-TiO_2-W5 and (b) $^{13}C_6$-TiO_2-5 on same scale.

Annealing the sample for two hours, rather than 5 minutes (i.e., C-TiO_2-120) resulted in a material that was visibly lighter in color, and this is reflected quantitatively in the UV/Vis spectrum (Figure 4.1b) but the XPS data were essentially unchanged from C-TiO_2-5.

Insertion of a washing step before annealing (C-TiO_2-W5), as expected, resulted in a material in which no sodium nor chloride was detected by XPS. The carbon portion of the XP spectra was essentially unchanged. However, the C-TiO_2-W5 was a lighter color, quite similar to that of C-TiO_2-120, as reflected in the UV/Vis data. This suggested that there was less organic material, and pointed out some of the difficulty of quantifying the carbon by XPS.

XPS data were also collected for the undoped TiO_2-5 as a control. Neither sodium nor chloride was detected. However, a smaller but easily detectable amount carbon was seen, with weaker signals at 288.9 eV, 286.5 eV, and 284.7 eV.[76] Importantly, however, no carbon remained detectable after argon etching of thoroughly washed TiO_2-5.

4.4.3 NMR analysis.

The controls in the XPS data suggest that the those spectra indeed do reflect "ambient" carbon when obtained under ordinary aerobic conditions. NMR data were obtained for analogous materials prepared with ^{13}C-labeled glucose to increase sensitivity and allow for measurement of C-C coupling. Also, the NMR data reveal more detail about functional group identity and location.

Analysis of pre-annealed samples. ^{13}C NMR spectra of the samples after glucose is exposed to the titanium-containing precursor but before annealing ($^{13}C_6$-TiO_2-0) are shown in Figures 4.3 and 4.4. The reaction causes significant changes to glucose, as seen by the comparison to a reference spectrum in Figure 3a. The quantitative spectrum of Figure 4.3b exhibits many new bands, spanning much of the spectral range of ^{13}C. They can be assigned based on their chemical shifts and CH_n spectral editing, as shown in Figures 4.3b-4.3e. The strongest signal, at ~83 ppm, with a shoulder at ~73 ppm, is due to OCH methine groups (Figure 4.3d). Several unresolved bands of O-CH-O methine groups are detected between 100 and 115 ppm, but there are no signals of CH groups not bonded to O, which would resonate at ~ 50 ppm. In the CH_2-only spectrum of Figure

4.3e, we observe not only a C-CH_2-C resonance at 38 ppm and a CH_2-OH peak at 63 ppm, but also a strong OCH_2 methylene band with a maximum at an unusually high frequency chemical shift of ~78 ppm. A strong COO ester-type signal at 183 ppm, as well as weaker signals of ketones at ~210 ppm, of CH_3 groups at ~22 ppm, and of aromatic C (mostly furan at ~150 ppm) are identified after C-H dipolar dephasing (Figure 4.3b, thin line).

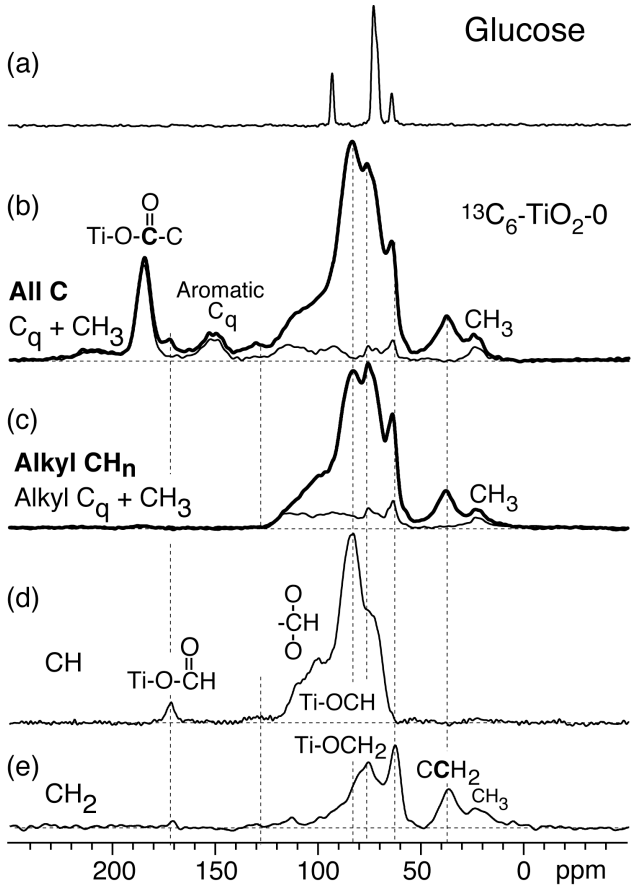

Figure 4.3 ^{13}C NMR spectra of materials before annealing. (a) Spectrum of glucose for reference. (b) – (e) Spectra of $^{13}C_6$-TiO_2-0 with spectral editing. (b) Quantitative spectrum of all C (thick line), and corresponding spectrum of nonprotonated C plus CH_3 (thin line) at 14 kHz MAS. (c) Spectrum after a chemical shift anisotropy (CSA) filter, which selects signals of sp^3-hybridized carbons (thick line), with signals extending to 120 ppm. The corresponding spectrum of quaternary carbon and CH_3 signals (thin line) was selected by 40 μs of gated decoupling before detection. (d) CH-only and (e) CH_2-only

spectra. All CH are polar alkyl and substituted by oxygen, according to their high-frequency chemical shift.

The resonance frequencies of the strongest OCH methine, O-CH-O methine, OCH_2 methylene, and COO ester-type signals are all at unusually high frequencies, by about 10 ppm, from their usual positions in organic compounds.[77] This is an indication of bonding to Ti via the O, since the literature shows a comparable chemical shift for ^{13}C in Ti-O-CH_2 groups.[78] After a chemical shift anisotropy filter that selects sp^3 hybridized carbons (Figure 4.3c), the alkyl signals are seen to extend to 130 ppm, again at unusually high frequency.

The CH-only spectrum (Figure 4.3d and Figure 4.4c) also reveals a small signal of an unusual methine resonating at 170 ppm, which is found to be an isolated ^{13}C (not bonded to other C) in J-dephasing experiments. On that basis, the peak at 170 ppm is assigned to a formate ester R-O-CHO, where the unusually high frequency chemical shift from 160-165 ppm for R = C[77] indicates that R = Ti. By control experiments described in the Supporting Information, we have excluded that the simple harshly acidic reaction conditions were responsible for the high-frequency chemical shifts (and the other rearrangements of glucose). We cannot rule out a small amount of direct C-Ti bonding, as hinted at by the XPS data, which might be obscured by other oxygenated functionality.[79]

Further information about the connectivity of the observed carbon species was obtained by selective labeling from glucose-$^{13}C1$ and by ^{13}C-^{13}C correlations on the fully ^{13}C-labeled sample. The spectrum of $^{13}C1$-TiO_2-0 (i.e., dried, but unannealed material) is dominated by the COO-Ti signal; comparison with the peak intensity for the fully labeled sample shows that glucose C1 accounts for only about half this species. This proves that significant rearrangement involving C1 has occurred. In addition, the glucose C1 site contributes to about half of the C-CH_3 species, but does not form C-CH_2-C methylenes and relatively little OCH methine or OCH_2 methylene. A large fraction of the O-CHR-O methine species comes from C1, as in the original structure glucopyranose.

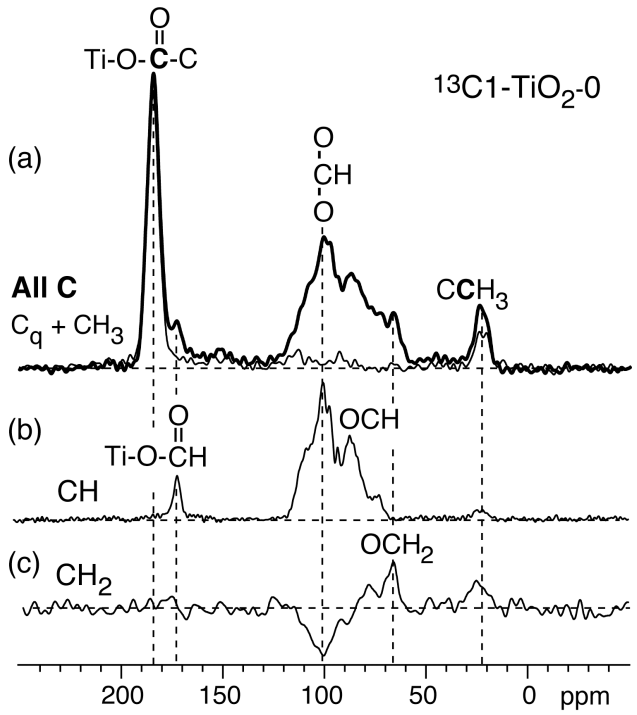

Figure 4.4 ^{13}C NMR of ^{13}C1-TiO$_2$-0 with spectral editing. (a) Quantitative spectrum of all C (thick line) and nonprotonated C (thin line) at 14 kHz MAS. (b) CH-only and (c) CH$_2$-only spectra. The negative signal intensity in (c) is an artifact of the dominant CH band present in the all-C spectrum.

The ^{13}C-^{13}C correlation spectrum of ^{13}C$_6$-TiO$_2$-0 is shown in Figure 4.5a. It shows pronounced cross peaks between COO and OCH methine, COO (ester-type) and CH$_2$ (meaning C-CH$_2$-C), OCH methine and other OCH methines, OCH methine and OCH$_2$ methylene, OCH and CH$_2$, as well as OCH and O-CH-O signals. Based on these and the ^{13}C1 labeling pattern, we propose two likely six-carbon fragments (Figure 4.5b). They account for the observed cross peaks of both CH$_2$ (not bonded to O) and Ti-O-CH carbons to COO groups, which were shown to be predominantly contributed by C1 of glucose. The CH$_2$-CH-O-Ti, OCH-CHO, and OCH-CH$_2$-O-Ti connectivities of the model structures are also seen in the spectrum. The cross-peak pattern of furan (150–110 ppm) is also detected. Other structures accounting for the remaining carbon species must also be present and might be identified in a more detailed study; however, since high-

temperature annealing greatly transforms the existing structures, the details of these structures may be of limited relevance for the final forms of carbon in the TiO_2 photocatalyst.

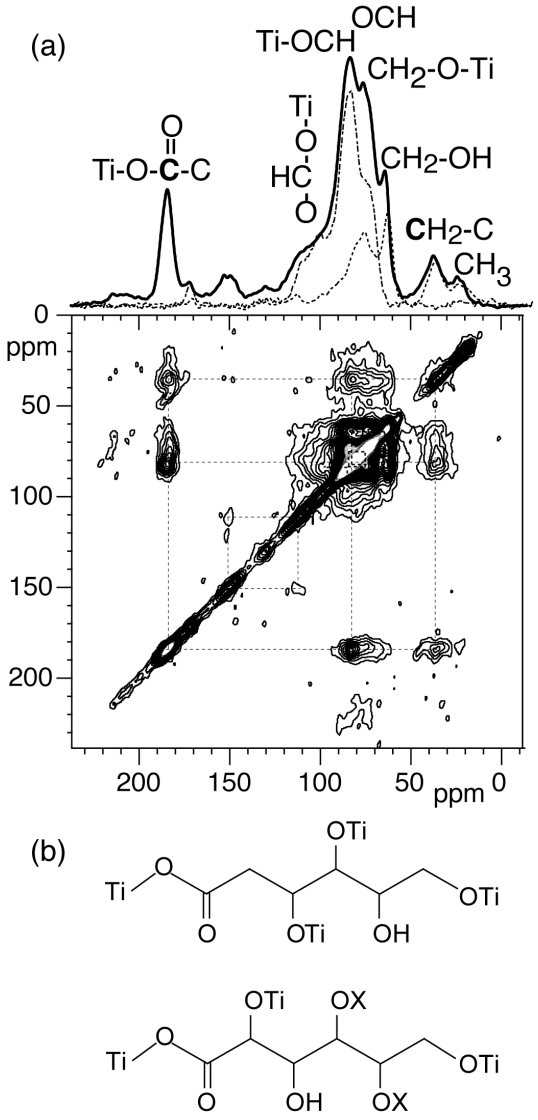

Figure 4.5 (a) Two-dimensional ^{13}C-^{13}C correlation spectrum of $^{13}C_6$-TiO_2-0 with a mixing time of 50 ms at 14 kHz MAS. At the top, one-dimensional spectra of all C (thick line), CH (dash-dotted line), and CH_2 (dashed line) are shown superimposed to facilitate peak assignment. (b) Two structural fragments consistent with the observed cross peaks in (a).

Figure 4.8 compares ^{13}C NMR spectra of samples with and without washing with water but without annealing (^{13}C-TiO_2-W0 vs. ^{13}C-TiO_2-0). Only subtle changes are observed (Figures 4.8a and 4.8b). Washing removes the minor furan-like components and increases the signal for some C=O species, which in effect fill the volume vacated by the components that were washed out. However, after collection and lyophilization of the aqueous washes, little organic material was observed by either ^{1}H or ^{13}C solution-phase NMR, confirming that most of the material removed by the washing step was NaCl.

NMR of annealed samples. High-temperature annealing dramatically alters the forms of carbon in the samples, mostly leading to dehydration and condensation. The spectra in Figure 4.6a,b for samples annealed at 500 ˚C for 5 and 120 minutes ($^{13}C_6$-TiO_2-5 and $^{13}C_6$-TiO_2-120), respectively, are dominated by a broad aromatic-carbon band at 130 ppm. Of these aromatics, 72 ± 2% are not protonated which suggests fused aromatic rings. (For example, all of the protons of benzene are protonated, and essentially none of those in a large graphene sheet are protonated.) In addition, a clear shoulder between 170 and 200 ppm, assigned to C=O species, is observed if the sample annealed for only 5 minutes ($^{13}C_6$-TiO_2-5), and the total signal intensity is greater.

When the washing step is inserted between drying and annealing (^{13}C-TiO_2-W5), an interesting and reproducible spectral feature is observed that is not found using any of the other protocols: a sharp peak at 126 ppm (Figure 4.7). This peak integrates to 37% of the total intensity, and it is also noted that the carbonate ester peak (Figure 4.8) is more pronounced. While the chemical shift of 126 ppm might initially suggest an aromatic carbon, spectral editing proves that it must be assigned to a tetracoordinate alkyl orthocarbonate (CO_4) functionality. Gated decoupling proves that this is a nonprotonated carbon (Figure 4.7a). It experiences no J-coupling to another ^{13}C, as proved by the absence of J-dephasing (Figure 4.7b); thus, it cannot be bonded to ^{13}C, which rules out an aromatic structure. This is confirmed by the minimal dephasing by a CSA-filter, which is characteristic of an sp^3-hybridized carbon with nearly tetrahedral bonding symmetry.[63]

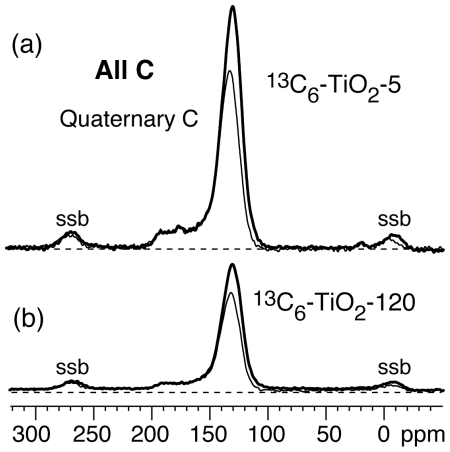

Figure 4.6 Comparison between the quantitative ^{13}C NMR spectra of (a) $^{13}C_6$-TiO_2-5 and (b) $^{13}C_6$-TiO_2-120, plotted on a correct relative vertical scale. Thick lines: spectra of all C; thin lines: spectra of quaternary C. Spinning frequency: 14 kHz. Spinning side bands are marked ssb.

Given that the four bonds cannot be to carbon or hydrogen, orthocarbonate is the only reasonable structure. Such a structure is in good agreement with the observed unusually high field chemical shift: ketals and acetals resonate around 100 ppm, orthoesters at approximately 115 ppm, and orthocarbonate bands generally arise around 120 ppm.[77] To the best of our knowledge, no previous reports of an orthocarbonate center in TiO_2 have been made. The narrow lineshape (Figure 4.7c) is indicative of a well-defined crystalline environment, strongly suggesting that the orthocarbonate centers are incorporated into the TiO_2 lattice. Direct substitution of C for Ti, which would result in hexacoordinate carbon, seems unlikely given the DFT calculations of Di Valentin *et al.*[42] which did not yield any low-energy structure with six-coordinate C for anatase or rutile. Instead, substitution of C for Ti ("$C_{S\text{-}Ti}$") in anatase has been predicted to result in a low-energy structure with C in a tetrahedral bonding environment.[42]

A distinct ^{13}C signal is also observed around 163 ppm. Lack of C-H dipolar and C-C J-dephasing (Figure 4.7a,b) shows that this carbon also is not protonated and not bonded to another C. However, its signal is suppressed by the CSA filter, proving that this is an sp^2-hybridized C. On this basis, we identify this as a CO_3 (regular carbonate) moiety,

which is in good agreement with its chemical shift. According to di Valentin et al., such a planar CO_3 unit can be formed by interstitial ("C_I") carbon in anatase.[42]

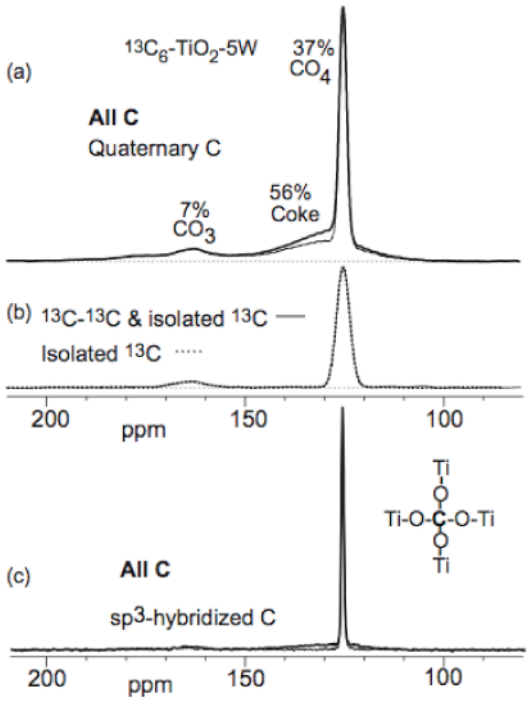

Figure 4.7 ^{13}C NMR spectra of $^{13}C_6$-TiO_2-W5. (a) Quantitative (DP) spectrum of all C (thick line) and corresponding spectrum of nonprotonated C (thin line). Strong line broadening was applied to make the coke and CO_3 bands better visible. (b) J-modulated dephasing spectra. Solid line: Reference spectrum S_0 of ^{13}C-^{13}C spin pairs and isolated ^{13}C spins. Dashed line: Spectrum S after dephasing by ^{13}C-^{13}C J-coupling. The two spectra are very similar and prove that the two sharp peaks are from isolated carbons. Strong line broadening was applied to make the CO_3 band better visible. (c) Selection of sp^3-hybridized C by a five-pulse CSA filter. Thick line: reference spectrum with minimum CSA dephasing time (1 μs). Thin line: spectrum after a CSA dephasing time of 38 μs at 6.5 kHz MAS. In this spectrum with minimal line broadening applied, the small natural width of the peak at 126 ppm is apparent.

The dephasing of the orthocarbonate signal in $^{13}C\{^1H\}$HARDSHIP[71] distance

measurements, is very slow compared to coke in the same sample and still slow relative to that of carbon in 4.8-nm diameter nanodiamond with protonated surfaces, as shown in Figure 4.9. This indicates that the orthocarbonate species is far (> 1 nm) from any ^{1}H: it is thus not a surface species, which may be why it is not observed in the XP spectrum. By contrast, the fast dephasing of the coke signal in Figure 4.9 demonstrates that the coke component is close to protons, suggesting this species is on the surface containing aromatic C-H and possibly nearby Ti-OH bonds.

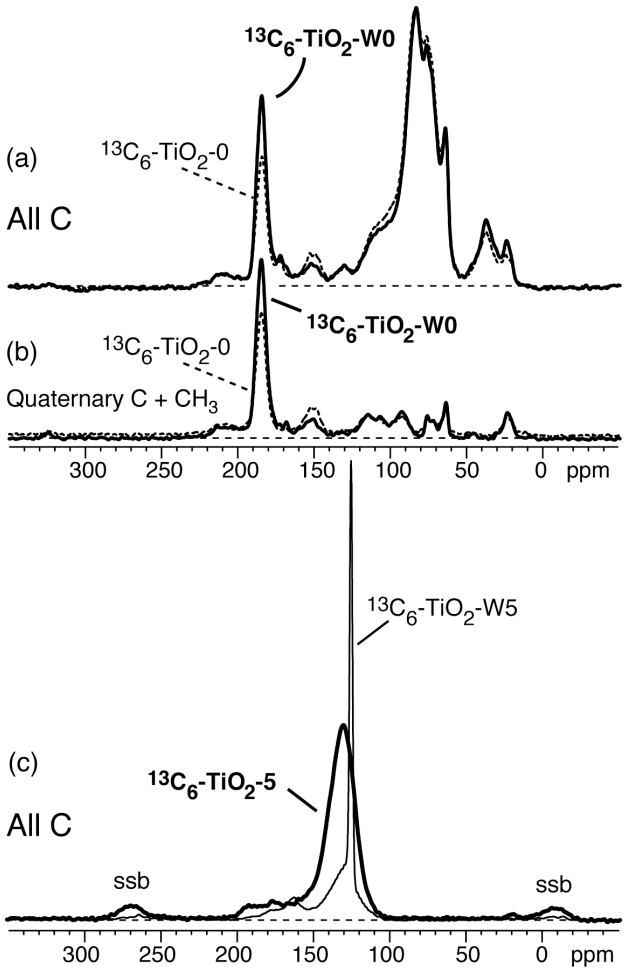

Figure 4.8 Effects of washing oven-dried material before annealing on ^{13}C spectra before and after annealing. (a) Quantitative ^{13}C NMR spectra of $^{13}C6$-TiO$_2$-W0 (solid line) and of $^{13}C6$-TiO$_2$-0 (dashed line) (b) Corresponding quantitative spectra of quaternary and methyl C. (c) Quantitative ^{13}C NMR spectra of $^{13}C6$-TiO$_2$-W5 (thin line) and of $^{13}C6$-TiO$_2$-5 (thick line).

Further structural information can be gleaned from the observed spin-lattice relaxation times. Figure 4.10 shows that the two major components of $^{13}C_6$-TiO_2-W5 have similarly short ^{13}C spin lattice relaxation times of near 3 seconds. These T_1 relaxation values are too short to be produced by the relevant internuclear couplings or chemical shift anisotropies. We conclude that the short T_1 must be attributed to fluctuating fields produced by unpaired electrons; these have been detected by epr and attributed to electron vacancies by other workers.[49] The nonexponential relaxation is typical of this process, with $T_1 \sim r_{Ce}^{-6}$, where r_{Ce} is the distance between the ^{13}C and the unpaired electron: Faster-decaying components arise from carbons closer to the unpaired electron center, and carbons further from the unpaired electron decay more slowly.

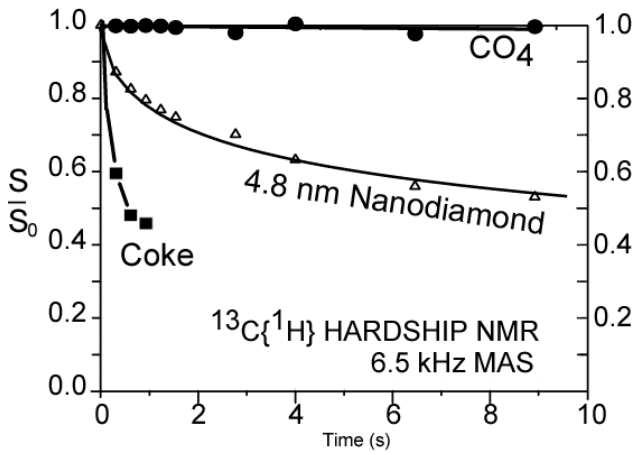

Figure 4.9 $^{13}C\{^1H\}$ HARDSHIP NMR decay curves of the CO_4 and coke signals in $^{13}C_6$-TiO_2-W5. The decay curve for 4.8-nm diameter nanodiamond is used as a reference. The slow decay of the CO_4 signals shows that orthocarbonate is located deep inside the TiO_2 nanoparticles.

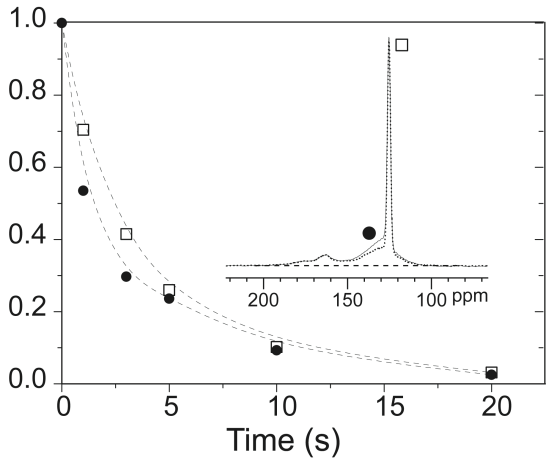

Figure 4.10 ^{13}C spin-lattice relaxation time measurements of orthocarbonate (CO_4) centers (squares) and coke (circles) in $^{13}C_6$-TiO_2-W5. The dashed lines are guides to the eye. These non-exponential decays have 1/e times of approximately 3.5 and 2.5 seconds, respectively.

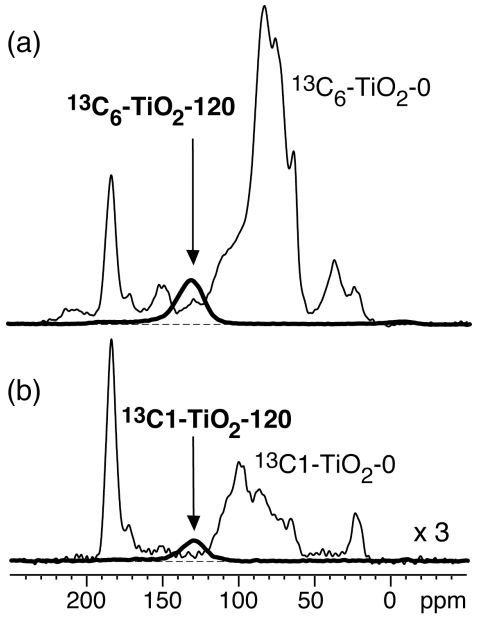

Figure 4.11 Comparison between the quantitative spectra of Ti-containing materials before and after annealing. (a) Comparison of $^{13}C_6$-TiO_2-0 (dashed line) and ^{13}C1-TiO_2-0 (solid line), plotted on a correct relative vertical scale. (b) Comparison of ^{13}C1-TiO_2-0 (thin line) and ^{13}C1-TiO_2-120 (thick line). (b) is scaled up by 300% relative to (a).

Carbon weight fractions from NMR. The amount of carbon is an important structural parameter of C-doped TiO_2. Traditional combustion analysis may not detect all C incorporated within the TiO_2 lattice; this limitation is not present in carbon quantification by ^{13}C NMR. Figure 4.11 compares the ^{13}C NMR signal intensity for samples before and after annealing, confirming a major loss of carbon. The carbon mass fractions in the six samples studied were determined from the total integrated intensity of the direct-polarization ^{13}C NMR spectra, normalized per scan and mass of sample in the rotor (Figure 4.12). Based on a calibration line determined by NMR and elemental analysis of several model compounds (circles) and validated on many samples of plant and soil organic matter (open triangles).[80] the measured ^{13}C NMR intensity of each sample studied here was converted to an approximate carbon weight % (taking into account the ^{13}C labeling level). The three samples before annealing have 5.5-6.5 wt% C, which corresponds to an organic volume fraction around 15%, given the ~2.5 times higher density of TiO_2 relative to glucose. Without washing, 5-minute annealing reduces the carbon to 1.2 wt%, and 120-minute annealing further to 0.6 wt%. After washing and 5-min annealing, the carbon weight fraction is also 0.6 wt%.

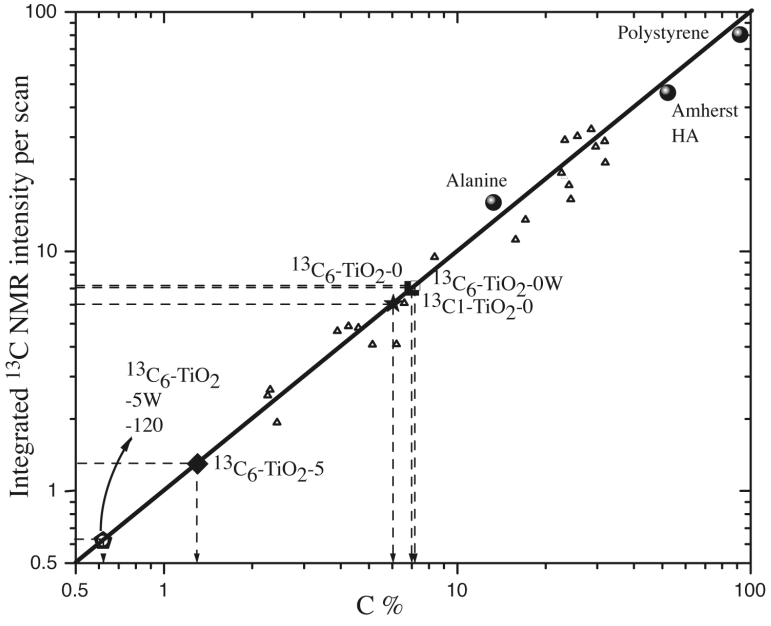

Figure 4.12 Carbon mass percentages in glucose-^{13}C modified TiO_2 from correlations of integrated DP ^{13}C NMR intensities per scan and mg of sample (ordinate) with the carbon

mass fractions from elemental analysis (abscissa), calibrated using alanine, polystyrene, humic acid from Amherst, and numerous soil samples (open triangles). $^{13}C_6$-TiO_2-0: filled square, $^{13}C_1$-TiO_2-0: star; $^{13}C_6$-TiO_2-W0: open small square; $^{13}C_6$-TiO_2-W5: filled diamond; $^{13}C_6$-TiO_2-120 filled pentagon; $^{13}C_6$-TiO_2-W5: open pentagon. The degree of ^{13}C labeling has been taken into account in determining the overall carbon percentage. Carbon content declines substantially on extended annealing.

In summary, the NMR data strongly suggest there is more than a physical interaction between the glucose and the titanium-containing precursor, and chemical reaction does occur during the aging and/or drying stages. Upon annealing of washed samples, carbon trapped inside the TiO_2 particles ultimately ends up substituting for a Ti atom and carbon nearer to the surface seems to be condensed into coke.

4.4.4 Photocatalytic activity.

The purpose of doping TiO_2 is to produce a catalyst with visible absorption that also at least maintains, if not improves on, the oxidative activity. Though NMR characterization of the carbon in C-TiO_2 is the central point of this paper, at least a meaningful screening for photocatalytic activity is essential. Ordinarily, TiO_2 photocatalyzes oxidative reactions either by initiating an oxidative single electron transfer (SET) or by invoking hydroxyl-radical-like reactivity. The dopant has the potential to hinder, as well as enhance, this property. For example, discrete dopant centers interject filled mid-gap orbitals into the semiconductor band structure, and their visible-light activation may result in much different and potentially less powerful oxidative behavior. Similarly, absorption by a color center such as graphite would set off a different set of microscopic events (e.g., electron injection into the TiO_2) that could again result in much different oxidative behavior. Thus, a short series of experiments was conducted to preliminarily screen the C-TiO_2 derivatives for their photocatalytic activity.

We chose quinoline as a preliminary probe for C-TiO_2 reactivity. Methylene blue has commonly been used as a probe for reactivity, but it has significant shortcomings that have been pointed out elsewhere.[81] We have advocated the use of 4-methoxyresorcinol,[82] but it and related molecules can form charge transfer complexes that are inherently

subject to visible light photolysis.[83-86] Quinoline does not have these problems. Its chemistry under photocatalytic conditions has been described in detail,[87,88] but the essential results of its earliest degradation steps are that it suffers SET mainly on the pyridine nucleus and hydroxyl attack mainly on the benzene nucleus, as illustrated in Figure 4.13.

The rates of the initial degradation steps of quinoline were within a factor of 1.5 of one another for TiO_2-5, C-TiO_2-W5, and C-TiO_2-5 for photolysis at pH 6 using irradiation centered at 350 nm (FWHM ~50 nm). Thus, the presence or absence of coke on the surface of TiO_2 did not have a large effect on the degradation rate. Full data are given in the supporting information.

None of the current carbon-doped materials did not show significant visible light photoactivity with quinoline upon ≥495 nm photolysis. These results clearly demonstrate that the presence of graphite on the TiO_2 surface is *not* the cause of any detected visible light activity. It is worth stressing that we believe quinoline is a fairly rigorous test of visible light reactivity, due to its lack of charge transfer bands and modest adsorption characteristics.

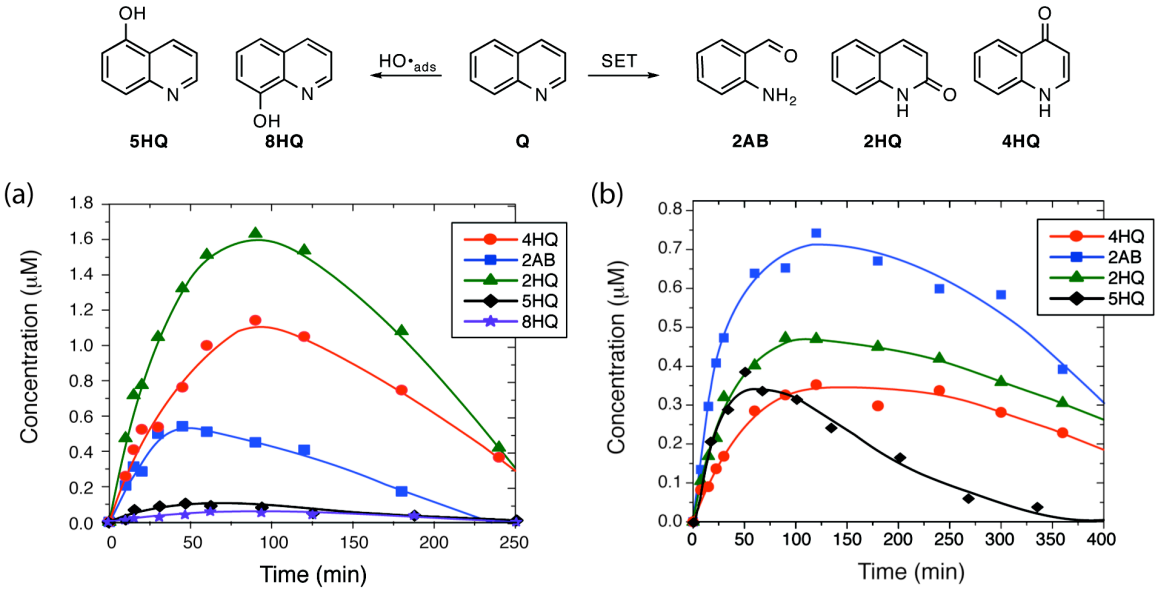

Figure 4.13 Photocatalytic degradation of quinoline: (a) loss of quinoline; formation of 4HQ, 2AB, and 2HQ mediated by (b) undoped TiO_2, (c) C-TiO_2-5, and (d) C-TiO_2-W5 under 350 nm irradiation.

The product distributions obtained with the broad 350 nm-centered irradiation were also examined. Undoped TiO_2-5 and C-TiO_2-5 led to similar early product distributions, with the SET-initiated products (functionalizing the pyridine nucleus) being the major pathways. Interestingly, C-TiO_2-W5 gave a significantly different product distribution than the other photocatalysts (Figure 13). The most significant difference is that 5HQ was formed as one of the major products, it representing the onset of the hydroxyl radical pathways. Among the SET products, 2HQ was still quite prominent, but 2AB was formed in greater proportion. It is tempting to correlate the product distribution change with the newly characterized orthocarbonate centers, but this must be seen as speculative, particularly since they are not associated with the surface, and their mechanism of action would thus have to be indirect.

4.5 CONCLUSIONS

NMR is shown to be a useful tool for probing the structure of magnetically accessible nuclei in carbon-doped TiO_2. It shows that a strategy of using glucose (as a representative poly-ol) as a dopant does provide true covalent interactions (Ti-O-C bonds) in the sol-gel stage of the catalyst preparation, and furthermore, that significant chemical change of the carbon structure occurs during this time. It confirms the previously somewhat ambiguous conclusion that coke is the major carbon-containing component of most of these hybrid materials, but also shows that orthocarbonate structures — with C-for-Ti substitutions deep inside the titania particles — and regular carbonate moieties do occur in annealed samples when a washing step is inserted between the initial drying and annealing. The removal of small amounts of furan-like materials by washing does not seem like an adequate rationalization to explain the changes. It is possible that this change is instead a result of the presence of water at the beginning of the annealing period, but this interpretation remains speculative.Carbon doping does not qualitatively affect the rate of photocatalytic degradation of quinoline, or the predominance of SET-induced products in the early stages of degradation, except for the C-TiO_2-W5 catalyst. Here, hydroxyl chemistry was more competitive, just as the orthocarbonate structure was only observed in this material. However, the causality of

this association is not established. Inasmuch as visible light irradiation (≥495 nm) does not photocatalyze decomposition of quinoline but that a reasonable rationalization for this exists through the intervention of the coke, we suggest that preparing coke-free C-TiO_2 may be critical for proving the utility of orthocarbonate-containing TiO_2 for visible-light applications.

4.6 ACKNOWLEDGEMENT

The authors thank the National Science Foundation (CHE 0518586) for financial support of this work. We are grateful to Clemens Burda for allowing us to obtain diffuse reflection spectra on his instrumentation. We also gratefully acknowledge the assistance of Jim Anderegg with the XPS data.

4.7 REFERENCES

(1) *Photocatalysis: Fundamentals and Applications*; Serpone, N.; Pelizzetti, E., Eds.; John Wiley & Sons: New York, 1989.

(2) Pichat, P.; Guillard, C.; Maillard, C.; Amalric, L.; D'Oliveira, J. C. *Trace Met. Environ.* **1993**, *3 (Photocatalytic Purification and Treatment of Water and Air)*, 207-223.

(3) Mills, A.; Davies, R. H.; Worsley, D. *Chem. Rev.* **1993**, *22*, 417-25.

(4) Malati, M. A. *Environ. Technol.* **1995**, *16*, 1093-1099.

(5) Bahnemann, D.; Cunningham, J.; Fox, M. A.; Pelizzetti, E.; Pichat, P.; Serpone, N. In *Aquatic and Surface Photochemistry*; Helz, G. R., Zepp, R. G., Crosby, D. G., Eds.; Lewis Publishers: Boca Raton, 1994, p 261-316.

(6) Serpone, N.; Khairutdinov, R. F. *Stud. Surf. Sci. Catal.* **1997**, *103*, 417-444.

(7) Konstantinou, I. K.; Albanis, T. A. *Appl. Catal. B* **2003**, *42*, 319-335.

(8) Fox, M. A.; Dulay, M. T. *Chem. Rev.* **1993**, *93*, 341-357.

(9) Legrini, O.; Oliveros, E.; Braun, A. M. *Chem. Rev.* **1993**, *93*, 671-698.

(10) Linsebigler, A. L.; Lu, G.; Yates, J. T., Jr. *Chem. Rev.* **1995**, *95*, 735-758.

(11) Thompson, T. L.; Yates, J. T., Jr. *Chem. Rev.* **2006**, *106*, 4428-4453.

(12) Choi, W.; Termin, A.; Hoffmann, M. R. *J. Phys. Chem.* **1994**, *98*, 13669-13679.

(13) Anpo, M. *Catal. Surv. Jpn.* **1997**, *1*, 169-179.

(14) Wang, C.-Y.; Bahnemann, D. W.; Dohrmann, J. K. *Chem. Commun.* **2000**, 1539-1540.

(15) Coloma, F.; Marquez, F.; Rochester, C. H.; Anderson, J. A. *Phys. Chem. Chem. Phys.* **2000**, *2*, 5320-5327.

(16) Burda, C.; Lou, Y.; Chen, X.; Samia, A. C. S.; Stout, J.; Gole, J. L. *Nano Letters* **2003**, *3*, 1049-1051.

(17) Sakthivel, S.; Kisch, H. *ChemPhysChem* **2003**, *4*, 487-490.

(18) Sakthivel, S.; Janczarek, M.; Kisch, H. *J. Phys. Chem. B* **2004**, *108*, 19384-19387.

(19) Chen, X.; Lou, Y.; Samia, A. C. S.; Burda, C.; Gole, J. L. *Adv. Funct. Mater.* **2005**, *15*, 41-49.

(20) Balcerski, W.; Ryu, S. Y.; Hoffmann, M. R. *J. Phys. Chem. C* **2007**, *111*, 15357-15362.

(21) Reyes-Garcia, E. A.; Sun, Y.; Reyes-Gil, K.; Raftery, D. *J. Phys. Chem. C* **2007**, *111*, 2738-2748.

(22) Ohno, T.; Mitsui, T.; Matsumura, M. *Chem. Lett.* **2003**, *32*, 364-365.

(23) Umebayashi, T.; Yamaki, T.; Itoh, H.; Asai, K. *Appl. Phys. Lett.* **2002**, *81*, 454-456.

(24) Ohno, T.; Tsubota, T.; Toyofuku, M.; Inaba, R. *Catal. Lett.* **2004**, *98*, 255-258.

(25) Ho, W.; Yu, J. C.; Lee, S. *J. Solid State Chem.* **2006**, *179*, 1171-1176.

(26) Lettmann, C.; Hildenbrand, K.; Kisch, H.; Macyk, W.; Maier, W. F. *Appl. Catal. B* **2001**, *32*, 215-227.

(27) Sakthivel, S.; Kisch, H. *Angew. Chem. Int. Ed.* **2003**, *42*, 4908-4911.

(28) Irie, H.; Watanabe, Y.; Hashimoto, K. *Chem. Lett.* **2003**, *32*, 772-773.

(29) Choi, Y.; Umebayashi, T.; Yoshikawa, M. *J. Mater. Sci.* **2004**, *39*, 1837-1839.

(30) Ohno, T.; Tsubota, T.; Nishijima, K.; Miyamoto, Z. *Chem. Lett.* **2004**, *33*, 750-751.

(31) Rincon, M. E.; Trujillo-Camacho, M. E.; Cuentas-Gallegos, A. K. *Catal. Today* **2005**, *107-108*, 606-611.

(32) Liu, H.; Imanishi, A.; Nakato, Y. *J. Phys. Chem. C* **2007**, *111*, 8603-8610.

(33) Dong, C. X.; Xian, A. P.; Han, E. H.; Shang, J. K. *Diffus. Defect Data, Pt. B* **2007**, *121-123*, 939-942.

(34) Irie, H.; Watanabe, Y.; Hashimoto, K. *J. Phys. Chem. B* **2003**, *107*, 5483-5486.

(35) Okato, T.; Sakano, T.; Obara, M. *Phys. Rev. B* **2005**, *72*, 115124/1-115124/6.

(36) Yang, K.; Dai, Y.; Huang, B. *J. Phys. Chem. C* **2007**, *111*, 12086-12090.

(37) Liu, S.; Chen, X. *J. Haz. Mat.* **2008**, *152*, 48-55.

(38) Asahi, R.; Morikawa, T.; Ohwaki, T.; Aoki, K.; Taga, Y. *Science* **2001**, *293*, 269-271.

(39) Asahi, R.; Morikawa, T. *Chem. Phys.* **2007**, *339*, 57-63.

(40) Batzill, M.; Morales, E. H.; Diebold, U. *Phys. Rev. Lett.* **2006**, *96*, 026103/1-026103/4.

(41) Batzill, M.; Morales, E. H.; Diebold, U. *Chem. Phys.* **2007**, *339*, 36-43.

(42) Di Valentin, C.; Pacchioni, G.; Selloni, A. *Chem. Mater.* **2005**, *17*, 6656-6665.

(43) Di Valentin, C.; Finazzi, E.; Pacchioni, G.; Selloni, A.; Livraghi, S.; Paganini, M. C.; Giamello, E. *Chem. Phys.* **2007**, *339*, 44-56.

(44) Kuznetsov, V. N.; Serpone, N. *J. Phys. Chem. B* **2006**, *110*, 25203-25209.

(45) Serpone, N. *J. Phys. Chem. B* **2006**, *110*, 24287-24293.

(46) Wang, H.; Lewis, J. P. *J. Phys.: Condens. Matter* **2005**, *17*, L209-L213.

(47) Ren, W.; Ai, Z.; Jia, F.; Zhang, L.; Fan, X.; Zou, Z. *Appl. Catal. B* **2007**, *69*, 138-144.

(48) Wang, X.; Meng, S.; Zhang, X.; Wang, H.; Zhong, W.; Du, Q. *Chem. Phys. Lett.* **2007**, *444*, 292-296.

(49) Li, Y.; Hwang, D.-S.; Lee, N. H.; Kim, S.-J. *Chem. Phys. Lett.* **2005**, *404*, 25-29.

(50) Khan, S. U. M.; Al-Shahry, M.; Ingler, W. B., Jr. *Science* **2002**, *297*, 2243-2245.

(51) Wong, M.-S.; Hsu, S.-W.; Rao, K. K.; Kumar, C. P. *J. Molec. Catal. A* **2008**, *279*, 20-26.

(52) Cui, X.; Gu, H.; Lu, J.; Shen, J.; Zhang, Z. *J. Nanosci. Nanotechnol.* **2007**, *7*, 3140-3145.

(53) Sakthivel, S.; Neppolian, B.; Shankar, M. V.; Arabindoo, B.; Palanichamy, M.; Murugesan, V. *Sol. Energy Mater. Sol Cells* **2003**, *77*, 65-82.

(54) Ohno, T.; Tsubota, T.; Nishijima, K.; Miyamoto, Z. *Chem. Lett.* **2004**, *33*, 750-751.

(55) Xu, C.; Killmeyer, R.; Gray, M. L.; Khan, S. U. M. *Electrochem. Commun.* **2006**, *8*, 1650-1654.

(56) Xu, C.; Killmeyer, R.; Gray, M. L.; Khan, S. U. M. *Appl. Catal. B* **2006**, *64*, 312-317.

(57) Xu, T.-h.; Song, C.-l.; Liu, Y.; Han, G.-r. *J. Zhejiang Univ., Sci., B* **2006**, *7*, 299-303.

(58) Xu, C.; Shaban, Y. A.; Ingler, W. B.; Khan, S. U. M. *Solar Energy Materials & Solar Cells* **2007**, *91*, 938-943.

(59) Xu, C.; Khan, S. U. M. *Electrochem. Solid-State Lett.* **2007**, *10*, B56-B59.

(60) Irie, H.; Watanabe, Y.; Hashimoto, K. *Chem. Lett.* **2003**, *32*, 772-773.

(61) TOtal Suppression of Sidebands

(62) Mao, J. D.; Hu, W. G.; Schmidt-Rohr, K.; Davies, G.; Ghabbour, E. A.; Xing, B. *Soil Sci. Soc. Am. J.* **2000**, *64*, 873-884.

(63) Mao, J. D.; Schmidt-Rohr, K. *Solid State Nucl. Magn. Reson.* **2004**, *26*, 36-45.

(64) Chan, J. C. C.; Tycko, R. *J. Chem. Phys.* **2003**, *118*, 8378-8389.

(65) Mao, J. D.; Schmidt-Rohr, K. *J. Mag. Res.* **2003**, *162*, 217-227.

(66) Mao, J. D.; Schmidt-Rohr, K. *J. Mag. Res.* **2005**, *176*, 1-6.

(67) Kolbert, A. C.; Griffin, R. G. *J. Magn. Reson.* **1990**, *66*, 87-91.

(68) Geen, H.; Bodenhausen, G. *J. Chem. Phys.* **1992**, *97*, 2928-2937.

(69) Schmidt-Rohr, K.; Spiess, H. W. *Macromolecules* **1991**, *24*, 5288-5293.

(70) Fang, X.-W.; Schmidt-Rohr, K. *manuscript in preparation* **2008**.

(71) Schmidt-Rohr, K.; Rawal, A.; Fang, X. W. *J. Chem. Phys.* **2007**, *126*, 054701/1-054701/16.

(72) Torchia, D. A. *Journal of Magnetic Resonance (1969-1992)* **1978**, *30*, 613-16.

(73) The Xu protocol called for a 5 minute annealing time.

(74) Moulder, J. F.; Stickle, W. F.; Sobol, P. E.; Bomben, K. D. *Handbook of X-Ray Photoelectron Spectroscopy*; Perkin-Elmer Corporation (Physical Electronics): Eden

Prairie, MN, 1992.

(75) The ordinary chemical shift for TiC is 281.7 eV.

(76) It should be noted that the fits were done using standard Gauss-Lorentz, symmetric peaks (70-95% Gauss) for the C1s region since there was no apparent reason to deviate for normal parameters (Figure 1d). It is possible that certain peaks could be made less significant or absent by changing certain parameter limits.

(77) Pretsch, E.; Bühlmann, P.; Affolter, C. *Structure Determination of Organic Compounds: Tables of Spectral Data*; Third Completely Revised and Enlarged English ed.; Springer: New York, 2000.

(78) Foris, A. *Magn. Reson. Chem.* **2000**, *38*, 1044-1046.

(79) Berger, S.; Bock, W.; Frenking, G.; Jonas, V.; Müller, F. *J. Am. Chem. Soc.* **1995**, *117*, 3820-3829.

(80) Fang, X.-W.; Chua, T.; Schmidt-Rohr, K.; Thompson, M. L. *manuscript in preparation* **2008**.

(81) Yan, X.; Ohno, T.; Nishijima, K.; Abe, R.; Ohtani, B. *Chem. Phys. Lett.* **2006**, *429*, 606-610.

(82) Hathway, T.; Jenks William, S. *J. Photochem. Photobiol. A* **2008**, *in press*.

(83) Agrios, A. G.; Gray, K. A.; Weitz, E. *Langmuir* **2003**, *19*, 1402-1409.

(84) Agrios, A. G.; Gray, K. A.; Weitz, E. *Langmuir* **2004**, *20*, 5911-5917.

(85) Kim, S.; Choi, W. *J. Phys. Chem. B* **2005**, *109*, 5143-5149.

(86) Orlov, A.; Watson, D. J.; Williams, F. J.; Tikhov, M.; Lambert, R. M. *Langmuir* **2007**, *23*, 9551-9554.

(87) Cermenati, L.; Pichat, P.; Guillard, C.; Albini, A. *J. Phys. Chem. B* **1997**, *101*, 2650-2658.

(88) Nicolaescu, A. R.; Wiest, O.; Kamat, P. V. *J. Phys. Chem. A* **2005**, *109*, 2829-2835.

4.8 SUPPORTING INFORMATION

4.8.1 Experimental

Chemicals. Chemicals, ordered at the highest commercially available purity, were used as received. ^{13}C-Labeled glucose was obtained in two forms: (1) uniformly and completely labeled and (2) labeled only at the anomeric (C1) carbon. Water was purified to a resistivity above 18 MΩ/cm.

Preparation of photocatalysts. The preparation is based on the procedure reported by Xu *et al.*[1] Glucose (0.02 M) was dissolved in ethanol, and the resulting solution was chilled to near 0 ºC. Neat $TiCl_4$ was added dropwise, and the temperature was maintained, until a final Ti concentration of 0.1 M was achieved. Aqueous NaOH (1 M) was added, also while maintaining the low temperature, until the pH reached 5.5, and a

precipitate formed. The solution was allowed to warm and then stand for ~150 hours at room temperature. The yellow-hued sol-gel was centrifuged and the solvent removed. It was placed in a 70 ˚C oven to dry for 12 hours. The dried material was hand-milled with an agate mortar and pestle resulting in a brown-orange solid, which was then annealed under air as indicated. After cooling, all annealed materials were thoroughly washed with purified water, filtered, and dried. As a control, undoped TiO_2 was prepared by the same process, save that no glucose was used.

In that one purpose of our investigation was to understand the chemical fate of the glucose throughout the process, certain samples were not carried all the way through the synthetic steps, e.g., not annealed. Also, to distinguish between chemically bound and physical mixtures (and remove water-soluble salts), a step consisting of thorough washing with water was sometimes added between the drying and annealing stages. To keep track of these varying materials, a notation is required, as outlined in the main text.

The nomenclature follows the format (C)-TiO_2-(prewashed or not)(calcination time, in minutes), as shown in Table 1 in the main text. "C" represents the presence of carbon and the type of glucose precursor: C is used when the glucose isotopes were at natural abundance, $^{13}C_6$ is for uniformly labeled glucose, and $^{13}C1$ is for the ^{13}C label only at carbon 1. The number after TiO_2 indicates the duration of the time spent at 500 ºC, in minutes. A "W" is added before the calcination number if the sample was washed before annealing. As an example, a material prepared in the presence of $^{13}C1$-labeled glucose that was washed after oven drying and then annealed for 5 minutes at 500 ºC is given the notation: $^{13}C1$-TiO_2-W5.

Routine physical characterization. Powder x-ray diffraction (XRD) spectra were taken with a diffractometer employing Cu K_α radiation. X-ray photoelectron spectroscopy (XPS) was done using a multitechnique spectrometer utilizing nonmonochromatized Al K radiation with a 1 mm^2 sampling area. The take-off angle was fixed at 45˚. In no case were either nitrogen or sulfur detected. Diffuse reflectance spectra were obtained with a UV/Vis spectrophotometer equipped with a diffuse reflectance attachment with MgO as a reference. For transmission electron microscopy (TEM) measurements, an aliquot of the powder was sonicated in purified water for 15

min. A single drop of this suspension was placed on a lacey-carbon-coated copper TEM grid and dried in air. The TEM examination was completed on an instrument operated at 200 kV with electron optical magnification of 64,000 to 550,000.

Degradations. The catalyst (70 mg) and water (35 mL) were placed in a cylindrical Pyrex reaction vessel and sonicated for 5 minutes. A stock solution of the organic was used to bring the final volume to 70 mL water and the quinoline concentration to 150 μM. The pH was adjusted to 6 and maintained throughout the photolysis by careful addition of aqueous NaOH. The solution was purged with O_2 and stirred in the dark for at least 30 minutes before photolysis. Reactions were irradiated using the output of broad range 4 W fluorescent tubes centered at 350 nm or light from a 75 W Xe arc lamp passed through a water filter and a 495 nm long pass filter. Potassium ferrioxalate was used as a chemical actinometer to normalize lamp intensities.[2-4] All reactions were carried out at ambient temperature with continuous stirring and O_2 bubbling.

For kinetics, 1 mL aliquots were removed from the sample and acidified with H_2SO_4, centrifuged, filtered through a syringe tip filter containing a PES membrane with a 0.2 μm pore size, and analyzed by HPLC using a reverse-phase column and diode array UV/Vis detector. Retention times and UV/vis spectra were compared to authentic samples to identify components. All rates were obtained as the mean of at least two reactions.

4.8.2 Control Experiments on Materials before Annealing

The conditions used to prepare the doped TiO_2 expose the glucose to a strongly acidic environment followed by the addition of base. To determine whether the harshly acidic reaction conditions were inherently responsible for the high-frequency shifts and molecular rearrangements observed in the NMR spectra, a control experiment was performed. The reaction was set up as described previously, except that HCl was added at the appropriate concentration instead of $TiCl_4$. The solution was concentrated by evaporation and a sticky solid residue was obtained after oven drying, and completely dried by lyophilization. The sample was analyzed in DMSO by solution ^{13}C NMR. No change in chemical shifts relative to those in the spectrum of unreacted glucose was

observed. This indicates that simple acidic conditions are not sufficient to explain the significant transformations of glucose. Presumably, specific Lewis acid catalysis by $TiCl_4$ or other intermediate Ti-containing products catalyze these reactions and/or drive dehydration.

4.8.3 Photocatalytic degradation of quinoline: a more extensive discussion

The major point of emphasis in the main text of the paper is the physical characterization of the catalysts, and thus the discussion of the choice of quinoline as a test degradation probe[5] is minimal. In this supporting information, the choice of quinoline to probe the two major classes of photocatalyst reactivity (oxidative SET and hydroxyl-like chemistry) is further explained. This is an important issue for examination of visible light activity, in that a catalyst that it active in the visible, but by only part of its normal chemical pathways will be less effective than one whose full oxidative repertoire is available.

Pichat and coworkers showed that the two different rings of quinoline are susceptible to different types of chemistry in ways that differentiate hole oxidation from hydroxyl attack. Electrophilic hydroxyl attack occurs mainly on the benzene moiety, whereas functionalization that begins with hole attack (single electron transfer, SET) affects mainly the pyridine nucleus.[5] Theoretical studies,[6] which are in agreement with the results obtained by Cermenati *et al.,*[5] show $HO^{\cdot}$ addition is most favorable at the 5 and 8 positions of quinoline, while $HO^{\cdot}$ addition at the 2 and 4 positions is extremely unfavorable. Oxidation at the 2 and 4 positions is therefore attributed to the reaction of the radical cation generated after single electron transfer (SET) and superoxide (or possibly molecular oxygen). Quinoline also has the advantage that no evidence has been reported for formation of charge transfer complexes between it and TiO_2, in contrast to some other phenol probe molecules.[7-10]

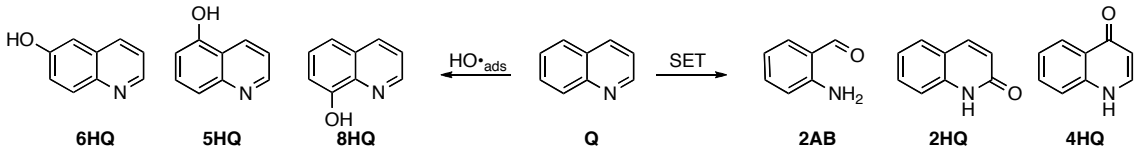

The results of heterogeneous photolysis at pH 6 under broad irradiation centered at 350 nm (FWHM ~50 nm) are given in Figure 4.S1. Loss of quinoline in the absence of light was less than 5% over 48 hours, and none of the expected oxidized products was observed. Figure 4.S1a shows that the rate of loss of quinoline with UV is similar for all three photocatalysts, with initial rates of 9.7×10^{-3} mM/min, 8.3×10^{-3} mM/min, and 6.8×10^{-3} mM/min for undoped TiO_2, C-TiO_2-W5, and C-TiO_2-5. The absolute rates, are of course, dependent on many variables, such as the photon flux, catalyst concentration, etc., but these rates are reliable relative to one another.

Figure 4.S1b-d demonstrates the growth and decay of oxidized products formed during the 350 nm photolysis. Undoped TiO_2 (Figure 4.S1b) and C-TiO_2-5 (Figure 4.S1c) lead to relatively similar early product distributions, with a somewhat lower concentration of 2HQ and 4HQ formed in the latter case. In both reactions, it is clear that SET is the dominant pathway, with 2HQ being the major initial product. In the report by Cermenati et al., in which the catalyst was Degussa P25, only small amounts of 2HQ were formed with 2AB being the predominant early product at pH 6. We reproduced this result with Degussa P25, a catalyst with both anatase and rutile phases, in contrast to the anatase-only catalysts discussed here.

As noted in the main text, C-TiO_2-W5 gave a different product distribution than the other photocatalysts (Figure 4.S1d). While 2HQ generation was still quite prominent, 2AB was formed in slight excess. The most significant feature is that $HO^{\cdot}$ addition appears to be more competitive with SET under these conditions. It was not possible to quantify 8HQ properly in this case because an unidentified peak grows in directly over the 8HQ peak in the HPLC trace, but it is reasonable to estimate a maximum concentration of 0.1-0.2 μM from the data. It is tempting to correlate the product distribution change with the newly characterized CO_4 sites, but this must be seen as speculative, particularly since they are not associated with the surface, and their mechanism of action would thus have to be indirect.

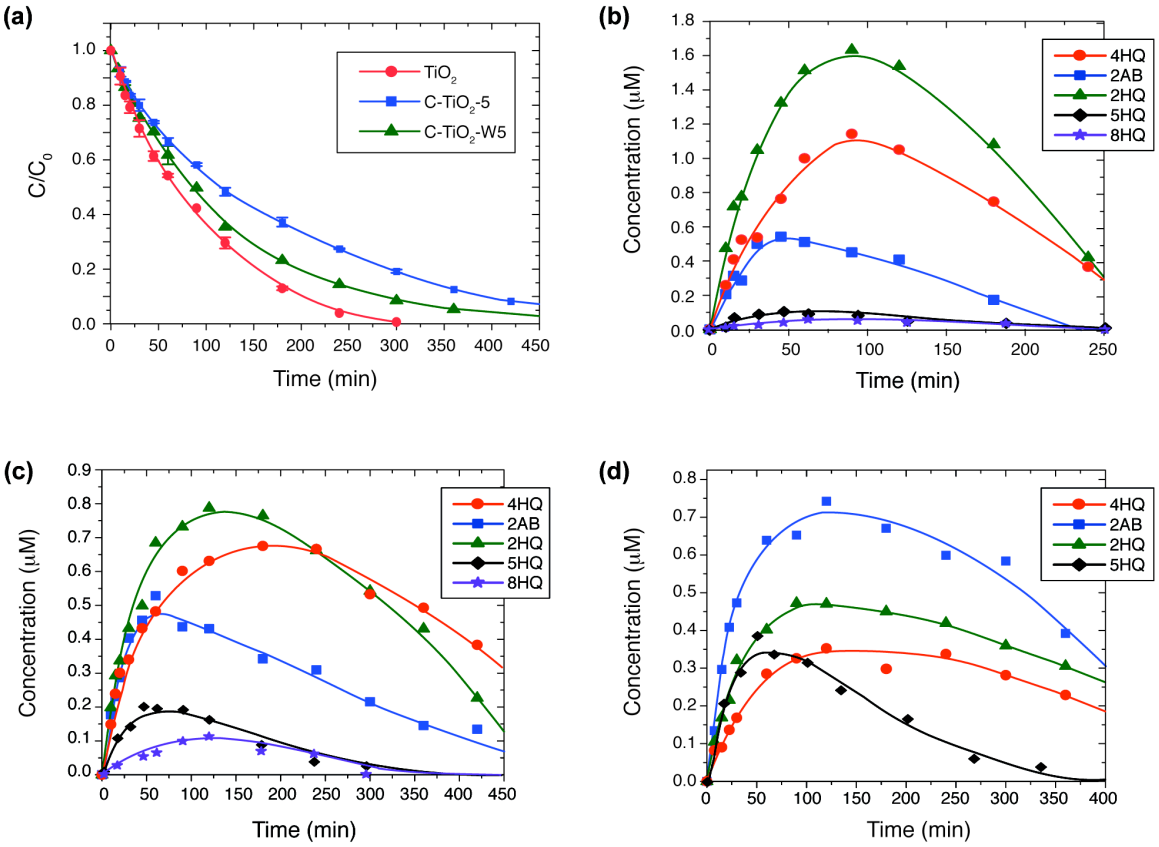

Figure 4.S1 Photocatalytic degradation of quinoline: (a) loss of quinoline; formation of 4HQ, 2AB, and 2HQ mediated by (b) undoped TiO_2, (c) C-TiO_2-5, and (d) C-TiO_2-W5 under 350 nm irradiation.

The current carbon-doped materials did not show significant visible light photoactivity with quinoline upon ≥495 nm photolysis. All three annealed photocatalysts gave ≤5% loss of quinoline with well over 100x the exposure that 5% degradation would require when using UV irradiation. Neither were any oxidation products observed. It is worth stressing that we believe quinoline is a fairly rigorous test of visible light reactivity, due to its lack of charge transfer bands and modest adsorption characteristics.

4.8.3 References

(1) Xu, C.; Killmeyer, R.; Gray, M. L.; Khan, S. U. M. *Appl. Catal. B* **2006**, *64*, 312-317.

(2) Hatchard, C. G.; Parker, C. A. *Proc. Royal. Soc. A* **1956**, *235*, 518-536.
(3) Calvert, J. C.; Pitts, J. N. *Photochemistry*; Wiley: New York, 1966.
(4) Bowman, W. D.; Demas, J. N. *J. Phys. Chem.* **1976**, *80*, 2434-2435.
(5) Cermenati, L.; Pichat, P.; Guillard, C.; Albini, A. *J. Phys. Chem. B* **1997**, *101*, 2650-2658.
(6) Nicolaescu, A. R.; Wiest, O.; Kamat, P. V. *J. Phys. Chem. A* **2005**, *109*, 2829-2835.
(7) Agrios, A. G.; Gray, K. A.; Weitz, E. *Langmuir* **2003**, *19*, 1402-1409.
(8) Agrios, A. G.; Gray, K. A.; Weitz, E. *Langmuir* **2004**, *20*, 5911-5917.
(9) Kim, S.; Choi, W. *J. Phys. Chem. B* **2005**, *109*, 5143-5149.
(10) Orlov, A.; Watson, D. J.; Williams, F. J.; Tikhov, M.; Lambert, R. M. *Langmuir* **2007**, *23*, 9551-9554.

CHAPTER 5

Is Sulfur-Doped TiO_2 an Effective Visible Light Photocatalyst for Remediation?

Reproduced from *Applied Catalysis, B: Environmental* **2009**, 91(1-2), 554, with permission from Elsevier.

Erin M. Rockafellow, Laine K. Stewart, and William S. Jenks*
Department of Chemistry, Iowa State University, Ames, IA 50011-3111

5.1 ABSTRACT

Doping titania with main group elements increases the visible light absorbance by introducing a localized band of orbitals within the band gap, but the effect of such dopants on the oxidizing power of the catalysts remains ambiguous. Three aromatic organic probe molecules — 4-methoxyresorcinol, quinoline, and 1-(*p*-anisyl)neopentanol — have been used to evaluate the oxidative chemistry of S-doped TiO_2 and test the efficacy of the catalyst with visible irradiation. With visible irradiation, a phenol is degraded efficiently, apparently through absorption by a CT band. For the other two probes, the most straightforward interpretation is that visible irradiation does not produce hydroxyl-type chemistry, but can accomplish single-electron transfers in favorable cases. The utility of sulfur-doped TiO_2 as a photocatalyst over undoped titania depends entirely whether the requirement for visible-light functionality, even if at low efficiency, outweighs a modest drop in the efficiency of catalysis using UV light.

5.2 INTRODUCTION

The use of titanium dioxide as a photocatalyst for the degradation of organic compounds in water has received a great deal of attention.[1-7] Titanium dioxide is of particular interest because it is robust, thermally stable, non-toxic, and cheap. Upon absorption of light with sufficient energy for band gap excitation, charge separation

occurs, promoting an electron (e^-) to the conduction band leaving a void, or hole (h^+), in the valence band. These photogenerated charges can migrate to the surface of the photocatalyst where charge transfer with surface-bound adsorbates and nearby molecules can occur in competition with recombination of the electron/hole pair. Nearby organic molecules can then undergo oxidative reactions by either indirect, hydroxyl-like pathways (hereafter referred to as $HO\bullet_{ads}$ to distinguish this chemistry from that of true bulk-solvated hydroxyl radicals, HO•) or single electron transfer (SET), which involves direct electron transfer from the organic molecule to the photogenerated hole ("hole attack") or potentially to another photogenerated reactive species, like HO•.[4,8-14]

Unfortunately, anatase, which is believed to be the most reactive phase of TiO_2, has a low quantum yield for oxidation steps (≤ 5%) as a result of rapid recombination of photogenerated charges. In addition, pure anatase is only able to use < 10% of the terrestrial solar spectrum because of its wide band gap (3.2 eV), with rutile having a slightly smaller band gap (3.0 eV), but generally lower activity.

Doping TiO_2 with metal cations or main group elements has been shown to induce extensions of the absorption spectrum into the visible.[4,15-18] Although transition metals give the desired red shift, many of them can act as recombination centers. This reduces the semiconductor's photochemical efficiency and therefore utility as a photocatalyst.[4,10] Recent research has focused greatly on doping TiO_2 with nonmetal main group elements to create materials we designate as N-TiO_2, C-TiO_2, etc., with S-TiO_2 being the focus of this paper.[15,19-56]

Understanding the origin of the shifted absorption and its relationship to the photocatalytic chemistry is essential. Asahi originally proposed that nitrogen doping creates a delocalized mixing between the O 2p and N 2p orbitals causing a rise in the valence band.[15] Most current research supports an alternative proposal in which the dopant atom orbitals generate an isolated mid-gap level above the valence band.[14,29,35,55,57-59] Intuitively, this point is a key one for understanding the chemistry that these catalysts will initiate, given that oxidation is the main TiO_2-mediated degradation pathway. Raising the bulk valence band energy level would necessarily lower the oxidizing power of the photochemically generated hole and potentially interfere with

certain reactions the pristine catalyst could perform. The role of isolated mid-gap level holes is less clear, though they also should result in low energy "hole traps" that were less chemically active than the main valence band holes. Excitation in the low energy edge of the absorption would presumably mean direct formation of such trapped holes, but UV excitation could also lead to low energy trapped holes via migration to the dopant center. It is thus apparent that at the limit of high charge mobility and rapid trapping, all excitations might have a lowered oxidation power over the undoped TiO_2. On the other hand, if oxidation of adsorbed substrates were competitive with charge migration within the particle, a wavelength dependence on the observed chemistry might be found.

Several key studies have reported on the differences in charge carrier mobility generated by irradiation with UV light versus visible light.[14,49,58,60] Others have recently noted wavelength-dependent chemistry for N-TiO_2 remediation of ethylene glycol in acetonitrile,[58] as well as C-TiO_2-mediated degradation of molecules with different binding abilities and oxidation potentials.[14]

To probe the photocatalytic activity of doped titania, many other studies have used dyes as chemical probes, some of which are prone to both oxidative and reductive degradation pathways and are often unrepresentatively easy to oxidize or reduce, compared to more common relevant pollutants. Dyes also absorb light is the visible region, which is an undesirable trait. The use of methylene blue, perhaps the most common of these, remains controversial for these and other reasons.[48,61,62] We prefer molecules more closely related to common pollutants such as aromatic pesticides, herbicides, manufacturing byproducts, or petroleum products that also have well-defined oxidative pathways.[2,63-65]

In this paper, we report the an investigation of S-TiO_2 prepared in two ways – a conventional sol-gel preparation.[38,46] and a modification of existing TiO_2 by annealing with S_8 – and an evaluation of the chemical reactivity of these catalysts in the UV and visible ranges. As chemical probes, we use three aromatic molecules with considerably different adsorption modes and modes of reactivity. These compounds, 4-methoxyresorcinol (**MR**, 4-methoxybenzene-1,3-diol), 1-(*p*-anisyl)neopentanol (**AN**, 1-(4-methoxyphenyl)-2,2-dimethylpropan-1-ol), quinoline (**Q**), have well established

patterns of oxidative reactivity.[12,63,66-68] By examining the partial degradation mixtures at low conversion of the starting material, reaction products can be used to distinguish between hydroxyl-type and single-electron transfer (SET) interactions with the catalyst, as shown in Scheme 5.1.

Scheme 5.1. Early photocatalytic degradation steps for **MR**, **Q**, and **AN.**

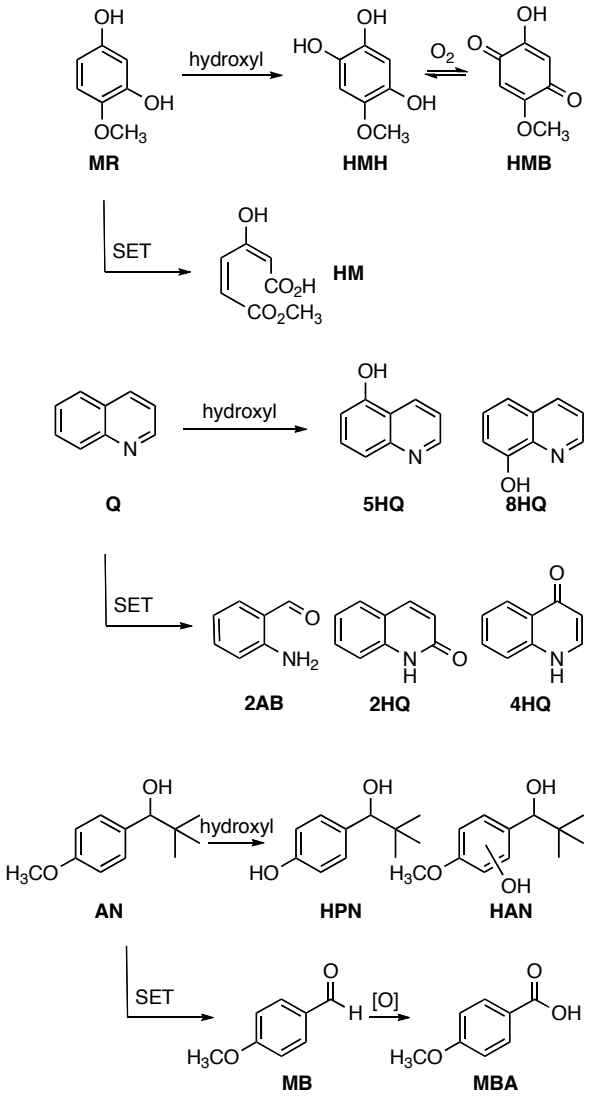

5.3 EXPERIMENTAL

5.3.1 Materials

Chemicals were purchased at the highest available purity and used as received, unless noted otherwise. 4-Methoxyresorcinol [69] and 1-(*p*-anisyl)neopentanol [66] were prepared by literature methods. Water was purified using a Milli-Q UV plus system with a resistivity above 18 MΩ/cm. PC500, a commercial anatase, was received from Millenium Chemical Company, and used only for the purpose of showing the anatase pattern in the powder XRD.

5.3.2 Photocatalyst Preparation

Sulfur-doped titanium dioxide (S-TiO_2) was prepared using a lightly modified literature procedure due to Ohno [38,46]. Thiourea (53.4 g) was dissolved in 550 mL 90% ethanol followed by drop-wise addition of titanium (IV) isopropoxide (51.5 mL) and vigorous stirring to yield a white precipitate. The solution was stirred at room temperature under aerated conditions for 48 hours to allow for complete hydrolysis. Solvent was removed under reduced pressure, and the remaining white powder was annealed at 450 ˚C for 4 hours. The material was then washed thoroughly with water to remove residual surface adsorbates and any surface sulfates. S-TiO_2 was obtained as a vivid yellow powder. Undoped TiO_2 was prepared by a similar method as S-TiO_2 without thiourea.

A second method was also used for the synthesis of sulfur-doped titanium dioxide, designated S_8-TiO_2. Samples of undoped TiO_2 obtained from the previous procedure were used as the starting material. Undoped (but otherwise identically prepared) unannealed, amorphous TiO_2 (5.00 g) and S_8 (2.00 g) were mixed and ground together thoroughly with a mortar and pestle, followed by annealing at 350 ˚C for 4 hours. (The boiling point of S_8 is 445 ˚C). The resulting grayish-tan powder was washed with water to remove surface adsorbates and sulfates. As a control, washing with CS_2, done to wash away any residual S_8 or related materials, was also performed, and no color change resulted.

5.3.3 Catalyst Charaterization

Powder x-ray diffraction (XRD) spectra were taken with a x-ray powder diffractometer employing Cu K_α radiation. Surface analysis of the materials was performed by nitrogen sorption isotherms in a sorptometer. The surface areas were calculated by the Brunauer-Emmett-Teller (BET) method. X-ray photoelectron spectroscopy (XPS) was done using a multitechnique spectrometer utilizing nonmonochromatized Al K radiation with a 1 mm^2 sampling area. The take off angle was fixed at 45˚. Spectra were calibrated to the C1s peak at 284.7 eV. Diffuse reflectance spectra (DRS) were generated with a UV-vis spectrometer equipped with a diffuse reflectance accessory. MgO was used as a background reference. For transmission electron microscopy (TEM) measurements, an aliquot of the powder was sonicated in nanopure water for 15 min. A single drop of this suspension was placed on a lacey carbon coated copper TEM grid and dried in air. The TEM examination was completed on a electron microscope operated at 200 kV to examine at electron optical magnification of 64,000 to 550,000.

5.3.4 Photocatalytic Measurements

Reaction mixture preparation, photolysis conditions, and analysis procedures were similar to previous work [70]. The suspensions contained doped or undoped titania at 1.00 mg/mL. The initial concentrations of probe molecules and solution pH values were as follows: 1.0 mM **MR** at pH 8.5 ± 0.5, 0.3 mM **AN** at pH 8.5 ± 0.5, 0.15 mM quinoline at pH 6.0 ± 0.5 or pH 3.0 ± 0.5. The pH was adjusted and maintained over the photolysis by careful addition of aqueous NaOH or HNO_3. The solution was purged with O_2 and stirred in the dark for a minimum of 30 minutes before reactions. Reactions were irradiated with 350 nm broad range 4-Watt bulbs in a Rayonet minireactor or light from 75-Watt Xe arc lamp passed through a water filter and a 495 nm longpass filter. Potassium ferrioxalate was used as a chemical actinometer [71,72]. All reactions were carried out at ambient temperature with continuous stirring and O_2 bubbling.

For kinetics, 1 mL samples were acidified, centrifuged, filtered and analyzed by HPLC. HPLC analysis was done using a C18 reverse phase column using a diode array

detector. Compounds were identified by comparison to authentic samples. **MR** degradation analysis was performed using 70% water containing 0.2% acetic acid and 30% methanol as the eluent at 1 mL/min and monitored at 290 nm. The eluent used for analysis of **AN** was 70% acetonitrile and 30% water at 1 mL/min and detected at 270 nm. Quinoline and the oxidized products were easily identifiable by HPLC. However, it was determined that using two different mobile phases was ideal for analysis of all the products, as there were some difficulties with overlap. For HPLC analysis of quinoline, 4-quinolinone (**4HQ**), 2-aminobenzaldehyde (**2AB**), and 2-quinolinone (**2HQ**), the solvent was 1:3 methanol:water with 0.2% acetic acid. Flow was 0.9 mL/min and traces were monitored at 230 nm and 325 nm. Analysis of 5-hydroxyquinoline (**5HQ**) and 8-hydroxyquinoline (**8HQ**) was done using 1:9 methanol:water with 0.2% acetic acid as the mobile phase with an elution rate of 0.75 mL/min and monitoring at 250 nm.

For product analysis for **MR** and **AN** degradations, GC-MS (or routine GC) was used and compounds were verified by comparison to authentic samples. Approximately 60 mL of the irradiated solution was acidified, centrifuged and filtered. Fifty mL of the filtrate was concentrated by evaporation under reduced pressure until 3 – 5 mL remained, which was then freeze-dried. For GC-MS analysis of **MR** reactions, 1 mL of a 0.5 mM dodecane in pyridine stock solution was added to the residual solid followed by silylation as previously described [67,70]. For GC-MS analysis of **AN** reactions, the lyophilized solid was dissolved in 0.5 mL methanol containing 0.5 mM docecane, followed by agitation and centrifugation. GC-MS was done by GC-TOF analysis with a 30 m DB-5 column.

5.4 RESULTS

5.4.1 Physical Charaterization of Photocatalysts

Powder diffraction data revealed that the prepared materials were anatase (Figure 5.1). The average crystallite size of S-TiO_2, S_8-TiO_2, and undoped TiO_2 were 13 nm, 13 nm, and 14 nm calculated using the Scherrer formula ($d = 0.9\lambda/\beta_{1/2}\cos\theta$). These values are consistent with the typical particle sizes of 5-15 nm observed in the transmission electron microscopy images (Figure 5.2). The BET surface was 93 m^2/g for S-TiO_2 and 69 m^2/g for undoped TiO_2.

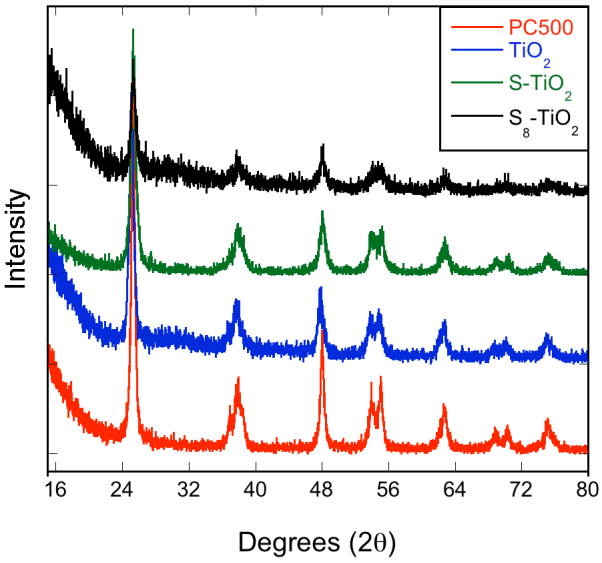

Figure 5.1 XRD of synthesized S-TiO_2 and TiO_2 compared to commercially available anatase (PC500).

Figure 5.3 shows the XP spectra of the S 2p region obtained under different conditions. The spectrum obtained from a dried, but un-annealed sample has a peak at 162 eV, which corresponds to S^{2-}. The spectra also indicated the presence of carbon and nitrogen derived from thiourea. After annealing, the 162 eV S^{2-} peak disappears and is replaced by a new one at 169 eV, indicating the presence of an S^{4+} and/or S^{6+} species [73-76]. Etching, which removes the first few atomic surface layers, reduced the signal strength by a factor of 2. In post-annealing spectra, no peaks corresponding to nitrogen were observed, and no carbon peaks were observed, outside of the ubiquitous carbon C 1s peak corresponding to adventitious/ambient carbon. By XPS, the total sulfur concentration was 0.8% (S-TiO_2) or 1.0% (S_8-TiO_2), determined before etching. In the S_8-TiO_2 sample, a small peak at 162 eV appears after etching, demonstrating the presence of S^{2-}. Diffuse reflectance data show that sulfur doping causes a significant red shift relative to the undoped titania prepared without the sulfur source (Figure 5.4).

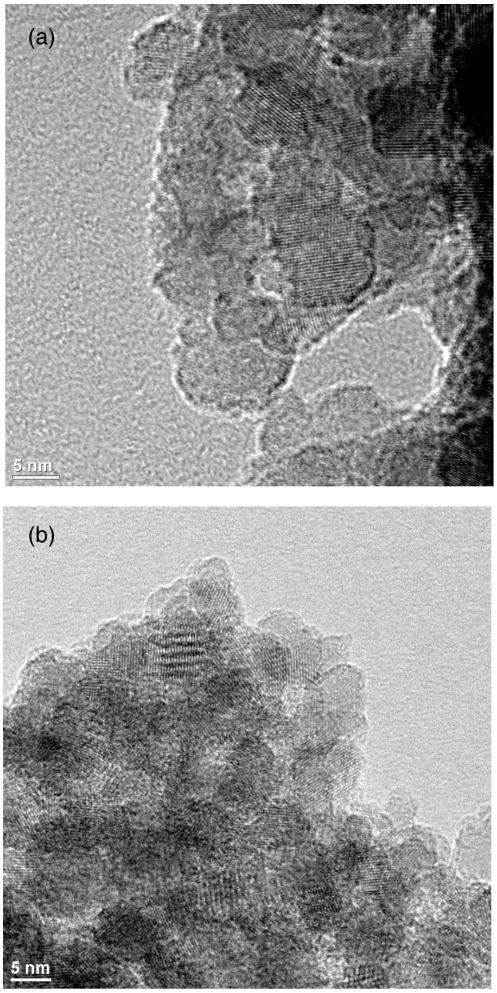

Figure 5.2 TEM images of (a) TiO_2 and (b) S-TiO_2.

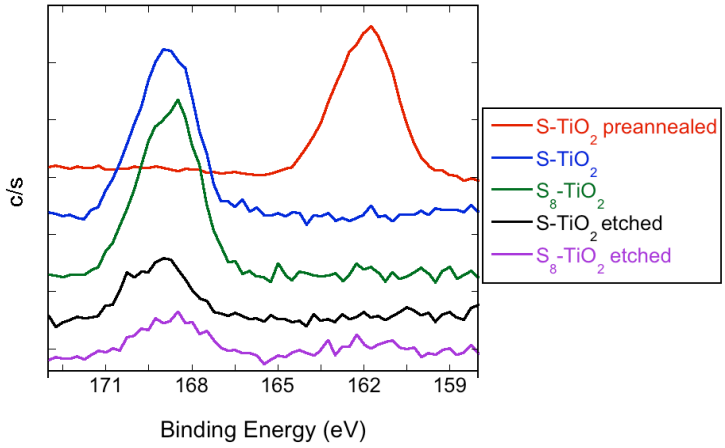

Figure 5.3 XP spectra of S-TiO_2.

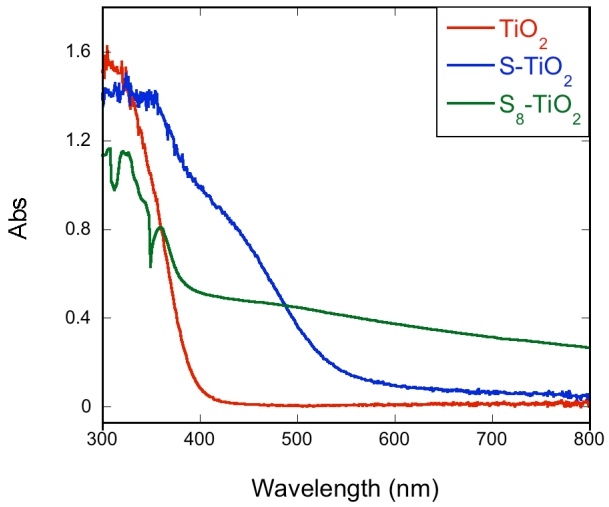

Figure 5.4 Diffuse reflectance spectra of undoped TiO_2 and S-TiO_2.

5.4.2 Photocatalytic Degradations

Figure 5.5 shows the initial zero-order rates of loss on a logarithmic scale for photocatalytic degradation of the probe molecules. The S_8-TiO2 behaved very similarly to S-TiO_2 in all tested cases. Control experiments showed that the organic compounds were stable under the conditions in the dark on the time scale of all reactions. Rates were normalized with actinometry from one light source to the other to account for varying photonic flux [77]. The light sources were fluorescent tubes with broad irradiation centered at 350 nm and a Xe arc lamp filtered through water (to remove excessive IR) and at 495 longpass filter. Thus, the latter is an exclusively visible (and IR) light source, while the former is fully in the UV. According to Figure 5.4, the undoped TiO_2, in the absence of any organic substrate, should not absorb any light from the >495 nm source, and such irradiation is also near the red edge of absorption for the doped catalyst. Under UV irradiation, the pristine TiO_2 degraded the probe compounds more rapidly than did S-TiO_2, by factors of approximately 2.

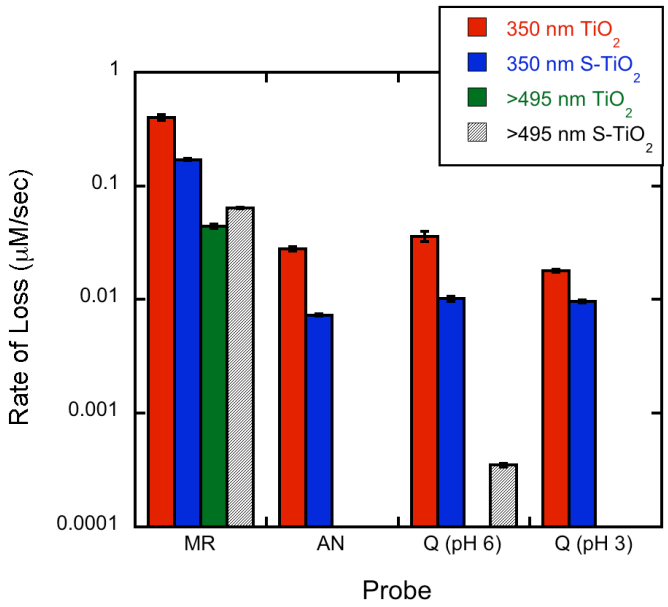

Figure 5.5 Comparison of probe molecule degradation rates for TiO_2 and S-TiO_2 photocatalytic degradation under UV and visible light. Rates are normalized for variances in light output using ferrioxolate actinometry.

Rates of degradation. **MR** was degraded faster than either of the other two probe molecules, regardless of conditions (Figure 5.5). Perhaps most interesting is the observation that **MR** is degraded at comparable rates when the naked catalyst does not absorb the light. Given that **MR** is an electron rich phenol, the most probably explanation is the formation of a charge transfer complex between it and TiO_2, which is irradiated even in the visible. The suspensions were not visibly colored, but the concentration of **MR** is sufficiently low that such obvious coloration is not expected. This type of CT complex has been documented in related molecules before [78-80]. Rates alone do not distinguish whether the >495 nm-initiated degradation with S-TiO_2 were based on the same CT interaction or on the visible absorption of the catalyst.

The rate of degradation of **AN** mediated by any of the catalysts under UV illumination is an order of magnitude lower than the rate of loss of **MR**. The rate for S-TiO_2 is smaller than that for TiO_2 by a factor of about 2.5, both under 350 nm irradiation. Over the course of 48 hours of irradiation (which was the practical limit for keeping the dark concentration the same within a few percent), no loss of **AN** was detectable when

using >495 nm irradiation, regardless of the catalyst.

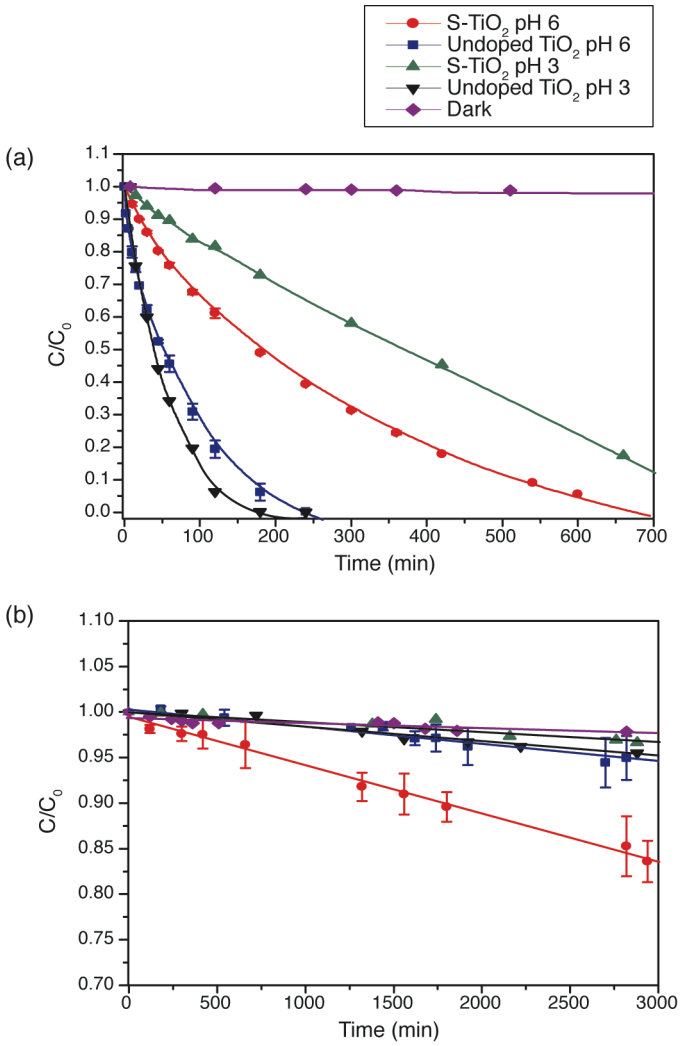

Figure 5.6 Heterogeneous photocatalytic degradation of quinoline under (a) 350 nm and (b) ≥495 nm.

Q was degraded efficiently with UV light, similarly to the other two probes, at either pH 3 or 6 by both S-TiO_2 and S_8-TiO_2 . Figure 5.6 shows the full set of kinetic data for degradation of **Q** using S-TiO_2. S_8-TiO_2 removes quinoline approximately 2.5 times faster than S-TiO_2 at pH 3, and 1.5 times faster at pH 6. Like **AN**, loss of **Q** when using TiO_2 and visible irradiation was not distinguishable from the dark background. This

same result was obtained when S-TiO_2 or S_8-TiO_2 was used as the photocatalyst at pH 3 under >495 nm irradiation. However, at pH 6, **Q** was reproducibly degraded at a normalized rate about two orders of magnitude more slowly than under UV irradiation (15% in 48 hours) by S-TiO_2 and wavelengths >495 nm. However, since the fraction of absorbed photons is not known, but is very likely lower for the visible irradiations, this should be taken as a lower limit of the relative rates and not an absolute ratio.

Product analysis. Product analysis at fixed low conversion can provide useful, if qualitative, information about the relative rates of formation of initial degradation products. The major concern is the secondary consumption of the intermediates; in extreme cases, no intermediates are observed at all because they are consumed much more rapidly than they are formed. However, the present compounds were chosen in large part because their early degradation products are observable and chemically interpretable. An admittedly simplified scheme for each molecule, based on previous studies, is given in Scheme 5.1. A few of these products clearly require more than one step (e.g., **MBA**, which is undoubtedly secondary to **MB**). Hydroxymethoxy hydroquinone (**HMH**) spontaneously oxidizes to the quinone in aerated water on handling, although the reverse reaction [81] almost certainly takes place with the light on.

Table 5.1 summarizes the results of product studies for all the probes and catalysts for low conversion, with the products grouped together as indicating hydroxyl-like chemistry or SET-initiated chemistry, as indicated in Scheme 5.1. The ratios given in Table 5.1 for **MR** show there is a slight excess of SET products over $HO\bullet_{ads}$ products, but both pathways are competitive. Moving from UV to visible, the product yield shifts for TiO_2, but does not do so for S-TiO_2.

For **AN**, no products were observed for the visible irradiations, as indicated by the kinetics experiments. For this poorly binding substrate, when UV irradiation at pH 8.5 was used, hydroxyl products predominate only slightly in the undoped TiO_2, but quite strongly when S-TiO_2 is the catalyst. (This latter result was also our observation using commercially available anatase catalysts [63].) The product peaks were smaller than expected, implying that even at modest degradation of the parent compound, secondary

degradation reactions were important. This phenomenon is not particularly surprising for poorly binding substrates; the more oxidized products may more easily be adsorbed to the catalyst.

Table 5.1 Ratios of early degradation intermediate products.

	Observed SET:$HO\bullet_{ads}$ intermediate product ratio[a]			
	TiO_2		S-TiO_2	
Probe molecule	UV	Visible	UV	Visible
4-methoxyresorcinol, **MR**[b]	1.3	1.7	1.2	1.2
p-anisyl-1-neopentanol, **AN**[b]	0.9[c]	--	0.1	--
quinoline, **Q** (pH 6)	4.2	--	6.2	SET only
quinoline, **Q** (pH 3)	0.2[d]	--[d]	0.04	--[d]

[a]**MR** and **AN** product ratios where found using GC peak areas relative to dodecane as an internal standard. **Q** product ratios were found by concentrations based on HPLC peak areas versus standard calibrations. [b]pH 8.5 ± 0.5. [c]Peak areas in the GC trace were very small, indicating intermediate products may be consumed faster than the parent probe molecule. [d]Trace amounts of 5HQ were observed.

Degradations were carried out at pH 3 and 6 for quinoline, which is below and above the pKa of quinolinium ion, respectively. Traces showing the product evolution as a function of irradiation time for quinoline, using TiO_2 as the catalyst, are given in Figure 5.7. Figure 5.8 shows the same data for quinoline and S-TiO_2, including the > 495 nm photolyses. S_8-TiO_2 behaved in the same manner as S-TiO_2 in >495 nm degradations of quinoline at both pH 3 and 6.

With UV exposure, the SET products were favored by a slightly larger margin with the sulfur-doped catalyst, compared to the undoped. A dramatic difference in the absolute ratio is seen for the quinoline (pH 6) vs. quinolinium (pH 3) case (Figures 5.7 and 5.8). Intermediate product studies after two hours of irradiation reveal that S_8-TiO_2

favored SET products by more than 10:1 at pH 6 and hydroxyl products by more than 23:1 at pH 3. In general, the favoring of SET products at pH 6 is very likely due to superior adsorption of the neutral compound through the nitrogen lone pair, favoring SET as a mechanism [12].

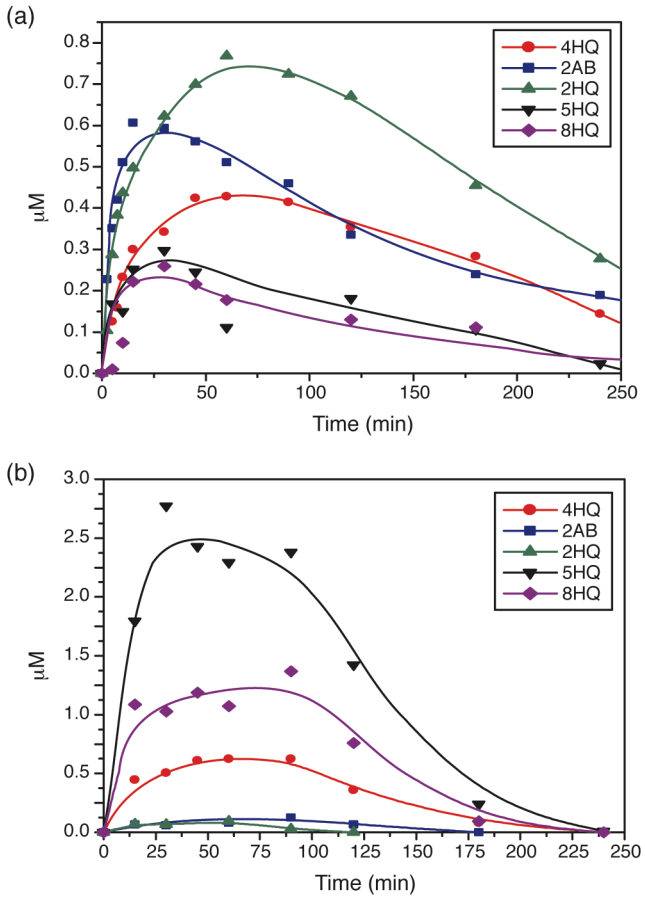

Figure 5.7 Intermediate products formed from the TiO_2-mediated degradation of quinoline at (a) pH 6 and (b) pH 3.

These results are consistent with those obtained by the Pichat group using P25 as the photocatalyst [12]. However, Pichat reports **2AB** as the major product, in contrast to the current observations. We were able to reproduce the Pichat result by using P25 as a photocatalyst instead of the pure anatase used in this study. Thus the internal change within the SET product distribution is attributable to differences in the catalyst.

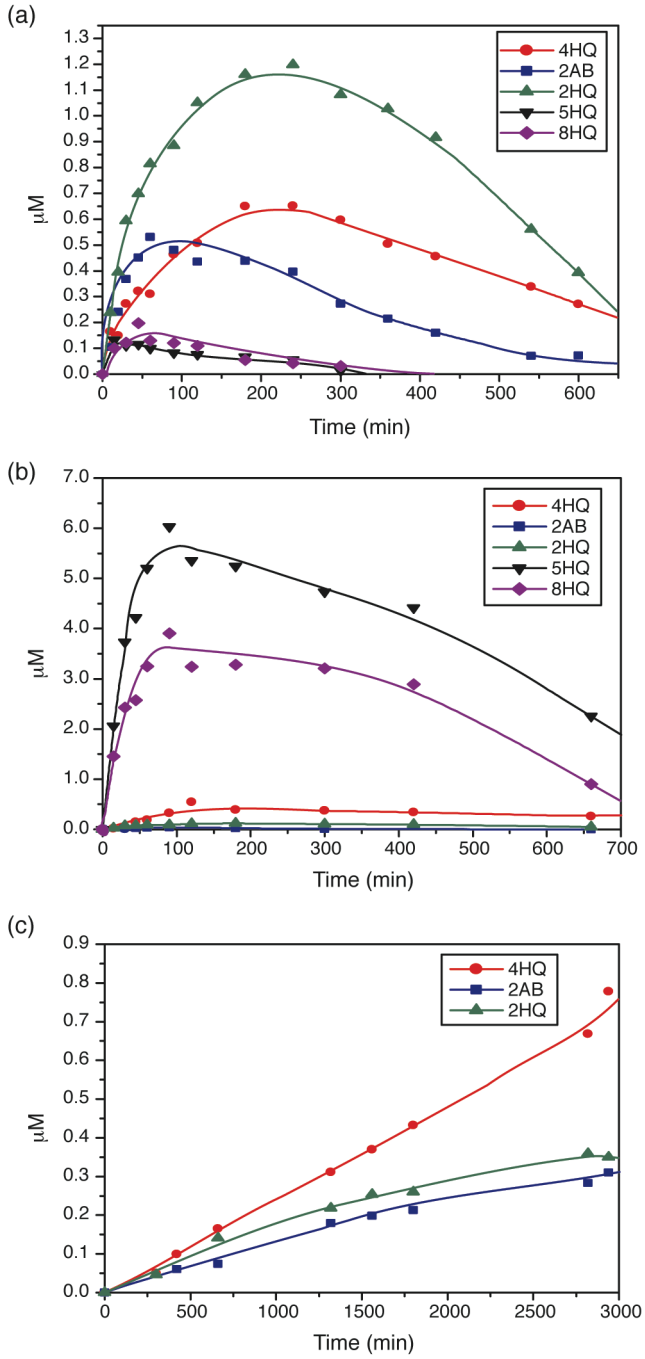

Figure 5.8 Intermediate products formed from the S-TiO_2-mediated degradation of quinoline at (a) pH 6 under 350 nm photolysis, (b) pH 3 under 350 nm photolysis, and (c) pH 6 under ≥495 nm.

A measurable difference in degradation rate of **Q** by S-TiO_2 and S_8-TiO_2 using UV light was observed, i.e., the latter provided faster removal by a factor of 2.5 at pH 3 and 1.5 at pH 6, and a rate closer to that of the undoped TiO_2. We presume (but cannot prove) that the S_8-TiO_2 has its sulfur localized in the several outer layers of the catalyst. If so, we may speculate that the sulfur sites that are throughout the interior of the S-TiO_2 do not contribute to the degradation in any useful way, but may represent recombination centers that lower the overall efficiency.

With visible photolysis of **Q**, there was a dramatic difference between the catalysts. The undoped TiO_2 did not catalyze any degradation as detected by kinetics at pH 6, but S-TiO_2 did, with the products being entirely SET-derived. Despite the loss of **Q** being indistinguishable from dark reaction at pH 3, trace amounts of **5HQ** could be detected.

Additional control experiments were done to determine if slightly higher energy visible light could be used to generate hydroxyl chemistry. Quinolinium degradation at pH 3 was the probe of choice for this. Instead of using 495 nm cutoff filters, two sets of otherwise identical experiments were carried out at pH 3, using 435 nm and 455 nm cutoff filters respectively. As shown in Figure 5.4, these cutoff wavelengths are both longer than the classical absorption of the TiO_2. Also, as a negative control, undoped TiO_2 was examined under the same conditions. The results for all three cutoffs (435 nm, 455 nm, and 495 nm) were the same within experimental uncertainty, i.e., no hydroxyl-mediated degradation.

5.5 DISCUSSION

5.5.1 Catalyst Physical Properties

The method of doping TiO_2 with thiourea, as per Ohno's procedure is now well established and reproducible. Thiourea is a good source of nucleophilic sulfur; in organic synthesis, it is used as a synthon for HS^-. (After initial reaction with an electrophile, a second step is usually used to hydrolyze the initial adduct and give urea as a byproduct.) To that extent, it is a sensible source of S for sol-gel preparations of TiO_2. XPS data obtained before annealing (showing S^{2-}) are consistent with either thiourea as a physical mixture with the titania or with a covalent modification in which the oxidation state of

sulfur has not changed. High temperature annealing under O_2 is necessarily oxidative, however, and S^{4+} and/or S^{6+} are what is observed thereafter. Since C and N are not detected by XPS, it is presumed that these are largely "burned off" by the high temperature annealing [82]. Indeed, Jin and coworkers showed through DSC measurements on similar preparations, that there is an exotherm near 220 ˚C attributable to decomposition of urea/thiourea, and others near 265 ˚C and 430˚C attributed to combustion of other organic substances [24]. It is also during the annealing process that the yellow color of the catalyst is developed, clearly indicating chemical incorporation of the S at this stage. The post-annealing spectra correspond to the sulfate oxidation state (or potentially SO_2), and suggest S-for-Ti substitution, as proposed by Ohno [38,47]. The etched XPS spectra show that the sulfur goes down at least several layers, though we presume it to be dispersed throughout.

The S_8-TiO_2 showed the same XPS data, save for a small S^{2-} peak after etching, which could suggest a minor fraction of S-for-O substitution. As with the Ohno-style, S-TiO_2, there could be a small amount of carbon also included in S_8-TiO_2; small amounts of residual solvent that remains after drying the material before the annealing. This is difficult to be certain of because the XPS for adventitious carbon adsorbed to the material from air overlaps strongly with the most likely resulting carbon product, i.e., coke condensation. (See ref [83].) The presence of small quantities of coke would also be consistent with the absorption tail that extends past 500 nm in the diffuse reflectance spectrum, as shown in Figure 5.4. The differing annealing temperatures could account for the differing amounts of coke between S_8-TiO_2 and S-TiO_2, but to argue more specifically would be overly speculative.

The mechanism for incorporation of S in S_8-TiO_2 is uncertain. At this high temperature, initiation of sulfur chemistry by both homolysis and nucleophilic type attack is reasonable. The fact that the S remains in the XPS spectra after Ar-etching does imply that significant rearrangement of the surfaces and nearby layers occurs at this temperature, in that "penetration" of the sulfur in the TiO_2 is required by this result. Since the material generated by annealing with S_8 appears to be functionally equivalent to that generated by preparation with thiourea, it would seem there are advantages to

preparing sulfur-doped TiO_2 in this manner: better optimization of the initial TiO_2 manufacture, and lower expense of the dopant. Optimization of the annealing step and/or use of other titania samples (e.g., P25) may result in a superior catalyst.

5.5.2 Photocatalytic Results

The specifics of the oxidations of these three compounds, of course, are much less valuable than the generalities that can be drawn from them; these results must be placed in the context of various other types of physical studies, and we review the available literature to put the current results in context. At least for this set of probes, a consistent result was that degradation using UV light was slowed by the sulfur doping. This is similar to the observations of Sun, who also found an inverse relationship between activity in the visible and UV for C- and S- doped TiO_2 [24].

Apparently, contradictory arguments are made by various authors for the chemistry that should be derived from doped TiO_2. These are manifest both in the explanation of kinetics and for the reactivity of the photogenerated holes. Consider, for example, the current observation that, under UV photolysis, S-TiO_2 always provided slower degradations than did TiO_2.

Sun attributed the lower UV activity to S centers acting as recombination sites [24]. On the other hand, Tachikawa, based on flash photolysis experiments, concluded that S sites did not act as recombination centers [49]. By time-resolved diffuse reflectance spectroscopy (in acetonitrile or methanol), Majima and coworkers determined that the yield of charge carriers with 355 nm excitation is greater for undoped TiO_2 than for S-TiO_2 (made by the sol gel method with thiourea). However, the efficiency of hole transport to the surface is comparable for the two materials and the S-centers do not act as special recombination points [49]. The lower total number of charge separations naturally leads to a lower observed rate of disappearance.

On the other hand, mainly on the basis of efficiency measurements over a series of catalysts, Jin and coworkers conclude quite the opposite. They argue that the sulfur defects do act as recombination centers, and it is by this means that the UV efficiency is slightly lowered [24]. The current results do not settle this particular dispute. Instead, they reinforce the observation that this effect (that UV photocatalytic efficiency for the S-

doped materials should be expected to be universally lowered, relative to the undoped case) is to be expected.

Thus, from a practical standpoint of optimizing a catalyst, the advantage or disadvantage of S-TiO_2 (in terms of speed of degradation) will depend entirely on the spectral distribution of the light source being used and the transmission of that light to the catalyst. The advantage of activity in the visible would have to make up for the loss of activity in the UV.

Therefore, to understand whether S-TiO_2 is an "improvement" over TiO_2, knowing how universal and efficient the degradation initiated by visible irradiation is critical. If only certain substrates will be oxidized, and others untouched, its utility would certainly be limited to niche applications.

Given the model that main group dopants provide mid-gap filled orbitals, rather than changing the band structure of TiO_2 in a more fundamental way, an intuitive argument can be made that the S-centers represent "deep" h^+ traps, i.e., high energy orbitals from which electrons may fall. This should inherently lower the oxidizing power of the hole, relative to undoped TiO_2 assuming charge migration is faster than reaction with the organic substrate. The consequences of the "deep hole trapping", however, remain a matter of discussion.

Majima and coworkers give a report that would be pessimistic regarding visible activity of their S-TiO_2 (also made by the Ohno method), at least in organic solvents. With 430 nm excitation, these authors report the formation of charge carriers, and formation of organic radical cations by direct irradiation of CT bands, but no SET oxidation of the organic adsorbate 4-(methylthio)benzyl alcohol after excitation [49].

Takeshita and coworkers contrasted the behavior of S-TiO_2 made by oxidative annealing of TiS_2 and by the Ohno method with thiourea [60]. Essential to their analysis was the observation that the sulfur remaining in the TiS_2-based catalyst was largely in the center of the particle, with very little remaining in the exterior. This is in contrast to the sol-gel method, assumed to produce approximately homogeneously dispersed S. They argue, on the basis of flash photolysis experiments, that the sol-gel materials produce near-surface holes that are not capable of oxidizing water to produce HO•, but are able to

oxidize methanol [60]. (This occurs whatever the excitation wavelength.) With the TiS_2-based material, visible irradiation does not produce photoactivity, which is rationalized by assuming that the sulfur centers are deep within the particle and the charge carriers cannot migrate to the surface.

By contrast, for carbon-doped TiO_2, Nakato reports that visible photooxidation of methanol goes by an indirect oxidation pathway functionally equivalent to $HO\bullet_{ads}$ chemistry. This conclusion is based upon measurement of photocurrent in the presence and absence of methanol. Although the catalyst is not identical to the present case, the authors discuss the generality of this mechanism [14]. The chemical contrast, in that case, is that hydrogen abstraction of the C-H is the first step of methanol oxidation, rather than SET, followed by deprotonation, current doubling, and so on. In principle, this might be distinguished by means of competition experiments with isotope labeling, where the hydrogen abstraction should show a kinetic isotope effect.

Our method, instead, depends on a different chemical outcome by the two mechanisms, and indirect reasoning about the physical processes. The three probes used here each demonstrate a different pattern of reactivity, but can be assembled into a sensible whole.

Photocatalytic degradation of MR. The pH of 8.5 was chosen to study the "remediation" of **MR** because this was the pH at which degradation was the most efficient, and intermediates from both SET and hydroxyl chemistry had been observed [67]. Indeed, **MR** was degraded under these conditions more rapidly than either of the other probes. This is presumably attributable to both stronger adsorption [63] and a lower oxidation potential, though reversible oxidation potentials are not available for these compounds.

The most important result with **MR**, however, was the observation of both major oxidation pathways, even with visible light well to the red of the absorbance cutoff of TiO_2. The chemistry occurring here could not result from the direct excitation of the undoped TiO_2 semiconductor since the light used here does not possess enough energy. We attribute this reactivity to the formation and direct irradiation of a charge transfer

(CT) complex, which has been directly observed between phenol compounds and TiO_2 [78-80,84]. Although the intuitive expectation is for CT irradiation to result in chemistry essentially identical to normal SET chemistry, the work of Agrios and Gray show wavelength dependence and multiple types of reactivity [79,80]. Indeed, we report a closely related phenomenon in Table 5.1, where the product ratios differ for the doped and undoped catalyst, presumably because some of the irradiation is direct to the catalyst in the case of S-TiO_2. Although interesting as an independent phenomenon, this CT-based degradation does not significantly bear on whether S-TiO_2 will be a broadly useful catalyst, since only a subset of pollutants will form such CT complexes.

Photocatalytic degradation of AN. The degradation of **AN** with the Millenium Chemicals PC series, reported on previously [63], showed hydroxyl products dominating at neutral and higher pH. This is similar to the result reported for S-TiO_2 and UV irradtiation in Table 5.1, but the total amount of observed intermediates was very small, in contrast, for undoped TiO_2. The smaller quantities are consistent with secondary degradation that is faster than the first step.

Loss of **AN** mediated by either S-TiO_2 or TiO_2 with > 495 nm light was insignificant. While this is the expected result for TiO_2, the S-TiO_2 shows modest absorption in this region and should be capable of generating charge carriers (and apparently does, given the results for quinoline). The lack of degradation of this molecule is thus reasonably damning to the prospects of S-TiO_2 as a versatile visible-light driven catalyst, at least this far into the visible. At least for this compound, both the SET and hydroxyl-like chemistry are shut down in the visible. The SET chemistry might be expected to be molecule-specific, i.e., that some more easily oxidized or better binding molecules might undergo SET even with the "weaker" holes due to the doping. However, though some controversy exists over the exact nature of the hydroxyl-like chemistry, it is widely believed to be "indirect", in that an intermediate (TiO•, HO•, etc.) is produced that in turn reacts with the substrate. As **AN** is dominated by this chemistry in the UV, the lack of degradation of **AN** with lower energy light is strongly suggestive that the indirect oxidizing center is not formed.

Photocatalytic Degradation of Q. The last probe, quinoline, leads to a variety of products under photocatalytic conditions, as a result of electronic demand differences in the benzene and pyridine rings. Pichat and coworkers showed that electrophilic hydroxyl radicals (e.g., Fenton conditions) favor addition to the benzene ring, and SET chemistry favors functionalization of the pyridine ring and formation of **2AB**, **2HQ**, and **4HQ** [12]. The product distribution results reported here follow the trends of Pichat and coworkers, save for the differences in internal ratios of SET products, but as noted, we were able to reproduce their results when using the same catalyst they did, i.e., P25.

Above the pKa of quinolinium, it is assumed that adsorption to the catalyst occurs largely through the nitrogen lone pair. At low pH, quinolinium is predominant and not as likely to adsorb to the also-positively-charged TiO_2 surface [85]. Not only does the poor binding suppress SET chemistry, but the protonation obviously increases the oxidation potential. We suggest that the approximate invariance in rate of degradation of **Q** with pH (Figures 5, 6) is merely coincidence.

Like **AN**, quinoline does not form a CT complex with TiO_2 that is degraded on visible excitation above the dark baseline, though trace **5HQ** is observed at pH 3. (We presume that this is diagnostic of a very minor amount of hydroxyl chemistry that was simply undetected in the **AN** case.) Both **5HQ** and **8HQ** were observed with UV irradiation and TiO_2 (Figure 5.7).

However, with S-TiO_2, **Q** is significantly degraded by visible light at pH 6, if only through the SET pathways. Only SET products **2AB**, **2HQ**, and **4HQ** (Figure 5.8) are observed. We inger that the reactive holes in S-TiO_2 are able to oxidize quinoline, even if they are not able to do the same for **AN**.

5.6 CONCLUSION

Information on the mechanistic differences between S-TiO_2 and undoped TiO_2 was obtained through the use of three probe molecules. **MR**, **AN**, and **Q** each showed a different pattern of reactivity with respect to visible irradiation, with activity from both catalysts, neither catalyst, and only S-TiO_2, respectively. The simplest interpretation of the results presented here is that S-TiO_2, prepared by the Ohno method, does not produce

active hydroxyl-like sites on excitation at > 495 nm. Furthermore, the sulfur doping sites do act as deep hole traps that diminish the oxidizing power of the hole. Moreover, we observe, consistent with previous workers, that the UV activity of S-TiO_2 is somewhat diminished from its parent. As a result, the utility of S-TiO_2 over a broadly useful TiO_2 catalyst such as P25 will come when extension of the absorption spectrum into the visible is more important than efficient use of UV photons, and when the target pollutants are relatively easy to oxidize. It is generally the case that the early degradation steps – at least of aromatic type pollutants – make the resulting compounds easier to degrade by photocatalysis, so this latter restriction may not be as daunting as it might seem at first glance. It may also be useful as a component of a catalyst mixture designed to efficiently use the UV and also derive some activity from visible irradiation. Finally, due to the very similar results obtained for S-TiO_2 and S_8-TiO_2 (without significant optimization of the S_8 annealing step), and the ease of preparation and low cost of the sulfur atoms, the annealing of S_8 into extant TiO_2 catalysts (e.g., P25) may turn out to be an attractive approach.

5.7 ACKNOWLEDGEMENT

The authors gratefully acknowledge the National Science Foundation (NSF CHE0518586) for support of this work, Prof. Clemens Burda for allowing us to obtain diffuse reflectance spectra on his instrument, Jim Anderegg for his assistance with XPS, and Brian Trewyn for obtaining TEM images and nitrogen sorption data.

5.8 REFERENCES

(1) Pichat, P. *Water Science and Technology* **2007**, *55*, 167-173.
(2) Ryu, J.; Choi, W. *Environmental Science & Technology* **2008**, *42*, 294-300.
(3) *Photocatalytic Purification and Treatment of Water and Air*; Ollis, D. F.; Al-Ekabi, H., Eds.; Elsevier Science Publishers: New York, 1993.
(4) Hoffmann, M. R.; Martin, S. T.; Choi, W.; Bahnemann, D. W. *Chem. Rev.* **1995**, *95*, 69-96.
(5) Robertson, P. K. J.; Bahnemann, D. W.; Robertson, J. M. C.; Wood, F. *Handbook of Environmental Chemistry* **2005**, *2*, 367-423.
(6) Fujishima, A.; Zhang, X.; Tryk, D. A. *Surface Science Reports* **2008**, *63*, 515-582.
(7) Kaneko, M.; Okura, I. *Photocatalysis: Science and Technology*; Springer-

Verlag: Berlin, 2002.

(8) Thompson, T. L.; Yates, J. T., Jr. *Chemical Reviews (Washington, DC, United States)* **2006**, *106*, 4428-4453.

(9) Fox, M. A.; Dulay, M. T. *Chem. Rev.* **1993**, *93*, 341-357.

(10) Linsebigler, A. L.; Lu, G.; Yates, J. T., Jr. *Chem. Rev.* **1995**, *95*, 735-758.

(11) Legrini, O.; Oliveros, E.; Braun, A. M. *Chem. Rev.* **1993**, *93*, 671-698.

(12) Cermenati, L.; Pichat, P.; Guillard, C.; Albini, A. *J. Phys. Chem. B* **1997**, *101*, 2650-2658.

(13) Park, J. S.; Choi, W. *Chemistry Letters* **2005**, *34*, 1630-1631.

(14) Liu, H.; Imanishi, A.; Nakato, Y. *Journal of Physical Chemistry C* **2007**, *111*, 8603-8610.

(15) Asahi, R.; Morikawa, T.; Ohwaki, T.; Aoki, K.; Taga, Y. *Science* **2001**, *293*, 269-271.

(16) Anpo, M. *Catalysis Surveys from Japan* **1997**, *1*, 169-179.

(17) Choi, W.; Termin, A.; Hoffmann, M. R. *J. Phys. Chem.* **1994**, *98*, 13669-13679.

(18) Highfield, J. G.; Pichat, P. *New Journal of Chemistry* **1989**, *13*, 61-6.

(19) Umebayashi, T.; Yamaki, T.; Tanaka, S.; Asai, K. *Chemistry Letters* **2003**, *32*, 330-331.

(20) Wang, H.; Lewis, J. P. *Journal of Physics: Condensed Matter* **2005**, *17*, L209-L213.

(21) Wang, H.; Lewis, J. P. *Journal of Physics: Condensed Matter* **2006**, *18*, 421-434.

(22) Wang, X.; Meng, S.; Zhang, X.; Wang, H.; Zhong, W.; Du, Q. *Chemical Physics Letters* **2007**, *444*, 292-296.

(23) Choi, Y.; Umebayashi, T.; Yoshikawa, M. *J. Mater. Sci.* **2004**, *39*, 1837-1839.

(24) Sun, H.; Bai, Y.; Cheng, Y.; Jin, W.; Xu, N. *Industrial & Engineering Chemistry Research* **2006**, *45*, 4971-4976.

(25) Chen, Z.; Yu, G.; Zhang, P.; Jiang, Z. *Huanjing Kexue* **2002**, *23*, 55-59.

(26) Chen, X.; Burda, C. *J. Phys. Chem. B* **2004**, *108*, 15446-15449.

(27) Chen, D.; Jiang, Z.; Geng, J.; Wang, Q.; Yang, D. *Industrial & Engineering Chemistry Research* **2007**, *46*, 2741-2746.

(28) Irie, H.; Watanabe, Y.; Hashimoto, K. *Chem. Lett.* **2003**, *32*, 772-773.

(29) Irie, H.; Watanabe, Y.; Hashimoto, K. *J. Phys. Chem. B* **2003**, *107*, 5483-5486.

(30) Irie, H.; Watanabe, Y.; Hashimoto, K. *Chemistry Letters* **2003**, *32*, 772-773.

(31) Li, Y.; Hwang, D.-S.; Lee, N. H.; Kim, S.-J. *Chemical Physics Letters* **2005**, *404*, 25-29.

(32) Yang, J.; Bai, H.; Tan, X.; Lian, J. *Applied Surface Science* **2006**, *253*, 1988-1994.

(33) Yang, K.; Dai, Y.; Huang, B. *Journal of Physical Chemistry C* **2007**, *111*, 12086-12090.

(34) Sakthivel, S.; Kisch, H. *Angewandte Chemie International Edition* **2003**, *42*, 4908-4911.

(35) Sakthivel, S.; Janczarek, M.; Kisch, H. *Journal of Physical Chemistry B* **2004**, *108*, 19384-19387.

(36) Xu, C.; Killmeyer, R.; Gray, M. L.; Khan, S. U. M. *Applied Catalysis, B: Environmental* **2006**, *64*, 312-317.

(37) Xu, T.-h.; Song, C.-l.; Liu, Y.; Han, G.-r. *Journal of Zhejiang University, Science, B* **2006**, *7*, 299-303.

(38) Ohno, T.; Akiyoshi, M.; Umebayashi, T.; Asai, K.; Mitsui, T.; Matsumura, M. *Appl. Catal. A* **2004**, *265*, 115-121.

(39) Ohno, T.; Tsubota, T.; Nishijima, K.; Miyamoto, Z. *Chemistry Letters* **2004**, *33*, 750-751.

(40) Reddy, K. M.; Baruwati, B.; Jayalakshmi, M.; Rao, M. M.; Manorama, S. V. *Journal of Solid State Chemistry* **2005**, *178*, 3352-3358.

(41) Zhang, Q.; Wang, J.; Yin, S.; Sato, T.; Saito, F. *J. Am. Ceram. Soc.* **2004**, *87*, 1161-1163.

(42) Umebayashi, T.; Yamaki, T.; Itoh, H.; Asai, K. *Appl. Phys. Lett.* **2002**, *81*, 454-456.

(43) Hamal, D. B.; Klabunde, K. J. *Journal of Colloid and Interface Science* **2007**, *311*, 514-522.

(44) Katoh, M.; Aihara, H.; Horikawa, T.; Tomida, T. *J. Coll. Interf. Sci.* **2006**, *298*, 805-809.

(45) Ho, W.; Yu, J. C.; Lee, S. *Journal of Solid State Chemistry* **2006**, *179*, 1171-1176.

(46) Ohno, T.; Mitsui, T.; Matsumura, M. *Chemistry Letters* **2003**, *32*, 364-365.

(47) Ohno, T.; Tsubota, T.; Toyofuku, M.; Inaba, R. *Catal. Lett.* **2004**, *98*, 255-258.

(48) Yan, X.; Ohno, T.; Nishijima, K.; Abe, R.; Ohtani, B. *Chemical Physics Letters* **2006**, *429*, 606-610.

(49) Tachikawa, T.; Tojo, S.; Kawai, K.; Endo, M.; Fujitsuka, M.; Ohno, T.; Nishijima, K.; Miyamoto, Z.; Majima, T. *J. Phys. Chem. B* **2004**, *108*, 19299-19306.

(50) Liu, S.; Chen, X. *Journal of Hazardous Materials* **2008**, *152*, 48-55.

(51) Crisan, M.; Braileanu, A.; Raileanu, M.; Zaharescu, M.; Crisan, D., Dragan, Nicolae; Anastasescu, M.; Iancucescu, A.; Nitoi, I.; Marinescu, V. E.; Hodoregea, S. M. *Journal of Non-Crystalline Solids* **2008**, *354*, 705-711.

(52) Yin, S.; Komatsu, M.; Zhang, Q.-w.; Li, R.-x.; Tang, Q.; Saito, F.; Sato, T. *Guocheng Gongcheng Xuebao* **2006**, *6*, 477-481.

(53) Zhou, Z.; Zhang, X.; Wu, Z.; Dong, L. *Chinese Science Bulletin* **2005**, *50*, 2691-2695.

(54) Li, H.; Zhang, X.; Huo, Y.; Zhu, J. *Environmental Science & Technology* **2007**, *41*, 4410-4414.

(55) Tian, F.; Liu, C. *J. Phys. Chem. B* **2006**, *110*, 17866-17871.

(56) Sato, S. *Chemical Physics Letters* **1986**, *123*, 126-8.

(57) Di Valentin, C.; Pacchioni, G.; Selloni, A. *Chemistry of Materials* **2005**, *17*, 6656-6665.

(58) Tachikawa, T.; Takai, Y.; Tojo, S.; Fujitsuka, M.; Irie, H.; Hashimoto, K.; Majima, T. *Journal of Physical Chemistry B* **2006**, *110*, 13158-13165.

(59) Kuznetsov, V. N.; Serpone, N. *Journal of Physical Chemistry B* **2006**, *110*, 25203-25209.

(60) Takeshita, K.; Yamakata, A.; Ishibashi, T.; Onishi, H.; Nishijima, K.; Ohno, T. *Journal of Photochemistry and Photobiology A: Chemistry* **2006**, *177*, 269-275.

(61) Tschirch, J.; Bahnemann, D.; Wark, M.; Rathousky, J. *Journal of Photochemistry and Photobiology, A: Chemistry* **2008**, *194*, 181-188.

(62) Tschirch, J.; Dillert, R.; Bahnemann, D.; Proft, B.; Biedermann, A.; Goer, B. *Research on Chemical Intermediates* **2008**, *34*, 381-392.

(63) Hathway, T.; Jenks, W. S. *J. Photochem. Photobiol. A* **2008**, *200*, 216-224.

(64) Enriquez, R.; Agrios, A. G.; Pichat, P. *Catalysis Today* **2007**, *120*, 196-202.

(65) Kominami, H.; Murakami, S.; Kato, J.; Kera, Y.; Ohtani, B. *Journal of Physical Chemistry B* **2002**, *106*, 10501-10507.

(66) Ranchella, M.; Rol, C.; Sebastiani, G. V. *J. Chem. Soc. Perkin Trans. 2* **2000**, 311-315.

(67) Li, X.; Cubbage, J. W.; Jenks, W. S. *J. Photochem. Photobiol. A* **2001**, *143*, 69-85.

(68) Cermenati, L.; Albini, A.; Pichat, P.; Guillard, C. *Res. Chem. Intermed.* **2000**, *26*, 221-234.

(69) Lang'at-Thoruwa, C.; Song Tong, T.; Hu, J.; Simons Andrean, L.; Murphy Patricia, A. *Journal of Natural Products* **2003**, *66*, 149-51.

(70) Li, X.; Cubbage, J. W.; Tetzlaff, T. A.; Jenks, W. S. *J. Org. Chem.* **1999**, *64*, 8509-8524.

(71) Bowman, W. D.; Demas, J. N. *Journal of Physical Chemistry* **1976**, *80*, 2434-2435.

(72) Hatchard, C. G.; Parker, C. A. *Proceeding of the Royal Society of London. Series A, Mathematical and Physical Sciences* **1956**, *235*, 518-536.

(73) Moulder, J. F.; Stickle, W. F.; Sobol, P. E.; Bomben, K. D. *Handbook of X-Ray Photoelectron Spectroscopy*; Perkin-Elmer Corporation (Physical Electronics): Eden Prairie, MN, 1992.

(74) Sayago, D. I.; Serrano, P.; Bohme, O.; Goldoni, A.; Paolucci, G.; Roman, E.; Martin-Gago, J. A. *Physical Review B: Condensed Matter and Materials Physics* **2001**, *64*, 205402/1-205402/7.

(75) Sayago, D. I.; Serrano, P.; Bohme, O.; Goldoni, A.; Paolucci, G.; Roman, E.; Martin-Gago, J. A. *Surface Science* **2001**, *482-485*, 9-14.

(76) Roman, E.; De Segovia, J. L.; Martin-Gago, J. A.; Comtet, G.; Hellner, L. *Vacuum* **1997**, *48*, 597-600.

(77) The rates are not quantum yields; no attempt was made to quantify the fraction of light absorbed.

(78) Kim, S.; Choi, W. *Journal of Physical Chemistry B* **2005**, *109*, 5143-5149.

(79) Agrios, A. G.; Gray, K. A.; Weitz, E. *Langmuir* **2003**, *19*, 5178.

(80) Agrios, A. G.; Gray, K. A.; Weitz, E. *Langmuir* **2004**, *20*, 5911-5917.

(81) Richard, C. *New J. Chem.* **1994**, *18*, 443-445.

(82) Small amounts of "atmospheric" carbon are always detected by XPS; we cannot eliminate the possibility of small amounts of graphitic type carbon in the final catalyst.

(83) Rockafellow, E. M.; Fang, X.; Trewyn, B. G.; Schmidt-Rohr, K.; Jenks William, S. *Chemistry of Materials* **2009**, *21*, 1187-1197.

(84) Orlov, A.; Watson, D. J.; Williams, F. J.; Tikhov, M.; Lambert, R. M. *Langmuir* **2007**, *23*, 9551-9554.

(85) Due to analytical difficulties the Pichat group was unable to quantify 8HQ, but we were able to separate this material chromatographically from the others.

CHAPTER 6

Redox Couples in Selenium-Modified TiO_2 and the Impact on Photocatalysis

In the style of a paper to be submitted to *Langmuir.*

Erin M. Rockafellow, Jessica M. Haywood, Travis Witte, Robert S. Houk,
and William S. Jenks*
Department of Chemistry, Iowa State University, Ames, IA 50011-3111

6.1 ABSTRACT

Several main-group doped TiO_2 photocatalysts have only been effective in degrading certain organic molecules under visible light. Consequently, the UV photocatalytic reactivity of non-metal doped titania is often sacrificed. This work describes the preparation of a selenium-modified TiO_2 photocatalyst and the evaluation of its photocatalytic activity. Se-TiO_2 displayed greater visible absorption than undoped TiO_2, but was still capable of degrading quinoline at a slightly faster rate under UV light. Se-TiO_2 was also able to degrade organic molecules under purely visible light by a single electron transfer pathway. Irradiation with > 435 nm light showed no evidence for efficient production of HO•-like species. Se-TiO_2 was also examined under hypoxic conditions, where the Se atoms were capable of trapping photogenerated electrons as evidenced by XPS.

6.2 INTRODUCTION

Titanium dioxide is a popular photocatalyst for air and water remediation as a result of several attractive properties such as low toxicity, inexpensive production, high thermal stability, and functionality. With exposure to UV radiation and O_2, TiO_2 degrades most organic compounds to CO_2, H_2O, and appropriate inorganic ions.[1-7] Unfortunately, pristine TiO_2 has a low quantum yield for generating the oxidative species responsible for degradation due to competition with recombination of photogenerated charges. In addition, anatase and rutile, the most commonly employed phases of TiO_2, are capable of

absorbing only ~5% of the solar light that reaches the Earth's surface due to their near-UV absorption cutoff. Therefore, it has been an important goal to improve upon pristine TiO_2 through modifications that prevent recombination and extend absorbance beyond 400 nm.[8-11]

Researchers have used several approaches to improve TiO_2 photocatalysts. One method has been to modify TiO_2 with metal doping or deposition.[2,8,11] Transition metal doping was found to extend absorbance into the visible region, but the metal often acted as a recombination center, reducing photonic efficiency. Noble metals used to modify TiO_2 are present as small pools on the surface of the particle. Platinum was effective in suppressing charge recombination by providing an efficient electron trap, but was not cost-effective for commercial use because the metal itself was oxidized by air leading to catalyst deactivation.[8,12]

Main group elements have been a recent focus for TiO_2 modification, and several methods to prepare titania doped with nitrogen, sulfur, and carbon using various dopant and titanium precursors have been published.[9-11,13-18] The major goal of this tactic is to extend the absorption range of the catalyst without reducing efficiency. Visible-light sensitivity is a result of localized states within the band gaps and induced oxygen vacancies (Ti^{3+} states).[13,18] In general, these photocatalysts have shown appreciable visible-light absorbance and photocatalytic activity. However, several reports have demonstrated lower quantum efficiencies under UV radiation and wavelength dependent chemistry for N, S, and C-doped TiO_2.[15,19-21] Therefore, careful consideration is essential for choosing applications for N, S, or C-doped TiO_2. If comparable photocatalytic activity to that of the unmodified parent material or broad functionality under visible light was achieved, the modified TiO_2 would be better suited for more universal applications.

One possible avenue to increase UV efficiency is through the addition of an internal electron trap within or on the surface of the catalyst itself. This has been successful in a number of reports using both homemade and commercially available non-metal doped titania that is either co-doped or modified with proficient electron-trapping metals, such as Fe, Cu, Ag, and Pt; however, little is known about the thermal stability of these materials.[22-26]

Larger main group elements with flexible oxidation states, such as iodine or selenium, can provide a center capable of trapping electrons. TiO_2 modified by either iodine doping or I_2 encapsulation has demonstrated interesting electronic properties.[27-29] Modification with selenium has not been widely studied, but Zhang et al. have prepared an SeO_2/TiO_2 composite that demonstrated redox chemistry.[30] Their material initially introduced an undesirable blue shift, but after chemical reduction to convert some of the SeO_2 centers to Se^0 metallic sites, which are capable of visible light absorption, a significant red shift occurred. Brief photocatalytic studies were done using organic dyes, which are unreliable mechanistic probe molecules. The authors also neglect to clearly indicate the wavelength used in their studies. Therefore, it is not known if the same problems that are encountered with other main group-doped TiO_2 nanoparticles are prevalent in their composite.

In this paper, we report a Se-doped titania that shows different properties than the SeO_2/TiO_2 composite prepared by Zhang *et al*.[30] The new photocatalyst exhibits an initial blue shift in absoption relative to pristine TiO_2, but directly after calcination without further modification, a modest red shift is achieved. We report that Se-TiO_2 exhibits unique oxidative chemistry with these selected organic probe molecules, chosen for their value as mechanistic probes. Photocatalysis studies in oxygen-rich and oxygen-deficient environments were conducted to investigate the ability and effects of Se acting as an electron trap.

6.3 EXPERIMENTAL

6.3.1 Chemicals

Chemicals, ordered at the highest commercially available purity, were used as received. Water was purified to a resistivity above 18 MΩ/cm. 1-(*p*-Anisyl)neopentan-1-ol (**AN**) was prepared as reported earlier.[31]

6.3.2 Photocatalyst Preparation

Se-TiO_2 was prepared by adapting a literature procedure, substituting SeO_2 for thiourea.[32] SeO_2 (1 eq.) was dissolved in 90% ethanol. To this, 2 eq. of titanium (IV)

tetraisopropoxide was added dropwise with vigorous stirring. The solution containing a white ppt. was stirred for 3 hours, followed by standing for 20 hours to allow for hydrolysis of the Ti precursor. The mixture was evaporated under reduced pressure leaving a white solid powder, which was then annealed in a quartz tube for 4 hours at 450 ˚C under air. The catalyst was washed with water and dried. A beige solid was obtained. Undoped TiO_2 was prepared using a similar procedure without the selenium source.[15]

It was found that some Se could be detected by ICP-MS in aqueous phases after photocatalytic degradations had been carried out. This is likely due to the slow hydrolysis of weakly bound surface Se species. Therefore, more vigorous efforts were made to ensure that the photocatalyst could be sufficiently cleaned so that no selenium leaching occurred. A sample of Se-TiO_2 was refluxed in Millipore water for 4 h, followed by careful filtration and rinsing. The filtrate was collected for analysis and the photocatalyst was subjected to three more identical reflux cycles. Analysis of solutions determined that no more selenium (detection limit of 7.93 ppb) was transferred to solution after one reflux cycle. A quadrupole ICP-MS device was used for all analyses performed. $^{84}Kr^{+}$ was monitored in order to account for potential isobaric interference of Kr with the measurement of $^{78}Se^{+}$. Analyses were done by employing either a standard additions or internal standard method using a Se or As standard, respectively. Results for each sample were reported from the background-subtracted integrated average peak intensities from at least 16 consecutive scans.

Careful control experiments using quinoline (**Q**) at pH 3 and pH 6 showed that there was not a significant difference between the thoroughly refluxed and washed Se-TiO_2 catalysts, either for degradation rates or product distributions.

6.3.3 Physical Charactization

Powder x-ray diffraction (XRD) spectra were taken with a diffractometer employing Cu K_α radiation. X-ray photoelectron spectroscopy (XPS) was done using a multitechnique spectrometer utilizing nonmonochromatized Al or Mg Kα radiation with a 1 mm^2 sampling area. The take-off angle was fixed at 45˚. Diffuse reflectance spectra were obtained with a UV/Vis spectrophotometer equipped with a diffuse reflectance

attachment with MgO as a reference. For transmission electron microscopy (TEM) measurements, an aliquot of the powder was sonicated in purified water for 15 min. A single drop of this suspension was placed on a lacey-carbon-coated copper TEM grid and dried in air. The TEM examination was completed on an instrument operated at 200 kV with electron optical magnification of 64,000 to 550,000. Surface area analysis of the materials was performed by nitrogen sorption isotherms in a sorptometer. Surface areas were calculated by the Brunauer-Emmett-Teller (BET) method. Point of zero charge estimates (PZC) were carried out by mass titration methods as described by Vakros *et al.*[33]

6.3.4 Degradations

UV and visible photolyses under O_2 were conducted as described in a previous report.[15] As noted, some photolyses were carried out in an O_2 deficient atmosphere. These samples initially were purged with argon prior to and during irradiations. This was used as a gauge for experiment length. Consecutive reactions were found to have unacceptable variablility as a result of residual O_2. To avoid reproducibility issues with significant residual O_2 concentrations, solutions were purged with argon and the headspace above the solution was pumped to 300 mTorr. The purge/pump cycles were done at least three times, and the solution was photolyzed under vacuum. In this case, only an initial and end point were sampled to determine conversion and produced intermediate products. Under evacuated conditions, percent conversions were reproducible within 5% error. Reactions were monitored and analyzed by HPLC or GCMS as reported earlier.[15]

In order to obtain physical evidence of any changes in the oxidation state of the dopant brought about during the photolysis (particularly under hypoxic conditions) samples of the post-photolysis catalyst were prepared using quinoline as a probe molecule under O_2-deficient conditions. The solution was not acidified to avoid sulfate contamination, because sulfate overlaps the Se 3p peak in the XP spectrum. The material was isolated by careful transfer under argon to a round bottom flask with two necks, one with a standard ground glass joint with a septum and one containing a stopcock and hose barb. The solution was kept under argon, frozen, and lyophilized. The sample was

plated for XPS in a glove box.

6.4 RESULTS

6.4.1 Photocatalyst Characterization

X-Ray powder diffraction revealed that Se-TiO_2 and undoped TiO_2 were anatase (Figure 6.1a). Diffuse reflectance showed that a blue shift occurs in the preannealed sample, but the annealed sample, which is beige instead of white, exhibits a modest tail extending into the visible region (Figure 6.1b). X-Ray photoelectron spectroscopy (XPS) confirmed the presence of Se, which appeared to be incorporated in the Se^{4+} oxidation state, the same as SeO_2 (Figure 6.1c and 6.1d). The Se 3p peak was used for quantification because the Se 3d peak overlaps the Ti 3s peak. The Se-TiO_2 was found to contain nearly 4 at. % Se after simply washing with water, and only about 2 at. % after refluxing in water. (This removes surface-bound Se, presumably.) After etching the washed sample, new features were present at chemical shifts at 55 eV and 161 eV indicative of a highly reduced oxidation state of Se^0.[34] The total at. % of Se was reduced to 2.5%.

The point of zero charge was found to be at a pH of ~3.5 compared to a value for P25 of 4.5. Thus Se-TiO_2 is more acidic than P25, although our value of 4.5 varies from many reports that are usually closer to 6.5.[33]

6.4.2 Photocatalytic degradations under oxygen rich conditions

Irradiations used either (a) the purely UV light from fluorescent bulbs centered around 350 nm or (b) the exclusively visible light of a 75 W Xe arc lamp passed through either a 495 or 435 nm longpass cut-off filter and a water filter to remove excessive IR. In order to gain a semi-quantitative comparison, ferrioxalate actinometry was done to normalize light sources.[35,36] As seen in Figure 6.1b, undoped TiO_2 does not absorb light with wavelengths longer than ~400 nm. Therefore, no photocatalytic reactivity is expected under these conditions, at least not though conventional semi-conductor band-gap excitation. The probe molecules were thermally stable over the reaction timescale and conditions based on the results of reactions carried out in the absence of any light

(dark reactions).

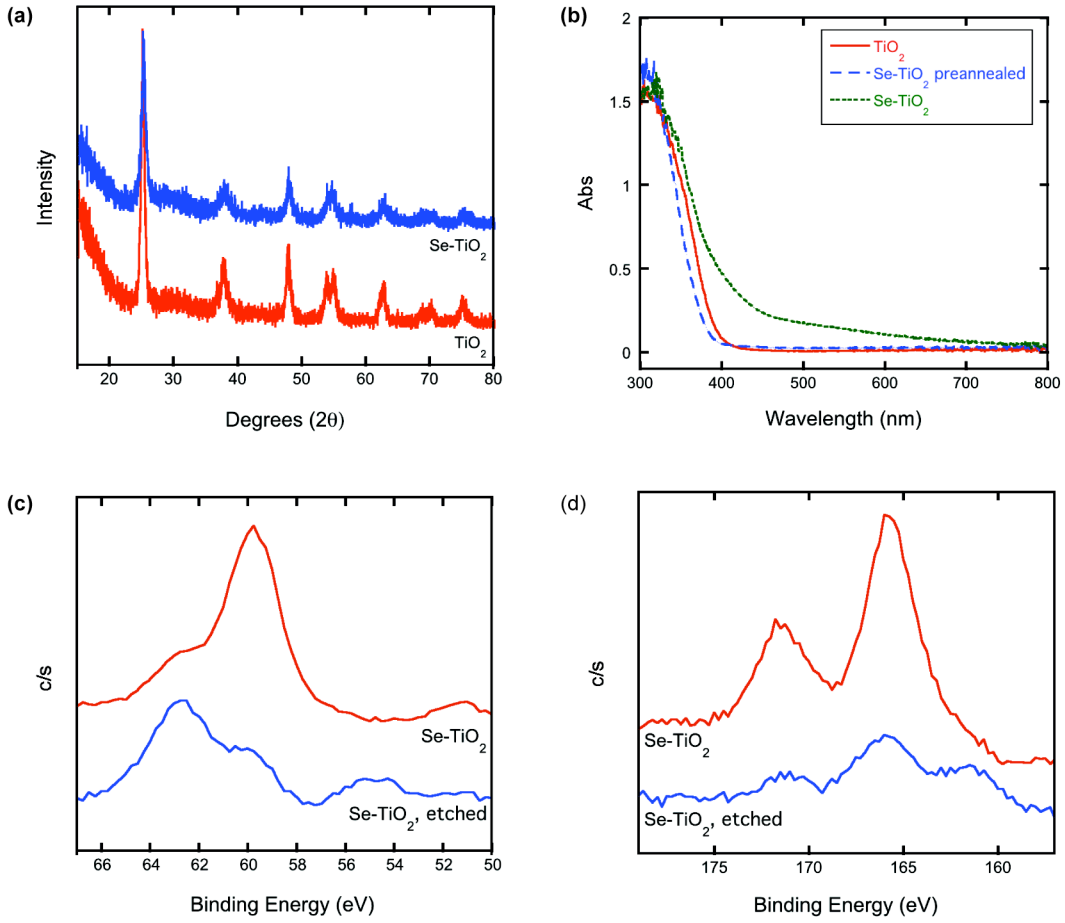

Figure 6.1 **(a)** X-Ray powder diffraction, **(b)** diffuse reflection spectra, and X-ray photoelectron spectra of the **(c)** Se 3d and **(d)** Se 3p regions of Se-TiO_2 and undoped TiO_2.

Rates of degradation. The initial zero-order rates of loss of both probe molecule under O_2-rich conditions are displayed on a logarithmic scale for both Se-TiO_2 and undoped TiO_2 in Figure 6.2. Se-TiO_2 degraded **Q** at a slightly faster rate than did undoped TiO_2 under UV light at both pH 3 and pH 6. However, the rate of loss of **AN** with Se-TiO_2 as the photocatalyst is roughly 3 times slower than TiO_2. Photolyses with Se-TiO_2 carried out using wavelengths longer than 495 nm showed insignificant degradation of the probe molecules, and were comparable to control experiments using undoped TiO_2 and to dark reactions. This is sensible as wavelengths longer than 495 nm

fall in the region of the extended tail of Se-TiO_2 where significant photocatalytic activity is doubtful. An appreciable loss of both **AN** and **Q** at pH 6 is seen under > 435 nm light with Se-TiO_2. This spectral output was in the region of the weak shoulder feature where slightly more light is absorbed. No significant reduction of **Q** at pH 3 is observed using > 435 nm irradiation of Se-TiO_2. Undoped TiO_2 under > 435 nm irradiation was no more effective in removing any of the probe molecules than the dark control reactions.

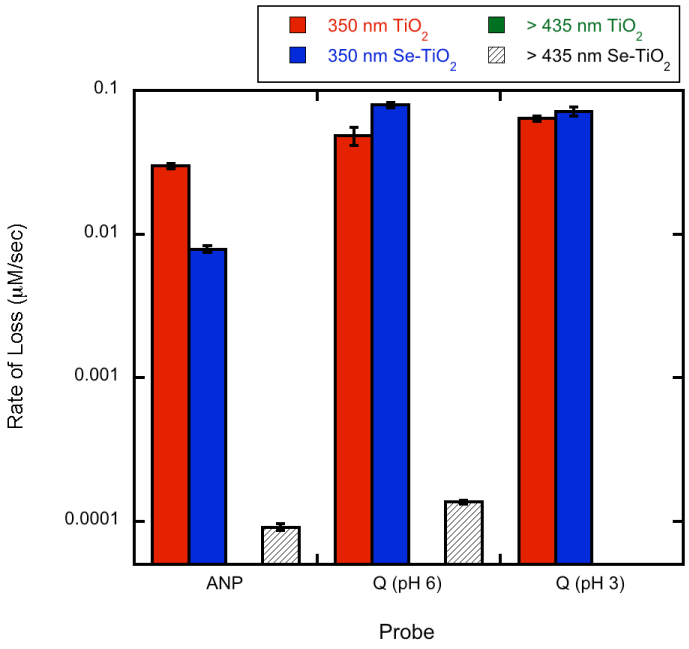

Figure 6.2 Rates of loss of probe molecules using TiO_2 or Se-TiO_2 under UV or visible light displayed on a logarithmic scale.

Intermediate products from Q degradations. Previous results using quinoline as a probe molecule have shown that SET chemistry is the dominant photocatalytic oxidation pathway at pH 6, while hydroxyl chemistry is favored at pH 3, as observed in product distributions (Scheme 6.1a).[15,37-39] Cermenati *et al.* found that addition of a hydroxyl radical occurs preferentially at the 5- and 8-positions of the electron rich benzene moiety of quinolinium (favored at pH 3) to yield 5-hydroxyquinoline (**5HQ**) and 8-hydroxyquinoline (**8HQ**), while SET is favored at the electron deficient pyridine ring of neutral quinoline (dominant at pH 6), leading to 2-quinolinone (**2HQ**), 4-quinolinone

(**4HQ**), and 2-aminobenzaldehyde (**2AB**).[37-39] Computations carried out by Wiest support experimental findings of hydroxylation patterns.[40]

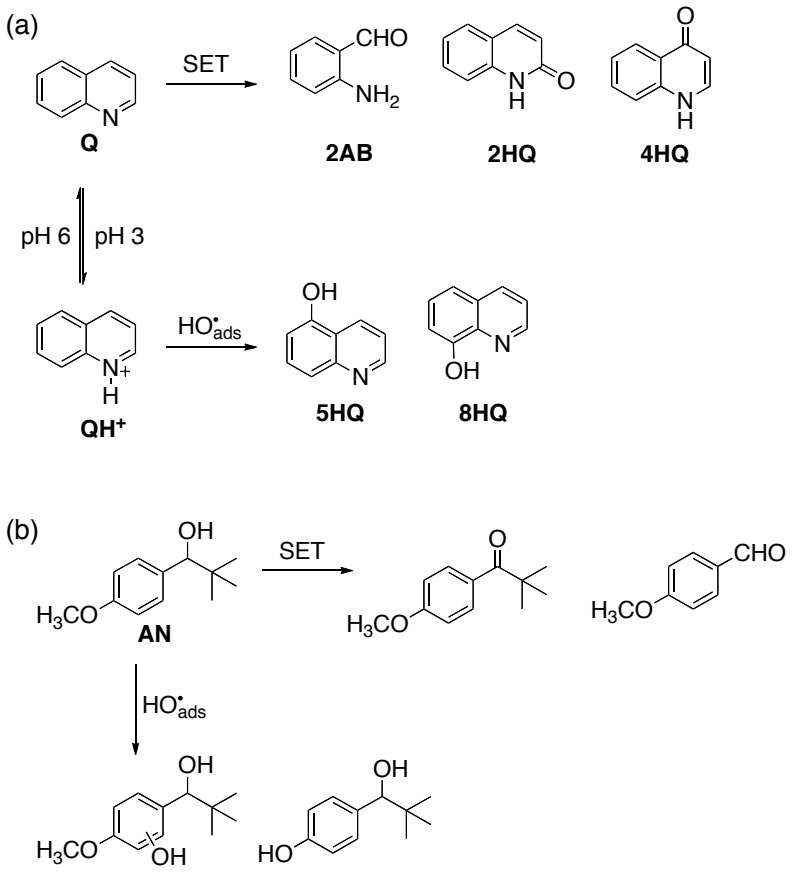

Scheme 6.1 TiO_2-mediated degradation pathways for (a) **Q** and (b) **AN**.

Figure 6.3 shows the distribution of observed products at 20% and 50% conversion.[41] Interestingly, intermediate products formed in Se-TiO_2 photocatalysis of quinoline at both pH 3 and 6 under UV light were predominantly HO•-like products. While significant amounts of SET products do grow in at pH 6, HO•-like chemistry was clearly the dominant path.

Only visible light irradiation of Se-TiO_2 at pH 6 led to any substantial degradation. Product analysis shows that SET products dominate and, in comparison to the UV radiation results, the hydroxyl-like pathway was essentially shut down.

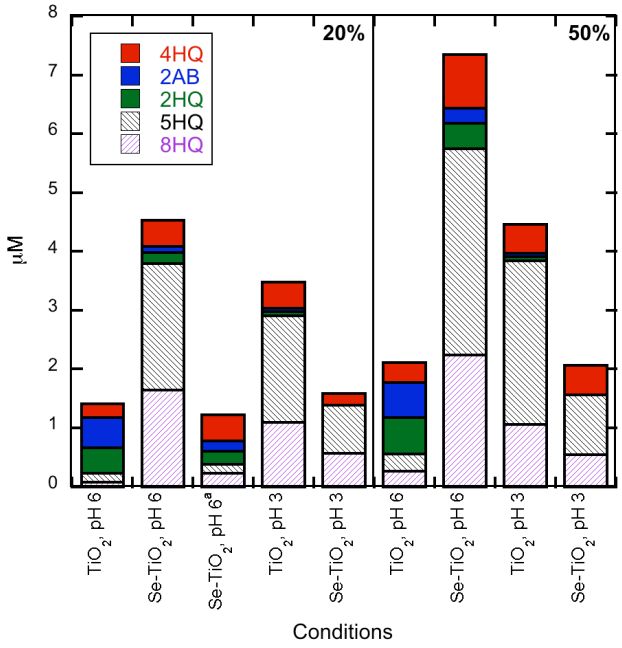

Figure 6.3 Intermediate products formed at 20% and 50% conversion of quinoline under UV light, except when noted. [a] > 435 nm.

Intermediate product analysis from AN degradations. **AN** also contains two sites of reactivity. Ranchella et al. originally reported that SET chemistry occurs primarily from the side chain, while HO•-like chemistry typically takes place at the benzene ring (Scheme 6.1b).[42] Using P25, Hathway and Jenks reported that hydroxyl-like reactivity is dominant at pH 8.5.[31] The results of UV photolysis at pH 8.5 reported here are in order with this finding as the SET: HO• product ratio was found to be 2:5 for Se-TiO_2-mediated degradation. Conversely, visible excitation of Se-TiO_2 resulted in exclusively SET products.

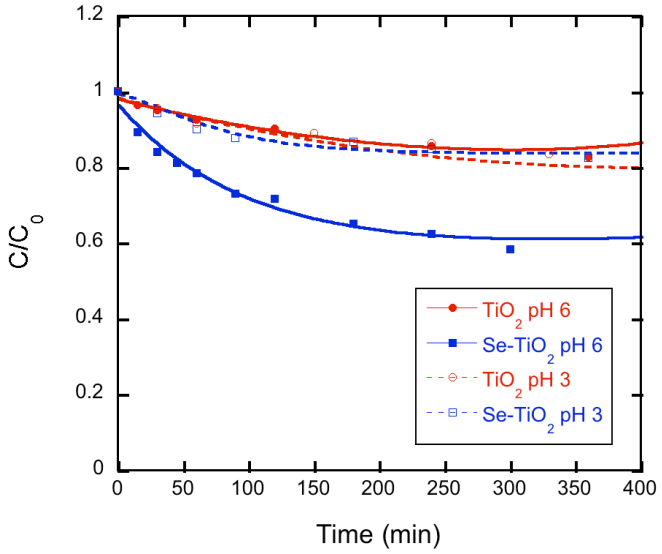

Figure 6.4 Loss of quinoline mediated by Se-TiO_2 under 350 nm and hypoxic conditions.

6.4.2 Photocatalytic degradations under oxygen deficient conditions

Without significant amounts of O_2 in solution to trap electrons and compete with recombination, the overall quantum efficiency of the photocatalyst should be greatly reduced. The Se center, if functional as an electron acceptor, could slow the recombination pathway and preserve some degree of photocatalytic functionality.

Quinoline degradation. To avoid unacceptably high variation in rates and product distributions due to residual oxygen, reactions were degassed by purging with argon and pumping cycles. Irradiations were done using 350 nm lamps. Since the reaction was carried out under vacuum, only initial and final samples could be taken for analysis. At pH 3, Se-TiO_2 and TiO_2 degraded 14% and 15% of the initial quinoline after 4 hours, respectively. At pH 6, Se-TiO_2 showed 35% loss of **Q**, while TiO_2 led to only 7% loss of **Q** after 4 hours of photolysis. Very careful photolyses using only Ar purging to remove O_2 were carried out so the loss of quinoline could be monitored over time as shown in Figure 6.4. The asymptotic curve indicates a finite reserve of electron storage at Se centers.

Figure 6.5 shows the intermediate products formed un these hypoxic conditions. Only very small amounts of products, mainly consisting of hydroxyl-substitution products, are observed, with the exception of Se-TiO_2-mediated degradation of quinoline at pH 6. This exceptional case results in roughly a four-fold increase of observable products, made up of HO•-like products as well as primary SET products.

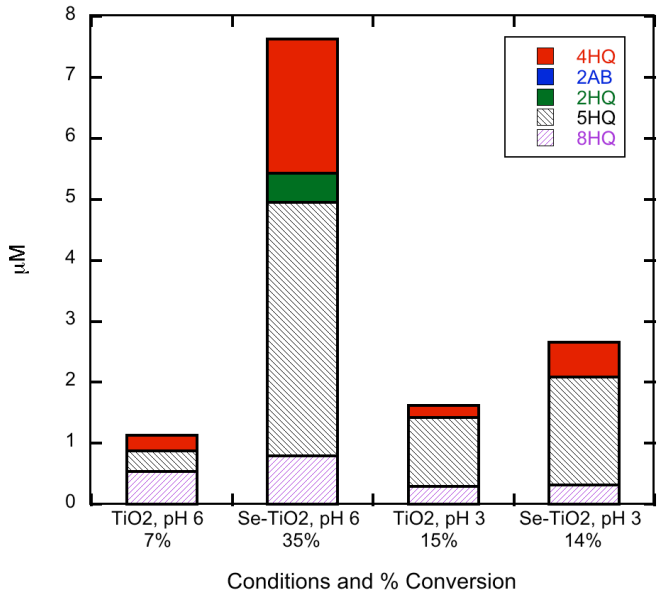

Figure 6.5 Intermediate products formed after 4 hours of photolysis with UV light under purged and evacuated conditions.

Photocatalyst changes. Physical changes that occurred over the photolysis provided further evidence for the reduction of Se centers by trapped electrons, such as an obvious darkening of the photocatalyst. The Se-TiO_2 was examined by XPS after irradiation to obtain direct evidence for any changes to the oxidation state of selenium. The XP spectrum obtained after photolysis that shows the subtle appearance of a reduced Se species after exposure to the photocatalytic conditions (Figure 6.6). Only the Se^{4+} was seen in material prior to irradiation in both refluxed and the raw washed samples. In addition, after exposure to ambient air for 24 hours, the reduced Se^0 species was partially re-oxidized, as indicated by the XP spectrum.

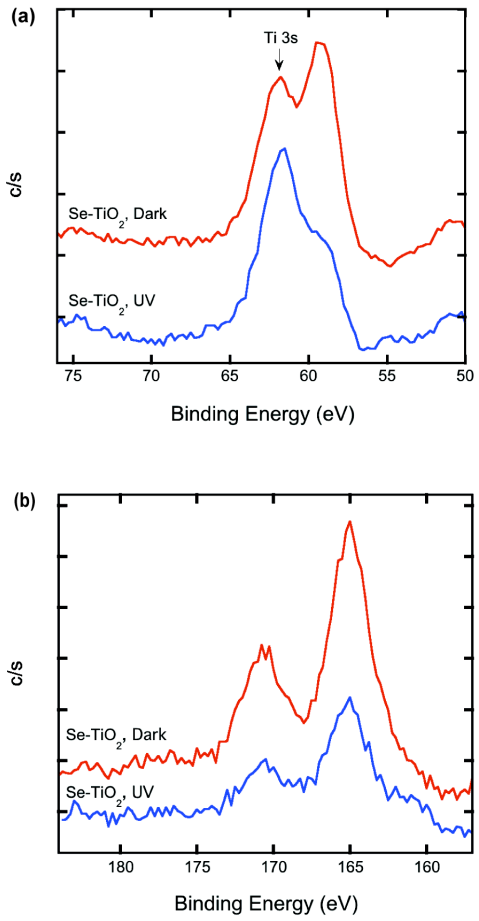

Figure 6.6 XPS measurements of the (a) Se 3d and (b) Se 3p regions of Se-TiO_2 before (dark) and after UV photolysis (UV) under oxygen deficient conditions.

6.5 DISCUSSION

6.5.1 Physical Properties

Selenium dioxide was selected as a selenium precursor because of its commercial availability, common use as an oxidant in synthesis, and potential to be incorporated into TiO_2. In the presence of water, selenium dioxide is readily hydrated and produces selenous acid (H_2SeO_3) and could be integrated into a growing TiO_2 lattice as Ti-O-Se-O linkages. However, the amorphous powder obtained after the sol-gel process was white and displayed a blue shift relative to anatase TiO_2 in the diffuse reflectance spectrum shown in Figure 6.1b, as reported in analogous cases.[43] After annealing, a beige powder

was produced, characterized by a slight red shift of the main band and an extended tail into the visible. These two spectral changes are attributed to (1) the induced crystallinity and particle growth that occurs through annealing and (2) effects brought about by the incorporation of Se atoms. Accordingly, the fraction of usable sunlight would be larger for Se-TiO_2. The SeO_2/TiO_2 composite prepared by Zhang and coworkers exhibited a blue shift, even after calcination, suggesting that the selenium is incorporated differently in their material.[30]

Etching with Ar^+ ions led to new features in the XP spectrum that are consistent with elemental selenium (Se^0). This is likely a result of the Se centers getting reduced during the etching process, but can also be explained by the possibility that surface species are being removed exposing deeper layers consisting of Se^0. The same XP spectral features ascribed to Se^0 were observed in the post-photolysis material used in hypoxic conditions.

While the obtained PZC value for commercial undoped TiO_2 (Degussa P25) was low (pH of 4.5 compared to literature values around pH 6.5), the results clearly indicate that Se-TiO_2 has a more acidic surface than undoped TiO_2 (pH of 3.5). This is not surprising as surface Se-OH bonds are possible and likely to act similarly to selenous or selenic acid. The greater surface acidity could potentially exhibit different chemistry, as it would likely effect specific binding, and is sometimes the attributed cause for activity.[44]

6.5.2 Photocatalysis Results

In order to discuss whether or not a new photocatalyst is an improvement over the known catalysts, comparisons to results in the available literature must be drawn. Similarities and differences between known photocatalysts and Se-TiO_2 will be addressed with a particular emphasis on our recent work using S-TiO_2 because it greatly parallels the mechanistic investigations described here.[15] In addition, by simply changing the chalcogen dopant, the chemistry could potentially be changed by the presence of new orbital energy levels.

UV irradiation. Under UV light, Se-TiO_2 exhibited a very comparable, or slightly improved, rate of degradation of **Q** at both pH 3 and 6 under oxygenated conditions. This result was often not found with other main group-doped TiO_2 photocatalysts. In fact, we

previously found that S-TiO_2 was slower than undoped TiO_2 in the degradation of quinoline.[15] At a simplified level, the observed improvement in rate could be due either to enhanced absorption of the substrate or an inherent increase in photocatalyst efficiency.

Product analysis of quinoline degradations revealed a unique result: HO•-like chemistry was dominant at *both* pH 3 and pH 6. This was different from Pichat's report using P25, as well as our results using S-TiO_2. The reason for the preference for HO•-like chemistry at pH 6 is not yet precisely understood. Since the solutions are buffered, it should not depend on the back equilibrium between **Q** and $\mathbf{QH^+}$. However, specific surface interactions may be very important.

Quinoline has been shown to weakly adsorb to TiO_2 at pH 6, whereas $\mathbf{QH^+}$ at pH 3 binds very poorly.[39] At pH 6, the Se-TiO_2 surface is likely to be closer to neutral, which would not negatively affect the binding of **Q** significantly. Therefore, a higher degradation rate could be due to an inherent increase in catalyst efficiency. The observed product distribution provides further support for this. The unique increase in HO•-like products seen at pH 6 could result from the presence of a second HO•-like pathway that is dependent on surface adsorption. Specifically, Pichat reports evidence for a "free HO•" pathway using P25 when binding is not favored in the case of $\mathbf{QH^+}$; however, the change in surface interactions with the new surface presented by Se-TiO_2 could favor an adsorbed species with HO•-like reactivity produced by "deep-trap" holes as described by Bahnemann.[38,45]

This same hypothesis could be used to elucidate quinoline degradation mechanisms operative with Se-TiO_2 at pH 3. Since the Se-TiO_2 surface is more acidic than that of undoped TiO_2, more neutral sites would be available at a lower pH value making it more attractive to $\mathbf{QH^+}$. Slightly more favorable surface interactions would allow for both types of HO•-like chemistry to occur, and could explain why Se-TiO_2 is more efficient than other main-group doped titania.

Photolyses using **AN** carried out at pH 8.5 also showed a preference for HO•-like chemistry when Se-TiO_2 was used as the photocatalyst. In contrast to quinoline degradations, but nearly identical to previous S-TiO_2 results, the rate of loss was

significantly lower with Se-TiO_2 than undoped TiO_2.[15] Intermediate degradation product distributions favored HO•-like products, which is qualitatively the same as previous results.[15,31]

AN rates and product distributions provide further evidence that surface interactions are important for efficient removal of organic molecules mediated by Se-TiO_2. Previous work shows that **AN** is a very poor binder, particularly at pH values higher than 7. This suggests that **AN** would be degraded by predominately the "free HO•" pathway, and the photocatalytic enhancement offered by Se-TiO_2 is very sensitive to surface interactions.

In the absence of O_2, Se-TiO_2 could be more efficient than undoped TiO_2 where no electron trap is present, and could lead to a greater conversion in a given amount of time. Only moderate removal of **Q** leading to the formation of HO•-like products at pH 3 was observed using both undoped TiO_2 and Se-TiO_2. This was not unsurprising for undoped TiO_2 if it is assumed that HO• chemistry results from trapping of holes in the catalyst since recombination of untrapped holes is not suppressed under hypoxic conditions. At pH 6, undoped TiO_2 led to very little overall removal of quinoline, since very little HO•-like chemistry is observed at this pH ordinarily. The Se-TiO_2-mediated degradation of quinoline at pH 6 gave the most significant removal. The stronger surface interaction between Se-TiO_2 and neutral **Q** present at pH 6 versus the weaker interaction with $\mathbf{QH^+}$ at pH 3 allowed for a greater loss of quinoline, and still showed that HO•-like chemistry is more significant than SET chemistry. This suggests that the Se centers acting as an internal electron trap is an important factor under hypoxic conditions, which is confirmed by XPS results (Figure 6.6), in addition to surface interactions. Figure 6.4 demonstrates that there is stoichiometric limit of available sites for reduction. Once the finite number of trap sites are consumed, the slow reaction observed for all the other cases becomes operative. This slow reaction is most likely some sort of photooxidation using residual O_2 or photohydration pathway that is generally too slow to compete with SET of HO•-like chemistry.

It is not completely understood degradations of quinoline at pH 6 mediated by Se-TiO_2 favored HO•-like pathways (under both O_2-rich and O_2-deficient conditions), but could be a result of improved photocatalytic efficiency. To account for the observed SET

products observed in hypoxic degradations, it is possible that some of the **2HQ** could be formed through hydroxyl-like pathways, while accumulation of **4HQ** indicates that the radical cation organic intermediate is formed through SET chemistry.[38] In the absence of O_2, charge carrier kinetics would be different, presumably leading to an increase of SET products since this is the faster pathway, in general. Without an excess of molecular oxygen, the **4HQ** radical cation precursor must be quenched by alternative nucleophiles, such as water. The absence of **2AB** is clearly correlated to the lack of oxygen required for its formation.[38]

Visible irradiation. Degradation of **Q** was only observed at pH 6 using visible light with the appropriate energy and Se-TiO_2. This result is identical to that previously reported for S-TiO_2.[15] Product analysis of Se-TiO_2-mediated degradation of **Q** at pH 6 shows that the SET products are formed, but the hydroxyl-like chemistry leading to **5HQ** and **8HQ** is nearly eliminated. This indicates that either HO•-like species were not sufficiently generated under visible irradiation or that the resulting products are consumed faster than they are formed. We conclude that HO•-like chemistry is suppressed because the photolysis at pH 3 (expected to undergo HO•-like reactions) showed no appreciable removal of **Q**. Although quinolinium might be more likely to interact with the surface of Se-TiO_2, SET was not successful at pH 3 as a result of the heightened ionization potential of quinolinium.

Se-TiO_2 was also able to modestly degrade **AN** under visible light, which was not the case for S-TiO_2. Only SET products were observable, providing further support for the conclusions drawn for the **Q** reactions. This demonstrates that Se-TiO_2 has a higher oxidizing power than the S-TiO_2 we have obtained, but is still unable to initiate HO•-like chemistry under visible light.

6.6 CONCLUSIONS

Se-TiO_2 was shown to be an improved visible light-active photocatalyst. Degradation rates of quinoline were comparable to undoped TiO_2 under UV light. Surface interactions appeared to play a very significant role in the degradation. It is likely that

higher concentrations of HO•-like species were generated, but are only useful if the molecule is in good proximity to the surface. Although visible light absorption is only moderately extended, the photogenerated hole induced by > 435 nm light is strong enough to oxidize difficult molecules by SET-initiated chemistry. No strong evidence for HO•-like pathways is observed when purely visible light is used. It was also shown that selenium atoms act as a trap for photogenerated electrons, and in turn is reduced to Se^0.

6.7 ACKNOWLEDGEMENT

The authors gratefully acknowledge the National Science Foundation (NSF CHE0518586) for support of this work, Prof. Clemens Burda for allowing us to obtain diffuse reflectance spectra on his instrument, and Jim Anderegg for his assistance with XPS.

6.8 REFERENCES

(1) *Photocatalysis: Fundamentals and Applications*; Serpone, N.; Pelizzetti, E., Eds.; John Wiley & Sons: New York, 1989.

(2) Hoffmann, M. R.; Martin, S. T.; Choi, W. Y.; Bahnemann, D. W. *Chemical Reviews* **1995**, *95*, 69-96.

(3) Pichat, P. *Environmental Science and Pollution Control Series* **2003**, *26*, 77-119.

(4) Jenks, W. S. In *Environmental Catalysis*; Grassian, V. H., Ed.; CRC Press: Boca Raton, 2005, p 307-346.

(5) Bahnemann, D. *Solar Energy* **2004**, *77*, 445-459.

(6) Robertson, P. K. J.; Bahnemann, D. W.; Robertson, J. M. C.; Wood, F. *Handbook of Environmental Chemistry* **2005**, *2*, 367-423.

(7) Fujishima, A.; Zhang, X.; Tryk, D. A. *Surface Science Reports* **2008**, *63*, 515-582.

(8) Linsebigler, A. L.; Lu, G. Q.; Yates, J. T. *Chemical Reviews* **1995**, *95*, 735-758.

(9) Serpone, N. *Journal of Physical Chemistry B* **2006**, *110*, 24287-24293.

(10) Tachikawa, T.; Fujitsuka, M.; Majima, T. *Journal of Physical Chemistry C* **2007**, *111*, 5259-5275.

(11) Thompson, T.; Yates, J. *Chemical Reviews* **2006**, *106*, 4428-4453.

(12) Nowotny, M. K.; Sheppard, L. R.; Bak, T.; Nowotny, J. *Journal of Physical Chemistry C* **2008**, *112*, 5275-5300.

(13) Qiu, X.; Burda, C. *Chemical Physics* **2007**, *339*, 1-10.

(14) Di Valentin, C.; Finazzi, E.; Pacchioni, G.; Selloni, A.; Livraghi, S.; Paganini, M. C.; Giamello, E. *Chemical Physics* **2007**, *339*, 44-56.

(15) Rockafellow, E. M.; Stewart, L. K.; Jenks, W. S. *Applied Catalysis, B: Environmental* **2009**, *91*, 554-562.

(16) Rockafellow, E. M.; Fang, X.; Trewyn, B. G.; Schmidt-Rohr, K.; Jenks, W. S. *Chemistry of Materials* **2009**, *21*, 1187-1197.

(17) Reddy, K. M.; Baruwati, B.; Jayalakshmi, M.; Rao, M. M.; Manorama, S. V. *Journal of Solid State Chemistry* **2005**, *178*, 3352-3358.

(18) Kuznetsov, V. N.; Serpone, N. *Journal of Physical Chemistry B* **2006**, *110*, 25203-25209.

(19) Irie, H.; Watanabe, Y.; Hashimoto, K. *J. Phys. Chem. B* **2003**, *107*, 5483-5486.

(20) Tachikawa, T.; Tojo, S.; Kawai, K.; Endo, M.; Fujitsuka, M.; Ohno, T.; Nishijima, K.; Miyamoto, Z.; Majima, T. *J. Phys. Chem. B* **2004**, *108*, 19299-19306.

(21) Yang, K.; Dai, Y.; Huang, B. *Journal of Physical Chemistry C* **2007**, *111*, 12086-12090.

(22) Ohno, T.; Miyamoto, Z.; Nishijima, K.; Kanemitsu, H.; Xueyuan, F. *Applied Catalysis A: General* **2006**, *302*, 62-68.

(23) Ohno, T.; Miyamoto, Z.; Nishijima, K.; Kanemitsu, H.; Xueyuan, F. *Applied Catalysis A: General* **2006**, *309*, 155-156.

(24) Morikawa, T.; Irokawa, Y.; Ohwaki, T. *Applied Catalysis A: General* **2006**, *314*, 123-127.

(25) Hamal, D. B.; Klabunde, K. J. *Journal of Colloid and Interface Science* **2007**, *311*, 514-522.

(26) Zhang, X.; Udagawa, K.; Liu, Z.; Nishimoto, S.; Xu, C.; Liu, Y.; Sakai, H.; Abe, M.; Murakami, T.; Fujishma, A. *Journal of Photochemistry and Photobiology, A: Chemistry* **2009**, *202*, 39-47.

(27) Usseglio, S.; Damin, A.; Scarano, D.; Bordiga, S.; Zecchina, A.; Lamberti, C. *Journal of the American Chemical Society* **2007**, *129*, 2822-2828.

(28) Yang, K.; Dai, Y.; Huang, B.; Whangbo, M.-H. *Chemistry of Materials* **2008**, *20*, 6528-6534.

(29) Hong, X.; Wang, Z.; Cai, W.; Lu, F.; Zhang, J.; Yang, Y.; Ma, N.; Liu, Y. *Chemistry of Materials* **2005**, *17*, 1548-1552.

(30) Zhang, S.-Y.; Chen, X.-J.; Tian, Y.-P.; Jin, B.-K.; Yang, J.-X. *Journal of Crystal Growth* **2007**, *304*, 42-46.

(31) Hathway, T.; Jenks, W. S. *Journal of Photochemistry and Photobiology A: Chemistry* **2008**, *200*, 216-224.

(32) Ohno, T.; Mitsui, T.; Matsumura, M. *Chemistry Letters* **2003**, *32*, 364-365.

(33) Vakros, J.; Kordulis, C.; Lycourghiotis, A. *Chemical Communications (Cambridge, United Kingdom)* **2002**, 1980-1981.

(34) Moulder, J. F.; Stickle, W. F.; Sobol, P. E.; Bomben, K. D. *Handbook of X-Ray Photoelectron Spectroscopy*; Perkin-Elmer Corporation (Physical Electronics): Eden Prairie, MN, 1992.

(35) Bowman, W. D.; Demas, J. N. *Journal of Physical Chemistry* **1976**, *80*, 2434-2435.

(36) Hatchard, C. G.; Parker, C. A. *Proceeding of the Royal Society of London. Series A, Mathematical and Physical Sciences* **1956**, *235*, 518-536.

(37) Cermenati, L.; Albini, A.; Pichat, P.; Guillard, C. *Research on Chemical Intermediates* **2000**, *26*, 221-234.

(38) Cermenati, L.; Pichat, P.; Guillard, C.; Albini, A. *Journal of Physical Chemistry B* **1997**, *101*, 2650-2658.

(39) Pichat, P.; Cermenati, L.; Albini, A.; Mas, D.; Delprat, H.; Guillard, C. *Research on Chemical Intermediates* **2000**, *26*, 161-170.

(40) Nicolaescu, A. R.; Wiest, O.; Kamat, P. V. *Journal of Physical Chemistry A* **2005**, *109*, 2829-2835.

(41) Data for 50% conversion of Q at pH 6 mediated by Se-TiO2 is not shown because this extent of degradation was not reached within the 48 hour photolysis.

(42) Ranchella, M.; Rol, C.; Sebastiani, G. V. *Journal of the Chemical Society, Perkin Transactions 2: Physical Organic Chemistry* **2000**, 311-315.

(43) Serpone, N.; Lawless, D.; Khairutdinov, R. *Journal of Physical Chemistry* **1995**, *99*, 16646-54.

(44) Sajjad, A. K. L.; Shamaila, S.; Tian, B.; Chen, F.; Zhang, J. *Applied Catalysis B: Environmental* **2009**, *91*, 397-405.

(45) Kormann, C.; Bahnemann, D. W.; Hoffmann, M. R. *Environmental Science & Technology* **1991**, *25*, 494-500.

CHAPTER 7

UV Treatment of Ammonia for Swine Barn Exhaust Applications

In the style of a paper to be submitted to *Atmospheric Environment.*

Erin M. Rockafellow,[1] Jacek A. Koziel,[2] and William S. Jenks[1]*
[1]*Department of Chemistry, Iowa State University, Ames, IA 50011-3111*
[2]*Department of Agricultural and Biosystems Engineering, Department of Civil, Construction, and Environmental Engineering, Iowa State University, Ames, IA 50011*

7.1 ABSTRACT

The feasibility of using deep UV treatment for abatement of ammonia in livestock and poultry barn exhaust was examined in a series of laboratory scale experiments. These experiments simulated moving exhaust air with controlled UV wavelength and dose, NH_3 concentrations, humidity, and presence of H_2S. Ammonia, initially at relevant barn exhaust concentrations in air, is completely, or at least substantially, reduced by irradiation with 185 nm light. Reactions were monitored using chemiluminescence detection, GC-MS, and high resolution FTIR, of which the latter was found to be the most informative and flexible. Detected nitrogen-containing products included N_2O, NH_4NO_3, and HNO_3. It is presumed that atomic oxygen is the primary photochemical product that begins the oxidative cascade. The data show that removal of NH_3 is plausible, but highlights concerns over ozone and N_2O emission.

7.2 INTRODUCTION

Agricultural ammonia (NH_3) emissions from commercial farms have significantly increased in recent years –animal waste and fertilizers are major sources of ammonia.[1,2] The 2002 EPA inventory estimated that agricultural sources contribute approximately 80% of the total ammonia emissions in the U.S.[3] Livestock farms were estimated to contribute 10% of NH_3 emissions (*ca.* 430,000 tons/year). Ammonia, hydrogen sulfide (H_2S), and other odorous compounds volatilized from commercial animal confinements negatively affect the local and regional air quality, create unpleasant conditions for

neighbors and people traveling on passing highways. Heightened ammonia levels raise the pH of soil and water and create untenable conditions for fish and plants through eutrophication.[1] Unsurprisingly, ammonia emissions are subject to considerable concern and regulation.

Ammonia is classified as a hazardous substance under the Comprehensive Environmental Response, Compensation and Liability Act (CERCLA) and the Emergency Planning and Community Right-To-Know Act (EPCRA). Livestock production facilities housing exceeding a certain threshold of animals are required to report NH_3 emissions greater than 100 lbs/day (45.5 kg/day), as required under the CERCLA and the EPCRA.[4] Production of more than 250 ton/y of any individual pollutant requires that the source obtain a permit. The US Environmental Protection Agency initiated the Air Compliance Agreement with US livestock industry through the National Air Emissions Monitoring Study (NAEMS) in which emissions from animal feeding operations (AFOs) were monitored over a two-year period that began in 2007.[5] The data collected will be used to develop methodologies to monitor emissions from AFOs, to determine emission limits, and help determine compliance of current regulations. Federal rules and regulations on NH_3 emissions, particularly related to AFOs, are currently being assessed.

Ammonia is also considered a secondary precursor to fine particulate matter ($PM_{2.5}$), as it suffers a number of chemical reactions in ambient air that lead to the formation of small particles.[2,6] The EPA's final rules do not require that NH_3 be regulated as a $PM_{2.5}$ precursor, but a State may choose to regulate ammonia emissions in nonattainment areas if it is proven to be a significant contributor to that area's fine particulate matter concentrations.[7] The EPA has elected this case-by-case policy as a result of substantial uncertainties in ammonia emission inventories and the "complex" nature of its involvement in $PM_{2.5}$ formation.

Ammonia emissions from AFOs have been measured in a number of previous studies in the US and Europe.[2,8,9] While the final estimates of NH_3 emissions are being developed, it is clear that larger AFOs will be subject to the mandatory reporting of NH_3 emissions (at emissions above 45.5 kg/day). As such, the AFOs are in need of reliable

mitigation technologies for NH_3 mitigation.

Livestock buildings have been reported to emit [NH_3] ranging from 0.2 to 9.2 g/h-AU.[2,8-11] It should be self-evident that NH_3, once produced, does not easily disappear. By ordinary chemical means, the best that can be achieved is to convert it to something less noxious, such as nitrate. Biological fixation to N_2 and reduction of its production are probably the only means by which to obtain no or truly benign byproducts. Clearly, the simplest way to reduce NH_3 emissions is to reduce the number of animals, but this seems politically difficult to accept and is generally not discussed.[12]

Other control strategies involve modifications of diet, animal housing, manure storage, and aerobic/anaerobic treatment.[13-17] Reduced protein feed can be used to optimize animal diets with regard to their amino acids requirements, which minimizes excretion of nitrogenous compounds in waste that are later converted to NH_3 by up to 39%.[12] Changes to building structure or the use of tie-stalls have reduced NH_3 volatilization anywhere from 27 to 80%.[1] However, tie-stalls bring about concern for animal welfare.[1,12] Changes in manure storage and treatment can be very effective, but often are not economical.[1]

Ultraviolet (UV) irradiation treatment has been very effective and economically practical for reducing odorous emissions in the food processing and recycling industries.[18] Exhaust is blown through a filter to trap aerosols and particulate matter, then passed through a UV chamber where irradiation with 254 nm light occurs. Using this method, odorous emissions have been reduced by up to 96%.[18] Therefore, it is practical to consider the use of UV light treatment as an option for the abatement of ammonia and other odorous compounds from commercial swine barns.

In the current work, the chemical fate of ammonia is determined after exposure to UV light (185 nm and 254 nm) in air. For this application, 185 nm light is essential for generation of the reactive species that degrade NH_3, as 254 nm light is not significantly absorbed by either ammonia or the major components of air. The concentration of remaining ammonia as well as the identity and quantity of new gases is established. The effects of added water and H_2S on ammonia removal and the growth/decay of nitrous oxide (N_2O) are studied. The results reported here provide a foundation for the

determination of the suitability of UV treatment for ammonia mitigation from commercial swine barn emissions.

7.3 EXPERIMENTAL

7.3.1 Materials

All gas blends were certified within ± 2% accuracy. Air contained 21.5% O_2, ≤ 10 ppm CO, ≤ 1000 ppm CO_2, and ≤ 24 ppm H_2O. Hydrogen sulfide and N_2O stock gases were blended with N_2 at 15 ppm and 5 ppm, respectively. Ammonia stock gases were 50 ppm in air, 500 ppm in air, and 500 ppm in N_2. Water was purified to a resistivity above 18 MΩ/cm.

7.3.2 Irradiations

Photolyses were carried out using a photochemical reactor containing thirteen 185/254 nm low pressure mercury lamps with quartz walls with an output power of approximately 0.02 watts and 8 watts for 185 nm and 254 nm light, respectively.[19] The 185 nm light was attenuated by passage through approximately 25 mm of ambient air before hitting the walls of the quartz reaction coil. Temperatures inside the reactor were kept very near ambient with a fan built into the reactor floor. All analyses were performed downstream from the reactor at room temperature (*ca.* 293 K) and atmospheric pressure. Gas flow rates were controlled using mass flow controllers. Figure 7.1 shows the gas delivery/reaction system using quarter-inch (*ca.* 6 mm) O.D. tubing and fittings made of a perfluoroalkoxy (PFA) material. The quartz reaction coil was constructed from a 7.6 m length of 185 nm-transparent quartz tubing with an 8 mm I.D. and 10 mm O.D., which allows for 65% transmission of 185 nm light at 1 mm wall thickness. The total interior volume of the coil exposed to irradiation was 394 mL. The setup is illustrated in Scheme 7.1.

7.3.2 Analysis

Reactions were analyzed by high resolution FTIR, chemiluminescence, or GC-MS. For IR measurements, 16 scans were taken over roughly 30 s while the gas was continuously passed through a 500 mL FTIR gas cell with a path length equal to 7.2 m

(15 cm, 48 reflections). The spectrometer was equipped with a DTGS detector and a 12 mm slit width allowing for 1 cm^{-1} resolution. The scanner was constantly purged with N_2 to reduce the background signal from air. The following frequencies were used to monitor and determine concentrations: 967 cm^{-1} for NH_3,[20] 1,040 cm^{-1} for O_3,[21] and 2,236 cm^{-1} for N_2O.[20] NH_3 (50 ppm) and N_2O (5 ppm) standards were diluted with air or N_2 respectively and the new concentrations were measured to obtain calibration curves (Figures 7.S1 and 7.S2).

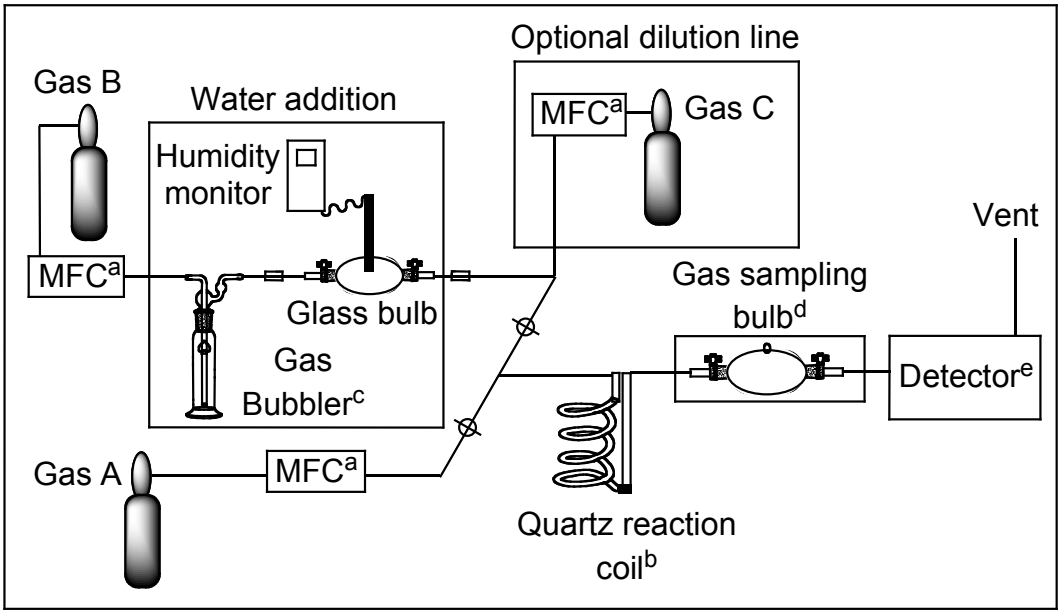

Scheme 7.1 Gas delivery and UV treatment system. The water addition segment and the gas sampling bulb were installed when appropriate. [a]MFC = mass flow controller. [b]Representation of the reaction coil which is placed inside the Rayonet photochemical reactor. [c]Contained 200 mL of water. [d]Used to collect samples for GC-MS analysis. [e]FTIR or NH_3 chemiluminescence analyzer.

FTIR results for NH_3 at higher flow rates and low concentrations were compared to measurements taken with a digitalized chemiluminescence ammonia analyzer, which could measure a maximum NH_3 concentration of 100 ppm with a minimum flow rate of 600 mL/min.

Analyses by GC-MS were performed using a 25 m CP Volamine column with 0.25 μm I.D. and 5 μm film thickness and a TOF mass spectrometer. The GC temperature program was 40 ˚C (2 min) ramped at a rate of 20 ˚C/min to 200 ˚C (2 min). Accurate mass was collected using 2,4,6-Tris(trifluoro-methyl)-1,3,5-triazine as a reference. Quantitative GC-MS calibrations for gas concentrations were not obtained since ammonia quantification was unreliable due to adsorption to the sampling flask walls.

7.4 RESULTS

7.4.1 Ammonia adsorption to walls

FTIR and chemiluminescence-based measurements of ammonia in dry air demonstrated that there was an initial period of time required to obtain a steady, constant signal from NH_3 under otherwise constant conditions. This was attributed to NH_3 adsorption to surfaces of the system and depended on both the initial concentration of ammonia ($[NH_3]_0$). The time required to reach a steady state in the adsorption/desorption equilibrium was particularly long with the IR system – far longer than the hydraulic residence time (HRT) of the gas in the system – typically 30 min for 500 ppm NH_3 and 210 min for 50 ppm NH_3. Nearly 4 h was required to achieve a constant absorption signal for 50 ppm $[NH_3]_0$ at a flow rate of either 100 or 600 mL/min, which suggested a flow rate independence in the range of concentrations being used. A representative IR response curve for constant $[NH_3]_0$ with no irradiation is illustrated in the supporting information (Figure 7.S3).

Once a steady state had been established in dark conditions, the lights were turned on and changes were monitored. At a flow rate of 600 mL/min (irradiation HRT 0.67 min), 50 ppm NH_3 was reduced to 25.5 ppm within 15 min, as detected by the chemiluminescence NH_3 analyzer, whereas FTIR showed a 45% reduction of NH_3 after 30 min. (Although the irradiation HRT remains constant at 0.67 min, the total HRT for the path of the gas to the IR detector is longer by approximately 1.5 min, due to the 500 mL gas capacity of the cell. There it is to be expected that the response times of the two measurements would differ somewhat. However, the ultimate reduction percentages

obtained by FTIR (45%) and chemiluminescence techniques (51%) are well within 10% of each other. This control clearly established that the variation in the length of time required to reach a steady state during the photolysis is likely an artifact of the difference in surface area to which ammonia adsorbs. In all cases, the observed time required to reach a steady state for $[NH_3]$ as detected by IR is limited by gas adsorption/desorption from the walls and does not directly measure the reaction kinetics or the actual HRT in the reactor coil. The latter are undoubtedly faster than the effective response time of the instrument. However, percent conversion and products could be determined and results acquired using the same analysis system can be compared.

Table 7.1 Percent of ammonia removed under varied flow rates, NH_3 starting concentration, and excitation wavelengths.[a]

$[NH_3]_0$ (ppm)	Wavelength (nm)	Flow rate (mL/min)	HRT (min)	% Removal
50	185 + 254	600	0.66	45
500	185 + 254	600	0.66	10
50	185 + 254	300	1.31	76
500	185 + 254	300	1.31	25
50	185 + 254	100	3.94	100[b]
500	185 + 254	100	3.94	83
500	254	100	3.94	3

[a] Irradiation chamber volume was 394 mL. Thirteen lamps, supplying 8 W 254 nm and 0.02 W 185 nm each, were used. [b]Minimum detection limit (MDL) of ca. 1 ppm.

7.4.2 Flow Rate Comparison

On a percentage basis, ammonia was removed to a greater degree when either the rate of flow was slowed or the initial concentration was lowered. For an $[NH_3]_0$ of 500 ppm, with a flow rate of 100 mL/min (4 min irradiation HRT), FTIR showed that over

80% of the ammonia was removed, i.e., the measured concentration at output was under 100 ppm. If the $[NH_3]_0$ was 50 ppm in dry air and the flow rate remained the same, then no ammonia could be detected at the output after achieving steady state. Products, of course, varied in quantity between these two runs, but their identities remained the same. Unless otherwise noted, all further experiments were carried out at 100 mL/min flow rate, giving the 4 min HRT with out setup.

To verify that 185 nm light is necessary for ammonia abatement, NH_3 in air was photolyzed with standard low-pressure mercury bulbs (254 nm with 185 nm filtered out). Only a 3% reduction of NH_3 was observed, monitoring the absorption at 967 cm^{-1} in the FTIR spectrum. These results are compiled in Table 7.1.

Table 7.2 Identification of components by GC-MS present after 185/254 nm photolysis of 500 ppm NH_3 after 30 min of flow at 100 mL/min.

Entry	Retention Time (min)	Observed Mass (M^+, m/z)	Compound
1	1.32	28.4045, 32.4056, 39.9686	Air (N_2, O_2, Ar)
2	1.43	43.9944	CO_2
3	1.53[a]	17.0284	NH_3
4	1.53[a]	44.0018	N_2O
5	1.88	18.3038	H_2O

[a]Peaks overlap in GC trace, but were resolved by single ion chromatograms.

7.4.3 Analysis of UV photolysis of NH_3 in dry air by GC-MS

Samples from the photolysis of 50 ppm NH_3 in air were not easily analyzed by GC-MS due to limits in sensitivity. Subsequent studies using this method were done using $[NH_3]_0$ = 500 ppm in air for this reason. In addition, a higher $[NH_3]_0$ led to a larger accumulation of photodegradation products, allowing for both FTIR and GC-MS to be

used for structural identification. Product identities by GC-MS are shown in Table 7.2. Entries 1-3 and 5 were observed in the unphotolyzed sample, as expected. After irradiation, N_2O (entry 4) was the major product, although it overlapped with the NH_3 peak in the chromatogram. The abundance of N_2O was large enough to obtain an accurate mass (m/z = 44.0018 observed vs. 44.0011 calculated), confirming the identity. Molecular ion peaks for NO, NO_2, HONO, HNO_3, and H_4N_2 were not observed, even when a single ion search was done. Ozone, shown to be a major component by IR, was not detected by the GC-MS method.

7.4.4 High resolution FTIR analysis of NH_3 photolysis in dry air

FTIR spectral changes were monitored over the course of the photolysis of 200 ppm NH_3 in air (Figure 7.1). The appearance of several new peaks accompanied the loss of NH_3 absorptions. Most of the new spectral features could be assigned to two major components. Absorptions around 2130, 1057, 1044, and 1030 cm^{-1} were assigned to O_3.[21] Bands at 3494, 2580, 2236, 2178, 1299, and 1258 cm^{-1} were attributed to N_2O.[20] No major changes occurred in the 1500 to 2000 cm^{-1} range that indicated the presence of NO_x compounds (NO, NO_2/N_2O_4). The broad bands at 3228, 3067, 2882, 1428, and 1367 cm^{-1} slowly grew in and were assigned to the presence of NH_4NO_3, which, of course, precipitates out under these conditions.[22,23] After ending the photolysis and purging the system with dry N_2, a spectrum of the purged cell was acquired. The FTIR spectrum revealed that the latter features remain after purging and exposed weaker absorptions at 1051, 1045, and 832 cm^{-1} (Figure 7.2). The frequencies reported here are all within expected ranges for various polymorphs of crystalline NH_4NO_3 films and aerosols.[22,23]

The observed steady state product distributions depended on $[NH_3]_0$, although the final O_3 concentration was not especially sensitive to $[NH_3]_0$. The absorbance shown in Figure 7.3 is typical and did not vary more than about ± 10% across all the irradiations using dry air.

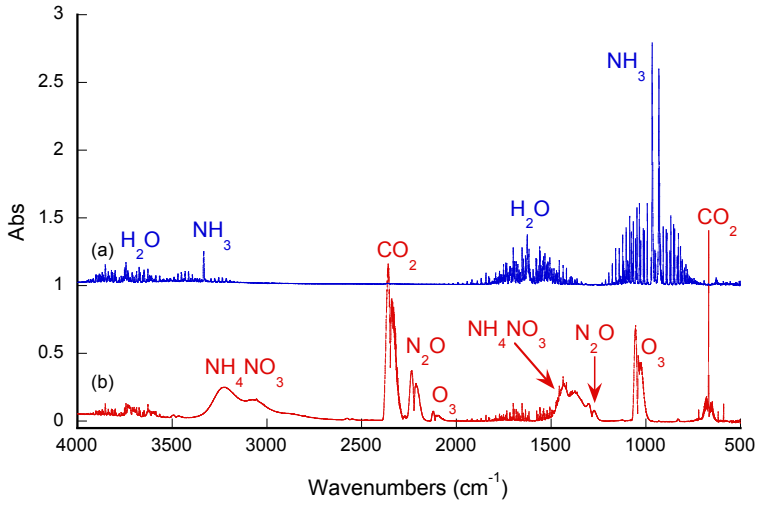

Figure 7.1 FTIR spectra of (a) 500 ppm $[NH_3]_0$ in air purged in the dark and (b) after 185 nm irradiation 200 ppm $[NH_3]_0$ in air at 100 mL/min (HRT = 3.9 min). The sample shown in (b) was diluted to 200 ppm $[NH_3]_0$ by addition of dry air that contained more CO_2 than the original 500 ppm $[NH_3]_0$ in air stock gas. The data in (b) were offset by 1.0 absorbance unit.

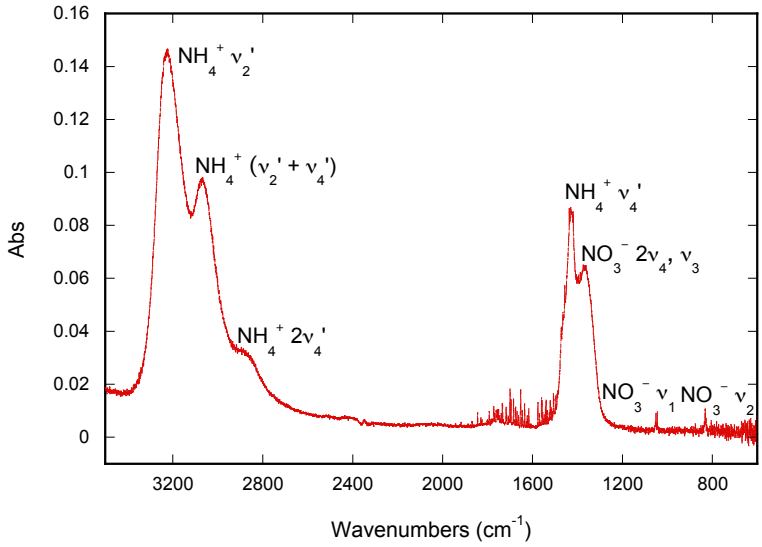

Figure 7.2 Spectrum obtained from static residue remaining in the IR gas cell under N_2 after the photolysis of 200 ppm NH_3 in air.

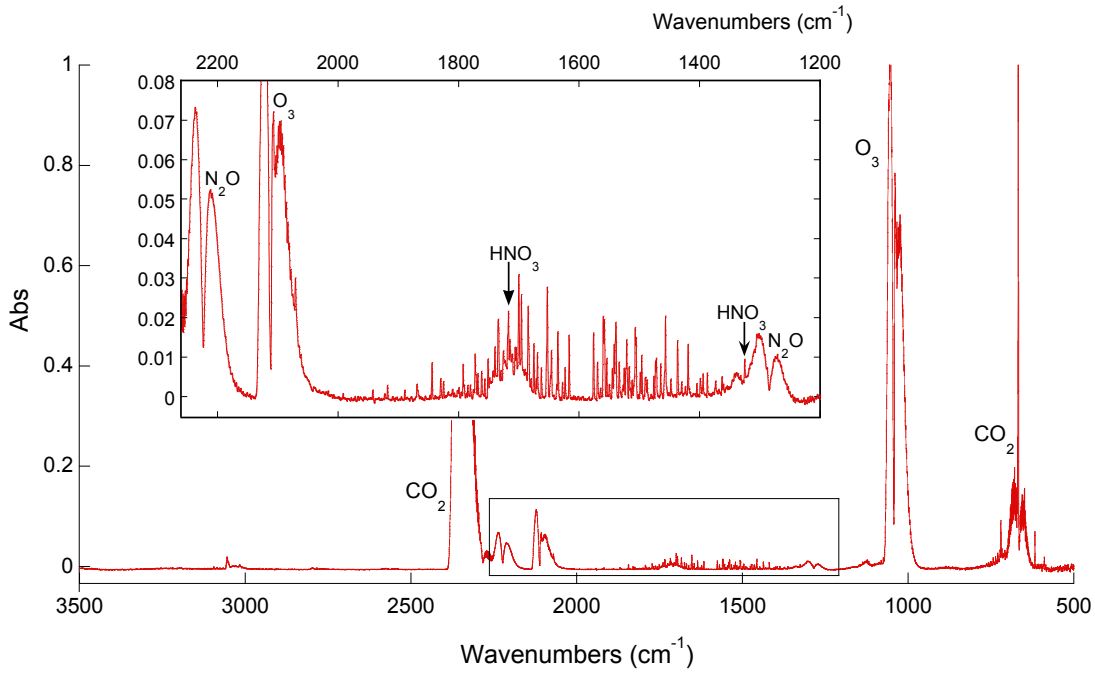

Figure 7.3 Extended 185/254 nm photolysis of 20 ppm $[NH_3]_0$ in dry air at 100 mL/min (Photolysis HRT = 3.9 min).

N_2O. Nitrous oxide was also observed at appreciable concentrations as a product of photolysis. Figure 7.4 illustrates the interesting result that N_2O formation was enhanced with increasing $[NH_3]_0$. With $[NH_3]_0$ < 100 ppm, N_2O formation exhibited an initial growth period followed by a decay to a lower steady state concentration. It is not clear whether this non-monotonic growth is "real" or entirely attributable to absorption/desorption artifacts. With $[NH_3]_0$ > 100 ppm, the N_2O reached a steady state at the maximum observed concentration.

HNO_3 and NH_4NO_3. After ammonia was no longer observed in the IR when low starting concentrations were used, a peak displaying a very distinctive Q-branch appeared at 1325 cm^{-1} in addition to broad bands at 1710 and 895 cm^{-1} indicated the presence of HNO_3 (Figure 7.3). At these low initial NH_3 concentrations, ammonium nitrate was not generally a significant feature in the IR spectrum until the lights were turned off and NH_3 was reintroduced to the system. At higher $[NH_3]_0$, where ammonia survived into the analysis chamber, the abundance of HNO_3 was low to undetectable, in favor of NH_4NO_3. (It is expected that the minimum detection limit of nitric acid would be comparable to

that of ammonia, but without nitric acid standards, it was not rigorously determined.)

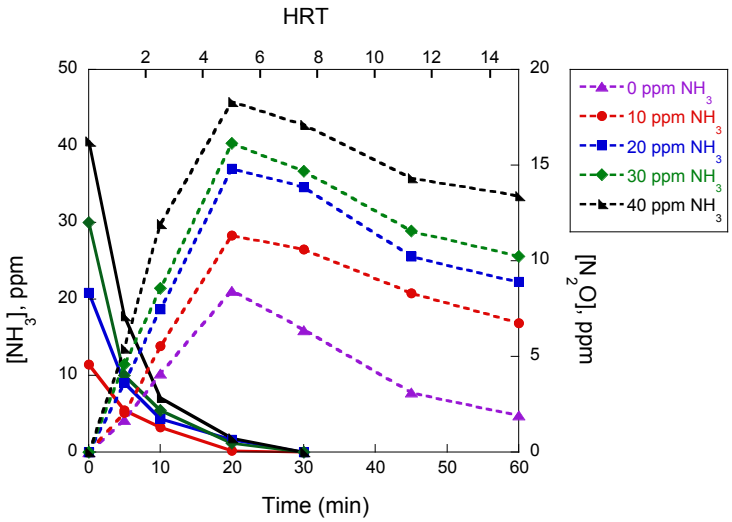

Figure 7.4. Photolysis (185/254 nm) of NH_3 in dry air. Solid lines represent the loss of NH_3. Dotted lines show the generation of N_2O.

7.4.5 High resolution FTIR analysis of NH_3 photolysis in the presence of H_2S

Hydrogen sulfide is also commonly found in livestock farm emissions. H_2S is a concern because of its unpleasant characteristic "rotten egg" odor and potential human health hazards.[1] Reports on typical H_2S emissions vary greatly from 0 to 3,400 ppb.[1] For purposes of reaching potential applications, it is desirable to determine whether NH_3 mitigation through UV treatment is affected by the presence of H_2S. The effect of H_2S on O_3 and N_2O (also objectionable gases to emit) was also a point of interest.

Experiments in which H_2S and N_2 were introduced into the gas mixture (Scheme 7.1, Gas B and Gas C) were conducted. These were conducted in such a way that the O_2 concentration was constant throughout the series, although it was lower than normal air, at about 8.6% instead of 21.5%; the sum of flow of a pure N_2 source and the H_2S source (in N_2) was kept constant. The $[NH_3]_0$ was kept constant at 20 ppm.

Figure 7.5 shows that the 185 nm photolysis of 20 ppm NH_3 in the presence of 9 ppm H_2S in this hypoxic "air" gave qualitatively similar product distributions to those observed during irradiations of low concentration ammonia in ordinary air. The FTIR

spectrum taken early in the photolysis (Figure 7.5a) shows that N_2O was the dominant product. However, after the observed NH_3 concentration fell below a detectable limit (*ca.* 1 ppm) for an extended period, the spectral features of HNO_3 grew in and the N_2O absorptions were reduced (Figure 7.5b). This is a natural consequence of there being no NH_3 for nitric acid to protonate. However, once the lights have been turned off, and the presence of ammonia was restored, features attributable to ammonium nitrate became apparent (Figure 7.5c).

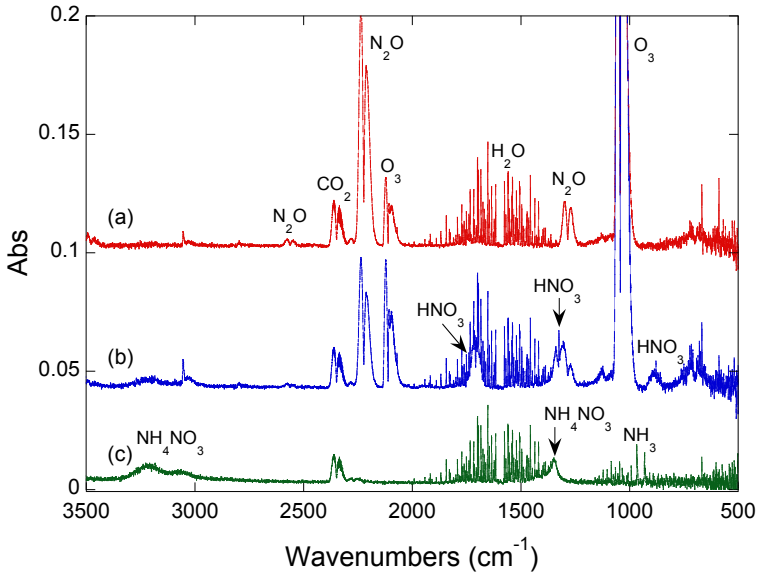

Figure 7.5 Comparison of FTIR spectra taken of the 185/254 nm photolysis of 20 ppm $[NH_3]_0$ flowing at 100 mL/min in hypoxic air (8.6% O_2) with 9 ppm H_2S after (a) 15 min and (b) 210 min of irradiation, and (c) extended photolysys, followed by 30 min continued flow in the dark.

Varying the concentration of H_2S showed that hydrogen sulfide had little effect on the observed rate of loss of ammonia (Figure 7.6). However, the length of time required for NH_3 to be undetectable by FTIR in the full set of H_2S experiments was longer than the photolysis in dry air, which is almost certainly a result of the lower O_2 concentrations in NH_3/H_2S gas mixtures used. This conclusion is buttressed by photolysis of NH_3 in air diluted solely with N_2 (0 ppm H_2S in Figure 7.6) without any H_2S added.

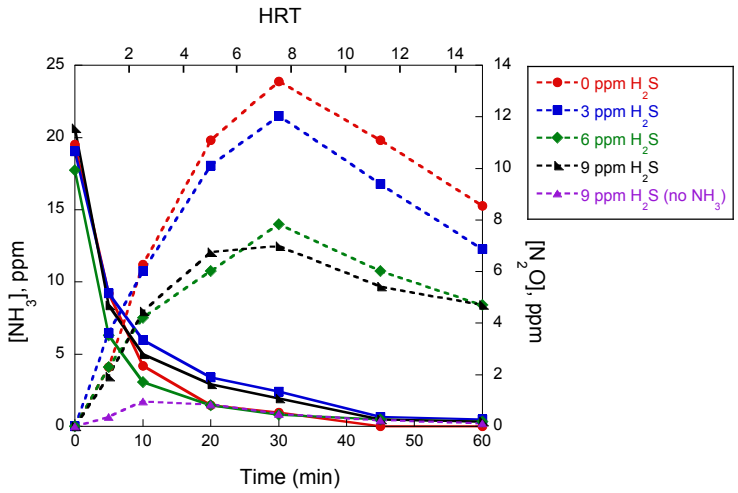

Figure 7.6 Photolysis (185/254 nm) of 20 ppm $[NH_3]_0$ in air in the presence of varied H_2S concentrations in N_2 balance flowed at 100 mL/min (HRT = 3.94 min). Solid lines represent the loss of NH_3. Dotted lines represent generation of N_2O.

The results suggest that H_2S does have a moderate effect on N_2O formation or consumption in the presence of ammonia, where steady state N_2O concentrations are lower at higher levels of H_2S. There does appear to be a saturation point for this effect, though, as indicated by the results for 6 ppm and 9 ppm H_2S. Nitrous oxide concentrations were reduced by more than half in the presence of these higher concentrations of H_2S. Figure 7.7 also shows that, in the absence of ammonia altogether, the formation of N_2O was suppressed even more greatly by 9 ppm H_2S. The maximum is earlier, and about 7 times lower, and the steady state concentration of N_2O is nearly zero. Table 7.3 provides a summary of the effects of H_2S and H_2O (discussed in the next section) addition.

Table 7.3 Qualitative summary of the effects of gas composition changes observed by FTIR.[a]

Additive to NH_3	Effect		
	N_2O	O_3[b]	NH_3
H_2S, 3 ppm	Slightly reduced (*ca.* 15%[c])	Not significant	Not significant
H_2S, ≥ 6 ppm	Appreciably reduced (*ca.* 50%[c])	Not significant	Not significant
H_2O[d]	Significantly reduced (*ca.* 80%[c])	Significantly lower (*ca.* 80 to 90%)	Incomplete removal[e]

[a]Initial NH_3 concentration was 20 ppm for all reactions. [b]Ozone measured by absorbance. [c]Approximate percent reduction. [d]Nearly identical results for 36% relative humidity (8400 ppm, 0.84%) and 58% relative humidity (13,600 ppm, 1.36%). [e]Ammonia displacement from walls was likely to contribute to this observation. See text for details.

7.4.6 High resolution FTIR analysis of ammonia photolysis in humid air

It is well known that NH_3 emission levels vary greatly by season.[1] Changes in temperature and humidity likely contribute to this.[1] Therefore, attempts were made to investigate the effect(s) of moisture. Higher concentrations of H_2O greatly affected the apparent abatement of ammonia. In the presence of water (Figure 7.6), a steady state of $[NH_3]$ was not achieved after 5 h of monitoring. This was probably a consequence of more complex adsorption/desorption equilibria, as well as partial solvation of ammonia by water, and the attendant acid/base chemistry, but the current data do not give a complete explanation.

An attempt was made to find out with experiments of manageable length whether ammonia remained at the end of a reasonable time period of photolysis. This was done by filling the IR detector with N_2 and disconnecting it from the system. Photolysis was conducted in the ordinary fashion for either 5 min or 135 min before reconnecting to the IR cell. By this method, if NH_3 remained after exposure to UV light, it would be forced

to "grow in" rather than "grow out", and a greater confidence that such a positive NH_3 signal would be obtained.

Ammonia was detected when the gas mixture (of either 36% or 58% rel. humidity) was photolyzed for 5 or 135 minutes before connecting to the N_2-filled FTIR gas cell. However, a steady state was not obtained, but rather an initial rise in NH_3 absorption, followed by a slow, steady drop occurred. This result implies that the survival of ammonia is "real", but that the final, steady state value is again dependent on complex equilibria involving water and NH_3, including interactions within the detection cell.

The effect of water on other gases was easier to quantify. As shown in Figure 7.8, the steady state $[N_2O]$ is significantly lower with water in the air. Nitrous oxide was found to reach a steady state of 3-4 ppm in the presence of water and 6-7 ppm in the absence of water. Ozone levels were also dramatically affected. The maximum IR absorbance obtained for ozone when water vapors were present were only 10-20% of those obtained for dry samples.

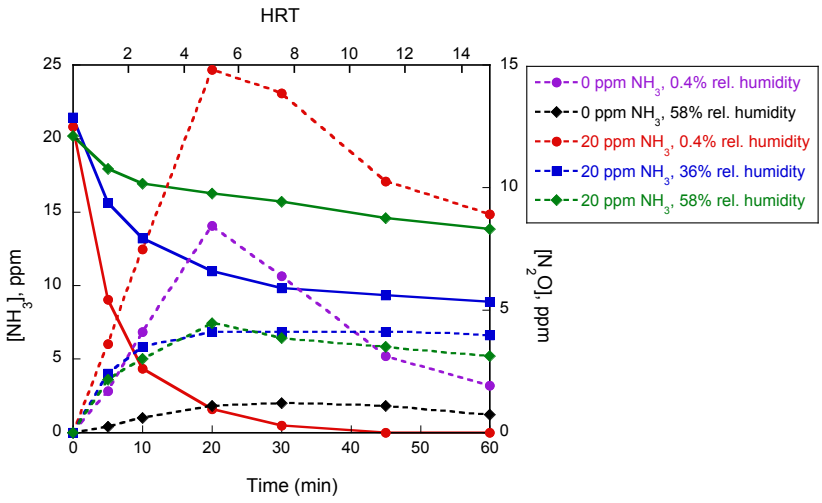

Figure 7.8 Effect of humidity on the 185/254 nm photolysis of 20 ppm $[NH_3]_0$ in air at 100 mL/min. [a]At higher concentrations of moisture, the NH_3 calibration was often skewed. In this case, the data were normalized to 20 ppm NH_3.

7.5 DISCUSSION

Considerable effort has long gone into understanding atmospheric chemistry and photochemistry. The application we consider here is simply a very special case of that broader effort. As a result, in this discussion, we are able to take advantage of considerable known data about reactions and rate constants that may be relevant to the abatement of ammonia via photochemical means. The interpretation is necessarily somewhat speculative, but considering known chemistry and rate constants can support or rule out certain possible pathways that could not be directly observed in this study.

7.5.1 The primary photochemical events

Under dry air conditions used this research, N_2 was the most abundant component at a concentration of approximately 780,000 ppm, followed by O_2 with a concentration of almost 215,000 ppm. Carbon dioxide and water were present at levels of ≤ 1000 ppm and ≤ 24 ppm, respectively. Added ammonia ranged from 10 - 500 ppm, depending on the dilution and gas standard used.[24,25] Under these conditions, the vast majority of 185 nm photons are absorbed by O_2, rather than any of the other components of the mixture, and it is thus the photochemistry of molecular oxygen that begins the reactive cascade.[26] (The absorption cross sections for the two gases are given in the supporting information.)

Upon 185 nm excitation, cleavage of O_2 occurs yielding two ground state oxygen atoms, $O(^3P)$ (eq 7.1).[27] Combination $O(^3P)$ with ubiquitous O_2 to generates (eq 7.2).[24,25] In a process commonly referred to as the Chapman cycle, however, O_3 also serves as a source of oxygen atoms: photolysis of ozone with *either* 185 or the more abundant 254 nm light produces O_2 and atomic oxygen in its first excited state, $O(^1D)$ (eq 7.3).[27] The quantum yield for the photochemical dissociation of ozone is near unity.[25]

$$O_2 + h\nu \longrightarrow O(^3P) + O(^3P) \quad (7.1)$$

$$O(^3P) + O_2 + M \longrightarrow O_3 + M \qquad k^a = 6.0 \times 10^{-34}\ cm^6\ molecules^{-2}\ s^{-1} \quad (7.2)$$

$$O_3 + h\nu \longrightarrow O_2 + O(^1D) \quad (7.3)$$

[a]Rate constant at the low pressure limit.

Using an estimate of 2.5×10^{19} molecules cm^{-3} at 300 K, the pseudo-second order rate constant for reaction in eq 7.2 is 1.5×10^{-14} cm^3 $molecules^{-1}$ s^{-1}. Evaluating the rate constant for direction reaction between $O(^3P)$ and NH_3 (eq 7.12) at 300 K gives 4.6×10^{-17} cm^3 $molecules^{-1}$ s^{-1}. Thus, also given the overwhelmingly large pool of O_2 relative to NH_3, it is safe to conclude that only a vanishingly small fraction of $O(^3P)$ reacts directly with NH_3. Instead, most of it participates in the ordinary Chapman cycle, combining with molecular oxygen to produce ozone. Ozone can then absorb light *at either 185 or the much more abundant 254 nm wavelength* to produce O_2 and the first excited state of atomic oxygen, $O(^1D)$. (This conclusion does not necessarily imply, however, that the small fraction of $O(^3P)$ that does react with ammonia is not significant to ammonia consumption.)

7.5.2 Relevant reactions of $O(^1D)$

Reactions involving $O(^1D)$ are very important in atmospheric chemistry, and this almost certainly holds true here. While much of the $O(^1D)$ is collisionally quenched to $O(^3P)$ (eq 7.4),[25] it also suffers very rapid reactions with water, N_2O, and NH_3 (eqs 7.5, 7.6, and 7.11). Although under "dry" conditions ($\leq$ 24 ppm in the stock gas supplied here), the great majority of $O(^1D)$ is quenched to $O(^3P)$, the Chapman cycle ensures that that it is continuously produced, so the reactions with low concentration components (e.g., H_2O, N_2O, NH_3, H_2S, and VOCs) remains important to their chemistry.

The reaction of $O(^1D)$ with H_2O produces 2 HO with a second order rate constant of 2.2×10^{-10} cm^3 $molecules^{-1}$ s^{-1}. The stock "dry" air may contain enough H_2O ($\leq$ 24 ppm) for this to be significant in competition with direct reaction with NH_3, at least at lower $[NH_3]_0$ and in the absence of significant humidity. HO, however, is also a critical oxidative species.

$$O(^1D) + M \longrightarrow O(^3P) + M \qquad k = \sim 3 \times 10^{-11}\ cm^3\ molecules^{-1}\ s^{-1} \qquad (7.4)$$

$$O(^1D) + H_2O \longrightarrow HO + HO \qquad k = 2.2 \times 10^{-10}\ cm^3\ molecules^{-1}\ s^{-1} \qquad (7.5)$$

$$O(^1D) + N_2O \xrightarrow{60\%} NO + NO \qquad k = 6.7 \times 10^{-11}\ cm^3\ molecules^{-1}\ s^{-1} \qquad (7.6a)$$

$$\xrightarrow{40\%} N_2 + O_2 \qquad k = 4.9 \times 10^{-11}\ cm^3\ molecules^{-1}\ s^{-1} \qquad (7.6b)$$

7.5.3 N_2O formation and removal

Peak N_2O concentrations reported here range up to almost 20 ppm, but were lower with the addition of water or H_2S. The detailed mechanism of the formation of N_2O through the photolysis of air is still under debate.[28-31] It has been proposed that N_2O is formed through either an association reaction between N_2 and $O(^1D)$ (eq 7.7) or through the reaction of an undissociated electronically excited state of O_3 with N_2 (eq 7.8). While the pseudo-second order rate constant estimated for eq 7.7 is small, the huge concentration of N_2 may make up for this compared to other molecules that are 3 to 5 orders of magnitude less prevalent. The unknown rate constant for interaction of excited (pre-dissociated) ozone with N_2 means we cannot speculate much further.

$$O(^1D) + N_2 \xrightarrow{M} N_2O \qquad k = 7.8\text{x } 10^{-17} \text{ cm}^3 \text{ molecules}^{-1} \text{ s}^{-1} \qquad (7.7)$$

$$O_3^* + N_2 \longrightarrow N_2O + O_2 \qquad k = ? \qquad (7.8)$$

N_2O reacts with $O(^1D)$ and can follow two possible pathways. The major reaction (eq 7.6a) yields 2 NO (60%), while the minor pathway regenerates O_2 and N_2 (eq 7.6b).[25,28] Our results also demonstrated a significant increase in N_2O concentration with NH_3 present. Possible pathways to yield nitrous oxide from ammonia are discussed below in the next section. Lastly, while N_2O is also destroyed under 185/254 nm irradiation, much as O_3 is, a control photolysis of 5 ppm N_2O in N_2 exhibited no net loss, which indicates a reformation reaction analogous to the Chapman cycle is operative.[26]

7.5.4 Ammonia Degradation

Several pathways for the oxidative removal of NH_3 are feasible. Given a survey of the available literature, the first step almost certainly involves generation of the amino radical, NH_2. Four pathways are envisioned, some more important than others. Direct photolysis of ammonia (eq 7.9) appears negligible, given the high concentration of O_2. A second possibility, as shown in eq 7.10, is the reaction of NH_3 with hydroxyl radical (eq 7.5).[25,32] Although the rate constant is slower for other processes, the concentration of hydroxyl radical is not known, relative to other active oxygen species. (At high water

concentrations, this route may be more significant, *vide infra*.) The reaction between NH_3 and $O(^1D)$ (eq 7.11) is a probable route under dry conditions, particularly for high $[NH_3]_0$.[33] As noted previously, the direct reaction between $O(^3P)$ and NH_3 seems very unlikely to be important.[34,35]

$$NH_3 + h\nu \longrightarrow NH_2 + H \quad (7.9)$$

$$NH_3 + HO \longrightarrow NH_2 + H_2O \qquad k = 1.6 \times 10^{-13}\ cm^3\ molecules^{-1}\ s^{-1} \quad (7.10)$$

$$NH_3 + O(^1D) \longrightarrow NH_2 + HO \qquad k = 2.5 \times 10^{-10}\ cm^3\ molecules^{-1}\ s^{-1} \quad (7.11)$$

$$NH_3 + O(^3P) \longrightarrow NH_2 + HO \qquad k(T) = (1.8 \times 10^{-18})T^{2.1}\exp(-2620/T)\ cm^3\ molecules^{-1}\ s^{-1} \quad (7.12)$$

On the other hand, if the reaction between NH_3 and HO (eq 7.10) is a major process, the addition of water to the photolysis would, intuitively, be expected to enhance the degradation of NH_3. This was not observed. While it is tempting to suggest that this implies that reaction with $O(^1D)$ is the major initiating pathway, the water addition experiments (*vide infra*) also make it clear that this is not the exclusive channel, either.

7.5.5 Reactions of downstream nitrogen-containing intermediates

The only nitrogen-containing downstream compounds detected were HNO_3 and NH_4NO_3 (in addition to N_2O). No hydrazine, which could be formed by dimerization of NH_2, was observed. The FTIR spectrum of hydrazine is strikingly similar to that of NH_3, but some frequencies are shifted by more than 2 cm^{-1} and would have been detected. It is more likely that the amino radical will be oxidized, eventually yielding NO. (We assume NO would rapidly be oxidized further and not accumulate.) Again, the detailed pathways remain a matter of some debate in the literature, and the current experiments do not shed further light on those matters.[24-26,32,36] Nonetheless, a quick walk-through is merited for this discussion.

The initial step involves the reaction of NH_2 with either O_2, O_3, HO_2, or $O(^3P)$. Although the reaction with O_2 is intuitively satisfying because of the latter's high concentration, the rate constant is very low (eq 7.13), and this reaction is not considered important.[32] Under less pristine conditions, formation of NH_2O through reaction of NH_3

with HOO or O_3 (eqs 7.14 and 7.15). [26,36] (In dry air photolysis, O_3 would seem rather more abundant.) NH_2O would likely collide with O_2 very rapidly, forming HNO and the peroxy radical (eq 7.16). Equation 15b shows an alternative outcome for the reaction of NH_2 with HO_2 producing HNO and H_2O, which is argued to be dominant product outcome.[32,36] The collision of NH_2 with $O(^3P)$ can lead to three possible product outcomes (eq 7.17a-c), but eq 7.17b is the major reaction pathway, again favoring the production of HNO.[26,36,37]

$NH_2 + O_2 \longrightarrow$	NH_2OO	$k = < 6 \times 10^{-21}$ cm^3 molecules^{-1} s^{-1}	(7.13)
$NH_2 + O_3 \longrightarrow$	$NH_2O + O_2$	$k = 1.9 \times 10^{-13}$ cm^3 molecules^{-1} s^{-1}	(7.14)
$NH_2 + HO_2 \longrightarrow$	$NH_2O + HO$	$k = ?$	(7.15a)
$\longrightarrow$	$HNO + H_2O$	$k = 7 \times 10^{-12}$ cm^3 molecules^{-1} s^{-1}	(7.15b)
$NH_2O + O_2 \longrightarrow$	$HNO + HO_2$	$k = 1 \times 10^{-13}$ cm^3 molecules^{-1} s^{-1}	(7.16)
$NH_2 + O(^3P) \longrightarrow$	products	$k = (9 - 15) \times 10^{-11}$ cm^3 molecules^{-1} s^{-1}	(7.17)
$\xrightarrow{5\text{-}13\%}$	$NH + OH$		(7.17a)
$\xrightarrow{87\%}$	$HNO + H$		(7.17b)
$\xrightarrow{\text{minor}}$	$NO + H_2$		(7.17c)

Regardless of the details, nitrosyl hydride (HNO) is almost certainly formed during the oxidation of ammonia.[37] Several steps are required to go from here to HNO_3 through the NO_x compounds, and the major possibilities[25,32,36-38] are given in eqs 7.18-7.25. (Notably, $O(^3P)$ is thought to play a role here.[25]) None of these compounds accumulated enough to be observed by IR at steady state concentrations until the formation of nitric acid.

$$HNO + HNO \longrightarrow N_2O + H_2O \qquad k = 4 \times 10^{-15}\ cm^3\ molecules^{-1}\ s^{-1} \qquad (7.18)$$

$$HNO + h\nu \longrightarrow NO + H \qquad (7.19)$$

$$HNO + O(^3P) \longrightarrow NO + HO \qquad k = 3.8 \times 10^{-11}\ cm^3\ molecules^{-1}\ s^{-1} \qquad (7.20)$$

$$NO + O(^3P) \xrightarrow{M} NO_2 \qquad k = 3 \times 10^{-11}\ cm^3\ molecules^{-1}\ s^{-1} \qquad (7.21)$$

$$NO_2 + O(^3P) \xrightarrow{M} NO_3 \qquad k = 2.2 \times 10^{-11}\ cm^3\ molecules^{-1}\ s^{-1} \qquad (7.22)$$

$$NO_2 + NH_2 \longrightarrow N_2O + H_2O \qquad k = 1.9 \times 10^{-11}\ cm^3\ molecules^{-1}\ s^{-1} \qquad (7.23)$$

$$NO_2 + NO_3 \xrightarrow{M} N_2O_5 \qquad k = 1.4 \times 10^{-12}\ cm^3\ molecules^{-1}\ s^{-1} \qquad (7.24)$$

$$NO_2 + HO \xrightarrow{M} HNO_3 \qquad k = 2.5 \times 10^{-11}\ cm^3\ molecules^{-1}\ s^{-1} \qquad (7.25)$$

At low enough [NH_3], HNO_3 was the major form of nitrate observed. However, as [NH_3] was increased, NH_4NO_3 became the major product. When the atmosphere is saturated with ammonium nitrate, a fraction is transferred to the aerosol phase, which was observed as a thin film on the mirrors and windows of the IR cell that eventually formed during the photolysis of higher NH_3 concentrations (> 200 ppm).[25] A white residue could also be seen on parts of the quartz reaction coil near the outlet in these reactions.

$$NH_3 + HNO_3 \rightleftharpoons NH_4NO_3 \qquad (7.26)$$

7.5.6 Effects of water vapor

Compared to "dry air", introduction of humidity may be the greatest perturbation, compared to addition of other components of livestock barn air such as VOCs.[39] Although water is often thought of as benign, it is present at high concentration and reacts with at least one of the key intermediates in this chemistry. Fully humid (100% relative humidity) air at 1 atm and 25 ˚C contains slightly over 3% water, i.e., > 30,000 ppm. Even very dry air (10% RH) would have > 3000 ppm water, two orders of magnitude greater than most realistic ammonia concentrations in barn air.

Although, even at these high concentrations, most of the $O(^1D)$ is deactivated to $O(^3P)$, the fraction of $O(^1D)$ that reacts chemically is diverted strongly toward water (to produce HO), going from "dry" to moist air, and thus away from reaction with NH_3 or N_2. The qualitative observations reported Table 7.3 are that addition of water during

photolysis reduces steady state concentrations of N_2O and O_3, and that the steady state concentration of ammonia goes up. Although we do not report proper simulations with all the reactions discussed here, surely the increase of water from ~20 ppm to thousands of ppm will reduce the rate of formation of ozone and N_2O by providing this additional channel of $O(^1D)$ consumption. Similarly, a reduction in the initiation of ammonia consumption by reaction shown in eq 7.11 is expected. Finally, a qualitative reduction in O_3 is expected if hydroxyl radical is produced, due to its reaction to form hydroperoxyl radical and molecular oxygen, eq 7.27. Indeed, a reduction of O_3 levels was observed.

$$O_3 + HO \longrightarrow HO_2 + O_2 \qquad k = 6.8 \times 10^{-14}\ cm^3\ molecules^{-1}\ s^{-1} \qquad (7.27)$$

However, the additional hydroxyl radical formed by $O(^1D)$ reacting with water is apparently not enough to compensate for the lost direct reaction of $O(^1D)$ with NH_3. Although final steady state levels of ammonia were not obtained in all cases in the reported experiments, it is clear that the addition of water reduced the amount of NH_3 removal in a qualitative sense.

7.5.6 Effects of H_2S

In the presence of H_2S added to dry air, NH_3 was still successfully removed, at least reduced to levels undetectable by FTIR. Although hydrogen sulfide is a very reactive species (generally much more so than water), its effect on ammonia abatement is much smaller simply because so much less of it is added than with water (Figure 7.6). It is also worth noting again that the percentage of O_2 in the total atmosphere of these experiments was lower by 60% than normal because the H_2S standard was in N_2, and all experiments regarding H_2S were kept with this same quantity of O_2. Of course, H_2S itself is a gas that is a target for abatement in barn exhaust. H_2S could be removed through similar oxidation pathways to NH_3 (eqs 7.28 – 7.30) except the reaction with $O(^3P)$ and HO should be faster.[26,33] In more general atmospheric chemistry, it is accepted that the major pathway for H-abstraction from H_2S occurs through the reaction with HO (eq 7.28).[24,26]

The reaction rate of H_2S with $O(^1D)$ is not reported in most literature sources, so this pathway cannot be ruled out (eq 7.30).

$$H_2S + HO \longrightarrow HS + H_2O \qquad k = 4.8 \times 10^{-12}\ cm^3\ molecules^{-1}\ s^{-1} \qquad (7.28)$$

$$H_2S + O(^3P) \longrightarrow HS + HO \qquad k = 2.2 \times 10^{-14}\ cm^3\ molecules^{-1}\ s^{-1} \qquad (7.29)$$

$$H_2S + O(^1D) \longrightarrow HS + HO \qquad k = ? \qquad (7.30)$$

It is both notable and very important that N_2O emissions are reduced by the presence of H_2S (although, again, the O_2 concentration also changed). N_2O is a known sink for NO_2, as discussed earlier.[25] However, in the presence of HS, NO_2 is rapidly consumed at a greater rate than competitive pathways for its conversion to N_2O (eq 7.31).[26] Since nitrous oxide is a known oxidant, it is also possible that nitrous oxide directly reacts with H_2S, but there is little literature available on this reaction.

$$HS + NO_2 \longrightarrow HSO + NO \qquad k = 5.8 \times 10^{-11}\ cm^3\ molecules^{-1}\ s^{-1} \qquad (7.31)$$

Regardless of the details, however important they may be, it cannot escape mention that a significant potential limitation to the photochemical abatement of ammonia could result from regulation of N_2O and/or ozone emissions. The results reported here, however are tantalizing in their suggestion that the additional VOC (and, potentially, dust) pollutants would act as an internal "scrubber" for N_2O and ozone. Of course, such reactions would serve to oxidize the other pollutants as well. We are confident that various parameters, such as the 185/254 nm ratio, light intensity, flow rate, and potential diversion of the natural dust in real systems would allow for certain ranges of ozone or N_2O emissions to be achieved; we also believe such engineering-scale experiments will require pilot scale testing over the laboratory synthetic air experiments we report here.

7.6 CONCLUSIONS

Abatement of small molecule contaminants that exist in livestock barn exhaust but

do not themselves absorb direct irradiation at 254 nm can be brought about by indirect photochemistry initiated by absorption of 185 nm light, mainly by atmospheric oxygen. Formation of atomic oxygen follows, and in the absence of other "contaminants", atomic oxygen reacts with the species in air to form ozone, N_2O, and (when water is present) hydroxyl radical, HO. Hydroxyl radical and reactions of atomic oxygen are, presumably, the major agents involved in the oxidation of NH_3, H_2S, and similar species. In laboratory conditions, the complete removal (> 99%) of 50-10 ppm ammonia was obtained in the absence of significant concentrations of water. With 58% relative humidity, the ammonia abatement was less significant with only *ca.* 25% removal for 20 ppm $[NH_3]_0$.

The hydraulic residence times of this very inefficient irradiation system, of the order of a few minutes, suggest that the much more efficient irradiations that could be obtained by direct exposure of exhaust airs with turbulent air flow to high-flux lamps might be brought down to more practical HRTs of the order of seconds with proper design and lamp intensity.

FTIR spectra revealed spectral features consistent with HNO_3, NH_4NO_3, N_2O, and ozone as the major downstream photolysis products. Under the current reaction conditions, NH_3 degradation likely begins with the reaction of $O(^1D)$ to generate the NH_2 radical, putting the nitrogen into the manifold of reactive species that will oxidize further. Once NO is generated, the products observed in the FTIR spectrum, N_2O, NH_4NO_3, and HNO_3, are readily formed. Nitrous oxide is a greenhouse gas whose formation will be at least as important as ozone to consider in further development of this technology.[40]

When H_2S was present in the reaction mixture, N_2O formation was reduced. It is possible (we believe likely) that in the presence of other components found in swine farm exhaust, such as other VOCs, the generation of nitrous oxide could be further reduced and the steady state concentration of ozone is likely to be lower, due to the consumption of atomic oxygen by the other oxidizable species. Elimination of water from barn air is thoroughly impractical, so the somewhat lower efficiency of ammonia abatement in humid air is a factor that will have to be dealt with in further studies. We speculate that the effect of VOCs, present in much smaller concentrations, on ammonia treatment will

be much smaller than that of water, but experiments are required to verify this. Particulate matter in the barn air is also a concern due to its light scattering effects, but would also consume some of the undesirable ozone and possibly N_2O. Ammonium nitrate could be removed mechanically along with other particulate matter, as needed.

The current experiments surely demonstrate that the photolysis method of ammonia abatement is viable at the level of proof of principle, but more realistic models would be required to see how well the higher energy input and the shorter HRTs of barn exhaust manifolds could be implemented.

7.7 ACKNOWLEDGEMENT

The authors thank the National Pork Board (Project # 15027) for support of this work, Steve Veysey for his assistance with GC-MS and FTIR analyses, Prof. Steven Hoff for the use of his chemiluminescence ammonia analyzer, and Prof. Jeffery Zimmerman for the use of his humidity monitor.

7.8 REFERENCES

(1) *Animal Agriculture and the Environment*; Rice, J. M.; Caldwell, D. F.; Humenik, F. J., Eds.; American Society of Agricultural and Biological Engineers: St. Joseph, MI, 2006.

(2) Academies, N. R. C. o. t. N. *Air Emissions from Animal Feeding Operations: Current Knowledge and Future Needs*; National Academies Press: Washington, D.C., 2003.

(3) Aneja, V. P.; Blunden, J.; James, K.; Schlesinger, W. H.; Knighton, R.; Gilliam, W.; Jennings, G.; Niyogi, D.; Cole, S. *Journal of Environmental Quality* **2008**, *37*, 515-520.

(4) USEPA. *Federal Register* **2008**, *73*, 76948-76960.

(5) USEPA. *Federal Register* **2005**, *70*, 4958-4977.

(6) USEPA. *Federal Register* **2007**, *72*, 20586-20667.

(7) USEPA. *Federal Register* **2008**, *73*, 28321-28350.

(8) Arogo, J.; Westerman, P. W.; Heber, A. J. *Transactions of the ASAE* **2003**, *46*, 805-817.

(9) Wheeler, E. F.; Casey, K. D.; Gates, R. S.; Xin, H.; Zajaczkowski, J. L.; Topper, P. A.; Liang, Y.; Pescatore, A. J. *Transactions of the ASABE* **2006**, *49*, 1495-1512.

(10) Groot Koerkamp, P. W. G.; Metz, J. H. M.; Uenk, G. H.; Phillips, V. R.; Holden, M. R.; Sneath, R. W.; Short, J. L.; White, R. P. P.; Hartung, J.; Seedorf, J.; Schroder, M.; Linkert, K. H.; Pedersen, S.; Takai, H.; Johnsen, J. O.; Wathes, C. M. *Journal of Agricultural Engineering Research* **1998**, *70*, 79-95.

(11) Wathes, C. M.; Holden, M. R.; Sneath, R. W.; White, R. P.; Phillips, V. R. *British Poultry Science* **1997**, *38*, 14-28.

(12) *Emissions of Air Pollutants*; Friedrich, R.; Reis, S., Eds.; Springer-Verlag: Berlin, 2004.

(13) Hoeksma, P.; Verdoes, N.; Oosthoek, J.; Voermans, J. A. M. *Livestock Production Science* **1992**, *31*, 121-132.

(14) Jongbloed, A. W.; Lenis, N. P. *Livestock Production Science* **1992**, *31*, 75-94.

(15) Melse, R. W.; Ogink, N. W. M. *Transactions of the ASAE* **2005**, *48*, 2303-2313.

(16) Melse, R. W.; Ogink, N. W. M.; Rulkens, W. H. *Biosystems Engineering* **2009**, *104*, 289-298.

(17) Parker, D. B.; Pandrangi, S.; Greene, L. W.; Almas, L. K.; Cole, N. A.; Rhoades, M. B.; Koziel, J. A. *Transactions of the ASAE* **2005**, *48*, 787-793.

(18) Oppenlander, T. *Photochemical Purification of Water and Air*; WILEY-VCH Verlag: Weinheim, Germany, 2003.

(19) Lamp output values were supplied by the manufacturer.

(20) Pouchert, C. J. *The Aldrich Library of FT-IR Spectra Vapor Phase*; 1st ed.; Aldrich Chemical Company, Inc.: Milwaukee, WI, 1989; Vol. 3.

(21) NIST Mass Spec Data Center, S. E. S., director, "Infrared Spectra" in **NIST Chemistry WebBook, NIST Standard Reference Database Number 69**, Eds. P.J. Linstrom and W.G. Mallard, National Institute of Standards and Technology, Gaithersburg MD, 20899, http://webbook.nist.gov, (retrieved June 9, 2009).

(22) Theoret, A.; Sandorfy, C. *Canadian Journal of Chemistry* **1964**, *42*, 57-62.

(23) Wu, H. B.; Chan, M. N.; Chan, C. K. *Aerosol Science and Technology* **2007**, *41*, 581-588.

(24) Levine, J. S.; Editor *The Photochemistry of Atmospheres: Earth, the Other Planets, and Comets*, 1985.

(25) Seinfeld, J. H.; Pandis, S. N.; Editors *Atmospheric chemistry and physics: from air pollution to climate change, 2nd Edition*, 2006.

(26) Warneck, P. *Chemistry of the Natural Atmosphere, Second Edition*, 2000.

(27) Finlayson-Pitts, B. J.; Pitts, J. N. *Chemistry of the Upper and Lower Atmosphere: Theory, Experiments, and Applications*, 1999.

(28) Estupinan, E. G.; Nicovich, J. M.; Li, J.; Cunnold, D. M.; Wine, P. H. *Journal of Physical Chemistry A* **2002**, *106*, 5880-5890.

(29) Prasad, S. S. *Journal of Chemical Physics* **2002**, *117*, 10104-10108.

(30) Prasad, S. S.; Zipf, E. C. *Journal of Geophysical Research, [Atmospheres]* **2008**, *113*, D15307/1-D15307/17.

(31) Zipf, E. C.; Prasad, S. S. *Geophysical Research Letters* **1998**, *25*, 4333-4336.

(32) Tyndall, G. S.; Orlando, J. J.; Nickerson, K. E.; Cantrell, C. A.; Calvert, J. G. *Journal of Geophysical Research, [Atmospheres]* **1991**, *96*, 20761-20768.

(33) DeMore, W. B.; Sander, S. P.; Golden, D. M.; Hampson, R. F.; Kurylo, M. J.; Howard, C. J.; Ravishankara, A. R.; Kolb, C. E.; Molina, M. J. *JPL Publication 97-4* **1997**, 1-266.

(34) Cohen, N. *International Journal of Chemical Kinetics* **1987**, *19*, 319-362.

(35) Espinosa-Garcia, J. *The Journal of Physical Chemistry A* **2000**, *104*, 7537-7544.
(36) Alfassi, Z. B.; Editor *N-Centered Radicals*, 1998.
(37) Inomata, S.; Washida, N. *The Journal of Physical Chemistry A* **1999**, *103*, 5023-5031.
(38) Frenck, C.; Weisweiler, W. *Chemical Engineering and Technology* **2002**, *25*, 123-128.
(39) Lo, Y.-C. M.; Koziel, J. A.; Cai, L.; Hoff, S. J.; Jenks, W. S.; Xin, H. *Journal of Environmental Quality* **2008**, *37*, 521-534.
(40) USEPA. http://www.epa.gov/climatechange/emissions/index.html

7.8 SUPPORTING INFORMATION

7.8.1 Calibrations and Control Experiments

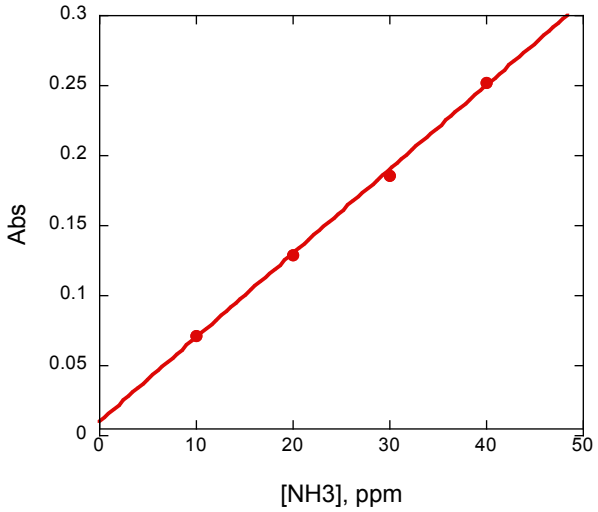

Figure 7.S1 FTIR response curve for air dilutions of 50 ppm $[NH_3]_0$ at 100 mL/min (1 HRT unit = 3.94 min).

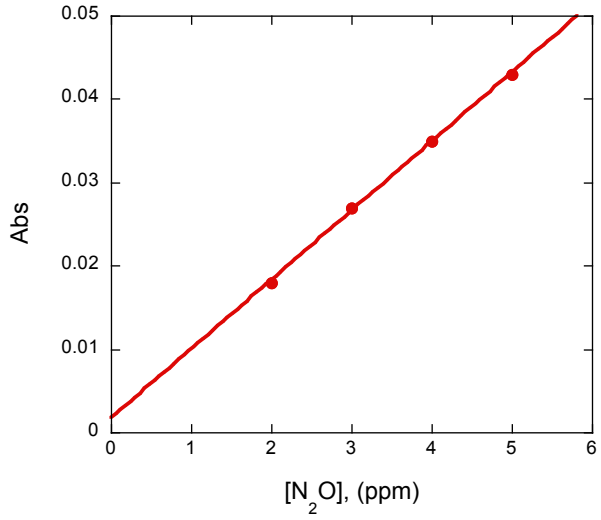

Figure 7.S2 FTIR response curve for N_2 dilutions of 5 ppm $[N_2O]_0$ at 100 mL/min (1 HRT unit = 3.94 min).

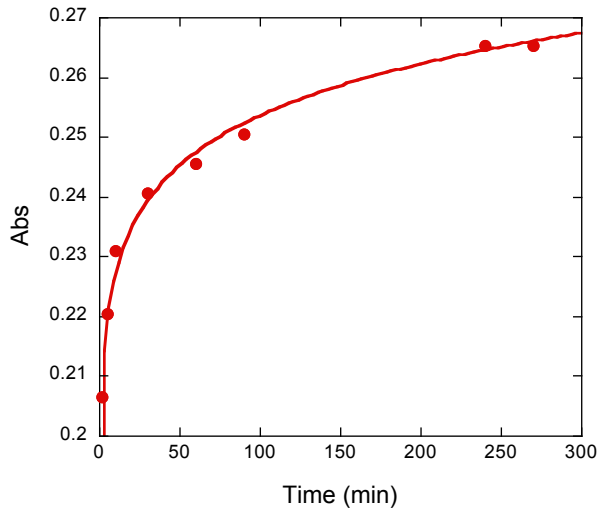

Figure 7.S3 Dark adsorption/desorption equilibration of 50 ppm $[NH_3]_0$ at 600 mL/min (1 HRT unit = 0.66 min).

7.8.2 Additional FTIR Spectra

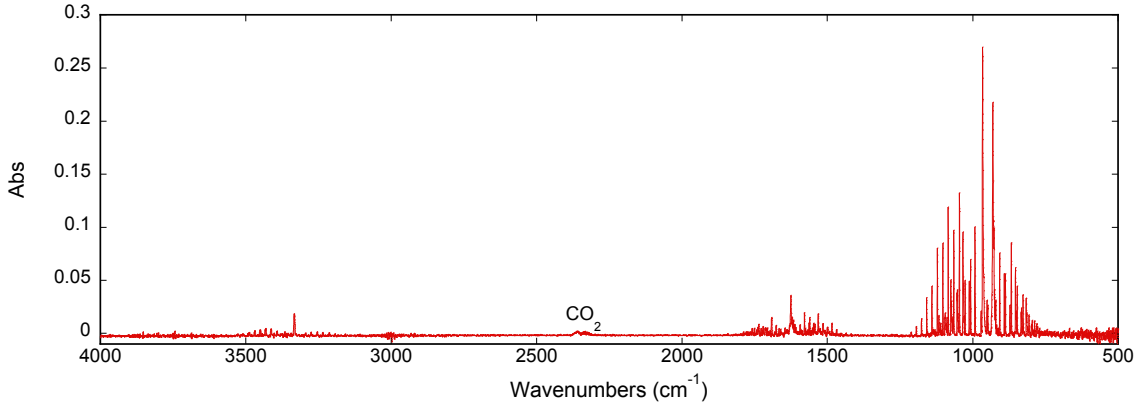

Figure 7.S4 FTIR spectrum of 50 ppm NH_3 in dry air.

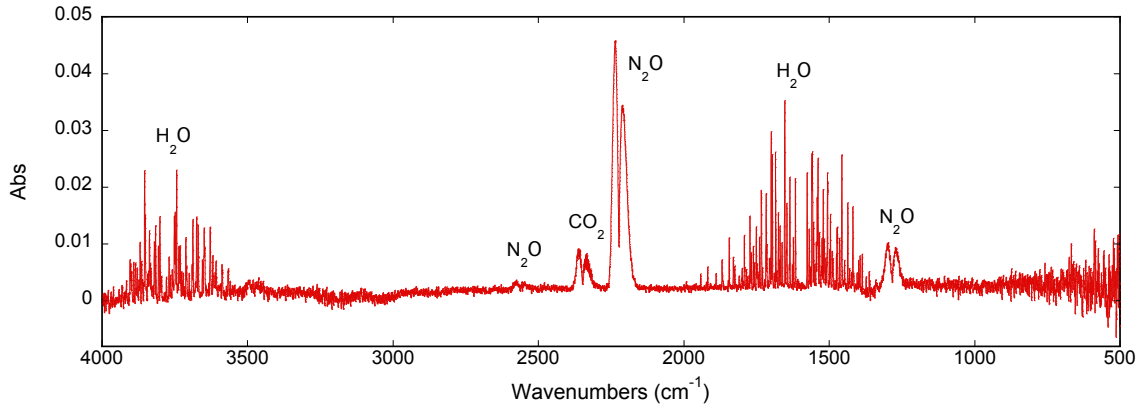

Figure 7.S5 FTIR spectrum of 5 ppm N_2O in N_2.

7.8.3 Absorption Cross Sections

Table 7.S1 Absorption cross sections (σ_λ) at 300 K used for rate comparisons.

Molecule	σ_{185} (cm^2 $molecule^{-1}$)	σ_{254} (cm^2 $molecule^{-1}$)	Ref
NH_3	*ca*. 1 x 10^{-17}	--	1
O_2	*ca*. 1 x 10^{-20}	--	2-4
O_3	6 x 10^{-19}	1 x 10^{-17}	4-6
H_2O	7 x 10^{-20}	--	7,8

7.8.4 References

(1) Chen, F. Z.; Judge, D. L.; Wu, C. Y. R.; Caldwell, J. *Planetary and Space Science* **1999**, *47*, 261-266.

(2) Kessler, K.; Kleinermanns, K. *Journal of Chemical Physics* **1992**, *97*, 374-78.

(3) Yoshino, K.; Esmond, J. R.; Cheung, A. S. C.; Freeman, D. E.; Parkinson, W. H. *Planetary and Space Science*, *40*, 185-192.

(4) Brion, J.; Daumont, D.; Malicet, J.; Marche, P. *Journal de Physique, Lettres* **1985**, *46*, 105-10.

(5) Mauersberger, K.; Barnes, J.; Hanson, D.; Morton, J. *Geophysical Research Letters* **1986**, *13*, 671-3.

(6) Molina, L. T.; Molina, M. J. *Journal of Geophysical Research, [Atmospheres]* **1986**, *91*, 14501-8.

(7) Creasey, D. J.; Heard, D. E.; Lee, J. D. *Geophysical Research Letters* **2000**, *27*, 1651-1654.

(8) Chan, W. F.; Cooper, G.; Brion, C. E. *Chemical Physics* **1993**, *178*, 387-400.

CHAPTER 8

General Conclusions

8.1 DEOXYGENATION OF DBTO AND DBSeO

The Jenks group has proposed the unimolecular deoxygenation of DBTO and DBSeO to generate O(^{3}P) and the corresponding sulfide or selenide.[1,2] The original hypothesis was that cleavage occurs during the S-O bond stretch that accompanies intersystem crossing (ISC) to T_1. Cleavage directly out of the spectroscopic triplet is energetically unfavorable since T_1 is lower energy (~61 kcal/mol) than the S-O bond strength (72 kcal/mol), and occurrence from S_1 is spin-forbidden.

Further evidence for this mechanism, albeit indirect, was presented in Chapter 2. It was shown through "oxidative fingerprinting" that triplet sensitization of DBTO led to different product distributions than direct photolysis. Different oxidation patterns indicated the lack of a common intermediate between sensitized and direct photolysis. Therefore, deoxygenation cannot be occurring out of the spectroscopic triplet (T_1), and must result from an alternate mechanism, such as bimolecular reduction.[3] On the other hand, when a triplet sensitizer of the appropriate energy was used with DBSeO as a substrate, similar oxidized product ratios to those obtained upon direct photolysis of both DBTO and DBSeO were observed. This result suggested that DBSeO suffered homolytic cleavage of the Se-O bond directly from the T_1 state. Unlike DBTO, the Se-O bond strength (63 kcal/mol) was estimated to be around the triplet energy of DBSeO, which should be roughly equal to the triplet energy of DBTO (~61 kcal.mol) since the two chromophores are essentially the same.

More recently, multireference MP2 computations on similar systems (thiophene oxide and selenophene oxide) have shown that the T_2 state likely lies beneath the S_1 state.[4] While the surfaces have not yet been fully generated for DBTO, preliminary results have found a surface corresponding to a T_2 state that lies below the S_1 state. This provides an energetically favorable pathway for unimolecular deoxygenation.

8.2 DOPED TITANIUM DIOXIDE

The main focus of the work presented in this dissertation was on exploration of modifications to TiO_2 in order to improve absorption of terrestrial sunlight. Chapter 3 adds to the available literature on tungsten modified TiO_2. We have found that the lattice incorporation of WO_x in both commercially available (DT52) and homemade TiO_2 photocatalysts does not exhibit a significant increase in visible absorption. Sol-gel preparation of W-TiO_2 yielded material that did not exhibit photocatalytic enhancement, whereas surface-modified DT52 showed accelerated degradation rates and favored SET pathways.

Chapters 4, 5, and 6 investigated the functionality of non-metal doped TiO_2 in the degradation of well-studied organic probe molecules under purely UV and visible irradiation. Current literature on many of these catalysts, namely S-, C-, and N-doped TiO_2, is often contradictory regarding photocatalytic effectiveness. Therefore, it is important to identify the specific dopants and their chemical environments within the catalyst that improve upon pristine TiO_2. With this, any limitations that might restrict these doped TiO_2 photocatalysts to niche applications may be determined.

Carbon-modified TiO_2 was characterized using SS-NMR in order to overcome the inherent shortcoming of XPS analysis of carbon species. Our material contained mostly coke on the surface of the catalyst, which did significantly extend visible light absorption, but did not result in any photocatalytic improvement.

A popular literature method using thiourea and titanium (IV) isopropoxide was employed to prepare S-doped TiO_2.[5] The incorporation of S^{4+}/S^{6+} into the TiO_2 lattice led to a vivid yellow material displaying visible absorbance extending beyond 500 nm. S-TiO_2 was effective in degrading organic probe molecules under visible light, but this was limited to SET pathways for **Q**. No evidence of HO•-type chemistry was observed, and S-TiO_2 was not capable of mediating any appreciable degradation of **Q** at pH 3 or **AN** at pH 8.5. In addition, the rates of loss under UV light for S-TiO_2 were significantly reduced relative to those obtained with undoped TiO_2. It can be concluded that S-TiO_2 would be an improvement over standard TiO_2 for certain types of pollutants and applications that value visible light reactivity over that of UV irradiation.

Moving further down in the periodic table to selenium gave the most promising results of the photocatalysts studied in this dissertation. Se-TiO_2 degraded **AN** at rates similar to S-TiO_2, but was slightly faster than undoped TiO_2 in the removal of **Q** at both pH 3 and 6. While Se-TiO_2 was also apparently limited to SET initiated degradation under visible irradiation, it was capable of degrading **Q** at pH 6 as well as **AN** at pH 8.5. Additionally, XPS analysis showed that Se^{4+} centers were reduced to Se^0 over the course of the photolysis, which indicated that the selenium atoms were acting as a trap for photogenerated electrons, thus suppressing recombination.

Future work in this area will focus on catalyst optimization to enhance photocatalytic activity and explore alternative precursors to lower production costs. Other large atom dopants, such as iodine, also hold great promise and studies in the Jenks group are currently underway.

8.3 AMMONIA MITIGATION

The last chapter of this dissertation extends into gas-phase photochemistry to explore the feasibility of ammonia abatement from swine barn exhaust by UV treatment. Clearly, NH_3 does not simply disappear using standard chemical methods, but can be transformed to more tolerable compounds. Therefore, the main goals of this work were to determine how much ammonia could be removed and whether it could be converted to less noxious species such as nitrate. In short, our studies found that significant ammonia removal by 185 nm irradiation was possible through conversion to NO_3^- species and likely N_2O. The mitigation process most certainly involves the generation of reactive O-containing species upon air photolysis (ozone, $O(^3P)$, etc.). While the photolysis of air also generates nitrous oxide, the addition of NH_3 increased its formation. N_2O is an undesirable byproduct, but we have shown that its production can be decreased by the presence of other components of swine barn emissions, specifically H_2S. Future studies should determine the effects of the presence of other gaseous components, such as VOCs, as this would likely further decrease N_2O liberation. This report provides groundwork for gaining a greater understanding of the chemical pathways and mechanisms that occur, and is necessary for the development and design of suitable UV treatment systems.

8.4 REFERENCES

(1) Gregory, D. D.; Wan, Z.; Jenks, W. S. *Journal of the American Chemical Society* **1997**, *119*, 94-102.

(2) McCulla, R. D.; Jenks, W. S. *Journal of the American Chemical Society* **2004**, *126*, 16058-16065.

(3) Cubbage, J.; Tetzlaff, T.; Groundwater, H.; McCulla, R. D.; Nag, M.; Jenks, W. S. *J. Org. Chem.* **2001**, *66*, 8621-8628.

(4) Stoffregen, S. A., Iowa State University, 2007.

(5) Ohno, T.; Akiyoshi, M.; Umebayashi, T.; Asai, K.; Mitsui, T.; Matsumura, M. *Applied Catalysis, A: General* **2004**, *265*, 115-121.